

TR 2952 S

Stellingen  
behorende bij het proefschrift

**The Interconnected Fluidized Bed reactor  
for gas/solids regenerative processes**

door

*Onno C. Snip*

Delft, 1997

## Stellingen

---

1. Dit is geen stelling omdat er omdat in staat.

2. Ook oude literatuur is nuttig.

*Lamb, H., "A treatise on the mathematical theory of the motion of fluids", Cambridge University Press, Cambridge (1879).*

3. Het is op zijn minst bijzonder dat in vrijwel geen enkel onderzoek naar stroming uit een gefluïdiseerd bed, de invloed van schuifspanningen in de berekening van de wrijvingsverliezen wordt meegenomen.

4. Het Orifice-Shear getal is goed bruikbaar voor de afschatting van wrijvingsverliezen bij stroming van visceuze media door een vernauwing of opening.

*Dit proefschrift.*

5. Het is verbazingwekkend dat er in veel leerboeken over vloeistofmechanica bij problemen over doorstroming van vernauwingen stilzwijgend vanuit wordt gegaan dat de viscositeit van de vloeistoffen gelijk is aan 0. Dat een eenvoudige vloeistof als water wel degelijk een bepaalde viscositeit heeft wordt duidelijk geïllustreerd door het Elfstedentocht-begrip "dik water".

6. Bij het analyseren van fysische transportverschijnselen zijn macroscopische balansen moeilijker toe te passen dan microscopische.

7. Dat fysische transportverschijnselen niet altijd gemakkelijk zijn aan te voelen blijkt uit de uitspraak: 'De kou trekt in m'n voeten!'

8. In de analyse van deeltjesstroming in een IFB-reactor-systeem mag de invloed van de totale hoeveelheid deeltjes in de reactor niet ontbreken.

*Dit proefschrift.*

9. Ten aanzien van milieuproblematiek moet minder geschermd worden met getallen en modellen. Het ontwikkelen van alternatieven en het werken aan oplossingen is aanzienlijk zinvoller.

*Oudshoorn, O.L., Snip, O.C., "Echte vergelijking tussen vliegen, autorijden en reizen per trein niet mogelijk", Trouw, Podium, woensdag 3 juli (1996).*

10. Het is niet terecht dat helium-gevulde luchtschepen als alternatief vervoermiddel zo weinig aandacht krijgen.
11. 'Wel' en 'niet' zijn limietgevallen van 'makkelijk' en 'moeilijk'.
12. Het is jammer dat de milieubeweging aan geloofwaardigheid verliest door voorspellingen te doen die vaak slechts gedeeltelijk of in het geheel niet uitkomen.
13. Het woord theorie is bij de zogenaamde "Big-Bang theorie" niet op zijn plaats. Het moet worden vervangen door geloof.

*Boslough, J., "Meesters van de tijd: hoe de kosmologie haar onschuld verliest", Bert Bakker, Amsterdam (1993).*

*Schilling, G., "Het grootste deel van het heelal is zoek of bestaat niet", Wetenschap, 30 april, Volkskrant (1994).*

14. Tijdens college's en in leerboeken moet het woord 'simpel' worden vermeden.
15. Het is niet terecht dat laserafstandsmeting niet wordt genoemd als één van de mogelijke technieken voor niveaumeting in de procesindustrie.

*Knight, E.A., Pugh, J.R., "Properly select level-measurement devices for bulk solids", Chem. Eng. Progr., February, 50-55 (1996).*

16. Het gebruik van het E(t)-model zoals beschreven in hoofdstuk 6 van dit proefschrift is vanuit een reactorkundig oogpunt een meer praktische benadering bij het modelleren van verblijftijdspreiding in reactoren dan het gebruik van populatiebalans-modellen. Het E(t)-model is dus een nuttige aanvulling op de modellen die op dit moment worden beschouwd als *state-of-the-art* en wordt dus ten onrechte niet genoemd bij een beschouwing over modellering van verblijftijdspreiding in chemische reactoren.

*Kiparissides, C., "Polymerization process modelling: a review of recent developments and future directions", Plenary Lecture at the 14th International Symposium on Chemical Reaction Engineering, May 8, Brugge, Belgium (1996).*

17. Er is pas sprake van een open deur als de deur is opengezet.

18. Linus Pauling merkte reeds in 1960 op dat wetenschappers niet in staat zijn om op basis van quantummechanische berekeningen de eigenschappen van stoffen, zoals bijvoorbeeld het kookpunt van water, te bepalen. Dit is tot op de dag van vandaag het geval. Het is, mede daarom, ongepast dat een gezaghebbend tijdschrift overweegt om een boek te verbranden waarin een on-conventionele hypothese van de vormende oorzakelijkheid wordt behandeld.

*Pauling, L., "The nature of the chemical bond", 3rd edition, Cornell University Press, Ithaca (1960).*

*Nature, Vol. 293, 245-246 (1981).*

*Sheldrake, A.R., "A new science of life", Blond and Briggs, London (1981).*

*Velde van de, K., "Profeet Sheldrake strijdt tegen heidense wetenschap", Trouw, 26 februari (1996).*

19. De menselijke zienswijze op het universum laat zich goed samenvatten door de uitspraak: "Het Heelal: hoe verder men keek, hoe groter het leek !"

*Deelder, J.A., "Moderne gedichten", 2e druk, De Bezige Bij, Amsterdam (1981).*

*Beekman, G., "Kosmos opgerekt", Wetenschap en Onderwijs, 22 februari, NRC Handelsblad (1997).*



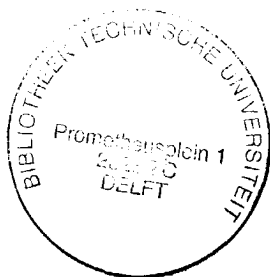
TR 2952

**The Interconnected Fluidized Bed reactor  
for gas/solids regenerative processes**

53500  
310200  
TR 53500



# The Interconnected Fluidized Bed reactor for gas/solids regenerative processes



## PROEFSCHRIFT

ter verkrijging van de graad van doctor  
aan de Technische Universiteit Delft,  
op gezag van de Rector Magnificus Prof.dr.ir. J. Blaauwendraad  
in het openbaar te verdedigen ten overstaan van een commissie,  
door het College van Dekanen aangewezen,  
op dinsdag 20 mei 1997 te 13.30 uur  
door

**Onno Cornelis SNIP**

scheikundig ingenieur  
geboren te Groningen

Dit proefschrift is goedgekeurd door de promotor: Prof.ir. C.M. van den Bleek

Toegevoegd promotor: Dr.ir. J.C. Schouten

Samenstelling promotiecommissie:

Rector magnificus, voorzitter

Prof.ir. C.M. van den Bleek, Technische Universiteit Delft, promotor

Dr.ir. J.C. Schouten, Technische Universiteit Delft, toegevoegd promotor

Prof.ir. J. Grievink, Technische Universiteit Delft

Prof.dr.ir. J.J.M. de Goeij, Technische Universiteit Delft

Prof.dr.ir. W.P.M. van Swaaij, Universiteit Twente

Prof.dr. Y. Molodtsov, Université de Technologie de Compiègne

Dr.ir. R. Korbee, Energie Centrum Nederland (ECN) Petten

Het onderzoek beschreven in dit proefschrift is in belangrijke mate financieel ondersteund door de Voortgangcommissie voor de Onderzoeksprofilering en Stimuleringsruimte (Commissie Beek), onder contractnummer 91-STM-2P en door de Commissie van de Europese Unie, onder contractnummers JOUF-CT91-0063 en JOU2-CT93-0431.

CIP-DATA KONINKLIJKE BIBLIOTHEEK, DEN HAAG

Snip, O.C.

The Interconnected Fluidized Bed reactor for gas/solids regenerative processes / O.C. Snip. - Delft : Delft University Press. - III.

Thesis Delft University of Technology. - With ref. - With summary in Dutch.

ISBN 90-407-1451-7

NUGI 813

Subject headings: fluidized beds / hydrodynamics / solids circulation / gas-solids regenerative processes / regenerative desulfurization / sulfur capture / Interconnected Fluidized Bed

Copyright © 1997 by O.C. Snip

All rights reserved. No part of the material protected by this copyright notice may be reproduced or utilized in any form or by any means, electronic or mechanical, including photocopying, recording or by any information storage and retrieval system, without permission from the publisher: Delft University Press, Mekelweg 4, 2628 CD Delft, The Netherlands.

Printed in the Netherlands.

Cover by E.J. Feenstra, Delft.

## Summary

This thesis concerns the development of Interconnected Fluidized Bed (IFB) reactor technology for gas-solids regenerative processes. The IFB reactor combines a high circulation rate of solids with a minimum amount of solids attrition. An IFB reactor system consists of multiple fluidized bed reactors connected by means of fluidized (or aerated) transport compartments. The difference in gas velocities to the IFB compartments is applied to induce a driving force for solids flow in the IFB system. The solids flow alternately through an orifice and over a weir. One objective in this study was to design and construct an IFB pilot plant facility for a Proof-Of-Concept test. Another objective was the development of insight in its hydrodynamics (solids circulation and solids distribution) in order to design and to operate IFB reactors.

The chemical performance of the IFB reactor system depends on the Circulation Rate of Solids (CRS), the amount of solids that circulates between the fluidized bed compartments. In general, the CRS in an IFB system depends on design parameters: 1. IFB geometry, 2. particle properties, and on operational parameters: 3. gas velocities to the compartments and 4. total IFB bed mass.

The solids flow (*viz.*, CRS) through the orifice that connects two compartments was studied in detail. A general orifice flow model was formulated on the basis of the main driving and resisting forces. This macroscopic model was derived from microscopic considerations of the flow phenomena. The effective orifice area is taken into account by means of the *empty annulus* approach. The *gas-solids drag* force is considered as the main driving force for solids flow. The difference in horizontally directed *particle pressure* between the aerated transport compartment and the fluidized bed reactor compartment determines whether this is a driving or a resisting force for solids flow. The particle pressure in the aerated bed is calculated on the basis of a force balance and the fluidized bed particle pressure is determined from an empirical correlation. The prediction of *shear friction* losses is based on a momentum analysis of the flow towards the orifice. A macroscopic pressure drop relationship relates shear friction to the apparent viscosity of the gas-solids mixture. An empirical relationship was developed on the basis of literature data that correlates the apparent viscosity of the aerated or fluidized bed to particle properties and operational parameters. The particle related properties that are required as model parameters were determined by small scale experiments. The model was validated with results that were obtained in two cold experimental facilities: the twin-bed facility and the jet facility. These facilities are simplifications of the IFB system and enable the direct measurement of solids and gas transport. The model proved to be able to describe solids and gas flows in both facilities satisfactory. The experimental as well as the modelling results give thus insight in the transport phenomena that determine solids discharge and gas flow through an orifice.

The orifice flow model is combined with models for weir flow and solids distribution resulting in an overall model for IFB hydrodynamics. The model predicts CRS and solids distribution in the IFB reactor on the basis of design and operational parameters. This IFB model is capable of explaining qualitatively the hydrodynamic phenomena that were experimentally observed. The influence of the total IFB bed mass and gas velocities to the IFB compartments on IFB hydrodynamics was revealed. It was further shown that the gas velocity to one of the transport compartments can be used to control the CRS in the IFB reactor.

The accomplishment of the high temperature IFB facility is considered as one of the main achievements of this Ph.D. study. The pilot plant facility is suitable for regenerative desulfurization during fluidized bed combustion of coal. Due to the severe conditions caused by the different chemical conditions (reducing, oxidizing and sulfurous gases) and high temperature (up to 1000 °C), special attention was given to the choice of the reactor material. Further, a number of safety measures was implemented in the design and process control devices. In order to measure the solids distribution in the IFB reactor, the bed heights in the four IFB compartments had to be determined. Two experimental methods for measuring bed heights in the IFB facility were developed and used during operation: Laser Light Reflection and Pressure Gradient Extrapolation. Both methods were used as complementary measuring methods. The measurement of gas compositions in the IFB reactor was carried out by an FT-IR apparatus that was calibrated and suited for the IFB facility.

The experimental results show that the IFB reactor is capable of integrating sulfur capture and regeneration by means of solids circulation within one reactor system. The IFB pilot plant facility was successfully operated for continuous regenerative desulfurization up to a five-day period after which the experiments were stopped intentionally. Further, a ten-hour test was carried out as well as various batch sulfur capture and regeneration experiments.

The CRS in the IFB reactor was estimated from the orifice flow model on the basis of pressure drop measurements across the rate limiting orifice. Temperature effects were verified on the sulfur capture and regeneration process.

The following important experimental findings can be identified:

- ▶ the IFB reactor proved to function at high temperature including continuous solids circulation, sulfur capture and regeneration;
- ▶ reactor performance could be controlled by means of manipulating the CRS through the hydrodynamics (gas velocities and bed mass);
- ▶ a high (> 90%) sulfur retention could be achieved in the IFB reactor that is thus suitable for regenerative desulfurization.

A dynamic model was developed for the IFB hydrodynamics. The model is capable of predicting the dynamic response of step-changes in the operational parameters (gas velocities and IFB bed mass). It is shown that the new steady-state for IFB hydrodynamics is reached within the time needed to redistribute the solids over the IFB compartments. This time is much smaller than the average IFB solids circulation time. It was further shown by means of dynamic modelling that it takes approximately five times the average IFB solids circulation time to reach a new steady-state with respect to gas-solids reactions. An alternative approach was developed in addition to population balance modelling for taking into account the effects of particle Residence Time Distribution (RTD) in a dynamically operated fluidized bed reactor system in which gas-solids reactions occur. This dynamic RTD approach was applied to regenerative desulfurization carried out in the IFB reactor. It was shown that the effects of particle RTD on the average conversion of the sorbent can be up to 30%.

It is concluded that the IFB system is a technically feasible reactor configuration that can be economically attractive for processes in which solids circulation is required. This is also illustrated by means of a preliminary design of a process for combined regenerative NO<sub>x</sub> and SO<sub>2</sub> removal from flue gas. This design study was carried out in cooperation with the NOXSO Corporation in the USA. Furthermore, a number of other potential IFB applications is presented.

# Contents

---

## Chapter 1. Introduction to IFB systems:

why and how; advantages and possibilities

<b>1.1</b>	<b>Solids circulation systems</b> . . . . .	<b>1</b>
<b>1.2</b>	<b>Developments in coal technology</b> . . . . .	<b>3</b>
1.2.1	The use of coal	
1.2.2	Fluidized Bed Combustion	
1.2.3	Integrated Gasification Combined Cycle processes	
<b>1.3</b>	<b>IFB history at DUT</b> . . . . .	<b>7</b>
1.3.1	Regenerative desulfurization	
1.3.2	IFB reactor development	
<b>1.4</b>	<b>Aim of the project</b> . . . . .	<b>10</b>
<b>1.5</b>	<b>Outline of the thesis</b> . . . . .	<b>11</b>

## Chapter 2. Hydrodynamics of the IFB system:

solids and gas transport between aerated and fluidized beds

<b>2.1</b>	<b>Circulation Rate of Solids as a function of design</b> . . . . .	<b>15</b>
	<b>and operational parameters</b>	
<b>2.2</b>	<b>Literature review on solids flow through orifices</b> . . . . .	<b>18</b>
<b>2.3</b>	<b>Modelling orifice flow in IFB systems</b> . . . . .	<b>25</b>
2.3.1	General	
2.3.2	Driving and resisting forces	
2.3.3	Consequences for modelling	
<b>2.4</b>	<b>On the viscosity of fluidized and aerated beds</b> . . . . .	<b>34</b>
2.4.1	Analogy of particle/gas-systems and Newtonian liquids	
2.4.2	Measuring apparent viscosities	
2.4.3	Theoretical models for fluidized bed rheology	
2.4.4	An empirical predictive relation for the viscosity	
<b>2.5</b>	<b>Shear friction in flow through orifices</b> . . . . .	<b>38</b>
2.5.1	A macroscopic description of shear friction losses	
2.5.2	Quantifying friction losses: experiments and predictions	
2.5.3	Shear friction in solids flow	
<b>2.6</b>	<b>Experimental results and model validation</b> . . . . .	<b>43</b>
2.6.1	Experimental facilities: twin-bed and jet facility	
2.6.2	Introductory experiments	
2.6.3	Experimental results and model validation	
<b>2.7</b>	<b>Discussion and conclusions</b> . . . . .	<b>53</b>

## Appendix

<b>2.A:</b>	Derivation of a macroscopic pressure drop relation for orifice flow. . . . .	<b>63</b>
<b>2.B:</b>	Outline of the mathematical model for orifice flow in the IFB system. . . . .	<b>65</b>

**Chapter 3. Solids distribution and dynamics of solids circulation in the IFB system:**

<b>3.1 Modelling IFB reactor hydrodynamics</b> . . . . .	69
3.1.1 IFB reactor hydrodynamics	
3.1.2 Solids distribution and solids transport in the IFB reactor	
3.1.3 Development of a mathematical model for IFB hydrodynamics	
<b>3.2 Steady-state modelling and comparison to experimental results</b> . . . . .	79
3.2.1 Orifice size and position	
3.2.2 Total IFB bed mass	
3.2.3 Gas velocities	
3.2.4 Comparison to experimental results	
<b>3.3 Dynamic modelling of the IFB reactor</b> . . . . .	87
<b>3.4 Discussion and conclusions</b> . . . . .	90
<b>Appendix</b>	
3.A: Outline of the mathematical model for IFB hydrodynamics. . . . .	94

**Chapter 4. IFB pilot plant facility for regenerative desulfurization:  
design, construction, and operation**

<b>4.1 Design of the IFB pilot plant facility</b> . . . . .	97
4.1.1 IFB reactor and flowsheet	
4.1.2 Safety and operation	
<b>4.2 Measuring in the IFB facility</b> . . . . .	104
4.2.1 Hydrodynamics	
4.2.2 Gas and solids analysis	
<b>4.3 Operational analysis of the IFB facility</b> . . . . .	108
4.3.1 Modelling the IFB reactor	
4.3.2 Results and consequences for design and operation	

**Chapter 5. IFB pilot plant facility for regenerative desulfurization:  
experimental and modelling results**

<b>5.1 Experimental work in the IFB pilot plant facility</b> . . . . .	113
<b>5.2 Hydrodynamics and solids circulation in the IFB reactor at high temperature</b> . . . . .	115
5.2.1 Minimum fluidization velocity	
5.2.2 Circulation Rate of Solids	
<b>5.3 Modelling regenerative desulfurization:</b> . . . . .	120
5.3.1 Sulfur capture	
5.3.2 Sorbent regeneration	
<b>5.4 Batch experiments:</b> . . . . .	133
5.4.1 Sulfur capture: experiments and modelling	
5.4.2 Sorbent regeneration: experiments and consequences for modelling	
<b>5.5 Continuous regenerative desulfurization experiments</b> . . . . .	140
5.5.1 Five-day test with step changes in operating parameters	
5.5.2 A ten-hour high temperature experiment	
5.5.3 Sulfur retention as a function of IFB hydrodynamics	
<b>5.6 Discussion and conclusions</b> . . . . .	147



## Chapter 6. Gas-solids reactions in the IFB reactor:

the influence of dynamics and particle residence time distribution  
on IFB reactor performance

<b>6.1</b>	<b>Dynamic modelling of regenerative desulfurization in the IFB reactor</b>	153
<b>6.2</b>	<b>Dynamic simulations</b>	158
<b>6.3</b>	<b>Particle residence time distribution</b>	163
6.3.1	The influence of particle RTD on the average conversion in a fluidized bed reactor	
6.3.2	Dynamic RTD in the IFB reactor	
6.3.3	The dynamic E(t) model	
6.3.4	Results of dynamic E(t) model simulations	
<b>6.4</b>	<b>Discussion and conclusions</b>	174
<b>Appendix</b>		
6.A:	Outline of the dynamic E(t) model for IFB regenerative desulfurization.	179

## Chapter 7. Combined NO<sub>x</sub> and SO<sub>2</sub> abatement:

IFB possibilities for the NOXSO process

<b>7.1</b>	<b>Introduction</b>	181
<b>7.2</b>	<b>Combined NO<sub>x</sub> and SO<sub>2</sub> removal processes</b>	181
<b>7.3</b>	<b>The NOXSO process in an Interconnected Fluidized Bed reactor</b>	183
7.3.1	NOXSO process layout	
7.3.2	Modelling the IFB-NOXSO process	
7.3.3	Design of the IFB reactor system	
7.3.4	Results and discussion	
<b>7.4</b>	<b>Analysis and comparison of the NOXSO and IFB-NOXSO process</b>	192
7.4.1	Exergy analysis	
7.4.2	Economic evaluation	
7.4.3	Discussion and comparison of exergy and economic analysis	
<b>7.5</b>	<b>Discussion and conclusions</b>	195

## Chapter 8. Outlook and applications of IFB technology:

<b>8.1</b>	<b>General design and operational considerations</b>	199	
<b>8.2</b>	<b>Applications of IFB technology: processes with solids circulation</b>	201	
8.2.1	Reaction-regeneration processes		
8.2.2	Processes for physical operation		
8.2.3	Combined gasification and novel combustion processes		
<b>8.3</b>	<b>Frequently Asked Questions: with answers</b>	210	
Samenvatting			217
List of abbreviations			219
List of publications			220
Dankwoord			221
Curriculum vitae			222



# Chapter 1

## Introduction to IFB systems

why and how; advantages and possibilities

---

### 1.1 Solids circulation systems

Earlier work on regenerative desulfurization in coal conversion processes carried out at Delft University of Technology (DUT) (Wolff, 1991; Wakker, 1992; Korbee, 1995) led to the investigation of solids circulation systems. A so-called *Interconnected Fluidized Bed (IFB)* system was proposed (Korbee, 1995) for the integration of sulfur capture and sorbent regeneration by means of solids circulation. The IFB reactor system is the main subject of this thesis. Initially proposed for regenerative desulfurization, the IFB reactor appeared to be suitable for several processes for which solids circulation is required. Therefore, the general backgrounds and motives for solids circulation are given below.

The discovery of how to maintain a stable and continuous circulation of solids in a gas-solid system has led to the development of various processes using such a scheme. The key to commercial success of these processes, large and small, depends on the proper design of the specific systems of circulating the solids. Knowlton (1986, 1997) and Kunii and Levenspiel (1991) provide the basic principles and relevant data to design such systems.

Solids circulation (or transfer) between fluidized or aerated solids-gas systems can be carried out for a number of specific motives. In Figure 1.1, a schematical representation is given of the relevant classes of solids circulation systems. The most important motives for solids circulation are:

► **Cyclic processes with reaction-regeneration.**

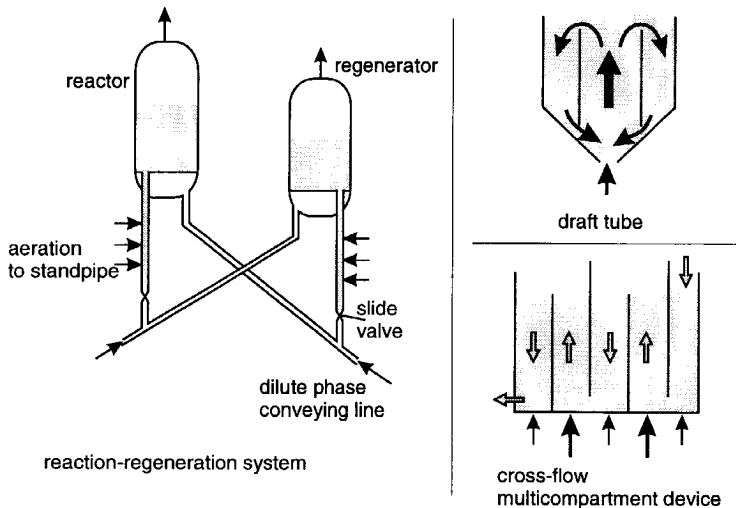
Examples are sorbent regenerative processes and processes in which a catalyst needs to be regenerated after deactivation in the reactor.

► **Mixing within a fluidized bed.**

In many fluidized bed devices, mixing is an important issue. The reason often is the elimination of temperature gradients or the reducing of segregation, caking and agglomeration (especially in drying and coating processes). A device that is frequently used for this purpose is the so-called draught (or draft) tube (see Figure 1.1). The solids are transported up the central tube. An effective density difference between the tube and the annulus is induced by the difference in gas velocity. This causes the solids to flow in a circulating pattern through the system. In case of large particle systems, such a device is also referred to as a spouted bed (Kalwar, 1993; Milne, 1992; Olazar, 1993).

A number of applications is proposed (He and Rudolph, 1993; LaNauze, 1976; Yang and

Keairns, 1978) for draught tube induced solids circulation systems. Some examples are coating and drying of solid materials, oil and coal gasification, and processing of caking coals.



**Figure 1.1** Schematic representations of solids circulation systems. Solids circulation is desired for: regeneration of the solid material, mixing enhancement within a reactor vessel (draft tube) and narrowing the residence time distribution of the solids (cross-flow multicompartiment device).

► **Cross-flow devices for physical operation.**

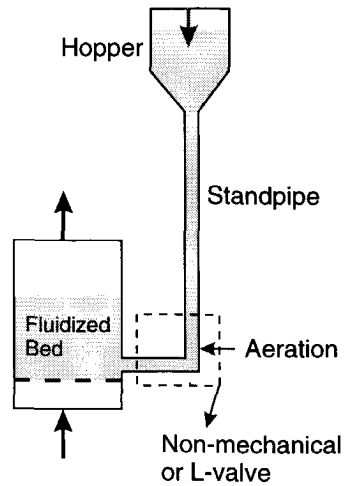
In chapter 8.2.2, a number of devices is presented and discussed that are being used for physical operations in which a solid material is undergoing some treatment (drying, heating, cooling and adsorption) by means of a gas. In many cases, a so-called cross-flow device (see Figure 1.1) is used to narrow the residence time distribution to yield a uniform product and to improve the efficiency of the apparatus compared to a one-stage facility (Kunii and Levenspiel, 1991).

Solids circulation systems are thus utilized for the purposes that are indicated above. In case of reaction-regeneration processes carried out in separate reactor vessels, solids transport can be carried out by means of mechanical and non-mechanical transport devices. Non-mechanical devices are advantageous because the stresses that are exerted on the particles are less severe than for mechanical devices. This results in a reduced loss of solid material. Further, non-mechanical devices are less sensitive for process disturbances such as blocking or break-down.

In non-mechanical transport devices, the solids are transported in dense or dilute phase transport lines between the reactor vessels. The connections can be made by means of valves and standpipes. The valves can be either mechanical or non-mechanical devices (see chapter 2.2 of this thesis). The main advantages of non-mechanical valves over mechanical valves are the simple and inexpensive construction with no moving mechanical parts (Knowlton,

1986). See Figure 1.2 for a simplified representation of a standpipe and non-mechanical valve configuration.

In order to avoid high velocity pneumatic transport of solids that is often used, high density circulating fluidized beds can be applied (Zhu and Bi, 1995). A development that combines the advantages of high density fluidized beds and non-mechanical valves without the need of transport lines is the Interconnected Fluidized Bed (IFB) system. See Figure 1.3 which shows a schematic representation of an IFB reactor. In this reactor system, the solids are transported through orifices and over weirs. The driving force for solids flow is induced by means of the differences in gas velocity to the compartments of the system. The transport compartments can be considered as a combination of a standpipe and non-mechanical valve.



**Figure 1.2** A standpipe and non-mechanical valve used to control the solids feeding rate to a fluidized bed reactor.

Due to the moderate solids transportation velocity and the lack of transport lines, the main advantages of the IFB reactor system are:

- ▶ compact and integrated reactor design, and
- ▶ less attrition compared to high velocity pneumatic transport.

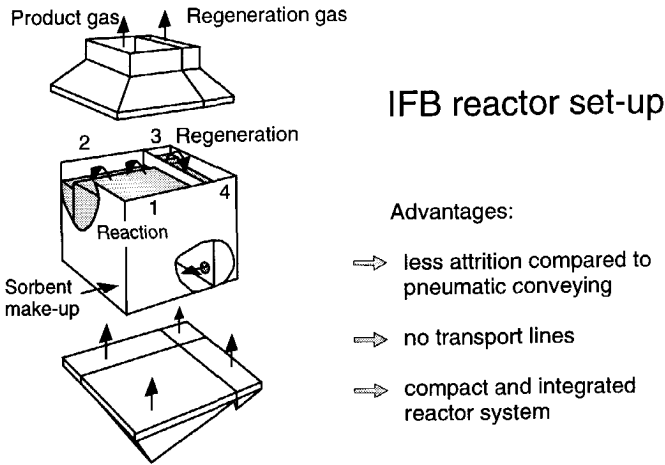
The IFB reactor system can be used for various applications such as reaction-regeneration processes or processes for physical operation (see chapter 8.2). The use of this reactor system will be further analyzed in this thesis.

## 1.2 Developments in coal technology

### 1.2.1 The use of coal

Coal is an important raw material in today's society. It is mainly used as an energy source (production of power), for the production of coke (in the steel industry), and as a feedstock for synthetic fuels and chemicals. Coal is the most abundant and widely dispersed fossil energy resource with an estimated worldwide reserve for 200-250 years (Shell, 1996; Sasol, 1996; Thambimuthu, 1993).

The number of energy sources as being used by the world population will grow and diversify in the coming years. Wind, solar energy (thermal and photovoltaic), nuclear power, wave and tidal energy, hydropower and biomass energy sources will be increasingly used. It is however expected that coal will continue to play a major role in the world's energy supply due to its large reserves and the spread across the world. It is therefore important that new technologies for conversion of coal into power are currently being developed.



**Figure 1.3** Schematic presentation of an IFB reactor suitable for solids circulation in a reaction-regeneration process.

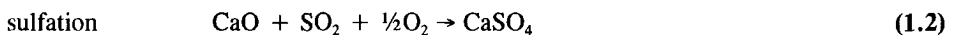
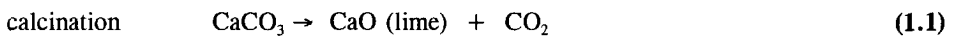
The main driving forces will originate from the need to:

- ▶ increase efficiency,
- ▶ fulfill environmental requirements, and
- ▶ improve process economics.

In chapters 1.2.2 and 1.2.3, Fluidized Bed Combustion (FBC) of coal and Integrated Gasification Combined Cycle (IGCC) processes are presented as two developments of coal technology for power production.

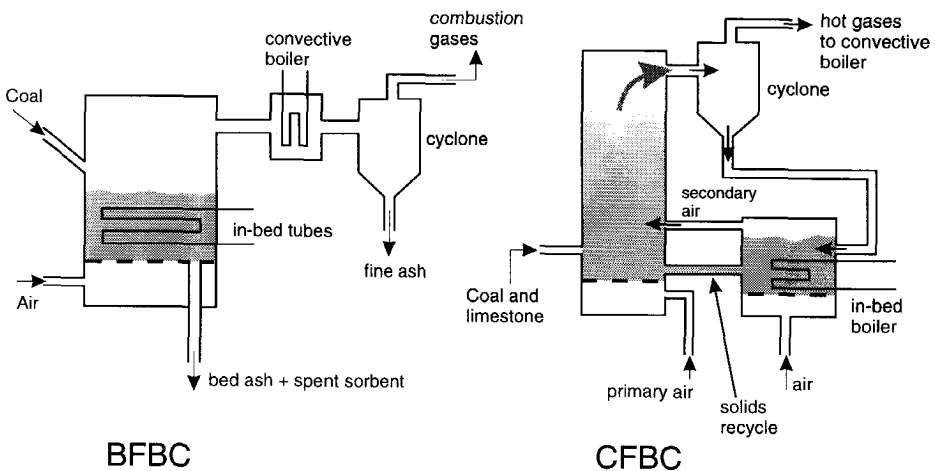
### 1.2.2 Fluidized Bed Combustion

The concept of Fluidized Bed Combustion (FBC) of coal was first proposed in the 1960s (Basu and Fraser, 1991; Davidson, 1992). The development of FBC has since then been steady and involved the evolution and demonstration of a number of variations to the original ideas (Anthony, 1995). Basically, coal is burned in a bed of hot ash or added sand through which air is blown. Due to the fluidized nature of the bed, heat is easily transferred to the wall or to tubes that are immersed in the bed. Because of the high reaction rates, fluidized beds are operated at temperatures typically 800 to 900°C, below that at which the ash particles start to agglomerate. At these temperatures, a sorbent (usually limestone) can be added to the bed that reacts with the sulfur that is released from the coal to form a solid compound that can be removed with the ash. The limestone (CaCO<sub>3</sub>) is calcined followed by sulfation according to:



No additional flue gas clean-up for sulfur compounds is needed. The relatively low bed temperature also limits the amount of nitrogen oxides formed during combustion (no thermal  $\text{NO}_x$  is formed).

Fluidized beds in which all chemical reactions and much of the heat transfer takes place in or just above the bed are referred to as stationary or bubbling fluidized bed combustors. More recently, boilers have been developed incorporating so-called Circulating Fluidized Beds (CFBs). High gas velocities are used to carry the hot particles and gases from the fluidized bed and combustion zones to separate heat exchangers. This results in improved process control and more efficient suppression of nitrogen and sulfur oxides (THERMIE, 1994). Further advantage of CFB boilers is the high combustion efficiency compared to bubbling fluidized bed combustors (Basu and Fraser, 1991). See Figure 1.4 for a schematic representation of a bubbling (BFBC) and a Circulating Fluidized Bed (CFBC) coal combustor.



**Figure 1.4** Schematic presentation of a bubbling (BFBC) and circulating fluidized bed combustor (CFBC).

In the CFB boiler, the combustion takes place in the furnace part of the facility. The air is added typically in points up to the chamber and the gas velocity is such that the solids are carried out of the top of the vessel. Some heat transfer takes place to the walls of the chamber but no cross tubes are present. The sulfur dioxide emissions are kept low due to the addition of limestone (reactions 1.1 and 1.2) and nitrogen oxides are kept low by using staged combustion (THERMIE, 1994). The combusted gases are separated from the particles in cyclones and the particles are recycled back to the combustion chamber after extraction of the heat. The hot gases from the cyclones are further cooled in superheaters and economisers.

The main advantages of fluidized bed combustion of coal compared to conventional pulverized coal combustion are the high volumetric energy release (compact installations), high fuel flexibility, low emissions of  $\text{NO}_x$  and the possibility of in-situ removal of  $\text{SO}_2$ . Disadvantages are the attrition of particles and the erosion of in-bed tubes and walls. Another disadvantage is the production of partly sulfated limestone that needs to be converted to a useful product or can be considered as a solids waste stream. Regenerative desulfurization can be applied to cope with this problem.

Economic evaluations have shown (see chapter 8.2.1 of this thesis) that bubbling FBC boilers are attractive for small scale power production (25-50 MWe). Circulating type boilers are economically more attractive for larger scale power plants.

Pressurized fluidized bed combustion can be applied to increase the efficiency with which the energy in a fossil fuel (such as coal) is transferred into electrical energy. The combustor type can be bubbling as well as circulating. A combination of a gas-fired turbine and a steam turbine is used. The efficiency of the 'combined cycle' is higher than for an atmospherically operated unit without a gas turbine. The overall efficiency of a pressurized fluidized bed combustor is estimated to be about 4% higher than the equivalent pulverized fuel-fired system (THERMIE, 1994).

### 1.2.3 Integrated Gasification Combined Cycle processes

The integration of a coal gasification step with a combined cycle plant is considered as one of the most promising ways of producing electricity from coal with respect to the process efficiency and its environmental impact (Richards, 1993; DeMoss, 1995; Joshi and Lee, 1996). In a so-called Integrated Gasification Combined Cycle (IGCC) process, coal is gasified to fuel gas that is purified before it is directed to the gas turbine. In this turbine, the fuel gas is combusted with compressed air yielding a stream of hot high pressure gas that drives the turbine.

Several processes are available for the gasification of coal to fuel gas (THERMIE, 1994; Joshi and Lee, 1996). The processes vary on the basis of:

- ▶ gasification reactor type: fixed, fluidized or entrained beds,
- ▶ conditions: pressure and temperature, and
- ▶ dry coal feed or slurry feed to the gasifier.

Another difference is the use of air or pure oxygen for gasification. Oxygen is needed for the partial combustion of the coal by which the heat is supplied for the endothermic gasification reactions.

Commercial scale demonstration units have been established both in Western Europe and in the USA (Joshi and Lee, 1996). In The Netherlands, a 253 MWe electric power producing IGCC facility based on Shell gasification technology is currently in its demonstration phase. In the USA, the so-called Cool Water IGCC plant (120 MWe) based on Texaco gasification technology already proved to be successful with respect to emission levels and efficiency of the process.

The conclusions of several studies (Joshi and Lee, 1996; THERMIE, 1994) are that the IGCC process based on coal is superior over other coal conversion techniques for large scale electricity production. The advantages of the process are its high efficiency of converting the energy of the coal into electrical energy and the minimization of the waste streams. Another



advantage of the IGCC technology is that further improvements can be expected with respect to the efficiency of the process.

The main directions for process improvements are:

- ▶ Introduction of a **fuel cell** into the combined cycle. In this configuration, the fuel cell is used for direct conversion of fuel gas into electricity. At this moment this is not a technically feasible option. Especially, gas cleaning systems need to be improved and problems of scale (stacking of the cells) with regard to fuel cells need to be solved (Thambimuthu, 1993; Joshi and Lee, 1996).
- ▶ Developments in **gas turbine** systems. The parameters affecting the improvement of the efficiency of the apparatus include cycle innovations, increased firing temperature, reduced cooling air usage and improved material/coating systems (Joshi and Lee, 1996).
- ▶ Introduction of **high temperature gas clean-up**. The fuel gas originating from the gasifier needs to be disposed of impurities such as dust, sulfur compounds ( $\text{H}_2\text{S}$ , COS,  $\text{CS}_2$ ), HCN,  $\text{NH}_3$ , heavy metals, alkali metals, and HCl and HF. The overall efficiency of the process can be improved by 1 to 3% when high temperature (450-650 °C) gas cleaning is applied in comparison to the conventional cold ( $< 100^\circ\text{C}$ ) gas clean-up (NOVEM, 1990; Thambimuthu, 1993).

High temperature desulfurization of fuel gas has received a lot of attention and various processes have been developed for this purpose. A large number of solid adsorbents based on metal oxides, mixed metal oxides, and supported metal oxides can be used for this purpose. An overview of high temperature desulfurization processes is given by Wakker (1992), Thambimuthu (1993) and van Yperen (1994).

Little attention was given to reactor developments that combine adsorption of the sulfurous components from the fuel gas with regeneration of the sorbent (NOVEM, 1990). The development of two new reactor types for continuous operation in a cyclic process is described by Bakker *et al.* (1996). The reactors that are under development at Delft University of Technology (DUT) are the Rotating Monolith (RM) reactor and the Interconnected Fluidized Bed (IFB) reactor. The IFB reactor is further described in this thesis.

### 1.3 IFB history at DUT

#### 1.3.1 Regenerative desulfurization

In 1932, the Battersea power station in London used water from the river Thames to dissolve sulfur oxides and returned the water to the river. This was the first flue gas desulfurization installation in history (Schobert, 1987). Since then, a large number of processes has been developed and improved for the removal of sulfur components from flue gas streams (Ellison, 1995). In general, the emission of sulfur dioxide in the production of electricity can be reduced in three ways:

- ▶ by coal cleaning,
- ▶ through treatment during combustion, and
- ▶ by flue gas desulfurization.

## Chapter 1

---

Coal cleaning has been found to be capable of removing only 5 to 30% of the sulfur. The remaining sulfur is bound within the coal structure and cannot be removed by physical processes. Flue gas desulfurization processes are in widespread use at pulverised power stations throughout the world. The costs of the additional plant that is required to clean the large amounts of flue gas, increase the cost of electricity or heat production considerably (THERMIE, 1994).

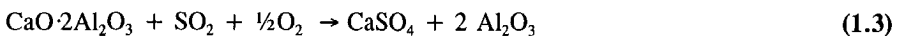
Processes in which the sulfur is removed before (IGCC) or during combustion (FBC) are therefore advantageous with respect to the costs of desulfurization. Regenerative sulfur capture is especially attractive because the elimination of SO<sub>2</sub> emissions is combined with the conversion of the sulfur compounds into useful products. The amount of solids waste is minimized as well. A description of developments in IGCC processes is given in chapter 1.2.3. A process for regenerative high temperature desulfurization developed at DUT is described by Wakker *et al.* (1993).

In case of Fluidized Bed Combustion of coal, limestone is usually added to the combustor to directly capture the SO<sub>2</sub> that is released. The limestone reacts according to reactions 1.1 and 1.2. The commercial application of the gypsum (CaSO<sub>4</sub>) that is produced during this once-through desulfurization is limited due to fact that no fully converted limestone (pure gypsum) is produced. Further limitations are the presence of ash and trace metals and the limited size of the gypsum market (Nilsson and Clarke, 1994). The sulfated limestone can therefore generally be considered as a solids waste stream that comprehends a serious disadvantage of FBC as a coal conversion technique.

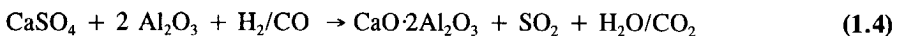
It would therefore be advantageous to apply regenerative desulfurization including sorbent regeneration in combination with the recovery of the sulfur from the coal as a useful product. The regeneration of natural sorbents, such as limestone, can only take place at relatively high temperatures (> 1100°C) compared to the combustion temperature (850°C). During cyclic sulfation and regeneration, the sulfur capture activity of the limestone decreases rapidly with the number of cycles. Further, the resistance of natural sorbents to attrition is poor. Due to these disadvantages of natural sorbents, a synthetic sorbent for regenerative desulfurization can significantly improve the process (Wolff, 1991). A schematic presentation of regenerative desulfurization in FBC is shown in Figure 1.5.

These considerations led to the design, development and testing of a suitable regenerable sorbent (Duisterwinkel, 1991; Korbee, 1995; Wolff, 1991). The sorbent, manufactured by means of the sol-gel (or oil-drop) method, consists of spherical particles of a  $\gamma$ -alumina carrier with highly dispersed calcium oxide (typically less than 10 wt%). Regenerative desulfurization by the synthetic sorbent can be represented by the following overall reactions:

sulfur capture:

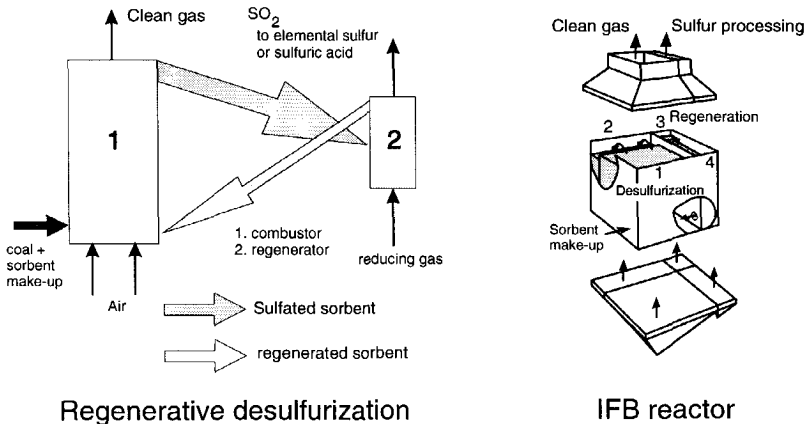


regeneration:



The formation of the stable calcium aluminates (represented by  $\text{CaO}\cdot\text{Al}_2\text{O}_3$ ) is the reason that sorbent regeneration can be carried out at much lower temperatures ( $850^\circ\text{C}$ ) than regeneration of sulfated limestones ( $1100^\circ\text{C}$ ). This enables the application of an *isothermal* process with respect to sorbent sulfation and regeneration.

The sorbent sulfation process was studied in thermogravimetric, fixed and fluidized bed equipment and a sorbent sulfation model was developed (Duisterwinkel, 1991; Wolff, 1991; Wolff *et al.*, 1993a; Schouten and van den Bleek, 1995). The sorbent showed satisfactory results with respect to sorbent deactivation and sulfation behaviour in a 100-cycle laboratory fluidized bed test and a 1.6 MWth PFBC pilot test (Korbee, 1995). The regeneration of sulfated sorbent and the development of a sorbent regeneration model is described by Korbee (1995). Several attrition tests carried out with the synthetic sorbent showed satisfactory results with respect to sorbent loss during fluidized bed operation. The synthetic sorbent showed a much higher resistance to attrition than limestone. However, when the sorbent is transported by means of a high velocity (20 m/s) pneumatic conveying system, many sorbent particles break causing a high (up to 83%) loss of sorbent (Wolff *et al.*, 1993b).



**Figure 1.5** Regenerative desulfurization in Fluidized Bed Combustion of coal. A sorbent is transported between combustor and regenerator. The IFB reactor is an integration of the combustor and regenerator in one reactor vessel.

### 1.3.2 IFB reactor development

An economic evaluation of regenerative desulfurization by means of the synthetic sorbent was carried out by Wolff (1991). This study revealed that regenerative desulfurization was not economically attractive compared to once-through processes. The major costs for regenerative desulfurization are the expenses for the synthetic sorbent. The amount of sorbent make-up (sorbent attrition) therefore needs to be minimized. It is of vital importance to avoid high velocity collisions during transport of sorbent between combustor and regenerator. This was the main driving force for the development of the IFB reactor as described by Korbee (1995).

## Chapter 1

---

This new type of reactor is shown in Figure 1.5 as the integration of combustor and regenerator in one reactor vessel. The sorbent is transported at moderate velocities ( $< 2$  m/s) respectively through an orifice and over a weir. The loss of sorbent is minimized, due to the relatively low (linear) particle velocities and the small distance between reactor compartments.

Cold experimental work was performed with respect to IFB hydrodynamics in order to obtain insight in the IFB reactor system. This resulted in the development of a hydrodynamic model that is able to describe solids and gas transport through the orifice between two IFB compartments (Korbee, 1995; Korbee *et al.*, 1994).

A preliminary design of a 100 MWe power plant based on the IFB reactor concept was presented by Korbee *et al.* (1993). In this design four compartments are considered:

1. a fluidized bed combustor with in-situ desulfurization, transporting the ash and sorbent over a weir to
2. a compartment with solids downflow and segregation of ash and sorbent to enable ash removal. From this compartment the solids are transported to
3. the regenerator, in which the sorbent is regenerated by means of reducing gases and transported over a weir to
4. a de-fluidized compartment (gas velocity below the minimum fluidization velocity). By means of adjusting the gas velocity to this compartment, the circulation rate of the solids is controlled.

The 100 MWe design of the IFB reactor system followed after an analysis of combustor and regenerator sizes, combustor emissions of  $\text{SO}_2$  and  $\text{NO}_x$ , regenerator off-gas and sorbent make-up. The design that was proposed showed that the solids waste stream is reduced by a factor of 35 in comparison to a once-through process with limestone. Further, a concentrated ( $> 6$  v%)  $\text{SO}_2$ -rich regenerator off-gas is obtained that is suitable for further treatment to elemental sulfur or sulfuric acid.

Another interesting result that was obtained, by permitting the synthetic sorbent to be sulfated for only 10-20%, is the (relative) small combustor size. In a once-through process, limestone is always maximally converted (usually 40%). Because of this, the average limestone reactivity in the combustor is small, and an increased reactor volume is therefore necessary. It was calculated that the size of the combustor in the regenerative process can be half the size of the combustor in the once-through process. This results in significant lower capital charges due to the investment costs. Although the regenerative process is still more expensive than a once-through process, the advantages of an IFB system for solids circulation are an encouragement for further development of regenerative desulfurization during Fluidized Bed Combustion of coal. Higher costs, that can be expected in the future, for disposing or processing the spent sorbent are also in favour of regenerative desulfurization.

### 1.4 Aim of the project

After the initial work on IFB systems (as described above in chapter 1.3.2), the general aim of the project is defined as: 'the development of rules for design and operation of IFB reactors'.

Following this general aim, more specific objectives are defined as:

1. Design and construction of an IFB facility for regenerative desulfurization as a Proof-Of-Concept (POC) test. Testing of the IFB concept at reaction conditions and pilot plant scale. The IFB reactor should be operated such that sulfation and regeneration are carried out continuously by means of sorbent recirculation.
2. Further development of the insight in the hydrodynamics of the IFB system. A mathematical model should be developed that predicts the Circulation Rate of Solids (CRS) and the solids distribution in the IFB system on the basis of design and operational parameters.
3. Development of the insight in IFB reactor dynamics. The dynamics of the IFB system are of influence on the overall chemical reactor performance. A mathematical model should be developed that describes the non-stationary behaviour. This should indicate how to operate the IFB reactor and should provide insight in the effect of operational parameters that can be used for process control purposes.

Another objective is:

4. The investigation of processes in which a solid material needs to be transported between fluidized bed type reactors. This investigation was started in order to verify the potential use of IFB reactor systems for other processes than regenerative desulfurization during FBC of coal.

These objectives were used as guidelines during the IFB research project that is described in this thesis. At the end of the project, it should be clear how the IFB reactor can be applied for gas/solids regenerative processes. Furthermore, it should be known what the main issues are concerning the design and operation of IFB reactors.

### 1.5 Outline of the thesis

The thesis starts with the further development of the hydrodynamic insights of the IFB reactor system. The IFB reactor system is characterised by the solids distribution and Circulation Rate of the Solids (CRS) in the IFB compartments. The parameters that determine the CRS and solids distribution are the particle properties and IFB geometry (design parameters) and gas velocities to the compartments and total IFB bed mass (operational parameters). Solids and gas transport through an orifice between two connected beds was already described by Korbee *et al.* (1994) by means of a hydrodynamic model. This model was the basis for further developments as described in this thesis. The solids and gas transport phenomena are experimentally studied in cold experimental facilities that are simplifications (twin-bed, jet, and Bernoulli facilities) of the IFB system. In chapter 2, a predictive model is developed for the description of solids and gas transport between aerated and fluidized beds including the prediction of shear friction losses in the solids flow towards the orifice.

## Chapter 1

---

In chapter 3, the hydrodynamic model for solids and gas transport through an orifice is extended with a weir flow and a solids distribution model. This results in an overall hydrodynamic IFB model that predicts the solids distribution and CRS in an IFB reactor system. The model is able to predict steady-state as well as dynamic behaviour of the IFB hydrodynamics. This indicates how to operate the IFB reactor and provides insight in the effects of operational parameters that can be used for process control purposes.

The design, construction and operation of an IFB pilot plant facility is described in chapter 4. In chapter 5, the experimental and modelling results that were obtained in this high temperature IFB pilot plant facility are presented and discussed. The experiments, including a continuous five-day test, are analyzed on hydrodynamic, sulfation and regeneration behaviour.

In chapter 6, a dynamic model for regenerative desulfurization is developed to reveal the influence of process dynamics on the chemical reactor performance of an IFB reactor system. Further, the effect of particle residence time distribution on the average conversion during steady-state as well as dynamic operation is estimated and discussed.

A suitable candidate process for accommodation in an IFB reactor is the so-called NOXSO process. This process for combined NO<sub>x</sub> and SO<sub>2</sub> removal from flue gases is studied and compared to other processes. In chapter 7, the IFB-NOXSO and the original NOXSO process are compared on the basis of exergy and costs.

Chapter 8 describes general design and operational strategies. In this chapter, different applications of IFB technology are suggested and frequently-asked-questions are presented with answers.

## References

- Anthony, E.J., "Fluidized bed combustion of alternative solid fuels; status, successes and problems of the technology", *Prog. Energy Combust. Sci.*, 21, 239-268 (1995).
- Bakker, W.J.W., Kapteijn, F., Moulijn, J.A., Korbee, R., Liang, B., Snip, O.C., Schouten, J.C., Bleek van den, C.M., "Regenerative sulphur capture in gases from coal gasifiers", Final report for the Joule-II Clean Coal Technology Contract No. JOU2/CT93/043, Delft University of Technology, The Netherlands (1996).
- Basu, P., Fraser, S.A., "Circulating fluidized bed boilers: design and operations", Butterworth-Heinemann, Chapter 1, 8-9 (1991).
- Davidson, J.F., "Fluidized combustion of solids gases and mixtures thereof", In: *Fluidization VII; Proceedings of the 7th Engineering Foundation Conference on Fluidization* (Eds: Potter, O.E. and Nicklin, D.J.), Brisbane, Australia, 15-26 (1992).
- DeMoss, T.B., "Gas, coal duke it out over repowering", *Power Engineering*, June, 21-24 (1995).
- Duisterwinkel, A.E., "Clean coal combustion with in-situ impregnated sol-gel sorbent", PhD thesis, Delft University of Technology, Delft, The Netherlands (1991).
- Ellison, W., "Limiting of SO<sub>2</sub> and NO<sub>x</sub> emissions in worldwide coal-power production", *Radiat. Phys. Chem.*, 45(6), 1003-1011 (1995).

- He, Y., Rudolph, V., "Control mechanism for gas crossflow in a compartmented dense phase CFB", In: CFB4; proceedings of the 4th International Conference on Circulating Fluidized Beds. (Ed.: Avidan, A.A.), 684-689 (1993).
- Joshi, M.M., Lee, S., "Integrated gasification combined cycle— A review of IGCC technology", Energy Sources, 18, 537-568 (1996).
- Kalwar, M.I., Raghavan, G.S.V., Mujumdar, A.S., "Circulation of particles in two-dimensional spouted beds with draft plates", Powder Technol., 77, 233-242 (1993).
- Korbee, R., "Regenerative desulfurization in an Interconnected Fluidized Bed System", PhD thesis, Delft University of Technology, Delft, The Netherlands (1995).
- Korbee, R., Grievink, J., Schouten, J.C., Bleek van den, C.M., "Preliminary design of a 100 MWe power plant with regenerative desulfurization applying Interconnected Fluidized Bed technology", In: Proceedings of the 12th International Conference on Fluidized Bed Combustion of coal, Vol. 2, (Eds: Rubow, L., Commonwealth, G.), San Diego, USA, 1143-1151 (1993).
- Korbee, R., Snip, O.C., Schouten, J.C., Bleek van den, C.M., "Rate of solids and gas transfer via an orifice between partially and completely fluidized beds", Chem. Eng. Sci., 49(24B), 5819-5832 (1994).
- Knowlton, T.M., "Solids transfer in fluidized systems", Chapter 12, in "Gas Fluidization Technology, Geldart, D. (Ed.), John Wiley & Sons, 341-414 (1986).
- Knowlton, T.M., "Standpipes and return systems", Chapter 7 in "Circulating Fluidized Beds" (Ed. Grace, J.R., *et al.*), Chapman & Hall, London, 214-259 (1997).
- Kunii, D., Levenspiel, O., "Circulation Systems", Chapter 15, in: "Fluidization Engineering", 2nd Ed., Butterworth-Heinemann, 359-395 (1991).
- LaNauze, R.D., "A circulating fluidised bed", Powder Technol. 15, 117-127 (1976).
- Milne, B.J., Berruti, F., Behie, L.A., "The Internally Circulating Fluidized Bed (ICFB): A novel solution to gas bypassing in spouted beds", Can. J. Chem. Eng., 70, 910-915 (1992).
- Nilsson, C., Clarke, L.B., "PFBC residues - characteristics, disposal and utilization", IEA Coal Reserach report, London (1994).
- NOVEM, "System study: High temperature gas cleaning for IGCC processes", The Netherlands, November (1990). (*in Dutch*)
- Olazar, M., San José, M.J., Aguayo, T., Arandes, J.M., Bilbao, J., "Design factors of conical spouted beds and jet spouted beds", Ind. Eng. Chem. Res., 32, 1245-1250 (1993).
- Richards, P.C., Wijffels, J-B., Zuideveld, P.L., "Clean and efficient power generation with the Shell coal gasification process", paper presented at the 11th Int. Conf. on Power Stations, Liège, Sept. 20-24 (1993).
- Sasol, "Annual Report 1996", Sasol Ltd., Johannesburg, Republic of South Africa (1996).
- Schobert, H.H., "Coal, the energy source of the past and future", American Chemical Society, Washington, DC (1987).
- Schouten, J.C., Bleek van den, C.M., "Sulfur retention and NOx reduction: the SURE model", in: "Atmospheric fluidized bed coal combustion - research, development and application", 22, Coal Science and Technology, (Ed: Valk, M.), Elsevier, Amsterdam, The Netherlands, 227-257 (1995).
- Shell, "Energy in profile", Shell Briefing Service (1996).
- Thambimuthu, K.V., "Gas cleaning for advanced coal-based power generation", IEA Coal Reserach report, London (1993).
- THERMIE, programme of the Commission of the European Communities Directorate-General for Energy (1990-1994) DG XVII, "Coal can be green: A review of Coal Technologies supported by the European Community" (1994).

## Chapter 1

---

- Wakker, J.P., "Development of a high temperature steam regenerative H<sub>2</sub>S removal process based on alumina supported MnO and FeO", PhD thesis, Delft University of Technology, Delft, The Netherlands (1992).
- Wakker, J.P., Gerritsen, A.W., Moulijn, J.A., "High temperature H<sub>2</sub>S and COS removal with MnO and FeO on gamma-Al<sub>2</sub>O<sub>3</sub> acceptors", *Ind. Eng. Chem. Res.*, 32, 139-149 (1993).
- Wolff, E.H.P., "Regenerative sulfur capture in fluidized bed combustion of coal: A fixed bed sorption study", PhD thesis, Delft University of Technology, Delft, The Netherlands (1991).
- Wolff, E.H.P., Gerritsen, A.W., Bleek van den, C.M., "Multiple reactor testing of a synthetic sorbent for regenerative sulfur capture in fluidized bed combustion of coal", *Can. J. Chem. Eng.*, 71, 83-93 (1993a).
- Wolff, E.H.P., Gerritsen, A.W., Verheijen, P.J.T., "Attrition of an alumina-based synthetic sorbent for regenerative sulphur capture from flue gas in a fluidised bed", *Powder Technol.*, 76, 47-55 (1993b).
- Yang, W.C., Keairns, D.L., "Design of recirculating fluidized beds for commercial applications", *AIChE Symp. Ser.* 74(176), 218-228 (1978).
- Yperen van, R., "On the high-temperature desulphurization of coal gas, the development of a regenerable absorbent", PhD thesis, State University of Utrecht, Utrecht, The Netherlands (1994).
- Zhu, J-X., Bi, H-T., "Distinctions between low density and high density circulating fluidized beds", *Can. J. Chem. Eng.*, 73, 644-649 (1995).



# Chapter 2

## Hydrodynamics of the IFB system

solids and gas transport between aerated and fluidized beds

---

### 2.1 Circulation Rate of Solids as a function of design and operational parameters

The overall performance of the IFB reactor depends on the Circulation Rate of the Solids (CRS), the amount of solids that are circulating between the reactors. By adjusting the CRS, the mean residence times in the reactors are changed. This results in a variable average conversion rate (or reactivity) of the solid material (regenerable catalyst or sorbent) by which the conversion of the reactor changes. It is therefore important to be able to predict the CRS as a function of the IFB design and operational parameters.

An IFB reactor system can be analyzed in terms of the parameters that determine the CRS and therefore the chemical performance of the reactor. It must be emphasized here that the IFB reactor consists of multiple fluidized bed reactors connected by means of (fluidized or aerated) transport compartments. These fluidized bed reactors should be designed and operated according to the requirements of the chemical process that will take place.

The consequence of this is that the IFB reactor system should be designed in such a way that transport of solids is established without influencing the chemical processes in the fluidized bed reactors except for the CRS influence.

An important aspect in properly designing and operating IFB reactors is a thorough understanding of the hydrodynamics. The term 'hydrodynamics' of the IFB system is meant to cover those transport phenomena that determine the CRS in the IFB system. In general one can divide the parameters influencing the CRS in design parameters and operational parameters.

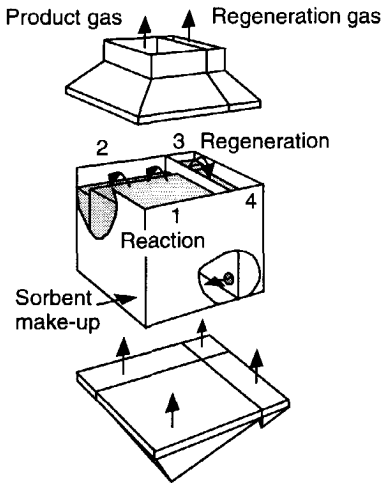
A close look at the IFB system (Figure 2.1) learns that one can further divide these parameters in four sets of parameters that determine the CRS:

#### Design parameters:

1. **IFB geometry:**  
orifice size, weir height and width, bed diameter and their relative sizes;
2. **particle properties:**  
density, size (and size distribution), sphericity and frictional properties;

#### Operational parameters:

3. **gas velocities** to the compartments, and
4. **total IFB bed mass.**

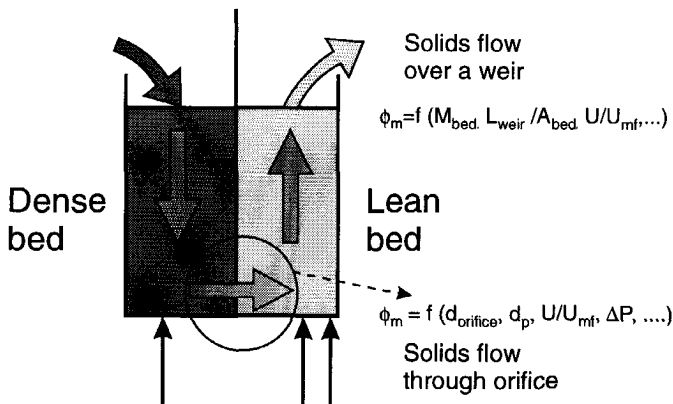


**Figure 2.1** A schematic representation of the IFB reactor system for regenerative gas-solid processes. Solids are transported between two fluidized bed reactors (1-reaction and 3-regeneration) by means of two interconnecting transport compartments (2 and 4).

of the gas velocity to a controlling transport compartment. This is, except for the desired influence of the CRS on the chemical process.

The first two sets consist of design parameters. The IFB geometry and sizes are fixed by the specific design. The particle properties are defined when the solid material is chosen according to the requirements of the process. These two sets cannot practically be altered during operation of the IFB reactor.

The second two sets are the operational parameters by which the CRS can be manipulated during operation of the process. Concerning the gas velocities it should be mentioned here that it will become clear that the CRS can be controlled by means of adjusting the gas velocity to one of the transport compartments. Thus, the chemical processes in the fluidized bed reactors are not unwantedly disturbed by adjustment of the CRS by means



**Figure 2.2** One set of Interconnected Fluidized Beds consisting of a dense (downflow) transport compartment and a lean (upflow) fluidized bed reactor compartment. Solids flow respectively over a weir and through an orifice mainly as a function of the indicated parameters.

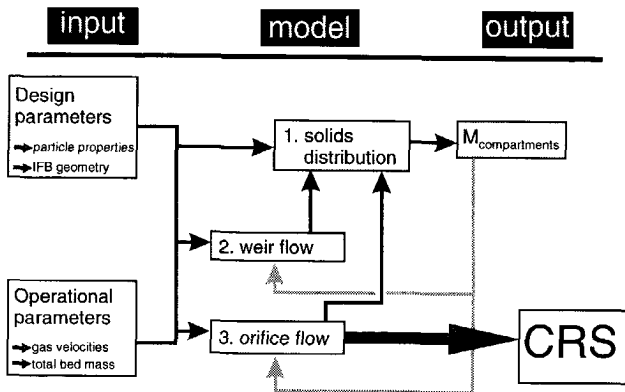
The total IFB bed mass is important for two reasons. The first reason is that by increasing it, the amount of solids in the respective fluidized bed reactors will change. This will have a direct influence on the conversion in these reactors.

Secondly, the total IFB bed mass influences the CRS in the system. This changes the mean residence times in the reactor compartments and thus the chemical reactor performance. Both influences can have opposite or mutual strengthening effects on the overall performance of the IFB system and therefore have to be known.

In Figure 2.1, a schematic view of the IFB reactor is given. This IFB reactor consists of two sets of dense (downflow of solids) and lean (upflow of solids) beds that are connected by means of an orifice. Two types of solids flow occur in the IFB reactor: in the upflow beds solids flow over a weir and in the downflow beds solids flow through an orifice. In Figure 2.2 this is shown.

In order to be able to predict the performance of an IFB reactor, both the distribution of the total IFB bed mass over the compartments ( $M_{\text{compartments}}$ ) and the CRS should be known as a function of design and operational parameters. In Figure 2.3 a scheme is presented which shows the interrelation. Models will be included for solids flow over a weir (chapter 3) and solids flow through an orifice (chapter 2). The solids distribution model (chapter 3) basically is a mass balance for the solids phase. The in- and out-terms in this model consist of weir- and orifice flow. For each compartment the terms are balanced and in an iterative way a solution can be found which yields the bed mass distribution over the IFB compartments.

The overall CRS is determined by the smallest net driving force for solids flow. Depending on the operational conditions and total bed mass in the IFB system, the CRS determining flow will be either the solids flow over a weir or the solids flow through an orifice. In chapter 3 these aspects are treated in detail. It is shown that it is advantageous to operate the IFB reactor such that solids flow through an orifice is CRS-determining. Therefore the attention in this chapter 2 is focused on solids flow through orifices.



**Figure 2.3** The solids distribution ( $M_{\text{compartments}}$ ) and Circulation Rate of Solids (CRS) are a function of design and operational parameters as indicated. Models for solids distribution and weir flow are described in chapter 3 and the orifice flow model is described in chapter 2.

## Chapter 2

This chapter starts with a literature review (2.2) on solids flow through orifices. Various authors describe experimental and modelling work on this subject. A number of driving and resisting forces are identified that were taken into account in their solids flow models. An overview is given of several experimental and modelling considerations.

Based on a momentum analysis, a predictive model for solids circulation in an IFB system is developed (2.3). The model consists of a number of driving and restricting contributions. Special attention is given to shear friction that is believed to play an important role as a resisting force in the solids circulation. Therefore the apparent viscosity of fluidized and aerated fluid particle systems is treated (2.4). An empirical predictive correlation for the viscosity as a function of particle properties and operational parameters is developed.

The shear friction in solids flow through orifices (2.5) is estimated according to a relationship that was derived from a microscopic momentum balance. The overall solids flow model is tested and validated in two experimental facilities (2.6).

Finally, discussion and conclusions are given on the possibilities and drawbacks of modelling solids circulation between aerated and fluidized beds.

### 2.2 Literature review on solids flow through orifices

A large number of publications can be found that is somehow related to solids flow through orifices. Depending on the research objectives and backgrounds of the authors attention is given to specific aspects of solids flow problems. Most authors describe experimental and modelling work.

The experimental work can be differentiated in many aspects. In Figure 2.4 an overview is given on the different approaches that can be found in literature concerning experimental studies on solids flow. This work provides insights that can be used for further analysis of solids circulation in IFB systems.

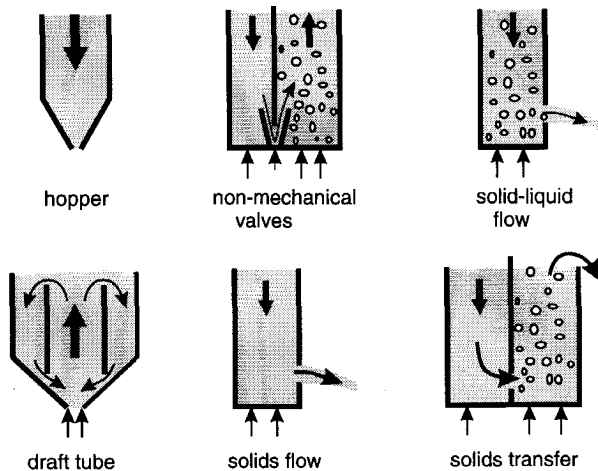


Figure 2.4 Overview of different approaches in experimental studies on solids flow.

High temperature or high pressure measurements are scarce in literature (Milne *et al.*, 1992; Reichold and Alexander, 1995; see also chapter 8 of this thesis). Furthermore, the experimental and operating conditions concerning solids flow are not properly defined. Therefore the results that are covered here concern measurements that were carried out at ambient conditions.

Experimental studies and modelling efforts are discussed on the basis of Figure 2.4. Only those aspects that give more insight in modelling solids flow through an orifice in IFB reactor systems are outlined.

### 1. Hoppers

An important distinction is the difference between aerated and non-aerated solids flow. The latter is mostly related to flow or discharge from hoppers and silo's. Therefore the flow direction will be mainly vertical and gravity is the main driving force.

Some early workers in the field (Franklin and Johanson, 1955; Brown and Richards, 1960; Beverloo *et al.*, 1961) studied the flow through a restricting orifice that was mounted in the bottom of the hopper.

In studies of de Jong (1969 and 1975) and de Jong and Hoelen (1975) solids flow from a bunker was studied under influence of aeration. Special attention was given to the particle size relative to the orifice size. Yamashiro (1985) and Marring (1989) also studied solids flow and the influence of particle size.

All authors suggest to use an orifice size correction in the modelling of solids flow. This is explained from the fact that not the entire orifice area is used. A stagnant zone adjacent to the wall is present in an orifice that effectively decreases the diameter of the orifice. They verified this idea with experiments using various solids and orifice sizes. The effective orifice size is calculated according to:

$$A_{eff} = \frac{1}{4}\pi(d_{orifice} - kd_p)^2 \quad (2.1)$$

in which  $k$  is an empirical constant that needs to be determined experimentally and depends on specific particle properties.

The influence of the interstitial gas and pressure field was studied by Molodtsov *et al.* (1992). They concluded that both interstitial gas and the assumption that the normal component of intergranular stresses is zero in the direction of particle flow are important. The latter is contrary to Janssen's equation which is commonly used; see Roberts (1995) for an overview of the use of this equation. The model of Molodtsov *et al.* (1992) showed to be able to predict the solids flow rate that was experimentally determined properly.

The effect of shear friction and the influence of the flow profile were experimentally studied by Zhang and Rudolph (1991). They assumed an accelerating and symmetric flow field towards the orifice. Shear stress only occurs at the edges between the flowing and non-flowing particles. It is shown that shear friction is an important factor which has to be taken into account.

The effect of fines and particle size distribution were studied by Arteaga and Tüzün (1990). Experimental results are presented and show a significant influence of particle size distribution and flow conditions on the microstructural properties (*viz.* porosity) of the bed. This is supported by theoretical analyses that extend the theory of Beverloo *et al.* (1960). Nedderman *et al.* (1982) provide a review on modelling solids flow from hoppers and silo's.

A critical remark is made with respect to continuum mechanics that, according to the authors, are not able to predict particle size effects fundamentally.

An extension of the Beverloo-correction is presented by Nedderman *et al.* (1982) that is able to predict the experimental observations. Reference is made to the so-called Hour Glass theory that is widely applied in non-aerated solids flow modelling (see Le Pennec *et al.*, 1995; Verghese and Nedderman, 1995). The Hour Glass theory relates particle properties to flow properties.

However, improvements can still be made since many of the so-called particle properties still have to be measured directly or indirectly. Furthermore no velocity profiles in the outlet of the hopper are predicted. This is provided by two fundamentally different modelling approaches. These are a *finite element* (continuum mechanics) analysis by Watson and Rotter (1996) and a *distinct element* simulation by Langston *et al.* (1996). The prediction of velocity profiles gives more insight in the solids flow phenomena.

An advantage of the distinct element simulation is, according to the authors, the prediction of flow instabilities and oscillatory features. Further, this simulation method links elementary particle properties directly to flow phenomena.

### 2. Non-mechanical valves

In solids circulation systems consisting of a riser reactor and a fluidized bed regenerator it is common practice to control the circulation rate of the solids by means of a standpipe and a specific type of non-mechanical valve.

The most primary type of non-mechanical valve is sometimes referred to as an O-valve. It is described by Masson (1989) and it comes down to an orifice in a separating wall between a downcomer or standpipe and a fluidized bed reactor. This is equivalent to what is encountered in an IFB reactor. Masson (1989) developed an empirical correlation based on the ratio of the size of the connecting opening and the diameter of the particles. A general pressure balance was used to describe the solids flow in terms of a density difference between the beds.

Alternatively, a standpipe joined to an L-valve is widely used. Yang and Knowlton (1993) and Picciotti (1995) give an overview of modelling and practical issues in using L-valves. Further considerations are given by Geldart and Jones (1991) and Rhodes and Cheng (1993). Standpipe modelling with reference to particle-wall frictional effects and stress distribution can be used for further modelling of solids flow in IFB reactors. See chapter 2.3, in which the particle-wall friction factor  $f$  and stress ratio  $K$  are related to a driving force for solids flow (the particle stress ( $\sigma_N$ ) directed to the wall). It is also appreciated that particle size effects are treated in a similar way as described in part 1 of this literature review.

In general, the combination of a high solids throughput with a limited gas-by-pass is highly attractive from an operational perspective. One possible configuration is a so-called V-valve described by He *et al.* (1993) and He and Rudolph (1996). The authors investigated the gas-cross-flow phenomenon and concluded that the particles are dragged by the flowing gas. A semi-empirical relationship was developed to describe their experiments. Li and Kwauk (1991) developed a more fundamental description of the flow phenomena in a V-valve, based on a pressure balance. The results of V-valve experiments show that stable operation can be obtained together with reduced gas-bypassing.

Stanley *et al.* (1984) also presented a type of valve consisting of restricting plates and a

narrow slot through which the solids are directed. Their modelling work consisted of a momentum analysis that was applied to the system. They assumed that interparticle and friction forces are not present. Especially this assumption limits the range in which their correlations can be used.

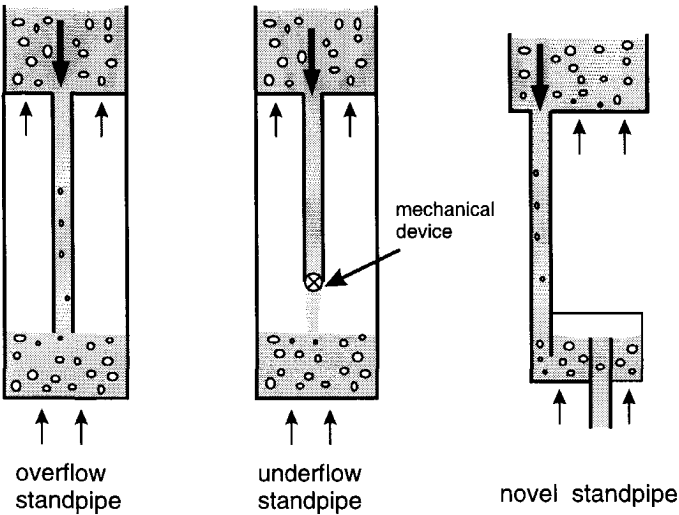


Figure 2.5 Overflow, underflow and novel standpipe.

Work on a so-called novel standpipe is described by Yang and Gautam (1992 and 1994). This novel standpipe offers advantages of an overflow and underflow standpipe (see Figure 2.5). The mechanical valve that is necessary in an underflow standpipe can be left out of the configuration. Excellent operating and gas by-passing characteristics are attributed to this type of solids transfer apparatus.

To quantify the gas by-passing advantages of the new developments in valves and standpipes van Oosterbaan (1995) performed some engineering calculations on gas transfer associated with solids transport in a V-valve. The calculations were based on the design equations presented by He *et al.* (1993). It appears that there is no significant improvement in the reduction of gas transfer relative to solids flow compared to an orifice and a transport bed.

### 3. Solid-liquid flow

In a study on liquid-particle jets from fluidized beds, Tan and Davidson (1989) investigated this particular type of solids flow. A theoretical model was developed that was able to describe the experimental results for differently shaped nozzles. The experiments were performed for pressures up to 20 bar. The solids flow rate appeared to obey Bernoulli's equation. The liquid flow rate could be well correlated by Bernoulli's equation if the liquid-solid drag was accounted for via the Richardson-Zaki equation for concentrated suspensions. The jet characteristics strongly resemble the solids gas jets. More studies on liquid jets and flow from orifices are described in chapter 2.5 of this thesis.

### 4. Draft tube

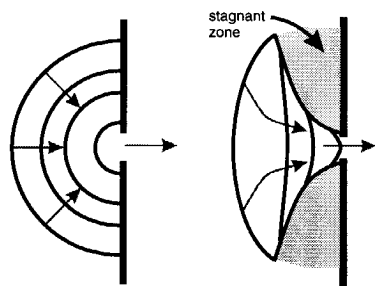
Draft tubes are widely used in reactors in which solids circulation is important. By setting a higher gas velocity in the centre part of the reactor (draft tube) a solids circulation pattern is established. This reactor type is common practice in large-particle systems because for these particles homogeneous fluidization cannot easily be obtained. The spouted beds, as they are referred to, can be equipped with or without a draft plate (Kalwar *et al.*, 1993; Olazar *et al.*, 1993).

Also in gas-liquid systems, the draft tube reactor is popular and mostly referred to as airlift reactor. An overview of the use of airlift reactors is given by Chisti and Moo-Young (1993). Yang and Keairns (1974 and 1978) describe a recirculating fluidized bed reactor that utilizes a draft tube. A mathematical model was developed based on pressure balances that describe the experimental results. They experienced a circulation-rate-determining phenomenon in the draft tube and explained this as choking which is well known in riser reactor technology. For a proper control of the solids flow, the draft tube should be operated such that the solids pick-up rate does not become limiting for solids flow.

A circulating fluidized bed making use of a draft tube was presented by La Nauze (1976). Based on a pressure balance, a model was developed to describe the experimental results. The particle-wall shear stress was included in the model. In further work, Bolton and Davidson (1987) developed a new model for solids circulation starting at the Beverloo equation (Beverloo *et al.*, 1961). An extra term was included to account for the wall shear stress while internal stresses were neglected. The gas pressure drop was included in the Hour Glass theory (Davidson and Nedderman, 1973) as a modified gravity term calculated by the Ergun (1952) equation. The model showed satisfactory agreement over a wide range of bed size and particle properties.

### 5. Solids flow from aerated and fluidized beds

Two pioneering articles on solids flow from aerated and fluidized beds were published by Massimilla *et al.* (1961) and Jones and Davidson (1965). These form the basis of the other work on this subject up to now. Massimilla (1971) gave an overview on solids discharge studies.



**Figure 2.6** Hemispherical flow profile (left) versus an experimentally determined (right) solids flow profile as reported by Massimilla (1971). The direction of solids flow is from left to right through the orifice.

Both Massimilla *et al.* (1961) and Jones and Davison (1965) assume the flow of solids to converge symmetrically towards the orifice. The interstitial gas was accounted for in both models. The total gas pressure drop is supposed to be caused by accelerating solids and gas and percolating gas through the solids. The voidage is assumed to be constant. Massimilla *et al.* (1961) determined a gas-solid drag coefficient experimentally. Massimilla (1971) further investigated the influence of particle diameter to orifice size and found that the orifice discharge coefficient approximates a constant value



of 0.5 for small  $d_p/d_{orifice}$ -ratio. However, velocity distributions determined experimentally in a 2-dimensional column do not support the hemispherical approach in the solids flow model (see Figure 2.6). Massimilla (1971) suggests that interparticle forces play an important role in the orifice flow phenomena. In most studies however these forces are neglected.

Jones and Davidson (1965) studied the influence of shaped (or tapered) nozzles on solids flow. They found significantly higher solids discharge coefficients for shaped orifices by measuring the solids flow rate and particle exit velocities.

Burkett *et al.* (1971) extended the theory of solids flow from fluidized beds to a model in which the voidage in the orifice region was not considered to be constant. The one-dimensional form of the momentum equations and the neglect of interparticle forces are considered to be the major drawbacks of their model.

Geldart and Haesebrouck (1983) studied the discharge of solids from fluidized beds. The experimental results have been correlated by a Bernoulli type correlation which included particle size effects. Also particle exit velocities and corresponding exit voidages were measured. It was found that the exit voidages were considerable higher than that at incipient fluidization. Jones and Davidson (1965) reported equivalent results.

Martin and Davidson (1983) found marked differences between ideal (*viz.*, frictionless) behaviour and their experiments. These differences are believed to be due to the high apparent viscosity of the fluidized bed.

In an extensive research program Sarkar *et al.* (1991a, b and c) studied the solids discharge from aerated and fluidized beds through inclined pipes. Mass flow was correlated including factors accounting for orifice size (correction as Beverloo *et al.* 1961), angle of inclination, feeding area and length of the pipe. In the aerated situation, mass flow is correlated as a combination of packed bed flow and fluidized bed flow according to:

$$\phi_{m,aerated} = \phi_{m,packed} (1-\delta) + \phi_{m,fluidized} (\delta) \quad (2.2)$$

$$\text{with: } \delta = (U/U_{mf})^{\frac{1}{3}}$$

Davies and Harris (1992) and Davies and Foye (1994) developed a device for measuring solids flowrates. This so-called Slot Flow Meter makes use of the relationship between solids flow rate through a vertical slot and height of the solids in the slot. The apparatus can be calibrated for a specific type of solid material and is then able to measure a solids flow rate accurately. Particle size effects were investigated by Davies and Fenton (1995, 1996) and were exploited in the development of an apparatus for continuously measuring particle size.

## 6. Solids flow between aerated and fluidized beds

At Delft University of Technology (DUT) an extensive research program resulted in various publications on solids flow between aerated and fluidized beds. See also chapter 1.2 for an overview of IFB history at DUT. Korbee (1995) and Korbee *et al.* (1991, 1994 and 1995) did both experimental and modelling work. A hydrodynamic model was developed that takes the particle pressure (*i.e.*, solids weight) into account in combination (or opposition) with the gas pressure drop as a driving force for solids flow. Further work on solids flow phenomena from and between aerated and fluidized beds was described by Snip *et al.* (1996). For a discussion see chapters 2.3 and 2.5.

## Chapter 2

Chen *et al.* (1979) used a macroscopic momentum balance to model the solids flow in an inclined pipe that connects two fluidized beds. In analogy to fluid flow, a friction factor was included that appeared to depend on the solids flow rate and pipe diameter.

Chin *et al.* (1980) studied dense phase powder feeding from an annular fluidized bed. Their experiments concerned various shapes for the opening. The solids flow equations proposed by Jones and Davidson (1965) appear to be able to describe the solids flow satisfactorily. However, the correlations of Jones and Davidson (1965) and Massimilla *et al.* (1961) for gas flow underestimate the amount of gas significantly. It is not clear if this is caused by the differences in the experimental set-ups or whether the particles do strongly differ from those used by the other authors.

Important studies on the solids flow between fluidized beds are presented by Kuramoto *et al.* (1985 and 1986). Their solids flow model is based on earlier work of Judd and Dixon (1978) in which the solids flow is given by:

$$\phi_m = C_D \epsilon_u^{2.35} A_o \sqrt{\frac{2\Delta P \rho_d}{1 - \left(\frac{A_o}{A_d}\right)^2}} \quad (2.3)$$

It was not explained what the term  $A_o/A_d$  (*viz.*, ratio of the cross-sectional area of the orifice to the dense bed area) represents. This extra friction term was introduced by Judd and Dixon (1978) without explanation. O'Dea *et al.* (1990) also took this term from Judd and Dixon (1978) and called it 'non-trivial momentum'. It is concluded from Bird *et al.* (1960) that this term originates from the difference between  $\langle v \rangle^2$  and  $\langle v^3 \rangle / \langle v \rangle$  (in which  $\langle v \rangle$  is the average velocity and  $\langle v^3 \rangle$  is the average value of the velocity to the third). The term  $(A_o/A_d)$  can be directly obtained from the application of Bernoulli's equation on the flow problem. In the form of Equation (2.3) it can only be used when a flat velocity profile is present in the vertical downflow of solids in the dense bed and in the solids flow after the orifice. Since this is doubtful in a solids circulation system the use of this extra term in the solids flow equation is not considered useful in this thesis.

An extra term is included by Judd and Dixon (1978) in the solids flow model (Equation 2.3) to account for the lean bed resistance (*viz.*,  $\epsilon^{2.35}$ ). In the derivation of the model it is assumed that all gas pressure drop is exerted as drag on the discharged particles. To determine the drag force on a particle in a fluid-multiparticle interaction system, a voidage function (*viz.*,  $g(\epsilon) = \epsilon^\beta$ ) was used. This function represents the ratio of the drag force on a particle in a fluid-particle system at given voidage ( $\epsilon$ ) and the drag force on an unhindered particle. For an overview on this subject, see di Felice (1994). Kuramoto *et al.* (1986) did not take into account that the exponent  $\beta$  in the voidage function can be a function of the particle Reynolds number. This limits the range over which the lean bed influence can be predicted.

Fox *et al.* (1989) performed a momentum analysis and measured horizontal and vertical friction forces and correlated this with operating conditions. They showed that it is advantageous from an operating point of view to control the solids flow rate by adjusting the vertical friction force by manipulating the gas supply to the dense bed.

## General considerations

Experimental and modelling insights from the literature as reviewed above can be used in the modelling and understanding of IFB hydrodynamics. In chapter 2.3 the driving and resisting forces that are considered to be important are discussed and the consequences for modelling the orifice flow are revealed.

Some properly defined experimental results obtained from literature are tabulated in a form that facilitates further analysis and use. It is especially interesting to relate this specific data from literature to the work on hydrodynamics at DUT. This will be further discussed in chapters 2.5 and 2.6. A selection of experimental results is summarized in Table 2.1 and grouped by author. The particle size is reported as an average value as given by the authors. The gas velocity mentioned is the dense bed gas velocity because in most cases this is determining the solids flow rate. The orifice is characterized by type, specific size and main direction of solids flow.

Estimations are determined for the minimum fluidization velocity ( $U_{mf}$ ) and the minimum fluidized bed porosity ( $\epsilon_{mf}$ ) when these are not given by the authors. The value for  $U_{mf}$  is calculated according to Wen and Yu (1966) and  $\epsilon_{mf}$  is estimated according to Kunii and Levenspiel (1991); the estimated values are given in Table 2.1 in *italic*. Values for the discharge coefficient ( $C_D$ ) are given despite the fact that these are difficult to interpret, because in general these values were obtained by the authors through fitting of their specific solids flow model to the experiments. For a more detailed analysis of the discharge coefficients mentioned in literature see Korbee (1995).

## 2.3 Modelling orifice flow in IFB systems

### 2.3.1 General

In an orifice flow model the solids flow needs to be predicted as a function of design and operational parameters (see Figure 2.3). A motivation to develop a fully predictive model can be found in the fact that many aspects are still not completely understood and therefore implemented in models as empirical constants that need to be determined experimentally.

From a better understanding of driving and resisting forces, a model can be developed that provides more insight in solids flow phenomena as a function of design and operational parameters. The idea is that this can reduce the amount of experimental work and increase the range in which the model can be used.

In earlier work at DUT described by Korbee *et al.* (1994, 1995), a model was formulated that included the most important contributions that determine solids flow through an orifice. This model provides the basis for the work described in this chapter.

In modelling stationary orifice flow, it is common practice to apply a macroscopic Bernoulli equation (Bird *et al.*, 1960):

$$\frac{1}{2}\rho \frac{\langle v_1^3 \rangle}{\langle v_1 \rangle} - \frac{1}{2}\rho \frac{\langle v_0^3 \rangle}{\langle v_0 \rangle} + (P_1 - P_0) = 0 \quad (2.4)$$

in which: (1) and (0) correspond to the positions far from the orifice and in the centre of the orifice respectively. It is further assumed that friction and contraction do not play a role and

**Table 2.1** Overview of experimental conditions and results from literature; estimated values for  $U_{mf}$  and  $\epsilon_{mf}$  are given in *italics*. The particle size is given as an average value of the particle diameter as given by the authors. The orifice is characterized by type, specific size and main direction of solids flow. The gas velocity is given as the superficial dense bed gas velocity.

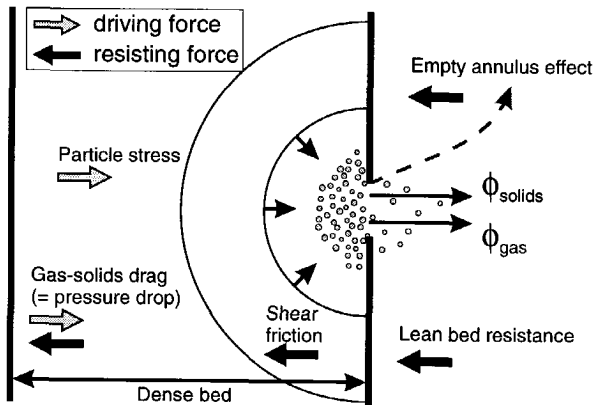
Reference	Particle type, density and diameter [kg/m <sup>3</sup> ] and [mm]	$U_{mf}$ and $\epsilon_{mf}$ [m/s] and [-]	Orifice type and size [mm or mm <sup>2</sup> ]	Gas velocity [m/s]	Solids flow [kg/s]	$C_b$ [-]
Fox <i>et al.</i> (1989)	sand 2600, 0.21	0.043 0.435	slot, horizontal 5-150x300 (heightxwidth)	0.03-0.09	0 - 2	-
Korbee <i>et al.</i> (1991)	sand, 2600, 0.8 silica, 740, 1.7 glass beads, 2880, 0.46	0.48, 0.45 0.41, 0.45 0.24, 0.41	circular, horizontal 15-40	1.14-1.84 1.25-1.88 1.53-2.19	0.055-0.544 0.007-0.170 0.026-0.505	0.5
de Jong (1969, 1975)	sand, 2590, 0.205 glass, 2950, 0.1 glass ballotini, 2950, 0.2	0.05-0.45 0.02-0.62 0.06-0.57	circular, vertical 5-17.9	aerated	0.12-0.6	0.50-0.64
Kuramoto <i>et al.</i> (1985, 1986)	alumina, 1570, 0.162	0.014, 0.52	circular, horizontal 62-140	0.017 - 0.11 1.2 - 8 $U_{mf}$	0.2-1.2	0.5-0.7
Geldart and Haesebrouck (1983)	'plastic', 1080, 0.212 polyethylene, 942, 0.82 alumina, 1900, 0.075	0.02-0.44 0.35-0.53 0.005-0.46	circular, horizontal 15-50	0.1 - 1.2 $U_{mf}$	0.1-1.3	0.4-0.6
Martin and Davidson (1983)	aluminium trihydrate 2420, 0.075	0.0069, 0.43 tube, 3.1	circular, 2.7-8 shaped, 3.1 (all horizontal)	1.5 - 2.5 $U_{mf}$ 0.005-0.035	0.01-0.03 0.70 0.01-0.06	0.58 0.56
Bolton and Davidson (1987)	sand 2630, 0.168	0.03, 0.47	draft tube: orifice area=0.0168 - 0.0304 m <sup>2</sup>	0.1-0.5	50-350	-

that the fluid density is constant. The fluid velocity far from the orifice ( $\langle v_i \rangle$ ) is considered to be negligible. This results in the following equation for the average fluid velocity ( $\langle v_0 \rangle$ ) and mass flow ( $\phi_m$ ):

$$\langle v_0 \rangle = \sqrt{\frac{2(P_1 - P_0)}{\rho}} \Rightarrow \phi_m = C_D A_o \sqrt{2\rho \Delta P} \quad (2.5)$$

All non-idealities are accounted for by the fluid discharge coefficient ( $C_D$ ). Some measured values for  $C_D$  that were found in literature are given in Table 2.1. It is the objective of this study to obtain insight in the non-idealities and relate them to particle and orifice properties and operational parameters. Some limitations on the use of macroscopic balances in orifice flow problems are given by Snip *et al.* (1997). For practical purposes however the macroscopic Bernoulli equation does provide a clear and straightforward basis for further modelling.

### 2.3.2 Driving and resisting forces



**Figure 2.7** Driving and resisting forces in solids ( $\phi_{solids}$ ) and gas ( $\phi_{gas}$ ) flow through an orifice from dense to lean bed.

In Figure 2.7 the solids flow through an orifice is schematically shown. It is stated that there are five main contributing forces that determine the solids flow rate from a dense transport bed to a lean upflowing bed. In Figure 2.7 these driving and resisting forces are shown. The arrows indicate the direction of the specific contributions. Only the gas-solids drag force can be acting in both directions. All five contributions can be implemented in the Bernoulli equation (Equation 2.4), resulting in:

$$\frac{1}{2} \rho_{bed} \langle v_0 \rangle^2 = \Delta P + \Delta \sigma_N - \Delta P_f \quad (2.6)$$

## Chapter 2

in which:

$\rho_{bed}$	= average bulk density of dense bed	[kg/m <sup>3</sup> <sub>bed</sub> ]
$\langle v_0 \rangle$	= average fluid velocity in the orifice	[m/s]
$\Delta P$	= pressure drop across the orifice	[Pa]
$\Delta\sigma_N$	= difference in particle pressure between dense and lean bed according to Equation 2.10 ( $\Delta\sigma_N = \sigma_N - P_p$ )	[Pa]
$\Delta P_f$	= shear frictional pressure drop	[Pa]

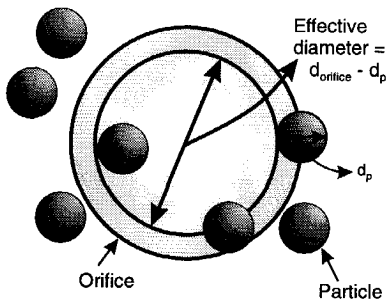
Rewriting the above equation and applying the effective orifice area ( $A_{eff}$ ) according to the empty annulus effect (see below) results in:

$$\phi_m = A_{eff} \rho_{bed} \sqrt{\frac{2(\Delta P + \Delta\sigma_N - \Delta P_f)}{\rho_{bed}}} \quad (2.7)$$

In the following paragraphs it will be explained that the specific forces mentioned are characteristic for solids flow phenomena in an IFB system. It is therefore believed that all non-idealities are accounted for. Further it will be shown how the specific contributions can be determined from particle and orifice properties and operational parameters.

### 1. Empty annulus effect: $A_{eff}$

The empty annulus effect is a phenomenon that has been observed experimentally. Actually it is not a 'real' resisting force but its effect can be considered as such. A region adjacent to the edge of the orifice is not used for solids flow. In Figure 2.8 this is schematically shown. In studies on discharge from hoppers an effective orifice area is calculated by means of Equation 2.1. A similar approach is used in studies on solids flow from and between aerated and fluidized beds (see chapter 2.2).



**Figure 2.8** Due to the empty annulus effect a region adjacent to the edge of the orifice is not used for solids flow resulting in an effective orifice diameter and area.

It was found that this type of orifice size correction does not offer a satisfactory way of accounting for the particle-orifice ratio since the empirical constant  $k$  varies considerable for different types of particles. In this empirical approach it is difficult to decide whether the decreased effective orifice area is a real empty annulus effect or caused by other flow phenomena.

Therefore a more systematic approach is needed (Zhang and Rudolph, 1991) and is obtained when the orifice area is observed in detail. It can be reasoned that a particle can flow through the orifice when its centre of gravity is within the opening. When this criterion is applied, the effective orifice diameter is reduced with one particle diameter ( $d_{effective} = d_{orifice} - d_p$ ). The effective orifice area is then easily calculated from Equation 2.1 by setting  $k$  to 1. In chapter 2.6 this approach is experimentally verified.

## 2. Gas-solids drag: $\Delta P$

In Figure 2.7 it is shown that the gas-solids drag can be acting in the direction of solids flow and opposite to the direction of solids flow. It can be either a driving or a resisting force depending on the pressures on both sides of the orifice. These gas pressures depend on the fluidizing conditions (*i.e.*, gas velocity) and the corresponding bed heights.

The importance of gas-solids drag in solids discharge of aerated and fluidized beds has been recognized since the first models were developed (Massimilla *et al.*, 1961; Jones and Davidson, 1965). Gas and solids are treated separately and their interaction is accounted for in gas-solids drag relationships. Mostly this is in the form of an Ergun (1952) equation. This equation was originally developed for predicting the pressure drop of a gas or liquid passing a stationary packed bed of solid material. A number of studies can be found in literature in which the use of the Ergun equation is extended to gas flow through moving particles (*e.g.*, Yoon and Kunii, 1970; Kim and Saeder, 1983; Rudolph *et al.*, 1990). This makes it possible to calculate gas-solids drag in solids flow through orifices.

When the particles are not in 'moving-bed-conditions' and when the voidage is higher than that at incipient fluidization, another approach would be more realistic. For such a case, Tan and Davidson (1989) and Kuramoto *et al.* (1985, 1986) show how the Richardson and Zaki (1954) relation can be used to relate gas-solids drag in a flowing gas-solids suspension.

However, the most relevant orifice flow phenomena at practical conditions in the IFB reactor are related to moving bed solids flow. It was therefore decided in this study to use the Ergun equation for further modelling work.

An important aspect in modelling gas-solids drag in orifice flow is the flow profile of both phases. In most studies, a hemispherical flow profile for both phases is assumed. The presence of such a profile can be doubted for the solids phase (see Figure 2.6). In chapter 2.5 possibilities are given to include this in the solids flow model. The gas phase flow profile is also not very likely to be hemispherical.

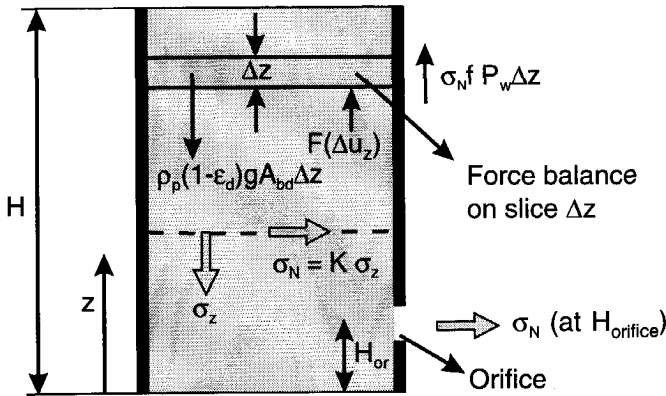
However, in this study, a hemispherical flow profile is nevertheless assumed for both the gas phase and solids phase as explained in chapter 2.5. The gas flow profile is experimentally verified in chapter 2.6.

## 3. Particle stress: $\sigma_N$

In addition to the gas pressure difference between dense bed and lean bed, the particle stress can also be a significant contribution to the driving force for solids flow (see Figure 2.7). Various authors report that the frictional forces and particle stresses in the dense bed should not be neglected, see Korbee (1995) and Korbee *et al.* (1994 and 1995).

A very clear motivation to include the particle stress in a predictive model is given by Korbee (1995): Particle flow in the opposite direction of the gas pressure gradient was experimentally observed. This phenomenon can only be explained if the particle stress is considered to be a driving force for solids flow.

The particle stress in a bed of particles relates to particle-wall friction that therefore needs to be considered (see Figure 2.9 for a schematic view of the forces acting in a packed aerated bed). In standpipe modelling the wall friction is mostly taken into account. See Picciotti (1995) for a review on standpipe modelling. Further studies that include wall shear friction in their models are from Yang and Kearns (1974), La Nauze and Davidson (1975), Bolton and Davidson (1987) and Zhang and Rudolph (1991).



**Figure 2.9** Forces acting in a packed aerated bed: gas-solids interaction force  $F(\Delta u_z)$ , gravity force  $(\rho_p(1-\epsilon_d)gA_{bed}\Delta z)$ , vertical particle pressure  $(\sigma_z)$  and particle wall frictional force  $(\sigma_N f P_w \Delta z)$ .

Ishida and Shirai (1975) developed a solids flow model based on a pressure balance for gas and particles. This resulted in a model that included normal stress as a driving force for solids flow. The derivation of the model and the influence of particle stress on the results is not explained in detail.

Due to the drawbacks of the models available, Korbee *et al.* (1994) developed a model that included particle wall friction in the dense bed and particle stress as a driving force. This model was described in detail by Korbee (1995) and will only be briefly explained here. The basis for the introduction of the particle stress in the calculations is provided by a particle pressure balance. See for an overview and considerations on stress distributions in granular materials the textbooks of Woodcock and Mason (1987), Shamlou (1988) and Nedderman (1992).

The general result of the particle pressure balance in a dense bed including a gravity term  $(\rho_p(1-\epsilon_d)gA_{bed}\Delta z)$  and a particle-wall friction term  $(\sigma_N f P_w \Delta z)$  (see Figure 2.9) is referred to as Janssen's equation (Roberts, 1995). It describes the vertical stress  $(\sigma_z)$  distribution in a packed bed of height  $H$ . Brandt and Johnson (1963) showed that Janssen's equation can also be applied for moving beds. For further solids flow modelling in IFB systems, the use of Janssen's equation needs to be extended from non-aerated to aerated beds. This was done (Korbee *et al.*, 1994) by introducing an extra term in the particle pressure balance taking into account the gas solids drag force  $(F(\Delta u_z))$ :

$$\sigma_z = \frac{A_{bed}}{fK P_w} (\rho_p(1-\epsilon_{bed})g - F(\Delta u_z)) \left( 1 - \exp\left(-\frac{z - H_{bed}}{A_{bed}} fK P_w\right) \right) \quad (2.8)$$

To calculate the force of interaction ( $F$ ) between solids and gas as a function of the slip velocity between both phases  $(\Delta u_z)$ , the Ergun (1952) equation is used. Further, the parameters related to the stress distribution ( $K$ ) and solid wall friction ( $f$ ) have to be determined as a function of the aeration rate.



Some empirical and theoretical relationships are available in literature that correlate the stress ratio ( $K = \sigma_N / \sigma_z$ ) to the angle of internal friction for non-aerated as well as aerated fluid particle systems. Nedderman (1992) showed that for cohesionless materials the angle of repose equals the angle of internal friction. This enables indirect experimental determination of the stress ratio in aerated beds of particles. See for example Judd and Dixon (1979) and Kono *et al.* (1994). It can be reasoned that the stress ratio changes from the value for a packed non-aerated bed (usually between 0.4 and 0.6, see Atewologun and Riskowski, 1991) to 1 for minimum fluidization conditions. In the model described by Korbee *et al.* (1994, 1995), the stress ratio decreases with increasing aeration rate. The resulting normal stress however that is predicted by the model is in accordance with the measured values for normal stress in aerated beds (Campbell and Wang, 1991; Chen *et al.*, 1995). The results obtained by the model can therefore be used for further analysis.

The friction factor  $f$  relates the upward frictional force to the horizontally directed normal stress  $\sigma_N$ . This factor is difficult to predict because it depends on particle properties as well as wall properties. It is therefore necessary to perform experimental work to find the appropriate solids wall friction force. The frictional upward force is depending on the extent of aeration through the normal stress ( $\sigma_N$ ); the friction factor itself is not considered to be a function of the aeration rate.

When  $K$  and  $f$  for a given fluid particle system and the gas-solids drag are known as a function of aeration rate, Equation 2.8 can be used to calculate the normal stress ( $\sigma_N = K\sigma_z$ ) at orifice height as a driving force for solids flow. In chapter 2.6 experimental work is related to the particle pressure.

#### 4. Lean bed resistance: $P_p$

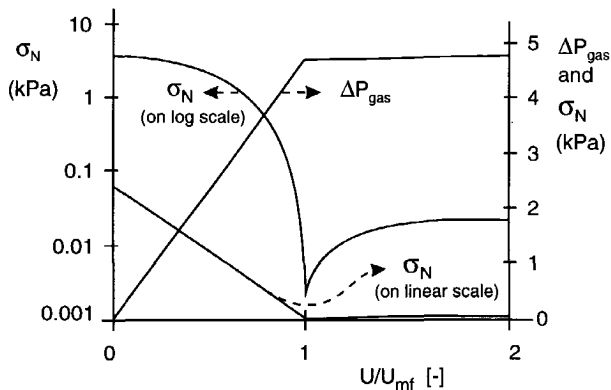
When solids are discharged into a fluidized bed instead of an empty vessel, this will give rise to an extra resistance caused by the presence of the particles. In the IFB reactor system, solids are transported between aerated and fluidized beds and it is therefore important to take this effect into account.

The only study that was found in literature in which a serious attempt was made to correlate the resistance of the lean bed to the solids flow was performed by Kuramoto *et al.* (1986). They derived a theoretical relationship for the resisting force as a function of the lean bed porosity. Due to the assumptions they made in deriving the model (see chapter 2.2), its applicability is limited. They also showed that the bubble frequency of the lean bed has no influence on the lean bed resistance.

In order to develop a lean bed resistance model that can be applied more general, the concept of particle pressure is used. This resembles to the previous section on particle stresses in aerated fluid particle systems. The lean bed is different compared to the dense bed with respect to its aeration rate. It is fluidized above the minimum fluidization velocity whereas in the aerated beds the superficial gas velocity is below  $U_{mf}$ .

Some studies report on the measurement of particle pressures in gas-solids suspensions. Chen and Weinstein (1994) measured particle stresses by means of bed collapse experiments. Campbell and Wang (1991) and Chen *et al.* (1994) used differential pressure transducers that measure only the stress transmitted by the particles. See Clift and Rafailidis (1993) for an overview of measuring and modelling particle stresses in fluidized beds.

Campbell and Wang (1991) systematically studied particle pressures in gas-fluidized beds. The general trend they found (see Figure 2.10) was that the particle pressure decreases with increasing gas velocity as progressively more of the bed is supported by fluid forces. The decrease is approximately proportional to the aeration rate. It reaches a minimum at minimum fluidization velocity and starts to rise again when the bed is fluidized, reflecting the agitation of the bed by bubbles.



**Figure 2.10** Particle pressure and gas pressure drop in a bed of solids as a function of the aeration rate (measured by Campbell and Wang, 1991).

With respect to lean bed resistance, the particle pressures measured above the minimum fluidization velocity are interesting. Campbell and Wang (1991) found that in this fluidized region, the particle pressure ( $P_p$ ) is proportional with the particle density ( $\rho_p$ ) and bubble size ( $D_e$ ):

$$\frac{P_p}{\rho_p g D_e} = \text{constant} \approx 0.08 \tag{2.9}$$

The correlation of Mori and Wen (1975) was used by Campbell and Wang (1991) to calculate  $D_e$  until the bubble diameter equalled the effective diameter of the fluidized bed after which it was assumed constant and equal to the average equivalent bed diameter. All of their data could be described by the empirical correlation of Equation 2.9.

See chapter 2.6 and Snip *et al.* (1996) for the experimental validation of using Equation 2.9 in predicting the lean bed resistance.

### 5. Shear friction: $\Delta P_f$

In the literature review on orifice flow phenomena (chapter 2.2), it was mentioned that various authors concluded that interparticle forces should not be neglected. The interparticle forces give rise to shear friction in the flow towards the orifice. Due to the complex nature of solids flow phenomena, shear friction was not included in any orifice flow model encountered in literature.

It is believed that phenomena such as the influence of the shape of the orifice on solids discharge can be better understood from a shear frictional point of view. It is therefore needed to derive a relationship for the shear frictional pressure drop ( $\Delta P_f$ ) that is included in Equation 2.7.

In chapter 2.5, a macroscopic relationship is derived that can be used to calculate the orifice shear friction. This relationship requires an input of the fluid viscosity. Due to the complex rheology of aerated and fluidized beds, it is necessary to find out if and how the viscosity of such a fluid-particle system can be determined. In chapter 2.4 an empirical relationship is developed that relates the apparent viscosity of an aerated or fluidized bed to particle properties and operational parameters.

### 2.3.3 Consequences for modelling

The orifice flow model represented in Figure 2.11 is now outlined in further detail. The term  $\Delta\sigma_N$ , representing the difference in particle pressure between dense bed and lean bed can be calculated from:

$$\Delta\sigma_N = \sigma_N - P_p \tag{2.10}$$

The dense bed particle pressure ( $\sigma_N$ ) and lean bed resistance ( $P_p$ ) are estimated from Equations 2.8 and 2.9 respectively.

A relationship for  $\Delta P_f$  representing the shear friction pressure drop will be derived in chapter 2.5. The empty annulus effect is taken into account according to Equation 2.1 (with  $k=1$ ).

For a predictive model for solids flow it is necessary to include the gas flow in the model for two reasons. Firstly, the gas-solids drag can be a driving or a resisting force as already mentioned. The second reason is that the orifice gas flow will change the effective gas velocity in both beds. This will influence the particle pressures and shear friction. The solids flow model therefore consists of a set of equations that needs to be solved in an iterative way to account properly for gas flow between dense and lean bed. In Figure 2.12 this is schematically shown for the case of a positive orifice pressure drop. The validity of the solids flow model is verified in chapter 2.6 by comparing model calculations to experimental results. The model is outlined in Appendix 2.B.

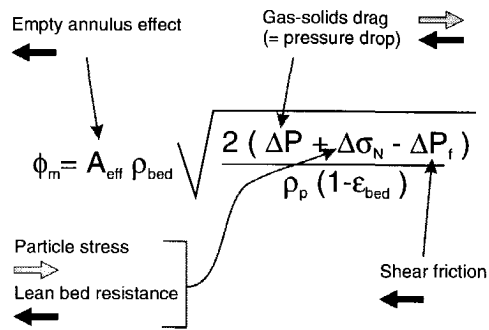
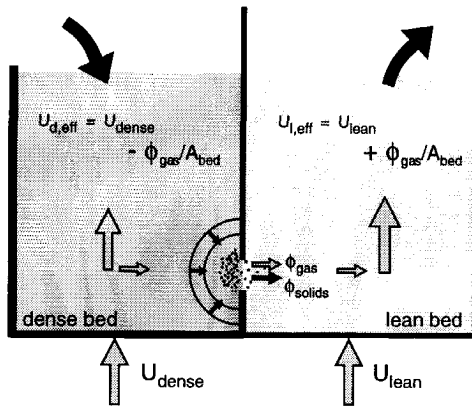


Figure 2.11 Macroscopic equation that predicts gas-solids flow through orifices on the basis of the driving and resisting forces that are indicated.



**Figure 2.12** Gas and solids flow through an orifice from a dense to a lean bed. Due to a gas flow ( $\phi_{gas}$ ) from dense to lean bed (in the case  $\Delta P > 0$ ), the effective gas velocities in the respective beds will decrease and increase.

## 2.4 On the viscosity of fluidized and aerated beds

### 2.4.1 Analogy of particle/gas-systems and Newtonian liquids

The analogy between gas-solid fluidized beds and Newtonian liquids has been recognized, criticized and discussed for a long time. The idea originates from the often surprisingly simple liquid-like behaviour of a fluidized bed. In reality however the system consists of a complex two phase structure on a microscopic scale.

Fluidized beds have been characterized by several rheological models:

- Newtonian* (Haygard and Sacerdote, 1966; Grace, 1970; Hoffmann *et al.*, 1994),
- pseudoplastic* (Botteril and Bessant, 1976; Botteril and Abdul-Halim, 1979),
- power-law* (Singh *et al.*, 1978) and
- Bingham* (Langenberg-Schenk and Rietema, 1984).

A critical remark with regard of treating a fluidized bed as a liquid was already made by Kramers (1951). According to this author a fluidized bed is essentially non-homogenous and non-uniform in its physical properties and has therefore in this respect nothing in common with the liquid state. This type of comment is justified because the rheology of a fluidized or aerated bed is essentially much more complex than it generally is for liquids. This is mainly caused by the complexity of the particle interactions and the non-isotropic features that originate from aeration in one direction.

Despite the complexities, some similarities between fluidized beds and liquids cannot be denied. This (liquid-like behaviour) can be used in a practical way which is the main reason that fluidized beds are used as chemical reactors (Kunii and Levenspiel, 1991) or for scale-up of multiphase reactors (Krishna and Ellenberger, 1995). It also offers an attractive way to

characterize the resistance to flow in aerated and fluidized beds by means of an apparent viscosity. It should be kept in mind however that a simplification is made with respect to the true rheology of the aerated or fluidized bed.

An overview of transport properties of fluidized solids and experimental methods to determine viscosity in a fluidized bed can be found in some textbooks on fluidization (Schügerl, 1971; Cheremisinoff and Cheremisinoff, 1984; Rietema, 1991).

The overall conclusion is that the true flow behaviour is fairly complex but can in a large number of cases be approximated by Newtonian behaviour. In further modelling work this approximation will be used.

#### 2.4.2 Measuring apparent viscosities

Several methods can be applied in measuring viscosities of aerated and fluidized beds. One can divide the measuring techniques in two categories:

1. methods that are adapted from measuring techniques in liquids and
2. indirect methods based on fluidization characteristics in analogy to liquids.

In the first category commonly used measuring techniques are: falling sphere, immersed rotor and pendulum method. These techniques utilize the drag force that is exerted on an object moving in a bed of particles. From the measured drag force, the apparent viscosity is determined. Another technique is to relate measured friction losses to viscosity in channel flow of fluidized solids. Two main problems of these measuring techniques are the disturbance of the fluidized suspension by an external object (for example defluidization in its vicinity) and slip at the solid boundaries.

An important advantage of indirect measurement of the viscosity is that the above mentioned problems are avoided. Two indirect methods are based on bubble shape and bubble rise velocity measurements. In analogy with liquids, the shape and rise velocity of a bubble are related to the viscosity of the dense phase. The main assumption is that bubble characteristics are the same as in liquids. The methods are limited to fluidized beds in which bubbles can be detected. This excludes viscosity measurements in aerated beds operated below the minimum fluidization velocity.

In view of the problems, restrictions and limitations in measuring viscosity in aerated and fluidized beds, the considerable scatter in the measured viscosity data is understandable (see Figure 2.13). When  $U_{mf}$  was not given by the authors it was estimated from the equation of Wen and Yu (1966). Experimental results of the following five studies are presented:

Author	Measuring technique
1. Schügerl <i>et al.</i> (1961);	immersed rotor
2. Haygard and Sacerdote (1966);	pendulum
3. Furukawa and Ohmae (1958);	immersed rotor
4. Daniels (1965);	falling sphere
5. Siemes and Hellmer (1962);	fluidized bed flow

Despite the scatter in the measured data two general features can be observed: the viscosity decreases with increasing gas flow rate and the viscosity is in the order of magnitude of 0.1 to 10 Pa·s.

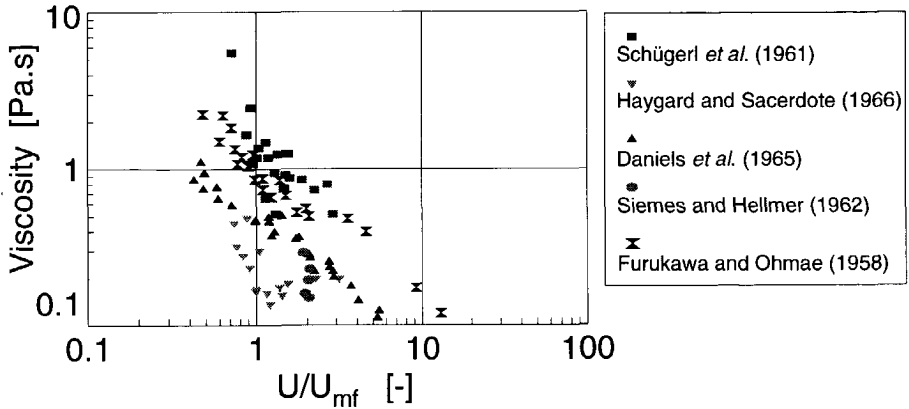


Figure 2.13 Viscosity as a function of  $U/U_{mf}$  as measured by the authors mentioned.

#### 2.4.3 Theoretical models for fluidized bed rheology

The apparent viscosity of an aerated or fluidized bed can be seen as its resistance to flow and is caused by friction between adjacent particles. When the particles can move around (as in a fluidized bed) collisions between the particles will also contribute to the viscosity. Modelling a fluidized bed including its rheological behaviour is a complex matter and still not fully developed. A number of models that were developed are empirical; see for example Cheremisinoff and Cheremisinoff (1984) and Kai *et al.* (1991). The application of this type of empirical models is limited to the experimental range that was taken into account in developing it.

Another approach in modelling is based on particle interactions on the microscopic scale. This is often referred to as the kinetic theory for granular flow. In this theory the concepts of the kinetic theory of gases are used to predict bulk properties such as viscosity; see for an overview of the possibilities of this type of modelling Gidaspow (1994) or Manger *et al.* (1995).

Brinkert (1993) and Brinkert and Davidson (1995) argue that in a fluidized bed, particles are not far apart (in comparison to their diameter), do not move through vacuum and have a considerable weight. They concluded therefore that the kinetic theory is not easily generalized and developed a new collisional model. The particle interactions do not resemble the kinetic theory but are based on a theory for suspension flow. The model is applied on solids flow down a slope but is not directly applicable to other situations.

The prediction of macroscopic properties of fluidized beds, and especially of aerated beds from microscopic particle interactions is still not a practical solution that can be used in modelling IFB hydrodynamics.

2.4.4 An empirical predictive relation for the viscosity

In modelling shear friction in IFB systems it is important to be able to predict the viscosity of an aerated bed. The difficulties and limitations of the theoretical models are the main reason that an empirical predictive correlation for the viscosity is developed.

Literature data of the viscosity is presented in Figure 2.13. In order to relate the measured viscosity to operational conditions and general particle properties, a dimensional analysis was performed. It is assumed that the viscosity ( $\mu$  in Pa.s) of an aerated or fluidized bed is related to the superficial gas velocity ( $U$  in m/s), minimum fluidization velocity ( $U_{mf}$  in m/s), particle density ( $\rho_p$  in kg/m<sup>3</sup>) and particle diameter ( $d_p$  in m):

$$\mu = c \cdot U^A U_{mf}^B \rho_p^C d_p^D \tag{2.11}$$

The dimensional problem given by Equation 2.11 is determined by five quantities (*viz.*,  $\mu$ ,  $U$ ,  $U_{mf}$ ,  $\rho_p$ ,  $d_p$ ) and three fundamental units (*viz.*, m, s, kg). According to the Buckingham  $\pi$ -theorem (see Bird *et al.*, 1960) this means that it can be characterized by two (=5-3) dimensionless groups. The dimensionless relationship that is obtained from the analysis is:

$$\left( \frac{\mu}{\rho_p d_p U} \right) = c \left( \frac{U}{U_{mf}} \right)^{-B} \rightarrow VN = c \left( \frac{U}{U_{mf}} \right)^{-B} \tag{2.12}$$

In this equation the two dimensionless groups that appear, are the viscosity number ( $VN$ ) and the dimensionless aeration rate ( $U/U_{mf}$ ). The parameters  $c$  and  $B$  need to be determined from experimental results. In Figure 2.14,  $VN$  is plotted against ( $U/U_{mf}$ ). Again it is obvious that the scatter in the data is considerable. A straightforward regression analysis yields for the parameters and their standard error:  $c = 29.3 \pm 2.9$  and  $B = 1.42 \pm 0.12$ . The correlation that is plotted in Figure 2.14 together with the experimental data is:

$$\left( \frac{\mu}{\rho_p d_p U} \right) = 29.3 \left( \frac{U}{U_{mf}} \right)^{-1.42} \tag{2.13}$$

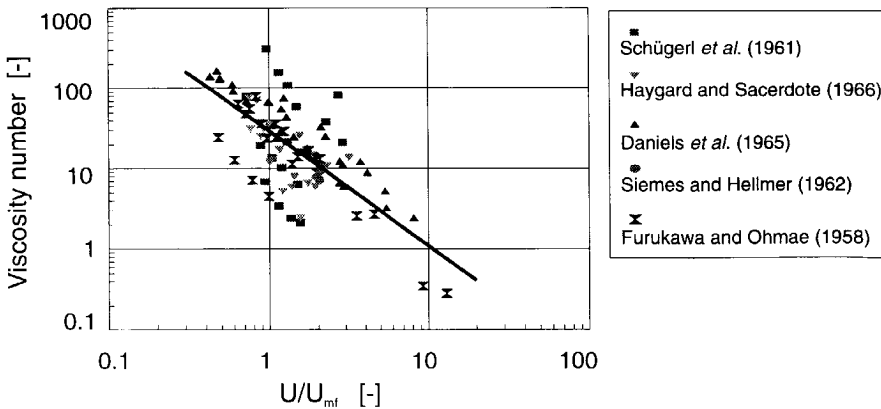


Figure 2.14 Viscosity number defined by Equation 2.12 versus  $U/U_{mf}$  including the fitted correlation

## Chapter 2

---

The empirical correlation (Equation 2.13) can only be safely used in the range of the hydrodynamic variables that was covered by the experiments; see Table 2.2.

**Table 2.2** Hydrodynamic variables and the experimental range that was applied in the development of the viscosity correlation, Equation 2.13.

Variable	Range
U [m/s]	0.015 - 0.47
$U_{mf}$ [m/s]	0.017 - 0.30
$U/U_{mf}$ [-]	0.43 - 13
$\rho_p$ [kg/m <sup>3</sup> ]	1150 - 2650
$d_p$ [ $\mu$ m]	75 - 588

The empirical predictive relation for the viscosity can be used for further modelling. An estimation of the viscosity can be made for the indicated range of the hydrodynamic variables. It provides an easy to use and straightforward basis to estimate the viscosity of aerated and fluidized beds. The scatter in the data on which the correlation is based is considerable. The value for the viscosity that is obtained from Equation 2.13 can therefore only be considered as a rough estimation.

## 2.5 Shear friction in flow through orifices

### 2.5.1 A macroscopic description of shear friction losses

It was already explained that shear friction is believed to play an important role in solids flow through orifices. In literature no attention was given to this phenomenon (see chapter 2.2) in relation to solids flow. Therefore it was investigated how the influence of viscosity on orifice flow of Newtonian liquids can be accounted for.

A significant number of textbooks was consulted with regard to this subject (for example Bird *et al.*, 1961; Schlichting, 1968; Fox and McDonald 1985; de Nevers, 1991; Holland and Bragg, 1995; Faber, 1995). Orifice flow problems are treated in almost every textbook. It appeared however that the friction losses are analyzed in terms of a discharge coefficient and the influence of shear stress in friction losses is not explained. The discharge coefficients need to be determined experimentally and depend on specific orifice and liquid properties. In general, the influence of shear friction is depending on the Reynolds number. Several experiments have shown that the discharge coefficient is practically constant at high ( $Re > 10^5$ ) Reynolds numbers (Street *et al.*, 1996). However, for smaller Reynolds numbers ( $< 10^5$ ) the influence is significant.

An attempt was made to predict the orifice discharge coefficient theoretically for high and low ( $Re < 10$ ) Reynolds numbers by Grose (1985) and Kiljański (1993), respectively. Despite their attempts, a clear understanding of the influence of shear friction is not available.



Kiljański (1993) states that even the outflow of Newtonian liquids at low Reynolds numbers has not been well examined.

In most discharge problems the Reynolds number is high (especially for low viscosity liquids like water). In that case the value for the discharge coefficient is mainly depending on the type of orifice. Four types of orifices are presented in Figure 2.15 together with their nominal coefficients. The discharge coefficient ( $C_D$ ) is considered as the product of a contraction coefficient ( $C_c$ ) and a velocity coefficient ( $C_v$ ).

Contraction is often referred to as the reason for low values of the discharge coefficient. This is not correct since the contraction of the flow has a true fluid dynamic cause. The so-called *vena contracta* originates from the flow profile towards the orifice. The fluid is not exiting perpendicular to the wall and the stream is still accelerating until the streamlines are parallel to each other. This causes the *vena contracta* that is quantified by the contraction coefficient. The upward flow profile depends partly on viscous effects and in particular on the shape of the orifice (see Figure 2.15).

A true frictional effect is represented by the velocity coefficient. The loss of mechanical energy is mainly caused by turbulence in the flow field at high Reynolds numbers. At lower Reynolds numbers viscous forces cause the shear friction losses.

The general concepts to explain non-idealities in orifice flow phenomena by contraction and frictional effects can be used in further considerations on orifice flow phenomena. In fluidized or aerated solids discharge, the Reynolds number will not be particularly high (due to the high apparent viscosities of the fluidized or aerated suspension). It is therefore believed that the friction losses will be mainly caused by 'viscous' effects. This is the reason that a macroscopic pressure drop relation is derived in Appendix 2.A that accounts for the viscosity of the fluid and also for the upward flow profile. In Figure 2.16 a schematic view of the flow field towards an orifice is shown. The flow profile is assumed to have the shape of a converging nozzle. The surface of the hyperboloid which coincides with the outer part of the flow tube is denoted as  $\zeta_0$ . The relation between the shape of the tube and  $\zeta_0$  is explained in Appendix 2.A. The following pressure drop relation was obtained:

$$\Delta P_f = \frac{3\pi\mu v}{d_{orifice} (1+2\zeta_0) (1-\zeta_0)^2} \tag{2.14}$$

For flow through an orifice, the flow field is often assumed to consist of symmetrical hemispheres converging towards the orifice. In that case the shape parameter  $\zeta_0$  is zero. In

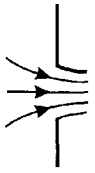

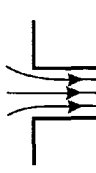
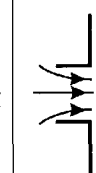
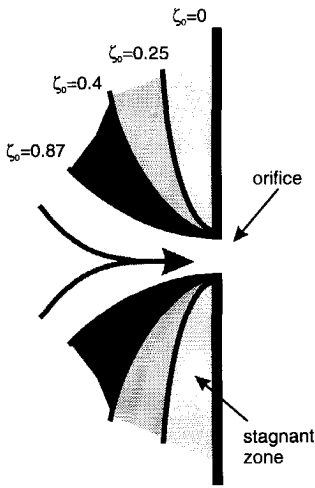
	Sharp edged	Rounded	Short tube	Borda
				
$C_D$	0.61	0.98	0.80	0.51
$C_c$	0.62	1.00	1.00	0.52
$C_v$	0.98	0.98	0.80	0.98

Figure 2.15 Four types of orifices and their corresponding coefficients of discharge ( $C_D$ ), contraction coefficient ( $C_c$ ) and velocity coefficient ( $C_v$ ) for high Reynolds number ( $>10^5$ ) discharge of liquids according to Street *et al.* (1996). The coefficient of discharge is considered as the product of  $C_c$  and  $C_v$ .



**Figure 2.16** Representative flow profiles and corresponding shape factors ( $\zeta_0$ ). The special situation of a hemispherical flow profile is characterized by  $\zeta_0=0$ . The mathematical description of the flow profiles is outlined in appendix 2.A.

Appendix 2.A the influence of the shape parameter  $\zeta_0$  on the resulting pressure drop is explained. These results and pragmatic considerations (such as the difficulty to predict the exact flow profile in solids flow) are a motivation to use the hemispherical approach ( $\zeta_0=0$ ) for further modelling. Equation 2.14 then simplifies to:

$$\Delta P_f = \frac{3\pi\mu v}{d_{orifice}} \tag{2.15}$$

In order to have a measure for the shear friction in flow through orifices, the Orifice Shear (OS) number is defined in this study. It represents the ratio of the pressure drop caused by shear friction and the total pressure drop:

$$OS = \left(1 + \frac{\rho v d_{orifice}}{6\pi\mu}\right)^{-1} \tag{2.16}$$

It resembles the Reynolds number, which is the ratio of convective to molecular momentum transport, but provides a more direct insight in the specific case of orifice flow. It can be used to estimate the importance of shear stress for a

specific flow problem. Values for the OS number range between the limits 0 to 1. For  $OS=0$ , no influence of shear friction is present and when  $OS=1$ , the pressure drop is totally caused by shear friction. From the OS number it can therefore be decided whether a more detailed study on the influence of shear friction on the flow is necessary or not.

The considerations on orifice flow apply for Newtonian liquids such as water. It is therefore surprising that in literature on air-lift reactors no detailed analysis is available that quantifies the friction losses due to shear friction. Merchuk and Berzin (1995) and Zehner and Benfer (1996) only include an empirical friction term in their fluid dynamic models to account for the energy dissipation.

Orifice flow phenomena for non-Newtonian fluids were studied by Salas-Valerio and Steffe (1989). They measured orifice discharge coefficients for power-law fluids. The results indicate that the orifice discharge coefficients are a function of orifice diameter, fluid velocity in the orifice and the fluid rheological properties. No efforts were undertaken by the authors to model the shear frictional influence. However, their results are a clear motivation to include shear friction in an orifice flow model.

In the following paragraph the validity of the use of the macroscopic pressure drop relationship (Equation 2.15) and the OS number will be verified by liquid flow experiments. The macroscopic shear friction approach will be further analyzed in relation to solids flow in chapter 2.5.3.

### 2.5.2 Quantifying friction losses: experiments and predictions

On the basis of the microscopic equations of motion, a macroscopic pressure drop relationship was obtained (Appendix 2.A). An analysis on the use of microscopic and macroscopic transport equations is given by Snip *et al.* (1997). In this paper the influence of the fluid viscosity in orifice flow is discussed in detail.

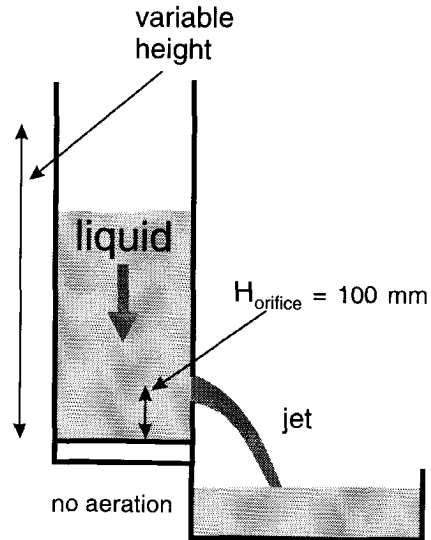
The influence of the viscosity on friction losses was experimentally studied in the so-called Bernoulli facility (see Figure 2.17). This is basically a square vessel (100x100 mm<sup>2</sup>) from which a liquid can be discharged batchwise to the atmosphere. In addition to the experiments, a resembling geometry was analyzed by Computational Fluid Dynamics (CFD). The 2-dimensional CFD geometry consisted of an equally sized vessel compared to the experimental set-up with an opening based on a short tube (see Figure 2.15) of 25 mm at a height of 100 mm. The results of CFD calculations and experiments are summarized in Table 2.3.

Experiments and CFD calculations show that shear friction should not be neglected in calculating the orifice flow behaviour for the high viscosity liquid (glycerol). This is also clearly illustrated in the values of the OS number. The predicted values for the discharge coefficient ( $C_{D, PRED}$ ) are calculated on the basis of the assumption that all friction losses are caused by shear friction. The macroscopic relationship for orifice flow can then be written as:

$$v_0 = \sqrt{\frac{2(\Delta P - \Delta P_f)}{\rho}} \quad (2.17)$$

in which  $\Delta P_f$  is calculated according to Equation 2.15. In this way, a relationship is obtained that predicts the fluid velocity ( $v_0$ ) in the orifice as a function of the pressure drop across the orifice ( $\Delta P$ ), the fluid properties ( $\rho$  and  $\mu$ ) and orifice diameter ( $d_p$ ). The predicted value for the discharge coefficient ( $C_D$ ) is the ratio between the fluid velocity calculated by Equation 2.5 and Equation 2.17.

From the predicted results that are given in Table 2.3, it is concluded that the macroscopic pressure drop relationship can reasonably predict the friction losses in orifice flow. Further, the OS number is helpful in predicting the relative influence of shear friction.



**Figure 2.17** Bernoulli facility for studying the batchwise discharge of liquids of various viscosity and density.

## Chapter 2

It is further revealed by CFD and experiments that the flow profile does resemble to a great deal the hemispherical profile that was assumed in the derivation of the macroscopic pressure drop relation and the OS number. The approach therefore seems to be useful and will be applied on solids flow through orifices.

**Table 2.3** Calculated and experimental results for the indicated liquids and temperatures.

Liquid	T [°C]	$\mu$ [Pa s]	$C_{D, CFD}$ [-]	$C_{D, EXP}$ [-]	$C_{D, PRED}$ [-]	$OS_{EXP}$ [-]	$Re_{EXP}$ [-]
water	23	0.001	0.99	0.96	0.99	0.0005	27000
glycerol	30	0.62	0.68	0.80	0.89	0.19	44
glycerol	23	1.3	0.53	0.77	0.79	0.32	20

### 2.5.3 Shear friction in solids flow

The study of shear friction was initiated in order to quantify the effect of interparticle forces on friction losses in solids flow through orifices. Massimilla (1971) describes experimental work in which a flow profile was observed including stagnant zones (see Figure 2.6). This indicates the fact that interparticle forces do play a role in gas-solids flow through orifices. Furthermore, Watson and Rotter (1996) and Langston *et al.* (1995, 1996) showed by modelling that a flow profile of the solids flow towards the orifice (similar to Figure 2.6) is obtained when the microscopic particle interactions are taken into account.

Various authors observed a high exit voidage in a jet that is discharged from a fluidized or aerated bed (see for example Jones and Davidson, 1965; Geldart and Haesebrouck, 1983). Viscous effects are also important in explaining this phenomenon. It is caused by shear friction in the solids flow towards the orifice. The particles can be decelerated causing a somewhat higher slip velocity between the two phases. The relative effect will, in most cases however, be stronger for the solids than for the gas phase resulting in a higher jet voidage fraction.

A shear frictional approach thus gives a better understanding of solids flow phenomena that are caused by particle interactions. To quantify the shear frictional effects, the macroscopic equations (derived in the preceding sections on solids flow) can be used. In that case it must be assumed that the gas-solids mixture can be treated as a continuum. The interaction between the two phases can be accounted for by the Ergun equation.

In chapter 2.4 the analogy between Newtonian fluids and aerated and fluidized beds was explained and discussed. A relationship was developed (Equation 2.13) by which it is possible to estimate the apparent viscosity of a gas-solids mixture.

The literature data of Table 2.1 were used to evaluate the use of the shear frictional approach in solids flow. The average values for the OS and Reynolds numbers were calculated on the basis of the average particle velocity in the orifice and orifice size. The viscosity was calculated on the basis of Equation 2.13 for the minimum and maximum gas velocity. In Table 2.4, the average OS and Reynolds numbers are shown. The values for the OS number indicate that shear friction is an important restriction in solids flow. It should be mentioned

that the estimated OS number is an average value and its particular value can be higher or lower depending on the specific conditions during the experiments. The Reynolds number is also an indication of the role of shear friction. The OS number however is a direct measure of the shear friction losses and is therefore preferred for evaluating purposes. The calculations that were carried out on the basis of the literature data show that:

1. shear friction can in most solids flow problems not be neglected and
2. the OS number is a convenient measure for shear friction losses.

**Table 2.4** Minimum, maximum and average values for the apparent viscosity of the gas-particle system ( $\mu_{\min}$ ,  $\mu_{\max}$ ,  $\mu_{av}$ ), average particle velocity ( $v_{av}$ ) and average OS and Reynolds numbers.

Reference	$\mu_{\min}$ [Pa.s]	$\mu_{\max}$ [Pa.s]	$\mu_{av}$ [Pa.s]	$v_{av}$ [m/s]	$OS_{av}$ [-]	$Re_{av}$ [-]
Fox <i>et al.</i> (1989)	0.50	0.80	0.65	0.62	0.17	9.2
Korbee <i>et al.</i> (1991) <sup>(1)</sup>						
1. sand	16	20	18	0.43	0.93	1.5
2. silica	8.0	9.5	8.7	0.45	0.95	0.96
3. glass beads	3.7	4.3	4.0	0.32	0.76	5.9
Kuramoto <i>et al.</i> (1985, 1986)	0.04	0.10	0.07	0.12	0.07	260
Geldart and Haesebrouck (1983)						
1. 'plastic'	0.12	0.35	0.24	1.23	0.94	1.2
2. polyethylene	7.3	21	14	2.0	0.82	4.2
3. alumina	0.02	0.06	0.04	0.61	0.02	992
Martin and Davidson (1983)	0.02	0.03	0.03	0.74	0.06	320
Bolton and Davidson (1987)	0.12	0.23	0.17	0.06	0.11	150

<sup>(1)</sup> particle size for sand and silica and particle density of glass beads are not within the range that is required to use Equation 2.13 (see Table 2.2)

## 2.6 Experimental results and model validation

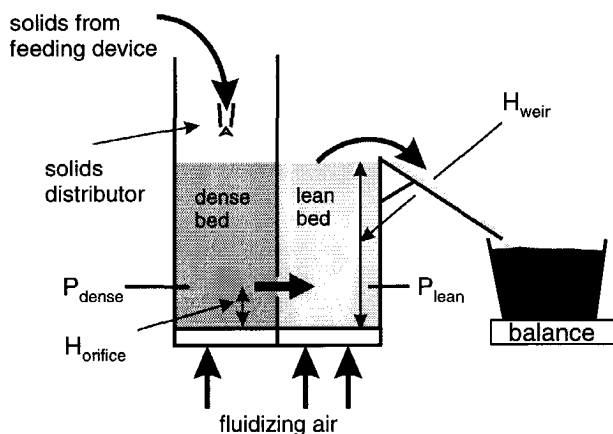
### 2.6.1 Experimental facilities: twin-bed and jet facility

The experimental work on two cold facilities was performed in order to develop insight in solids and gas transport from and between aerated and fluidized beds. The so-called twin-bed facility and the jet facility are simplifications of the IFB system. These transformations serve the purpose of enabling direct measurement of gas and solids transport.

The two facilities are used to reveal the mechanisms which determine the solids and gas transport phenomena. Special attention will be given to the sorbent material that is used in the hot IFB pilot plant facility (see chapter 5). Details on the experimental facilities, particle properties, experimental procedures and experimental results can be found in the M.Sc reports of Iversen (1995) and Roodenburg (1995).

### Twin-bed facility

Korbee *et al.* (1994) describe the twin-bed facility in detail. This simplification of the IFB system consists of two beds that are connected by means of an orifice (see Figure 2.18). The surface area of each bed is  $100 \times 100 \text{ mm}^2$  and the height of the weir is fixed at 300 mm. The solids are introduced to the dense bed by means of a vibrating feeding device. Subsequently, the solids are transported through an orifice to the lean bed. The lean bed, which is operated at the higher gas velocity, discharges the solids (by means of a slide) to a collecting vessel that is positioned on a balance.



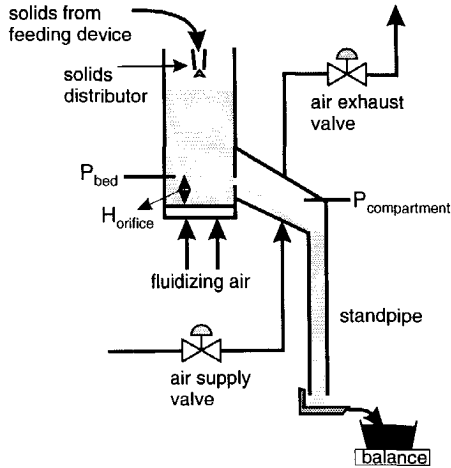
**Figure 2.18** Twin-bed facility; an experimental apparatus for measuring solids and gas transport between aerated and fluidized beds.

The solids flow rate can be determined since the weight of the vessel is measured on-line. The orifice gas flow is determined by means of pressure drop measurements in the dense bed, which are compared to pressure drops obtained in a single bed with a fixed gas velocity. Pressures are measured by means of pressure transducers (Validyne DP 15) which are connected to a process control and data acquisition interface. The signals from balance and transducers are simultaneously recorded for further use.

The diameter of the orifice is adjustable between 10 and 30 mm (orifice depth = 20 mm). The orifice is inserted in the separating wall at a height of 100 mm. The solids and gas flow through a specific orifice can be determined as a function of the gas velocities in dense and lean bed. The measurements are carried out at a fixed bed height in the dense bed, equal to the height of the weir. This procedure enables the translation to a 4-bed IFB system (see chapter 3).

### Jet facility

The jet facility is a further simplification of an IFB system (see Figure 2.19). The lean bed is substituted for a pressurized compartment. The size of the bed equals the dense bed size in the twin-bed facility. Position and sizes of the orifices are also identical. The solids are introduced to the system by means of a feeding device (equivalent to the twin-bed facility). During an experiment the bed height is controlled at a constant level.



**Figure 2.19** Jet facility; an experimental apparatus for measuring solids and gas transport between an aerated or a fluidized bed and a pressurized compartment.

In this experimental set-up it is thus possible to vary the pressure drop across the orifice as an independent hydrodynamic variable. At a specified pressure difference, gas and particles flow from the aerated or fluidized bed into the pressurized compartment. The pressure in the compartment is controlled by means of a gas supply valve and gas exhaust valve. The pressures in the bed at orifice height and in the pressurized compartment are measured by manometers.

The standpipe serves the purpose of maintaining an excess pressure in the compartment together with continuous solids removal from the system. The standpipe level is maintained constant by means of a solids flow controller (equivalent to the feeding device). The solids flow rate can be measured at the bottom of the standpipe by means of weighing.

In the jet facility, the lean bed resistance can be determined by comparing an equivalent (equal pressure drop) measurement in the twin-bed facility; see Figure 2.24. In this way, an important resisting contribution in solids flow between IFB compartments can be revealed. Furthermore, a direct measurement of gas flow through the orifice is possible by means of flow meters (gas that is escaping through the standpipe needs to be corrected for). An estimation of the linear solids velocity can be obtained through measuring the jet trajectory. From a mass balance for the solids and gas phases, the voidage fraction and the absolute gas velocity in the jet can be determined. A detailed analysis of solids and gas transport from an aerated or fluidized bed is thus possible in the jet facility.

## 2.6.2 Introductory experiments

*Measurement of K and f*

Several parameters in the hydrodynamic model presented in chapter 2.3 concern particle related properties. Experiments were therefore carried out for the sorbent particles to reveal those parameters that are used in modelling. In Table 2.5, the particle properties are given. The particle size was measured by means of image analysis and could be described by a normal distribution ( $N(2.66, 0.006)$ ). Further, the fixed bed voidage and minimum fluidization velocity were determined before and after the experiments and appeared not to have changed. The stress ratio  $K$  and friction factor  $f$  are important parameters in predicting the normal stress in a bed of particles. Friction between wall and particles was determined by means of a weighing experiment. A square vessel (identical to the twin-bed and jet facility) made of perspex (PMMA) was positioned on a balance without making contact. It was then filled with a fixed amount of solids and the weight was registered on the balance. The solid wall frictional force can be obtained from Equation 2.8 for the un-aerated situation ( $F(\Delta u_z)=0$ ). Integration yields an expression for the solid-wall friction force ( $F_{sw}$ ) and the weight on the balance ( $W_{balance}$ ):

$$W_{balance} = W_{solids} - \frac{F_{sw}}{g} \quad (2.18)$$

and:

$$F_{sw} = A_{bed} \rho_p (1 - \epsilon_{bed}) g \left( H - \frac{A_{bed}}{f K P_w} \left( 1 - \exp \left( \frac{-f K P_w}{A_{bed}} H \right) \right) \right) \quad (2.19)$$

From the measured weight and the above equations, the product of the friction factor and stress ratio ( $fK$ ) can be determined. Due to consolidation of the bed material, the recorded bed weight decreased during the experiment for approximately three hours and then levelled off at a constant value. The decrease corresponds to a solids weight of 3% of the total bed mass. In the steady state, 68% of the bed mass was sustained by the wall. The product  $fK$  was calculated according to Equation 2.18 and 2.19. A value of  $0.25 (\pm 0.01)$  was found based on the steady-state measurements of the solids weight.

In a so-called Jenike shear cell (see van der Kraan, 1996), experiments were performed to determine the friction factor  $f$  between the perspex (poly methyl methacrylate or PMMA) wall and the particles. In a Jenike shear cell, the relation between a normal stress that is applied (by means of a variable weight) and the subsequent shear stress is determined. The shear stress is determined from the measured force that is necessary to slide a packing of solids over the specific wall material for different normal stresses.

When the shear stress is plotted against the normal stress, the friction factor can be determined from the slope of the curve. The friction factor appeared to be independent of the applied normal stress and weakly dependent on the shear velocity in the cell. In the range of particle velocities (5-50 mm/s) that can be encountered in the dense bed of the IFB system, the friction factor is constant at a value of  $0.401 \pm 0.005$ . The latter value of the friction factor ( $f$ ) is averaged on the basis of nine measurements. The experimentally determined stress ratio  $K$  then is  $(0.25/0.401) = 0.62 \pm 0.03$ .



**Table 2.5** Particle properties of the SGC-500 sorbent.

$d_p$	= 2.66	$\pm$ 0.08	[mm]	K	= 0.62	$\pm$ 0.03	[-]
$\rho_p$	= 1400		[kg/m <sup>3</sup> ]	$f^{(1)}$	= 0.401	$\pm$ 0.005	[-]
$\epsilon_{\text{fixed}}$	= 0.463	$\pm$ 0.005	[-]	$U_{mf}$	= 0.75	$\pm$ 0.03	[m/s]
$\alpha_r$	= 24	$\pm$ 3	[°]				

<sup>(1)</sup> the friction factor is a particle-wall interaction parameter

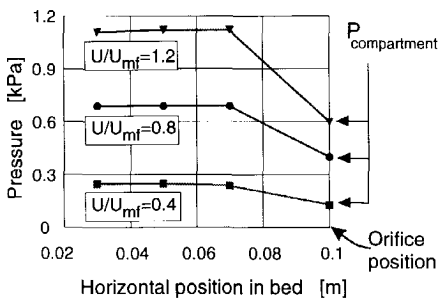
### Measuring gas flow through the orifice

In the jet facility, the gas flow through the orifice could be measured directly whereas in the twin-bed facility an indirect method was necessary. Korbee (1995) describes a helium tracer method that was applied to determine the gas flow. The problems with this technique are the diffusion effects and concentration profiles requiring a large number of measurements to determine the gas flow at one set of conditions.

For practical purposes it was therefore decided to utilize the effect of the gas that is flowing from one compartment to the other on the hydrodynamics in dense and lean bed. The hydrodynamic properties that depend on the effective gas velocity in each bed are the pressure gradient and voidage in both beds. The pressure gradient in the dense bed is most influenced by an alteration in effective gas velocity due to orifice gas transfer. It was therefore chosen as the basis for the orifice gas flow measurement. The actual (measured) pressure gradient is related to the effective gas velocity in the dense bed. From the difference between the actual and set gas velocity, the orifice gas flow can be determined.

The method was tested in the jet facility and the results were compared to directly measured gas flows. The measurement is based on the determination of the pressure gradient in the centre of the dense bed over a distance of 0.08 m. The pressure gradient method proved to be reproducible with a relative deviation of less than  $\pm$  10%.

### Measuring the pressure drop across the orifice



**Figure 2.20** Pressure in the dense bed of the jet facility for a 10 mm orifice at the three indicated gas velocities as a function of the horizontal position.

Another important issue that needs to be discussed is how to measure the pressure drop across the orifice. In Figure 2.20 the measured pressures in the jet facility are shown as a function of measuring position for the indicated gas velocities. The profiles indicate that measuring close to the wall opposite to the orifice is an effective way of characterizing the pressure drop across the orifice. According to the measured horizontal pressure gradients in the bed it can be concluded that the gas flow through the orifice is determined in the region close to the orifice. This is particularly important with regard to predicting the gas flow from a pressure drop across the orifice.

2.6.3 Experimental results and model validation

Twin-bed results

In the experiments, the gas velocities were varied in the ranges:  $0.4 < U_d/U_{mf} < 1.5$  and  $1.5 < U_l/U_{mf} < 2.5$  for orifice sizes 10, 20 and 30 mm.

A typical result is shown in Figure 2.21. The solids flow is plotted as a function of the dense bed gas velocity ( $U_d/U_{mf}$ ) at a constant lean bed gas velocity ( $U_l/U_{mf}=1.5$ ) for three different orifice sizes. It can be seen that increasing the orifice size clearly results in higher solids flows. The maximum in the curve originates from the fact that the height of the dense bed was kept constant during the experiments. At higher gas velocities, the bulk density starts to decrease. Therefore the driving force for solids flow decreases as well.

The same trend can be observed in Figure 2.22 in which the solids flow is shown as a function of the dense bed gas velocity for different lean bed gas velocities. The solids flow rate is larger for the higher lean bed gas velocities. This is caused by a decreasing bed height in the lean bed. The height of the weir is constant in the experiments. Due to the higher gas velocity, the stationary bed mass will be less. This results in a larger pressure drop across the orifice and subsequently a larger solids flow. See chapter 3 for a detailed analysis of weir flow phenomena.

The measured orifice gas flow was in the range of -5% to +20% of the dense bed gas flow. A negative gas flow corresponds to a net gas transport from the lean bed to the dense bed. The gasflow is proportional to the pressure drop across the orifice.

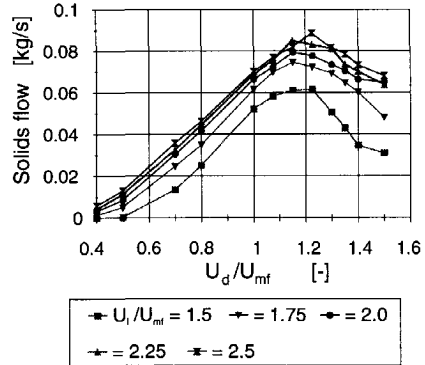
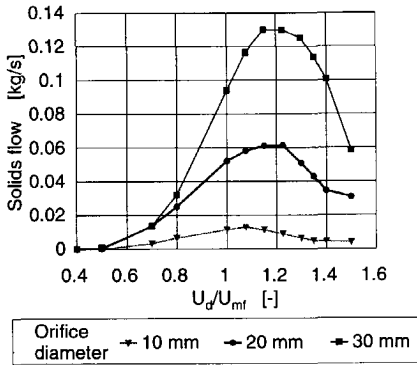


Figure 2.21 Solids flow measured in the twin-bed facility as a function of the dense bed gas velocity ( $U_d/U_{mf}$ ) for the indicated orifice diameters and constant lean bed gas velocity ( $U_l/U_{mf}=1.5$ ).

Figure 2.22 Solids flow measured in the twin-bed facility as a function of the dense bed gas velocity ( $U_d/U_{mf}$ ) for the indicated lean bed gas velocities ( $U_l/U_{mf}$ ) and an orifice diameter of 20 mm.

Jet facility results

The jet facility experiments were carried out, equivalent (with respect to the experimental procedures of solids feeding and pressure measurements) to the twin-bed experiments. The gas velocity in the bed varied between  $0.4 < U_d/U_{mf} < 1.5$  for orifice sizes of 10 and 20 mm.

In Figure 2.23, the solids and gas flows are shown as a function of the pressure drop across the orifice for a set of experiments applying the 10 mm orifice. The trends for gas and solids flow are nearly equivalent. The main difference is a negative gas flow (from compartment to bed) at negative pressure drop at which no solids flow is observed.

It is further recognized that for low pressure drop, the solids flow is relatively higher than the gas flow. This is a direct effect of the normal stress of the solids ( $\sigma_N$  in Equation 2.10). At higher pressure drop, the driving force for gas and solids transport is similar. This indicates the decreasing influence of the normal stress under these conditions.

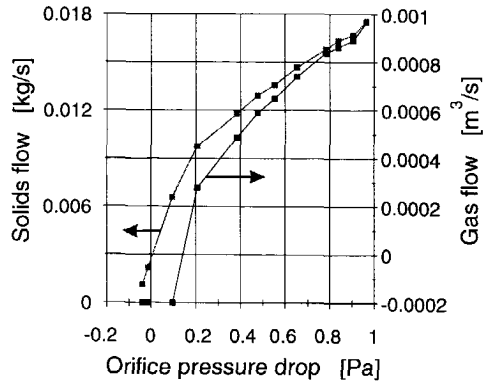
Based on visual jet trajectory observations in the pressurized compartment of the jet facility, the average particle velocities in the jet were determined. Due to gravity, the particles in the jet will travel a distance ( $y$ ) downwards in vertical direction. It is assumed that the horizontal displacement of the particles in the jet ( $x$ ) is a function of the constant horizontal exit velocity in the orifice ( $v_0$ ). The relation between horizontal and vertical displacement and the jet exit velocity can then be written as:

$$v_0 = \frac{x}{\sqrt{2y/g}} \tag{2.20}$$

The jet trajectory measurements for the average horizontal jet velocity ( $v_0$ ) proved to be reproducible with a relative deviation of  $\pm 10\%$ . The corresponding voidage fraction in the jet and velocity of the gas phase can be obtained from a mass balance for gas and solids phases. In Table 2.6, the ranges that were found for the jet properties are shown.

**Table 2.6** Jet properties and flow characteristics in twin-bed orifice. The properties in the twin-bed orifice that are represented, were calculated on the basis of the assumption that the voidage in the orifice is equivalent to the dense bed voidage.

Property	Jet	Twin-bed orifice
particle velocity [m/s]	1 - 1.5	0.05 - 0.35
voidage [-]	0.7 - 0.8	0.46 - 0.65
gas velocity [m/s]	18 - 22	0 - 10



**Figure 2.23** Solids and gas transport measured as a function of orifice pressure drop in the jet facility for an orifice diameter of 10 mm.

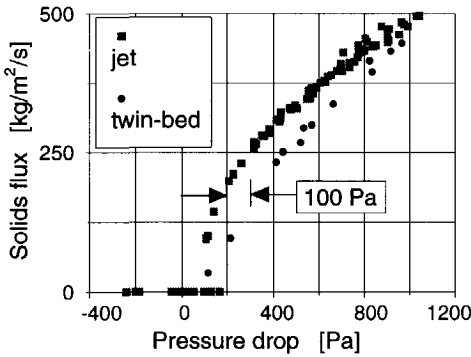
## Chapter 2

The high voidage fraction in the jet is in accordance with literature on particle jets (see Massimilla *et al.*, 1961; Jones and Davidson, 1965; Burkett *et al.*, 1971; Geldart and Haesebrouck, 1983) and visual observations during the experiments. It was also observed that the voidage in the bed close to the orifice was not significantly higher than the average bed voidage. The conclusion is therefore that the increase in the voidage is occurring right after the solids exit the orifice.

### Comparison of jet and twin-bed results

First, the orifice flow characteristics in jet facility and twin-bed facility are compared. The average linear particle velocity and the gas velocity in the twin-bed experiments were calculated on the basis of the assumption that the voidage in the orifice was equal to the dense bed voidage. Experiments in the jet facility have shown that this assumption is reasonable. The dense bed voidage was estimated experimentally by means of pressure gradient measurements.

In Table 2.6, the flow characteristics in both facilities are given. It is clear that the particle velocities and subsequently the voidage and gas velocity are much higher in the jet than in the twin-bed orifice. This is explained from the fact that the jet can accelerate freely after exiting the orifice. In the twin-bed facility this is hindered by the particles that are present in the lean bed. It is therefore believed that the characteristics of the flow towards and inside the orifice for the jet facility are equivalent to the solids flow in the twin-bed facility.



**Figure 2.24** Solids flux as a function of pressure drop across the orifice measured in jet and twin-bed facility. For an equivalent solids flux in the twin-bed facility compared to the jet facility, an approximately 100 Pa higher pressure drop is required.

This idea is confirmed by analysing the solids flow as a function of the pressure drop for both facilities. In Figure 2.24, the solids flow is plotted as a function of the orifice pressure drop. The solids flow is expressed as a flux, based on the effective orifice area. It can be seen that the dependency of the pressure drop is identical. The measured solids flux in the twin-bed facility is shifted to the right compared to the jet results, corresponding to an approximate pressure difference of 100 Pa. Since the conditions in the dense bed of the twin-bed facility and the jet facility are equivalent, the shift in the measurements of Figure 2.24 is caused by lean bed resistance.

### Model validation

The model that was developed in chapter 2.3, expressed by Equation 2.7 and outlined in Appendix 2.B can now be validated on the basis of the experiments that were performed in the jet facility and in the twin-bed facility. In Figure 2.25, the measured solids flux based on the effective orifice area ( $A_{eff}$  defined by Equation 2.1) is shown. The results for the 10 and 20 mm orifice show an identical trend which indicates the correctness of the use of the effective orifice area.

The term  $\Delta\sigma_N$  (Equation 2.10) consists of a driving force ( $\sigma_N$ ) and a resisting force ( $P_p$ ). The influence of  $\sigma_N$  can be observed in Figure 2.23. At negative pressure drop across the orifice, a solids flow is observed that can only be explained by the particle pressure ( $\sigma_N$ ) that acts in the direction of the solids flow.

The influence of the lean bed particle pressure ( $P_p$ ) is shown in Figure 2.24. The particle pressure can be calculated according to Equation 2.9 for the experimental situation in the lean bed that was operated in the slugging regime. Therefore, the size of the effective bubble diameter ( $D_e$ ) was set at the bed diameter of the bed (0.1 m). A value of 110 Pa is then found for the particle pressure in the lean bed. This accounts for the extra resisting force of the lean bed and thus explains the shift of the twin-bed results in Figure 2.24.

The experimentally determined friction factor and stress ratio are used in model calculations (Table 2.5). The stress ratio  $K$  is assumed to depend linearly on the effective gas velocity in the bed according to:

$$K = K_0 + (1 - K_0) \frac{U_{eff}}{U_{mf}} \quad (2.21)$$

in which  $K_0$  is the stress ratio for the non-aerated situation. The value for  $K_0$  was determined by means of the introductory measurements mentioned in chapter 2.6.2 ( $K_0=0.62$ ).

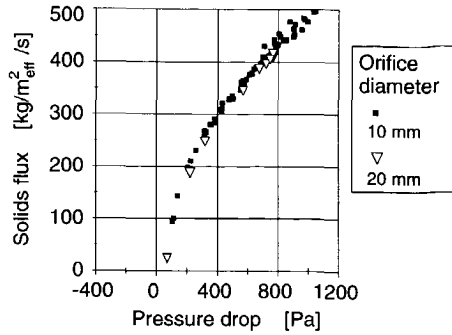
The gas-solids drag term ( $\Delta P$ ) is calculated according to the Ergun equation. The flow profile for the gas phase is assumed to converge symmetrically to the orifice. The acceleration of the gas is assumed to take place within 30 mm from the orifice. See Figure 2.20 for an experimental motivation of this assumption.

To calculate the friction losses ( $\Delta P_f$ ) according to Equation 2.15, an expression for the viscosity is needed. Equation 2.13 can unfortunately not be used because the particle properties are not within the range that is required (Table 2.2). It therefore overpredicts the viscosity of the bed to unrealistic values.

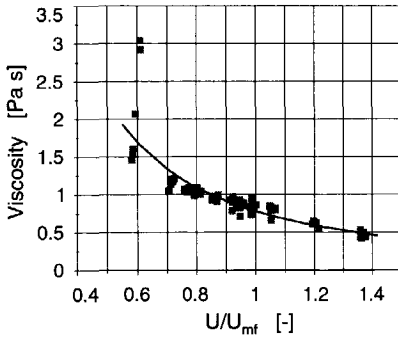
It was decided to determine the pressure loss due to shear friction experimentally from the jet facility results (as plotted in Figure 2.25), applying Equation 2.7. The apparent viscosity of the fluid-particle system can then be calculated by:

$$\mu = \frac{\Delta P_f d_{orifice}}{3 \pi v_{solids}} \quad (2.22)$$

in which  $\Delta P_f$  and  $v_{solids}$  (linear horizontal particle velocity in the orifice) were determined experimentally.



**Figure 2.25** Solids flux based on effective orifice area plotted as a function of orifice pressure drop and measured in the jet facility for the indicated orifice diameters. The solids flux was calculated based on the area of the orifice that is effectively used for solids flow according to Equation 2.1.



**Figure 2.26** The apparent viscosity of the gas-solids mixture in the dense bed of the jet facility plotted as a function of the effective relative gas velocity. The shear frictional pressure drop and particle velocity were determined experimentally and the viscosity was calculated on the basis of Equation 2.22. The fitted correlation is represented by Equation 2.23.

The value for the viscosity that is obtained for all experiments is then plotted as a function of  $U/U_{mf}$ . A correlation was fitted that is given by:

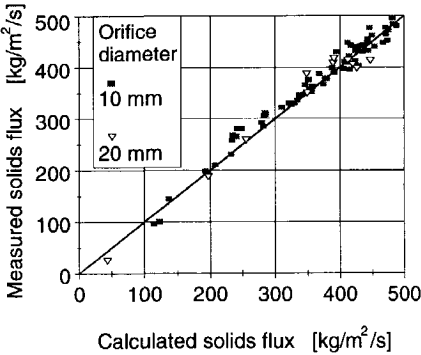
$$\mu = 0.8 \left( \frac{U_{eff}}{U_{mf}} \right)^{-1.52} \quad (2.23)$$

and is shown in Figure 2.26.

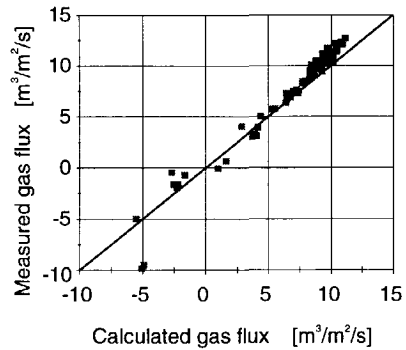
The values for the viscosities that were obtained in this way are in the range that was experimentally found by other investigators (see Figure 2.13). Furthermore the trend of the viscosity as a function of the gas velocity strongly resembles the empirical predictive correlation (Equation 2.13). These aspects thus confirm the value of the shear frictional model for solids flow through the orifice.

The experimentally determined viscosity relation (Equation 2.23) is then used to calculate shear friction losses in solids flow in the jet facility (Figure 2.27). The solids flow is obviously adequately described because the viscosity relationship was based on these experiments.

In Figure 2.28, the experimental gas flow is compared to the calculated (Ergun equation) gas flow. It is observed that the gas flow is also predicted satisfactory.



**Figure 2.27** Experimental solids flux versus calculated solids flux in jet facility. Shear frictional pressure drop is taken into account according to equation 2.15 and the apparent viscosity of the gas-solids mixture is estimated by Equation 2.20.



**Figure 2.28** Experimental gas flow as determined in the jet facility versus calculated gas flow by means of the Ergun equation in the jet facility.

Measurements in the twin-bed facility show (Figure 2.29) that the solids flux can also be reasonably described applying the same model (including the lean bed resistance term  $P_p$ ). This indicates that the characteristics of solids flow are equivalent in both facilities. Further, the overall solids flow model appears to be useful in predicting the experimental orifice flow phenomena.

The experiments can also be analyzed in terms of the OS number. When the twin-bed experiments are considered (Table 2.6), it is found that the

OS numbers are in the range of 0.5 to 0.95. This indicates that the pressure drop due to shear friction ranges from 50 to 95% of the total pressure drop. The importance of shear friction losses is thus confirmed by the OS number.

## 2.7 Discussion and conclusions

Solids flow through orifices is treated in this chapter. On the basis of a literature review, the main driving and resisting forces are identified. This lead to the formulation of a general solids flow model that is represented by Equation 2.7. This macroscopic equation was derived on the basis of microscopic considerations of the flow phenomena.

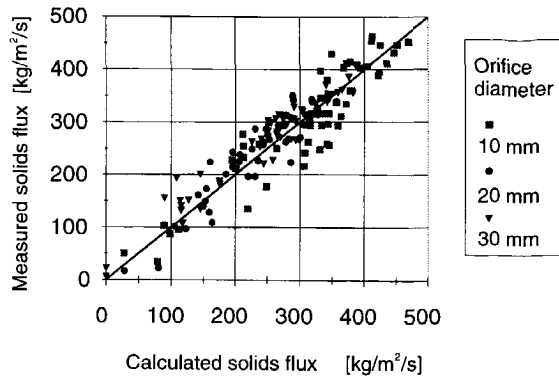
This model is able to describe orifice flow phenomena of experiments in two experimental (twin-bed and jet) facilities. It is appropriate however to discuss the *driving and resisting forces* that were formulated in chapter 2.3.2 successively.

It was shown (Figure 2.25) that the effective orifice area calculated by Equation 2.1 is an adequate way of taking into account the *empty annulus effect*.

The *gas-solids drag* was calculated by means of the Ergun equation assuming a hemispherical flow profile for the gas phase. In Figure 2.28, it is shown that this approach is sufficient to be able to predict the gas flow through the orifice in the experiments that were carried out in this study. However, this approach can give rise to serious miscalculations if the flow profile is different. This could be the case when:

1. the orifice is positioned close to the distributor plate or
2. a large orifice is applied compared to the dense bed size.

The influence of *particle pressure* on solids flow is expressed by the term  $\Delta\sigma_N$ . This represents the difference in the horizontally directed particle stress in the dense bed and the



**Figure 2.29** Experimental solids flux as determined in the twin-bed facility plotted as a function of the calculated solids flux in the twin-bed facility for the indicated orifice diameters.

lean bed. The lean bed particle pressure (or lean bed resistance) could be adequately predicted by means of an empirical correlation from literature (Equation 2.9). This was revealed by comparing jet facility to twin-bed experimental results (Figure 2.24).

The particle pressure in the dense bed is calculated according to Equation 2.8 which is based on Janssen's equation. The main assumption that is made in deriving it, is the fact that the stresses and stress distributions are uniform across any horizontal section. In practice this will not be completely true, especially in the orifice region at large solids flow rates. Despite this failing assumption, Janssen's equation and Equation 2.8 proved to be very useful in explaining solids flow phenomena in practice (see Nedderman, 1992 and Korbee *et al.*, 1994). In the experiments carried out in this study, the horizontally directed particle stress also appeared to be useful in explaining the experimental results (see for example Figure 2.23). Values for the stress ratio ( $K$ ) and friction factor ( $f$ ) can be obtained from straightforward experiments (see chapter 2.6.2). The dependency of the stress ratio on aeration rate could be determined from measuring the angle of repose at different gas velocities. The angle of repose equals the angle of internal friction for non-cohesive particles. The stress ratio can then be calculated according to (Picciotti, 1995):

$$K = \frac{1 - \sin(\alpha_r)}{1 + \sin(\alpha_r)} \quad (2.24)$$

Despite the importance of the particle pressure at low gas velocities, it should be mentioned however that its value decreases almost proportionally to the gas velocity. At gas velocities close to minimum fluidization its influence can be neglected.

**Shear friction** is included in the model by the term  $\Delta P_f$ . The prediction of shear friction losses in solids flow through orifices is based on a microscopic analysis of the flow towards the orifice. This resulted in a macroscopic pressure drop relationship. The most critical aspects in this description are the assumed flow profile towards the orifice and the apparent viscosity of the solid-gas mixture. It can be argued and it was also experimentally observed that for gas velocities close to the minimum fluidization gas velocity ( $U/U_{mf} > 0.8$ ), the flow profile strongly resembles a converging hemisphere ( $\zeta_0 = 0$ , Figure 2.16). Further experimental conditions that will meet this assumption closest, are:

1. a small orifice compared to dense bed size and
2. an orifice position far ( $> 10 \cdot d_{\text{orifice}}$ ) from the distributor plate.

The influence of the shape of the orifice can also be explained from this analysis. Various authors (for example Jones and Davidson, 1965; Geldart and Haesebrouck, 1983) report on the influence of orifice shape. Higher discharge coefficients were found for smoothly shaped orifices. This can be ascribed to a changing flow profile (decreasing  $\zeta_0$ ) and a subsequent decrease in shear frictional pressure drop.

The apparent viscosity of the aerated or fluidized dense bed can be predicted by an empirical correlation (Equation 2.13). It should be mentioned however that the calculated value is only an indication of the true rheological behaviour of the solid-gas mixture. The prediction of shear friction in modelling solids flow through orifices is nevertheless considered useful since shear frictional phenomena are encountered in practice and can therefore not be neglected. Furthermore, the OS number is proposed as a measure for shear friction losses. It represents



the ratio of pressure drop caused by shear friction to the total pressure drop. The OS number can be estimated from basic preliminary calculations. When its value exceeds 0.1, it is in general advisable to perform a more detailed study on shear friction losses.

The overall solids flow model was finally used to predict experimental results in the twin-bed experimental facility. These results (Figure 2.29) show that the model is fairly capable of predicting the experimental results. The apparent viscosity was estimated from separate experiments in the jet facility (Figure 2.26). Its value appeared to be in the range that was expected on the basis of experimental values found in literature (Figure 2.13). The modelling approach is therefore considered to be useful.

A different approach in modelling that can be followed is based on the elementary particle properties. Promising advances have been recently made in modelling solid-gas fluid dynamics in aerated beds (Langston *et al.*, 1996) and in fluidized beds (Hoomans *et al.*, 1996). To relate the results of such calculations to the experimental data however, it is common to apply one or more parameters to fit the data. These type of models still require fit parameters and furthermore require extensive computational power. It is therefore concluded that the approach based on elementary (or microscopic) particle properties (size and shape) is (at this moment) of less practical value than a model that is based on particle related properties (such as the minimum fluidization velocity and stress ratio).

The model that was developed in this work is capable of describing the orifice flow phenomena in Interconnected Fluidized Beds. The input of the particle related properties that are necessary to perform the calculations can be obtained from straightforward small scale experiments. In chapter 3, the solids flow through orifices will be related to the solids circulation in IFB systems.

**Notation**

$A_d$	: cross sectional area of dense bed	[m <sup>2</sup> ]
$A_{eff}$	: effective orifice area (defined by Equation 2.1)	[m <sup>2</sup> ]
$A_o$	: cross sectional area of the orifice	[m <sup>2</sup> ]
$B$	: empirical constant (defined by Equations 2.12 and 2.13)	[-]
$c$	: empirical constant (defined by Equations 2.11 and 2.12)	[-]
$c$	: radius of the orifice defined in Appendix 2.A	[m]
$C_c$	: contraction coefficient	[-]
$C_D$	: discharge coefficient	[-]
$C_v$	: velocity coefficient	[-]
$D_e$	: effective bubble size	[m]
$d_{orifice}$	: orifice diameter	[m]
$d_p$	: particle diameter	[m]
$F$	: force	[N]
$f$	: friction factor	[-]
$F(\Delta u_z)$	: solid-gas frictional force per unit bed volume or solid-gas frictional pressure drop per unit bed height	[N/m <sup>3</sup> ] [Pa/m]
$g$	: gravitational constant	[m/s <sup>2</sup> ]
$H_{bed}$	: expanded bed height	[m]
$K$	: stress ratio	[-]

## Chapter 2

$K_0$	: stress ratio at $U=0$	[-]
$k$	: orifice correction factor	[-]
OS	: Orifice Shear number (defined by Equation 2.16)	[-]
$P_0$	: pressure at orifice position (Equation 2.4 and 2.5)	[Pa]
$P_1$	: pressure at a position far from the orifice (Equation 2.4 and 2.5)	[Pa]
$P_{\text{compartment}}$	: pressure in pressurized compartment of the experimental jet facility	[Pa]
$P_w$	: perimeter of dense bed	[m]
$\Delta P$	: pressure drop across the orifice	[Pa]
$\Delta P_f$	: shear frictional pressure drop	[Pa]
$P_p$	: particle pressure	[Pa]
Re	: Reynolds number	[-]
T	: temperature	[°C]
U	: superficial gas velocity	[m/s]
u	: absolute or interstitial gas velocity	[m/s]
v	: linear fluid or particle velocity	[m/s]
VN	: dimensionless viscosity number (defined by Equation 2.12)	[-]
W	: weight	[kg]
z	: vertical coordinate	[m]

### Greek

$\alpha_r$	: angle of repose	[°]
$\Delta\sigma_N$	: difference in particle pressure between dense bed and lean bed	[Pa]
$\delta$	: $(U/U_{mf})^{1/2}$ (defined by Equation 2.2)	[-]
$\epsilon_{\text{fixed}}$	: fixed bed voidage	$[\text{m}^3_{\text{gas}}/\text{m}^3_{\text{bed}}]$
$\epsilon_u$	: voidage of the upflowing bed	$[\text{m}^3_{\text{gas}}/\text{m}^3_{\text{bed}}]$
$\zeta_0$	: shape parameter (Equation 2.14)	[-]
$\mu$	: dynamic viscosity of fluid	[Pa.s]
$\sigma_N$	: horizontally directed particle pressure	[Pa]
$\sigma_z$	: vertical particle pressure	[Pa]
$\rho_d$	: bulk density of dense bed	$[\text{kg}/\text{m}^3_{\text{bed}}]$
$\phi_m$	: solids mass flow	[kg/s]

### Subscripts

av	: average
CFD	: computational fluid dynamics
comp	: compartment
d	: dense
eff	: effective
EXP	: experimental
l	: lean
m	: mass
max	: maximum
mf	: minimum fluidization
min	: minimum
o	: orifice
p	: particle
PRED	: predicted
sw	: solid-wall
w	: wall

## References

- Arteaga, P. Tüzün, U., "Flow of binary mixtures of equal-density granules in hoppers-size segregation, flowing density and discharge rates", *Chem. Eng. Sci.*, 45(1), 205-223 (1990).
- Atewologun, A.O., Riskowski, G.L., "Experimental determination of Janssen's stress ratio by four methods for soyabeans under static conditions", *American Soc. of Agricultural Engineers*, 34(5), 2193-2198 (1991).
- Beverloo, W.A., Leniger, H.A., Velde van de, J., "The flow of granular solids through orifices", *Chem. Eng. Sci.*, 15(3), 260-269 (1961).
- Bird, R.B., Steward, W.E. and Lightfoot, E.N., "Transport phenomena", John Wiley and Sons (1960).
- Bolton, L.W., Davidson, J.F., "Dense phase circulating fluidised beds", *Chem. Eng. Comm.*, 62, 31-51 (1987).
- Botteril, J.S.M., Abdul-Halim, B.H., "The open-channel flow of fluidized solids", *Powder Technol.*, 23, 67-78 (1979).
- Botteril, J.S.M., Bessant, D.J., "The flow properties of fluidized solids", *Powder Technol.*, 14, 131-137 (1976).
- Brandt, H.L., Johnson, B.M., "Forces in a moving bed of particulate solids with interstitial fluid flow", *AIChE J.*, 9(6), 771-777 (1963).
- Brinkert, J., "Particle jets in fluidised beds", PhD Thesis, University of Cambridge, Cambridge (1993).
- Brinkert, J., Davidson, J.F., "Fluidised Bed Behaviour: a New Collisional Model", In: *Fluidization VIII; Proceedings of the 8th Engineering Foundation Conference on Fluidization*, Vol. 1, Tours, France, 593-600 (1995).
- Brown, R.L., Richards, J.C., "Profile of flow of granules through apertures", *Trans. Inst. Chem. Eng.*, 38, 243-256 (1960).
- Burkett, R.J., Chalmers-Dixon, P., Pyle, D.L., "On the flow of fluidised solids through orifices", *Chem. Eng. Sci.*, 26, 405-417 (1971).
- Campbell, C.S., Wang, D.G., "Particle pressure in gas-fluidized beds", *Journal of Fluid Mechanics*, 227, 495-508 (1991).
- Chen, T.Y., Walawender, W.P., Fan, L.T., "Moving-bed solids flow between two fluidized beds", *Powder Technol.*, 22, 89-96 (1979).
- Chen, L., Weinstein, H., "Measurement of normal stress and hindrance factor in a collapsing fluidized bed", *Chem. Eng. Sci.*, 49(6), 811-819 (1994).
- Chen, J.C., Polashenski, W., Tuzla, K. "Normal stress in Fluidized Beds". In: *Preprints of Fluidization and Fluid-Particle Systems, 1994 Annual meeting of the AIChE, San Francisco, U.S.A. (Ed.: AIChE)*, 14-19 (1994).
- Cheremisinoff, N.P., Cheremisinoff, P.N., "Rheological behaviour of fluidized solids", Chapter 3, in: *Hydrodynamics of gas-solids fluidization*, Gulf Publishing Co., 91-136 (1984).
- Chin, E.J., Munz, R.J., Grace, J.R., "Dense phase powder feeding from an annular fluidized bed", *Powder Technol.*, 25, 191-202 (1980).
- Chisti, Y., Moo-Young, M., "Improve the performance of airlift-reactors", *Chem. Eng. Prog.*, June, 38-45 (1993).
- Clift, R., Rafailidis, S., "Interparticle stress, fluid pressure and bubble motion in gas-fluidised beds", *Chem. Eng. Sci.* 48(9), 1575-1582 (1993).
- Daniels, T.C., "Measurement of the drag on spheres moving through gaseous fluidized beds", *J. of Mech. Eng. Sci.*, 4, 103-110 (1965).
- Davidson, J.F., Nedderman, J.C., "The hour-glass theory of hopper flow", *Trans. Inst. Chem. Eng.*, 51, 29-35 (1973).

## Chapter 2

---

- Davies, C., Foye, J., "Flow of granular material through vertical slots", *Trans. IChemE* 69(A), 369-373 (1994).
- Davies, C.E., Harris, B.J., "A device for measuring solids flowrates; characteristics and application in a circulating fluidized bed", In: *Fluidization VII; Proceedings of the 7th Engineering Foundation Conference on Fluidization*. (Eds.: Potter, O.E.; Nicklin, D.J.), Brisbane, Australia, 741-748 (1992).
- Davies, C., Fenton, K., "Particle size effects in the discharge of fluidized solids through orifices and vertical slots", In: *Fluidization VIII; Proceedings of the 8th Engineering Foundation Conference on Fluidization*, Vol. 2, Tours, France, 1059-1066 (1995).
- Davies, C.E., Fenton, K., "Continuous estimation of particle size using a fluidized bed with a vertical slot", *Powder Technol.* 88, 89-93 (1996).
- Denn, M.M., "Process fluid mechanics", Prentice-Hall Inc. (1980).
- Di Felice, R., "The voidage function for fluid-particle interaction systems", *International Journal of Multiphase Flow*, 20(1), 153-159 (1994).
- Ergun, S., "Fluid flow through packed columns", *Chem. Eng. Progr.*, 48(2), 89-94 (1952).
- Faber, T.E., "Fluid dynamics for physicists", Cambridge University Press, New York (1995).
- Fox, D., Molodtsov, Y., Large, J.F., "Control mechanisms of fluidized solids circulation between adjacent vessels", *AIChE J.*, 35(12), 1933-1941 (1989).
- Fox, R.W., McDonald, R.W., "Introduction to fluid mechanics", 3rd edition, Wiley, New York (1985).
- Franklin, F.C., Johanson, L.N., "Flow of granular material through a circular orifice", *Chem. Eng. Sci.*, 4, 119-129 (1955).
- Furukawa, J., Ohmae, T., "Liquidlike properties of fluidized systems", *Ind. Eng. Chem.*, 50, 821-828 (1958).
- Geldart, D., Haesebrouck, M., "Studies on the intermittent discharge of coarse solids from fluidized beds", *Chem. Eng. Res. Des.*, 61, 162-166 (1983).
- Geldart, D., Jones, P., "The behaviour of L-valves with granular powders", *Powder Technol.*, 67, 163-174 (1991).
- Gidaspow, D., "Multiphase flow and fluidization and kinetic theory descriptions", Academic Press, New York (1994).
- Grace, J.R., "The viscosity of fluidized beds", *Can. J. Chem. Eng.*, 48, 30-33 (1970).
- Grose, R.D., "Orifice contraction coefficient for inviscid incompressible flow", *Trans. of the ASME*, 107, 36-43 (1985).
- Happel, J., Brenner, H., "Low Reynolds Number Hydrodynamics with special applications to particulate media", Prentice-Hall Inc. (1966).
- Haygard, T., Sacerdote, A.M., "Viscosity of suspensions of gas-fluidised spheres", *Ind. Eng. Chem. Fundam.*, 5, 500-508 (1966).
- He, Y., Rudolph, V., Nicklin, D.J., Chong, Y.O., "Circulating fluidized oil shale retort", *Fuel* 72(6), 879-883 (1993).
- He, Y., Rudolph, V., "A model for the riser of a dense phase circulating fluidized bed", In: *CFB5; Preprints of the 5th International Conference on Circulating Fluidized Beds*, May 28 to June 1, Beijing, Peoples Republic of China, MSS2 (1996).
- Hershey, D., "Transport analysis", Plenum Press, New York-London (1973).
- Hoffmann, A.C., Hartholt, G.P., Yates, J.G., "On the rheology of the dense phase of a gas fluidized bed", *Chem. Eng. Comm.*, 130, 31-44 (1994).
- Holland, F.A., Bragg, R., "Fluid flow for chemical engineers", 2nd edition, Arnold, London (1995).
- Hoomans, B.P.B., Kuipers, J.A.M., Briels, W.J., van Swaaij, W.P.M., "Discrete particle simulation of bubble and slug formation in a two-dimensional gas-fluidised bed: A hard-sphere approach", *Chem. Eng. Sci.*, 51(1), 99-118 (1996).

- Ishida, M., Shirai, T., "Circulation of solid particles within the fluidized bed with a draft tube", *J. Chem. Eng. Jpn.*, 8(6), 477-481 (1975).
- Ishida, M., Shirai, T., "Equilibrium bed heights when a fluidized and a fixed bed are connected through an opening - effect of contracting the bed columns at the gas exit -", *J. Chem. Eng. Jpn.*, 9(3), 249-250 (1976).
- Iversen, K.S., "Hydrodynamics of the Interconnected Fluidized Bed system", MSc report, Technical University of Denmark and Delft University of Technology (1995).
- Jones, D.R.M., Davidson, J.F., "The flow of particles from a fluidised bed through an orifice", *Rheol. Acta*, 4, 180-192 (1965).
- Jong de, J.A.H. "Vertical air-controlled flow from a bunker through circular orifices", *Powder Technol.*, 3, 267-278 (1969)
- Jong de, J.A.H., Hoelen, Q.E.J.J.M., "Cocurrent gas and particle flow during pneumatic discharge from a bunker through an orifice", *Powder Technol.*, 12, 201-208 (1975).
- Jong de, J.A.H., "Aerated solids flow through a vertical standpipe below a pneumatically discharged bunker", *Powder Technol.*, 12, 197-200 (1975).
- Judd, M.R., Dixon, P.D. "The flow of fine, dense solids down vertical standpipe", *AIChE Symp. Ser.*, 74(176), 38-44 (1978).
- Judd, M.R., Dixon, P.D., "The effect of aeration on the flowability of powders", *Trans. IChemE*, 57, 67 (1979).
- Kai, T., Murakami, M., Yamasaki, K.I., Takahashi, T., "Relationship between apparent bed viscosity and fluidization quality in a fluidized bed with fine particles", *J. of Chem. Eng. of Jpn.*, 24(4), 494-500 (1991).
- Kalwar, M.I., Raghavan, G.S.V., Mujumdar, A.S., "Circulation of particles in two-dimensional spouted beds with draft plates", *Powder Technol.*, 77, 233-242 (1993).
- Kececioglu, I., Yang, W., Keairns, D.L., "Fate of solids fed pneumatically through a jet into a fluidized bed", *AIChE J.*, 30(1), 99-110 (1984).
- Kiljański, T., "Discharge coefficient for free jets from orifices at low Reynolds number", *J. of Fluids Engineering*, 115, 778-781 (1993).
- Kim, J.M., Saeder, J.D., "Pressure drop for cocurrent downflow of gas-solid suspensions", *AIChE J.* 29(3) (1983).
- Knowlton, T.M., Hirsan, I., "L-valves characterized for solids flow", *Hydrocarbon Processing*, 149-156 (1978).
- Kono, H.O., Aksoy, E., Itani, Y., "Measurement and application of the rheological parameters of aerated fine powders - A novel characterization approach to powder flow properties", *Powder Technol.*, 81, 177 (1994).
- Korbee, R., "Regenerative desulfurization in an Interconnected Fluidized Bed System", PhD thesis, Delft University of Technology, Delft, The Netherlands (1995).
- Korbee, R., Schouten, J.C., Bleek van den, "Modelling Interconnected Fluidized Bed systems", *AIChE Symp. Series*, 281, 70-77 (1991).
- Korbee, R., Snip, O.C., Schouten, J.C., Bleek van den, C.M., "Rate of solids and gas transfer via an orifice between partially and completely fluidized beds", *Chem. Eng. Sci.*, 49(24B), 5819-5832 (1994).
- Korbee, R., Snip, O.C., Schouten, J.C., Bleek van den, C.M., "Solids and gas transfer via an orifice between partially and completely fluidized beds -design equations and considerations for operation", In: *Fluidization VIII; Proceedings of the 8th Engineering Foundation Conference on Fluidization*, Vol. 1, Tours, France, 665-672 (1995).
- Kraan van der, M., "Techniques for the measurement of the flow properties of cohesive powders", PhD thesis, Delft University of Technology, Delft, The Netherlands (1996).
- Kramers, H., "On the viscosity of a bed of fluidized solids", *Chem. Eng. Sci.*, 1, 35 (1951).

## Chapter 2

---

- Krishna, R., Ellenberger, J., "A unified approach to the scale-up of 'fluidized' multiphase reactors", *Chem. Eng. Res. Des.*, 73(A3), 217-221 (1995).
- Kunii, D., Levenspiel, O., "Fluidization Engineering", 2nd Ed., Butterworth-Heinemann (1991).
- Kuramoto, M., Furasawa, T., Kunii, D., "Development of a new system for circulating fluidized particles within a single vessel", *Powder Technol.*, 44, 77-84 (1985).
- Kuramoto, M., Kunii, D., Furasawa, T. "Flow of dense fluidized particles through an opening in a circulation system", *Powder Technol.*, 47, 141-149 (1986).
- Lamb, H., "A treatise on the mathematical theory of the motion of fluids", Cambridge University Press, Cambridge (1879).
- La Nauze, R.D., "A circulating fluidised bed", *Powder Technol.*, 15, 117-127 (1976).
- La Nauze, R.D., Davidson, J.F., "The flow of fluidized solids", In: Fluidization; proceedings of the Engineering Foundation Conference on Fluidization, (Ed.: Keairns, D.L.), Hemisphere, Washington, 113-125 (1975).
- Langenberg-Schenk van den, G., Rietema, K., "The rheology of homogeneously solids, studied in a vertical standpipe", *Powder Technol.*, 38, 23-32 (1984).
- Langston, P.A., Tüzün, U., Heyes, D.M., "Discrete element simulation of internal stress and flow fields in funnel flow hoppers", *Powder Technol.*, 85, 153-169 (1995).
- Langston, P.A., Tüzün, U., Heyes, D.M., "Distinct element simulation of interstitial air effects in axially symmetric granular flows in hoppers", *Chem. Eng. Sci.*, 51(6), 873-891 (1996).
- Leung, L.S., Chong, Y.O., "Operation of V-valves for gas-solids flow", *Powder Technol.*, 49, 271-276 (1987).
- Li, H. Kwauk, M. "Hydrodynamics of the V-valve", *Chem. Eng. Res. Des.*, 69, 355-360 (1991).
- Manger, E., Solberg, T., Hjertager, B.H., Vareide, D., "Numerical simulation of the ticking hourglass", *Int. J. Multiphase Flow*, 21(4), 561-567 (1995).
- Marring, E., "Fluidization and discharge of cohesive powders", PhD thesis, State University of Groningen, Chapter 1, 1-31 (1989).
- Martin, P.D., Davidson, J.F., "Flow of powder through an orifice from a fluidised bed", *Chem. Eng. Res. Des.*, 61, 162-166 (1983).
- Massimilla, L., "Flow properties of the fluidized dense phase", In: "Fluidization", (Eds.: Davidson, J.F., Harrison, D.), Academic Press, 651-675 (1971).
- Massimilla, L., Betta, V., Rocca Della, C., "A study of streams of solids flowing from solid-gas fluidized beds", *AIChE J.*, 7(3), 502-508 (1961).
- Masson, H., "Design of a compact twinned FB system", In: Fluidization VI; proceedings of the 6th Engineering Foundation Conference on Fluidization. (Eds.: Grace, J.R., Shemilt, L.W., Bergougnou, M.A.), Banff, Canada, 383-392 (1989).
- Merchuk, J.C., Berzin, I., "Distribution of energy dissipation in airlift reactors", *Chem. Eng. Sci.*, 50(14), 2225-2233 (1995).
- Milne, B.J., Berruti, F. Behie, L.A., "The Internally Circulating Fluidized Bed (ICFB): A novel solution to gas bypassing in spouted beds", *Can. J. Chem. Eng.*, 70, 910-915 (1992).
- Molodtsov, Y., Ould-Driss, A., Bogнар, G., "Particle flow through orifices and solids discharge rate from hoppers" In: Fluidization VII; Proceedings of the 7th engineering foundation conference on fluidization. (Eds.: Potter, O.E.; Nicklin, D.J.), Brisbane, Australia, 361-370 (1992).
- Mori, S, Wen, C.Y., "Estimation of bubble diameters in gaseous fluidized beds", *AIChE J.* 21, 109-115 (1975).
- Nedderman, R.M. (Ed.), "Statics and kinematics of granular materials", Cambridge University Press (1992).
- Nedderman, R.M., Tüzün, U., Savage, S.B., Houlsby, G.T., "The flow of granular materials -I- discharge rates from hoppers", *Chem. Eng. Sci.*, 37(2), 1597-1609 (1982).
- Nevers de, N., "Fluid mechanics for chemical engineers", 2nd edition, Mc.GrawHill (1991).

- O'Dea, D.P., Rudolph, V., Chong, Y.O., "Gas-solids flow through the bottom restriction of an inclined standpipe", *Powder Technol.*, 62, 291-297 (1990).
- Olazar, M., San José, M.J., Aguayo, T., Arandes, J.M., Bilbao, J., "Design factors of conical spouted beds and jet spouted beds", *Ind. Eng. Chem. Res.*, 32, 1245-1250 (1993).
- Oosterbaan van, G., "Gas-solid transport in non-mechanical valves and standpipes", Internal report, Delft University of Technology (1995).
- Pennec Le, T., Ammi, M., Messenger, J.C., Truffin, B., Bideau, D., Garnier, J., "Effect of gravity on mass flow rate in an hour glass", *Powder Technol.*, 85, 279-281 (1995).
- Picciotti, M., "Specify standpipes and feeder valves for packed beds", *Chem. Eng. Progr.*, January, 54-63 (1995).
- Reichold, A., Hofbauer, H., "Adsorptionsprozesse in intern zirkulierender Wirbelschicht", *Chemie Ingenieur Technik*, 67(11), 1476-1480 (1995).
- Rhodes, M., Cheng, H., "Operation of an L-valve in a circulating fluidized bed of fine solids", In: CFB4; proceedings of the 4th International Conference on Circulating Fluidized Beds. (Ed.: Avidan, A.A.), 284-289 (1993).
- Richardson, J.F., Zaki, W.N., "Sedimentation and fluidisation. Part 1", *Trans. Inst. Chem. Eng.* 32, 35-53 (1954).
- Rietema, K., "Rheology of fluidized powders", Chapter 9, in: "The dynamics of fine powders", Elsevier Applied Science, 162-186 (1991).
- Roberts, A.W., "100 Years of Janssen", In: Partec 95, 3rd European Symposium Storage and Flow of Particulate Solids (Janssen Centennial), Preprints, (Ed.: Schwedes, J.), Nurnberg, 6-44 (1995).
- Roodenburg, D., "Mechanisms for flow through the orifice in the Interconnected Fluidized Bed - gas and particle flow", MSc report, Delft University of Technology, (1995).
- Rudolph, V., Chong, Y.O., Nicklin, D.J., "Standpipe modelling for circulating fluidized beds", In: CFB III; Proceedings of 3rd International Conference on Circulating Fluidized Beds, (Eds.: Basu, P., Horio, M., Hastani, M.), Nagoya, Japan, 49-64 (1990).
- Salas-Valerio, W.F., Steffe, J.F., "Orifice discharge coefficients for power-law fluids", *Journal of Food Process Engineering*, 12(2), 89-98 (1989).
- Sarkar, M., Gupta, S.K., Sarkar, M.K., "Experimental investigation of solids flow from aerated beds through inclined pipes", *Trans. IChemE* 69(A), 361-368 (1991a).
- Sarkar, M., Gupta, S.K., Sarkar, M.K., "An experimental investigation of the flow of solids from a fluidized bed through an inclined pipe", *Powder Technol.*, 64, 221-231 (1991b).
- Sarkar, M., Gupta, S.K., Sarkar, M.K., "Experimental investigation on gravity flow of solids through inclined pipes", *Chem. Eng. Sci.*, 46, 1137-1144 (1991c).
- Schlichting, H., "Boundary-Layer Theory", 6th edition, New York (1968).
- Schügerl, K., "Rheological behaviour of fluidized systems", Chapter 6, in: "Fluidization", Davidson, J.F.; Harrison, D. (Eds.), Academic Press London, 261-291 (1971).
- Schügerl, K., Merz, M., Fetting, F., "Rheologische Eigenschaften von Gasdurchströmten Fließbettssystemen", *Chem. Eng. Sci.*, 15, 1-38 (1961).
- Shamlou, P., (Ed.), "Handling of bulk solids; theory and practice", Butterworth, London (1988).
- Siemes, W., Hellmer, L., "Die Messung der Wirbelschicht viskosität mit der pneumatischen Rinne", *Chem. Eng. Sci.*, 17, 555-571 (1962).
- Singh, B. Callcott, T.G., Rigby, G.R., "Flow of fluidized solids and other fluids in open channels", *Powder Technol.*, 20, 99-113 (1978).
- Snip, O.C., Korbee, R., Schouten, J.C., Bleek van den, C.M., "Solids and gas transport from and between aerated and fluidized beds", *AIChE Symp. Series*, 92 (313), 76-80 (1996).
- Snip, O.C., Schouten, J.C., Bleek van den, C.M., "Micro- and macroscopic transport phenomena -On the use of transport equations: theory and experiments", to be submitted to *Chem. Eng. Education* (1997).

## Chapter 2

---

- Stanley, C.K., Bridgewater, J., Botteril, J.S.M., "Solids flow between Interconnected shallow Fluidized Beds", *Chem. Eng. Sci.*, 39(12), 1797-1806 (1984).
- Street, R.L., Watters, G.Z., Vennard, J.K., "Elementary fluid mechanics", 7th edition, John Wiley & Sons (1996).
- Takeshita, T., Harada, M. Yoshima, H; Yamazaki, R., Jimbo, G., "Characteristics of discharge of aerated granular materials through an orifice", *Int. Chemical Engineering*, 30(2), 268-273 (1990).
- Tan, R.B.H., Davidson, J.F., "Liquid-particle jets from fluidised beds", *Chem. Eng. Sci.*, 44(12), 2899-2907 (1989).
- Verghese, T.M., Nedderman, R.M., "The discharge of fine sands from conical hoppers", *Chem. Eng. Sci.*, 50(19), 3143-3153 (1995).
- Watson, G.R., Rotter, J.M., "A finite element kinematic analysis of planar granular solids flow", *Chem. Eng. Sci.*, 51(16), 3967-3978 (1996).
- Wen, C.Y., Yu, Y.H., "A generalized method for predicting the minimum fluidization velocity", *AIChE J.*, 12, 610-615 (1966).
- Woodcock, C.R., Masson, J.S. (Eds.), "Bulk solids handling", 1st Ed., Chapman and Hall, New York, 47-55 (1987).
- Yang, H., Gautam, M., "The design and performance of a novel standpipe", *Industrial and Environmental Applications of Fluid Mechanics*, 145, 33-39 (1992).
- Yang, H., Gautam, M., "Gas-solid flow in a novel standpipe", *Powder Technol.*, 78, 91-98, (1994).
- Yang, W.C., Keairns, D.L., "Recirculating fluidized bed reactor data utilizing a two-dimensional cold model", *AIChE Symp. Series*, 70, 27-40 (1974).
- Yang, W.C., Keairns, D.L., "Design of recirculating fluidized beds for commercial applications", *AIChE Symp. Ser.*, 74(176), 218-228 (1978).
- Yang, W.C., Knowlton, T.M., "L-valve equations", *Powder Technol.*, 77, 49-54 (1993).
- Yamashiro, M., Yuasa, Y., "Effects of opening diameter of orifice at the bottom of a cylindrical vessel and the height of solids layer on flow rates of particles", *J. of Powder & Bulk Solids Technology*, 9(1), 9-15 (1985).
- Yoon, S.M., Kunii, D., "Gas flow and pressure drop through moving beds", *Ind. Eng. Chem. Process Des. Develop.*, 9(4), 559-565 (1970).
- Zehner, P., Benfer, R., "Modelling fluid dynamics in multiphase reactors", *Chem. Eng. Sci.*, 51(10), 1735-1744 (1996).
- Zhang, J.Y., Rudolph, V., "Effect of shear friction on solid flow through an orifice", *Ind. Eng. Chem. Res.*, 30(8), 1977-1981 (1991).



## Appendix 2.A:

### Derivation of a macroscopic pressure drop relation for orifice flow.

The shear frictional pressure drop is caused by microscopic forces within the fluid. It is therefore necessary to start the derivation of a macroscopic pressure drop relation for orifice flow at the microscopic equations of motion.

Which type of coordinate system is preferred to solve the flow problem depends on the geometry. Subject to the symmetry of the flow, it can be solved in one or more dimensions. The analytical solutions of the equations of motion are mainly limited to steady flow in two dimensions. In some textbooks (Bird *et al.*, 1960; Hershey, 1973; Denn, 1980) the flow through various geometrical configurations is treated.

The problems are solved in rectangular ( $x,y,z$ ), cylindrical ( $r,\theta,z$ ) or spherical ( $r,\theta,\phi$ ) coordinate systems. Due to the symmetry in the flow field, the problem is generally reduced to two dimensions. This leaves a set of two partial differential equations to be solved.

For several classes of flows with constant density ( $\rho$ ) and viscosity ( $\mu$ ), the differential equations may be somewhat simplified by formulation in terms of a stream function  $\psi$ . The velocity components are expressed as derivatives of  $\psi$  (see Bird *et al.*, Table 4.2-1, 1960) in such a way that the equation of continuity is automatically satisfied. The physical significance of the stream function is that lines of constant  $\psi$  are the curves or streamlines actually traced by the particles of the fluid. The flow problem is transformed to a problem in which a solution for  $\psi$  as a function of the coordinates needs to be found.

The so-called oblate spheroidal coordinates (see Figure 2.A.1) are particularly useful in the case of orifice flow or flow through a converging section towards the orifice (see Lamb, 1879; Happel and Brenner, 1966). Three coordinates ( $\xi, \eta, \phi$ ) are defined that determine the points in space. The relationships between rectangular and oblate spheroidal coordinates are:

$$\begin{aligned} x &= c \sinh \xi \cos \eta \\ y &= c \cosh \xi \sin \eta \end{aligned} \quad (\text{A.2.1})$$

The ranges for the coordinates have to be limited to:

$$0 \leq \xi < \infty, \quad 0 \leq \eta \leq \pi, \quad 0 \leq \phi < 2\pi \quad (\text{A.2.2})$$

In order to simplify mathematics and to obtain more insight,  $\lambda$  and  $\zeta$  are defined as:

$$\lambda = \sinh \xi, \quad \zeta = \cos \eta \quad (\text{A.2.3})$$

The coordinate  $\lambda$  can be considered as the distance from the orifice. The widening in the stream tube is characterized by  $\zeta$ . The surface of the hyperboloid which coincides with the tube is denoted by  $\zeta_0$  (see Figure 2.16). When it is assumed that the stream surfaces coincide with the surfaces of the hyperboloids, *i.e.*  $\zeta = \text{constant}$ , it follows that the stream function is only a function of  $\zeta$ . It is further assumed that a converging section as defined in this coordinate system is representative for flow towards an orifice.

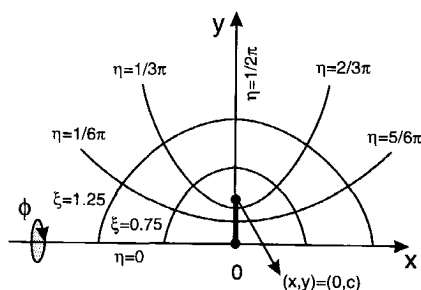


Figure 2.A.1 Oblate spheroidal coordinate system.

## Appendix 2.A

For steady creeping flow (= low Reynolds number), the solution of  $\psi$  has to satisfy the following differential equation (see Bird *et al.*, Table 4.2-1, 1960):

$$E^4 \psi = 0 \rightarrow E^2 (E^2 \psi) = 0 \quad (\text{A.2.4})$$

Happel and Brenner (1966) give an expression for the operator  $E^2$  in oblate spheroidal coordinates ( $c$  is the radius of the orifice):

$$E^2 = \frac{1}{c^2(\lambda^2 + \zeta^2)} \left( (\lambda^2 + 1) \frac{\partial^2}{\partial \lambda^2} + (1 - \zeta^2) \frac{\partial^2}{\partial \zeta^2} \right) \quad (\text{A.2.5})$$

A detailed analysis of this problem leads to the following expression for the stream function:

$$\psi(\zeta) = \frac{q}{2\pi} \frac{\zeta(\zeta^2 - 3\zeta_0^2) - (1 - 3\zeta_0^2)}{(1 + 2\zeta_0)(1 - \zeta_0)^2} \quad (\text{A.2.6})$$

(in which  $q$  is the volumetric flow rate).

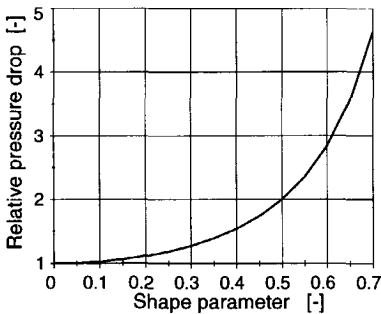
Relating the pressure distribution to the stream function yields a relationship for the pressure drop that is experienced by a fluid traversing the duct:

$$\Delta P = \frac{3q\mu}{c^3(1 + 2\zeta_0)(1 - \zeta_0)^2} \quad (\text{A.2.7})$$

Appreciating symmetry in the flow towards and after the orifice and rewriting Equation A.2.7 in terms of an orifice diameter ( $d_{\text{orifice}}$ ) and fluid velocity ( $v$ ) results in:

$$\Delta P = \frac{3\pi\mu v}{d_{\text{orifice}}(1 + 2\zeta_0)(1 - \zeta_0)^2} \quad (\text{A.2.8})$$

It is interesting to investigate the influence of  $\zeta_0$  on the pressure drop. It is convenient to relate the pressure drop for a given  $\zeta_0$  to the special case of  $\zeta_0 = 0$  which corresponds to a hemi-spherical flow towards the orifice. In Figure 2.A.2 this relative pressure drop is plotted as a function of the shape parameter  $\zeta_0$ .



**Figure 2.A.2** The influence of shape parameter  $\zeta_0$  on pressure drop.

For decreasing  $\zeta_0$ , the influence of the shape rapidly decreases. It is believed that in most flow problems encountered in practice, the shape factor  $\zeta_0$  is well below 0.4. Furthermore, it is very difficult to predict the exact flow profile in most flow problems. To estimate the influence of shear friction in a qualitative way it is sufficient to assume a hemi-spherical flow profile. Equation A.2.8 then becomes:

$$\Delta P = \frac{3\pi\mu v}{d_{\text{orifice}}} \quad (\text{A.2.9})$$

The macroscopic pressure drop relationship (A.2.9) is only valid under the assumptions of a hemi-spherical flow profile ( $\zeta_0 = 0$ ), for Newtonian fluids and at low Reynolds numbers.

## Appendix 2.B:

### Outline of the mathematical model for orifice flow in the IFB system.

In this appendix, an outline is given of the mathematical model for orifice flow of gas and solids in the IFB system. The main equations are derived, described and discussed in chapter 2. It is believed however that it is useful to provide a comprehensive overview of all equations that make up the mathematical model for orifice flow in the IFB system. For a detailed explanation of the various terms, reference is made to chapter 2.

The model is suited for the prediction of solids and gas flow through an orifice between a dense and a lean bed. The input of the following particle and gas properties, IFB geometry parameters and operational parameters is required.

#### Input variables and model parameters

##### Particle properties

$d_p$	particle diameter	[m]
$\rho_p$	density of the particles	[kg/m <sup>3</sup> ]
$\phi_s$	particle shape factor	[-]
$f$	solid-wall friction factor	[-]
$K_0$	stress ratio at $U_{eff}=0$	[-]
$\epsilon_{fixed}$	voidage at $U_{eff}=0$	[m <sup>3</sup> <sub>gas</sub> /m <sup>3</sup> <sub>bed</sub> ]
$U_{mf}$	minimum fluidization velocity	[m/s]

##### Gas properties

$\mu_{gas}$	dynamic gas viscosity	[Pa·s]
$\rho_{gas}$	gas density	[kg/m <sup>3</sup> ]

##### IFB geometry and model parameters

$d_{orifice}$	orifice diameter	[m]
$A_d, A_l$	cross-sectional area of dense and lean bed	[m <sup>2</sup> ]
$P_w$	perimeter of dense bed	[m]
$H_d, H_l$	expanded bed height of dense and lean bed	[m]
$H_{orifice}$	height of the orifice from distributor plate	[m]
$x$	radius of the hemisphere at which the solids and gas start to accelerate towards the orifice	[m]

##### Operational parameters

$U_d, U_l$	superficial gas velocity in dense and lean bed	[m/s]
$\epsilon_d, \epsilon_l$	dense and lean bed voidage fraction	[m <sup>3</sup> <sub>gas</sub> /m <sup>3</sup> <sub>bed</sub> ]

#### Model equations

The most important equation describing the solids flow as a function of the driving and resisting forces is given in chapter 2.3.2 (Equation 2.7):

$$\phi_m = A_{eff} \rho_d \sqrt{\frac{2(\Delta P + \Delta\sigma_N - \Delta P_f)}{\rho_d}} \quad (\text{A.2.1})$$

## Appendix 2.B

The volumetric gas flow through the orifice ( $\phi_{g,orifice}$ ) is related to the gas pressure drop across the orifice ( $\Delta P$ ) according to:

$$\Delta P = \frac{150}{2\pi} \left( \frac{1-\epsilon_d}{\epsilon_d} \right)^2 \frac{\mu}{(\phi_s d_p)^2} \Delta\phi \left( \frac{1}{r'_0} - \frac{1}{x} \right) + \gamma \frac{1.75}{12\pi^2} \left( \frac{1-\epsilon_d}{\epsilon_d} \right) \frac{\rho_g}{\phi_s d_p} \Delta\phi^2 \left( \frac{1}{r'_0{}^3} - \frac{1}{x^3} \right) \quad (\text{A.2.2})$$

in which  $\gamma=1$  if  $\Delta\phi > 0$  and  $\gamma=-1$  if  $\Delta\phi < 0$ . The terms  $\Delta\phi$  and  $r'_0$  are calculated from:

$$r'_0 = \left( \frac{1}{\sqrt{8}} \right) d_{orifice} \quad (\text{A.2.3})$$

and:

$$\Delta\phi = \frac{\phi_{g,orifice}}{\epsilon_d} - \frac{\phi_m}{\rho_p(1-\epsilon_d)} \quad (\text{A.2.4})$$

The terms  $r'_0$  and  $\Delta\phi$  represent respectively the radius of a hemisphere with an area equivalent to the orifice and the difference between volumetric gas and solids flow through the orifice. The gas flow is in this respect treated separately from the solids flow in order to calculate the interaction or drag force between the gas phase and the solids phase. The term  $r'_0$  follows from the assumption that the gas flows perpendicular to a hemisphere (centered around the orifice) and the equation of continuity for the gas phase (Korbee, 1995).

In order to solve the set of equations (A.2.1-A.2.4) in an iterative way, the effective gas velocities in dense and lean bed need to be calculated. In the general case of a positive driving force for both gas and solids flow (*viz.*, gas and solids flow from dense to lean bed), the effective gas velocities in dense and lean bed are calculated according to:

$$U_{eff,d} = U_d - \epsilon_d \frac{\Delta\phi}{A_d} \quad (\text{A.2.5})$$

$$U_{eff,l} = U_l + \epsilon_l \frac{\Delta\phi}{A_l} \quad (\text{A.2.6})$$

The slip velocity between solids and gas phase in the dense bed (in which the particles flow downwards against the gas flow) is determined from:

$$\Delta u_z = \frac{U_{eff,d}}{\epsilon_d} - \frac{\Delta\phi}{A_d} \quad (\text{A.2.7})$$

The pressure drop across the orifice depends on the pressure in dense ( $P_d$ ) and lean bed ( $P_l$ ) at orifice height:

$$\Delta P = P_d - P_l \quad (\text{A.2.8})$$

The pressures  $P_d$  and  $P_l$  are calculated according to:

$$P_d = \left( 150 \left( \frac{1 - \epsilon_{bed}}{\epsilon_{bed}} \right)^2 \frac{\mu_{gas}}{(\phi_s d_p)^2} \Delta u_z + 1.75 \left( \frac{1 - \epsilon_{bed}}{\epsilon_{bed}} \right) \frac{\rho_g}{\phi_s d_p} \Delta u_z^2 \right) (H_d - H_{orifice}) \quad (\text{A.2.9})$$

$$P_l = \rho_p (1 - \epsilon_{bed}) g (H_l - H_{orifice}) \quad (\text{A.2.10})$$

The effective orifice area ( $A_{eff}$ ) is calculated according to:

$$A_{eff} = \frac{1}{4} \pi (d_{orifice} - d_p)^2 \quad (\text{A.2.11})$$

The difference in horizontally directed particle pressure ( $\Delta\sigma_N$ ) is calculated from:

$$\Delta\sigma_N = K\sigma_z - P_p \quad (\text{A.2.12})$$

in which the terms  $\sigma_N (=K\sigma_z)$  and  $P_p$  represent the dense bed particle pressure and the lean bed resistance respectively. The lean bed resistance is determined from the empirical correlation presented in chapter 2 (Equation 2.9):

$$P_p = 0.08 \rho_p g D_e \quad (\text{A.2.13})$$

The horizontal particle pressure in the dense bed is calculated from:

$$\sigma_z = \frac{A_{bed}}{fKP_w} \left( \rho_p (1 - \epsilon_d) g - \frac{P_d}{(H_d - H_{orifice})} \right) \left( 1 - \exp \left( \frac{-fKP_w}{A_{bed}} (H_d - H_{orifice}) \right) \right) \quad (\text{A.2.14})$$

in which the stress ratio ( $K$ ) is calculated according to:

$$K = K_0 + (1 - K_0) \frac{U_{d,eff}}{U_{mf}} \quad (\text{A.2.15})$$

The shear frictional pressure drop ( $\Delta P_f$ ) is calculated from:

$$\Delta P_f = \frac{3 \pi \mu_{solids} v_{solids}}{d_{orifice}} \quad (\text{A.2.16})$$

in which the linear solids velocity in the orifice ( $v_{solids}$ ) and the apparent solids viscosity ( $\mu_{solids}$ ) are determined from:

$$v_{solids} = \frac{\phi_m}{\rho_p (1 - \epsilon_d) A_{eff}} \quad (\text{A.2.17})$$

and:

$$\mu_{solids} = 29.3 (\rho_p d_p U_{d,eff}) \left( \frac{U_{d,eff}}{U_{mf}} \right)^{-1.42} \quad (\text{A.2.18})$$

## Appendix 2.B

---

The latter correlation for the prediction of the apparent viscosity of a gas-solids mixture is based on literature data in the range of experimental conditions given in Table 2.2.

The solids and gas flows can be calculated on the basis of the above listed equations. The numerical solution is obtained in an iterative way. Driving and resisting forces are a function of the solids and gas flow. The model presented above is used in chapter 2.6.3 for the prediction of the orifice flow phenomena.

# Chapter 3

## Solids distribution and dynamics of solids circulation in the IFB system

---

### 3.1 Modelling IFB reactor hydrodynamics

#### 3.1.1 IFB reactor hydrodynamics

The chemical performance of the IFB reactor depends to a great extent on the Circulation Rate of the Solids (CRS); *viz.*, rate of solids circulation between the reactors. In chapter 2.1 (Figure 2.3) it is schematically shown how the CRS can be determined from:

- ▶ design parameters (particle properties and IFB geometry), and
- ▶ operational conditions (gas velocities and total IFB bed mass).

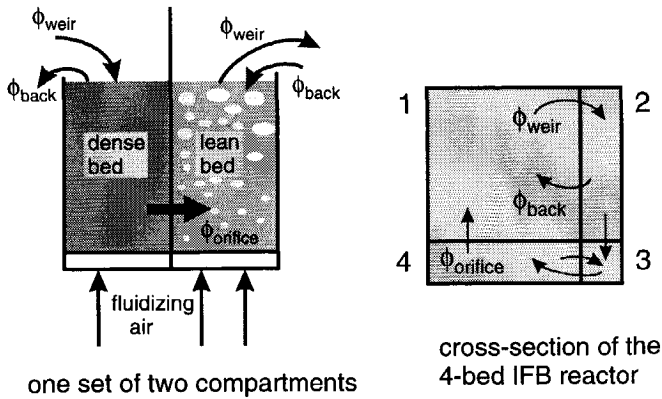
In order to predict the CRS in an IFB system, a model needs to be defined that predicts:

1. distribution of the solids over the compartments,
2. solids flow over the weir, and
3. solids flow through the orifice.

These models are interconnected as shown in chapter 2.1 (Figure 2.3). The orifice flow was studied and treated in detail in chapter 2. A model was developed that predicts the solids transport between two compartments that are connected by means of an orifice. In general the orifice connects two beds that are operated in such a way that there is a net driving force for solids flow. In practice this means that a dense bed (low gas velocity) is connected to a lean bed (high gas velocity) as shown in Figure 3.1. The orifice flow model can be used when the bed mass in the respective compartments is known. The driving and resisting forces for solids flow are determined by the solids holdup in dense and lean bed. The bed mass in the compartments thus needs to be predicted for an estimation of the orifice flow.

The CRS is determined by the smallest net driving force for solids flow. Depending on the operational conditions and the total bed mass in the IFB system, the CRS determining transport process can be either weir flow or orifice flow. The solids flow rate over the weir, from one compartment to the other, depends to a great extent on the bed mass in the overflowing compartment.

The weir flow phenomenon is experimentally studied, resulting in an empirical model. This is described in chapter 3.1.2. The orifice flow was treated in detail in chapter 2 and some aspects are briefly mentioned in this chapter. Finally, an overall mathematical model for the IFB hydrodynamics (*i.e.*, solids distribution and circulation) is developed in chapter 3.1.3.



**Figure 3.1** One set of two compartments of the IFB reactor system with the in- and outlet solids flow for dense and lean bed and a cross-sectional view of the 4 bed IFB reactor. The back flow of solids from a dense bed to a lean bed occurs when the orifice from a dense to a lean bed is rate limiting. The solids will thus accumulate in the dense bed until the bed is filled up to the weir.

The equations for the IFB model that are presented in this chapter concern the steady-state as well as the dynamic behaviour of the IFB system. A differential equation will thus describe each of the transport processes. The IFB hydrodynamics can be predicted when the resulting set of differential equations is simultaneously solved. The steady-state result can be predicted by the IFB model as well. The model is developed for the case of four interconnected fluidized beds. This is because the four beds represent the IFB reactor and its features for a reaction/regeneration process. At least four beds are necessary to carry out such a process. The mathematical model for the IFB hydrodynamics will be especially used to predict the steady-state and dynamic behaviour of the IFB pilot plant (as described in chapter 4). The dynamic behaviour of the IFB reactor is studied to obtain insight in the effect of external disturbances and the operational parameters that can be used to control the IFB reactor performance (as explained in chapter 3.3).

The development of the model and a detailed description is given by Verlaat (1995) and van Ling (1996). The mathematical model for IFB hydrodynamics is further described in Appendix 3.A.

### 3.1.2 Solids distribution and solids transport in the IFB reactor

#### *Solids distribution*

The solids distribution over the compartments of the IFB system determines the IFB reactor performance in two distinct ways. First, it will influence the CRS in the IFB system. This affects the reactor performance by means of the average particle residence times in the reactor and regenerator. Further, the total amount of solids and the solids distribution will determine the amount of solids that is available in each of the chemical reactive compartments of the IFB reactor. This will directly affect the chemical performance of the reactor and regenerator.



The solids holdup in the respective IFB compartments can be determined from the general mass balance:

$$\frac{dM_i}{dt} = \phi_{in} - \phi_{out} \tag{3.1}$$

in which  $M_i$  is the bed mass of compartment  $i$  and  $\phi_{in}$  and  $\phi_{out}$  are the inlet and outlet mass flows. Solving the mass balances for the four IFB compartments yields the solids distribution, *viz.*, the bed mass in each of the compartments.

Depending on the operating conditions, a compartment can be a dense (low gas velocity) or a lean bed (high gas velocity). Two types of flow can occur between the compartments (see Figure 3.1 for a schematic view of one set of two compartments of the IFB reactor): the solids can flow either over a weir or through an orifice.

The total amount of solids in the IFB system determines whether the beds are filled higher than or below the weir. The weir flow in the main direction of flow (from lean to dense bed) contributes to solids circulation in the IFB system. However, when the dense beds become filled above the weir some of the solids that cannot be transported through the orifice will return to the lean bed. This flow is denoted as back flow. The mass balance of each bed then becomes:

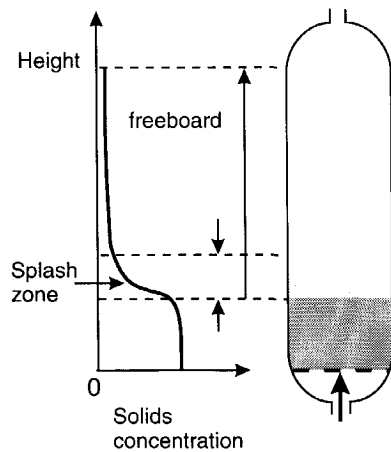
$$\frac{dM_i}{dt} = \phi_{in,or} + \phi_{in,weir} + \phi_{in,back} - \phi_{out,or} - \phi_{out,weir} - \phi_{out,back} \tag{3.2}$$

in which each term on the right-hand side of the equation is a mass flow as shown in Figure 3.1. The mass flows can be either inlet or outlet terms depending on the operational conditions of the compartment that is concerned.

**Weir flow**

In general, a fluidized bed consists of a dense bed zone with a relatively high solids concentration. Due to breaking of bubbles and slugs at the bed surface, a splash zone is formed by ejection of the particles. These phenomena are more or less separated from an upper zone in which the solids concentration is small and decreases with height. The flux of solids caused by the gas taking particles into the freeboard is called entrainment or carryover. A schematical representation of a fluidized bed and its freeboard is shown in Figure 3.2. Because the bulk density of solids decreases with height, increasing the height of the freeboard decreases the particle entrainment from the bed.

The Transport Disengaging Height (TDH) is referred to as the height above which



**Figure 3.2** Schematical representation of a fluid bed freeboard. The solids concentration decreases as a function of the height.

### Chapter 3

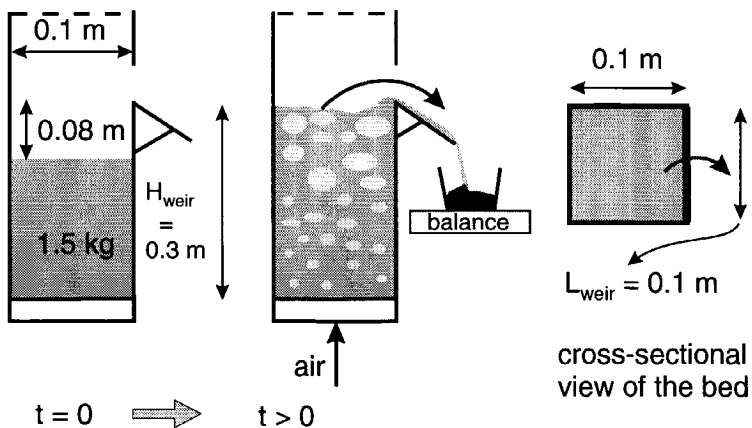
entrainment does not change appreciably. The phenomenon of elutriation refers to the effect of separation of large from small particles in the freeboard.

Particle entrainment and elutriation were studied by many investigators especially due to the relevance of these phenomena with respect to high velocity fluidization and riser reactor technology. See Geldart (1986) and Kunii and Levenspiel (1991) for an overview of experimental findings and theoretical considerations.

With respect to weir flow in the IFB reactor, these phenomena are relevant to the lower part of the freeboard, the splash zone. This is because the IFB reactor will be operated in a bubbling or slugging fluidization regime. In this regime, the solids flow over the weir can only reach a sufficient rate (for the regeneration of the solid material) if the bed is filled with an amount of solids such that the weir flow is related to the splash zone of the fluidized bed.

An important observation is reported by Caram *et al.* (1984). They found that the initial velocity of ejected particles is only dependent on the size (rise velocity) of the bubble and not on particle size and density. For weir flow in the IFB reactor it therefore seems reasonable to assume that the whole spectrum of particle sizes present in the bed is thrown into the freeboard and to the other compartment.

Many studies have been carried out on the lean zone above a fluidized bed. They give a qualitatively coherent picture of the freeboard behaviour. However, quantitatively a considerable disagreement between experimental results is observed. Sometimes this is an order of magnitude or more (Kunii and Levenspiel, 1991). The reasons for this, arise from the different and unaccounted physical conditions during the experiments. The most important differences are the size of the beds (small versus large) and the fluidized bed operating regime (bubbling versus slugging). The latter depends importantly on the type and size of the particles being used.



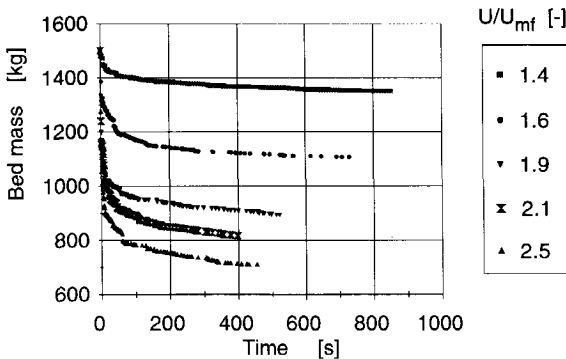
**Figure 3.3** Experimental facility for batch-wise weir flow experiments. The amount of solids that is thrown over the weir is recorded as a function of time until the solids flow approximates zero.

The above mentioned considerations were the reason that weir flow experiments were carried out for the sorbent particles (SGC-500; see Table 2.5 in chapter 2) in a separate fluidized bed facility. Representative, in this context, is the relation to the size of the IFB pilot plant (see Table 4.2, chapter 4). These experiments are used to formulate a model describing the weir flow from a lean bed to a dense bed compartment.

**Weir flow experiments**

The experiments were carried out in the experimental facility as shown in Figure 3.3. Before the start of the experiments the bed was filled with 1.5 kg of sorbent particles. The bed height without expansion reached up to 0.08 m from the height of the weir. This was enough to ensure that the initial weir flow was not caused by bed expansion.

The bed was subsequently fluidized until a steady-state bed mass was reached. The weight of the solids that leave the bed is recorded as a function of time by means of a balance. The relative gas velocity ( $=U/U_{mf}$ ) was varied between 1.4 to 2.5 at 12 different gas velocities. In Figure 3.4, the bed mass in the fluidized bed is shown as a function of time for the indicated relative gas velocities. It can be observed that initially the flow rate (slope of the curve) is high and decreases to a small value that is approximating zero. It is assumed that the last value measured is the steady-state bed mass ( $M_{ss}$ ).



**Figure 3.4** Actual bed mass in the fluidized bed during the weir flow experiments at the indicated gas velocities as a function of time. Initial bed mass for all experiments was 1500 g.

**Weir flow modelling**

On the basis of these experiments an empirical model is developed to describe the weir flow in the IFB reactor. When the steady-state bed mass is plotted against the relative gas velocity, Figure 3.5 is obtained. The steady-state bed mass decreases with increasing gas velocity. The particles are thrown higher in the freeboard at higher gas velocity by the increased slug rise velocity. The particles that were used show a typical slugging fluid bed behaviour.

An empirical equation that can describe the measured steady-state bed mass is:

$$M_{ss} = K_1 \left( \frac{U}{U_{mf}} \right)^{-1} + K_2 \tag{3.3}$$

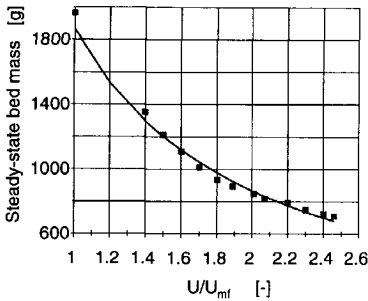
## Chapter 3

The above correlation is fitted to the experimentally determined steady-state bed mass. The result is shown in Figure 3.5 and the values for the constants  $K_1$  and  $K_2$  are given in Table 3.1. Values for  $K_1$  and  $K_2$  are based on data for bed mass measured in kg.

**Table 3.1** Constants in Equations 3.3 and 3.4 fitted to the experimental data of the weir flow experiments.

Constant	$K_1$	$K_2$	$C_1$	$C_2$
Value	$2.005 \pm 0.065$	$-0.134 \pm 0.037$	$10.5 \cdot 10^{-12} \pm 7.9 \cdot 10^{-12}$	$4.76 \pm 0.11$

The steady-state bed mass of the fluidized bed compartment can now be calculated from Equation 3.3 in the range of gas velocities from 1.0 to 2.4 m/s.



**Figure 3.5** Steady-state bed mass in the fluidized bed as a function of the relative gas velocity. The curve is fitted according to Equation 3.3.

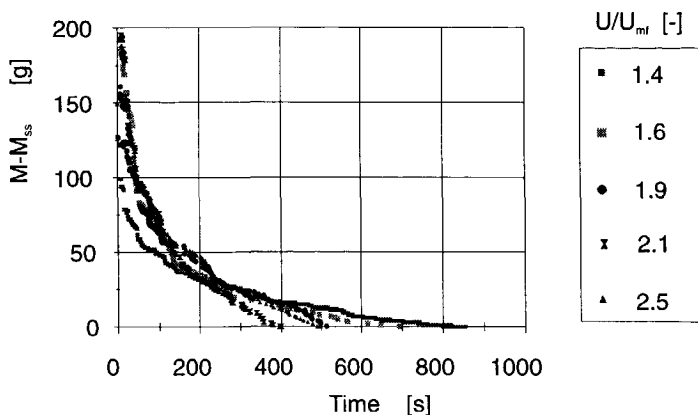
Further, a model for the non-stationary weir flow needs to be developed when the non-steady-state behaviour of the IFB reactor is to be predicted. In the IFB reactor the solids flow over the weir is a continuous process. Solids are transported into the lean bed through the orifice and carried away over the weir to the next dense bed. The steady-state bed mass (as determined in the weir flow experiments and predicted by Equation 3.3) will therefore not be reached when solids are circulating in the IFB reactor.

The driving force for solids transport over the weir is assumed to be the difference between the momentary bed mass and the steady-state bed mass.

In Figure 3.6, the momentary minus the steady-state bed mass ( $M - M_{ss}$ ) is plotted as a function of time. It is assumed that the gas velocity through the bed only affects  $M_{ss}$ . The mechanism of the entrainment from the bed is assumed to be equivalent for all gas velocities. The two constants ( $C_1$  and  $C_2$ ) in the empirical equation (3.4) are therefore assumed to be no function of the gas velocity. The non-steady-state weir flow is then described by:

$$\phi_{weir} = -\frac{dM}{dt} = C_1 (M - M_{ss})^{C_2} \quad (3.4)$$

This equation was fitted to the experimental data shown in Figure 3.4 and the resulting values for the constants  $C_1$  and  $C_2$  are given in Table 3.1. The non-stationary solids flow over the weir can be described by Equation 3.4 applying the constants  $C_1$  and  $C_2$  in the range of gas velocities from 1.0 to 2.4 m/s. The weir flow ( $\phi_{weir}$ ) is thus a function of the bed mass  $M$  at time  $t$ . The large error in the fitted constant  $C_1$  will result in a large error in the predicted value for the non-stationary weir flow.



**Figure 3.6** Actual minus steady-state bed mass in a batch-wise weir flow experiment as a function of time for the indicated relative gas velocities.

In the IFB reactor, a steady-state will be reached after some time (see chapter 3.3) with respect to the hydrodynamics of the reactor. This means that the solids distribution (bed mass in the compartments) and CRS (solids flow through the orifice and over the weir) are constant. The bed mass in the lean beds at this steady-state will be higher than the steady-state bed mass ( $M_{ss}$ ) that was determined in the weir flow experiments. This is due to the fact that during IFB operation a certain solids flow rate is established. To obtain this flow rate, the actual bed mass is higher than  $M_{ss}$ . The weir flow, described by Equations 3.3 and 3.4, thus determines the steady- and non-steady-state solids distribution. Since the distribution of solids also affects the orifice flow, the weir flow will thus influence the CRS in the IFB reactor (as schematically shown in Figure 2.3).

#### *Influence of bed geometry on weir flow*

The correlation to describe weir flow from a fluidized bed is based on batch experiments that were carried out in a  $0.1 \times 0.1 \text{ m}^2$  facility. For other sized compartments it is possible to use the same correlation if the effects of bed geometry are properly taken into account.

The two most important geometries that will affect the weir flow are:

- ▶ the bed surface area:  $A_{bed}$ ,
- ▶ the length of the weir:  $L_{weir}$ .

The bed surface area determines the entrainment capacity of the bed and will thus influence the rate of solids transport over the weir. In order to correct for differences in bed surface area, the bed mass should be related to the surface area of the bed. The bed mass in the equation for solids flow over the weir, Equation 3.4, is therefore substituted for the modified characteristic bed mass:

$$M^* = \frac{M}{A_{bed}} \quad (3.5)$$

This characteristic bed mass equals the product of bed height and bulk density. This is in agreement with the assumption that the distance between the bed height at steady-state and the height of the weir is equivalent for all bed sizes. The bulk density of the bed is assumed to be the same for similar fluidization velocities. Based on the experimental standard ( $A_{bed,exp}$ ), the weir flow equation (Equation 3.4) is corrected for the surface area of the bed. The following equation is obtained:

$$\phi_{weir} = C_1 \left( \frac{A_{bed,exp}}{A_{bed}} \right)^{C_2-1} (M - M_{ss})^{C_2} \quad (3.6)$$

By this equation, the rate of entrainment that was observed in the weir flow experimental facility is related to other bed geometries concerning the bed surface area. The rate of entrainment describes the process of particles that are thrown into the freeboard. However, some of these particles fall back onto the bed and do not leave the bed via the weir. The length of the weir controls to a certain extent the fraction of the particles that does leave the bed over the weir. Its effect is however not straightforward. From geometrical considerations it can be supposed that the weir flow is proportional to:

1. the length of the weir,
2. the ratio between weir length and bed surface area, and
3. the ratio between weir length and bed width (or length, the distance between weir and opposite wall).

The weir flow experiments were carried out in a square 0.1x0.1 m<sup>2</sup> bed with a weir length of 0.1 m. No other bed geometries were investigated experimentally on their weir flow characteristics. The main purpose of the model was to predict the hydrodynamic behaviour of the pilot plant facility IFB reactor. The compartment sizes of the lean beds in this reactor are 0.14x0.14 and 0.06x0.06 m<sup>2</sup>. The weir lengths are 0.14 and 0.06 m, respectively. These beds do resemble the cold weir flow experimental facility with respect to its size and geometry. It was therefore assumed that correcting for the length of the weir will be sufficient to predict the weir flow phenomenon in the IFB pilot plant reactor. The resulting equation that predicts the weir flow as a function of the bed geometry and driving force ( $M - M_{ss}$ ) then becomes:

$$\phi_{weir} = C_1 \frac{L_{weir}}{L_{weir,exp}} \left( \frac{A_{bed,exp}}{A_{bed}} \right)^{C_2-1} (M - M_{ss})^{C_2} \quad (3.7)$$

This empirical relationship predicts the rate of solids flow over the weir from a fluidized bed as a function of the actual bed mass and gas velocity. The use of the correlation is extended to other (than the experimental facility) geometries by taking into account the effect of the bed surface area and the length of the weir. Temperature effects will be taken into account by changing gas properties (density and viscosity) and a changed minimum fluidization velocity. These effects influence the weir flow through the prediction of the steady-state bed mass ( $M_{ss}$ ) (Equation 3.3) which is a function of the minimum fluidization velocity.

The weir flow model will be applied in chapters 3.2 and 3.3 to predict the hydrodynamic behaviour of the IFB pilot plant facility reactor.

**Backflow**

Back flow over the weir was defined as the solids flow that can occur when the weir flow from lean bed to dense bed is considerably higher than the orifice flow from this dense bed to the subsequent lean bed (see Figure 3.1). The solids will accumulate in the dense bed until the bed height reaches the height of the weir. In that case the particles will start to return to the lean bed. This phenomenon can take place especially when the lean bed is in the slugging regime. A periodic flow pattern is established between the beds. When the slugs that rise in the lean bed reach the bed surface, the solids will be entrained and partly be transported to the dense bed. When this bed is filled up to the height of the weir, the particles will return to the lean bed when this bed is collapsing. This cycle will be repeated at the slug frequency of the lean bed. A similar flow pattern is observed when the lean bed is in the bubbling regime. This phenomenon was experimentally (visually) observed in cold experimental facilities and in the IFB pilot plant reactor that was operated at high temperature.

The back flow is important with respect to the solids distribution when the total IFB bed mass is such that the dense beds are filled up to or higher than the height of the weir. In developing a model for back flow, it should be appreciated that the dense bed compartment is normally operated at defluidized or minimum fluidization conditions. The angle of repose of the particles will change with changing gas velocities below the minimum fluidization gas velocity. This will affect the rate of back flow from dense to lean bed through the distribution of solids over the dense bed surface area. Its value will change for unaerated solids from 24° (see Table 2.5) to 0° at minimum fluidization conditions. Because the gas velocities in the dense beds are close to the minimum fluidization gas velocity at a relative gas velocity of 0.7 to 1.0, it is assumed that the solids are evenly distributed over the dense bed surface. The back flow phenomenon is therefore considered to be no function of the gas velocity in the dense bed.

The back flow is then described by the following empirical equation:

$$\phi_{weir,back} = C_{bf}(M - M_{ss,dense}) , M \geq M_{ss,dense} \tag{3.8}$$

In this equation, the steady-state bed mass of the dense bed ( $M_{ss,dense}$ ) is equivalent to the amount of solids that is necessary to fill the dense bed up to the height of the weir at the gas velocity at which this bed is operated. The back flow equation is only valid for a situation in which the actual bed mass is equal to or exceeds the steady-state bed mass. If the bed mass is less than  $M_{ss,dense}$ , no back flow occurs.

The effects of bed geometry on back flow were taken into account for the specific experimental situation in the IFB reactor. The back flow is used to balance the solids distribution between an overflowing lean bed and a back-flowing dense bed. The back flow constant ( $C_{bf}$ ) is adjusted such that the calculated values for the backflow and weir flow did not exceed 50 times the calculated orifice flow during the simulations that were carried out. Higher values for the solids flow over the weir compared to the orifice flow were considered to be unrealistic. The values that were used during the IFB simulations were 20 and 2 for back flow from compartment 2 to 1 and from compartment 4 to 3 respectively.

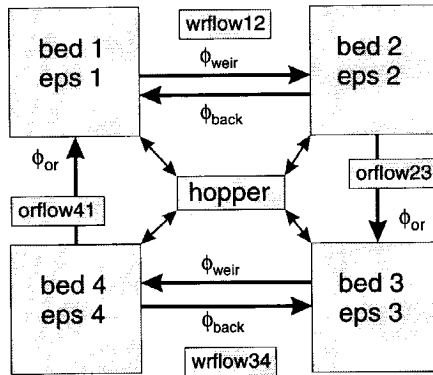
**Orifice flow**

The solids flow through an orifice that is connecting a dense bed to a lean bed is investigated and discussed in chapter 2 of this thesis. The orifice flow model is based on two driving forces that are taken into account: pressure drop across the orifice ( $\Delta P_{or}$ ), and particle stress acting in the horizontal direction at orifice height ( $\sigma_{N, or}$ ). To calculate these driving forces, the gas flow through the orifice needs to be predicted as well. The effective gas velocities in the compartments influence the driving forces. The equations concerning solids and gas flow and their respective driving forces therefore need to be solved simultaneously. The appropriate set of equations and model parameters with respect to orifice flow modelling can be found in Appendix 3.A of this thesis.

**3.1.3 Development of a mathematical model for IFB hydrodynamics**

The model needs to provide insight in the steady-state and dynamic behaviour of the IFB reactor. This information can be used to verify the effect of external disturbances and the operational parameters that can be used to control the IFB reactor performance. In order to develop a mathematical model for the IFB reactor hydrodynamics, the various mathematical sub-models have to be connected to each other. Further, a large number of algebraic and differential equations need to be solved simultaneously.

It was therefore chosen to solve the model equations by using the dynamic flowsheeting program Speedup (1993). When the sub-models are programmed in Speedup code, this program can be used to perform steady-state and dynamic simulations. The structure of the problem is represented by a flowsheet in which the various units are connected by means of "process streams". These connections are used to transfer values of the variables between the units that describe the Speedup problem. Each unit is set up from a model that describes the output of the unit as a function of its input.



**Figure 3.7** A schematic representation of the flowsheet of the IFB model. Each term represents a unit that is based on a specific mathematical model. The models "bed" and "eps" solve the general mass balances and calculate the voidage in each compartment of the IFB reactor. Solids flow over the two weirs is calculated by the models "wflow12" and "wflow34". The orifice flow through the connecting orifices follows from the models "orflow41" and "orflow23". The "hopper" model is implemented in the flowsheet to add or withdraw solids from the IFB reactor.



The flowsheet that describes the IFB reactor, consisting of four compartments, is schematically shown in Figure 3.7. The IFB reactor is defined by the hydrodynamic models for orifice flow, weir flow, back flow and the general mass balances for each compartment. In addition to this, a model ("*bedvoid*") is used to estimate the voidage in the lean bed. In the flowsheet this is represented as **eps1, 2, 3 and 4**. Further, a "*hopper*" is added to the flowsheet. This enables adding and removing of solids during a dynamic simulation. An amount of solids can be added to or removed from each of the four compartments at a user defined flow rate. The model "*fluidbed*" is represented by **bed 1, 2, 3 and 4** in the flowsheet and is equivalent to the mass balance for each compartment (Equation 3.2). The models "*orflow*" and "*wrflow*" correspond to the models for orifice flow and weir flow that are outlined in chapter 3.1.2 and described in Appendix 3.A.

The mathematical model for IFB hydrodynamics that is schematically shown in Figure 3.7 was used for steady-state and dynamic modelling. This is described in chapters 3.2 and 3.3, respectively.

### 3.2 Steady-state modelling and comparison to experimental results

The mathematical model for IFB hydrodynamics is capable of predicting the dynamic behaviour of the IFB reactor. An important feature of the model is however that it can also predict the steady-state hydrodynamics (solids distribution and CRS) on the basis of the relevant IFB parameters. In chapter 2, a model was presented that predicts the solids flow rate through an orifice on the basis of the known amounts of solids in the connected beds. The overall IFB model that is presented in this chapter predicts the solids distribution (by solving the general mass balances for each IFB compartment) and the CRS as well.

The parameters that determine the solids distribution and CRS can be sub-divided in design and operational parameters. The design parameters concern particle properties and IFB reactor geometry. The operational parameters are the gas velocities to the compartments and the total IFB bed mass. The simulations were carried out for variations of the design (see Table 4.2) and operational parameters that can be applied in the IFB pilot plant reactor. In this way, the calculated results could be compared to the experimental results.

The following parameters were varied in the indicated range:

<b>Parameters</b>	<b>Range</b>	
▶ orifice size:	10 - 30	[mm ]
▶ orifice position: (height measured from the distributor plate)	35 - 150	[mm]
▶ total IFB bed mass:	6.0 - 8.5	[kg]
▶ gas velocities $U_1$ and $U_3$ :	1.2 - 1.6	[m/s]
$U_2$ and $U_4$	0.7 - 1.0	[m/s]

These parameters were investigated for its influence on steady-state and dynamic IFB hydrodynamics. The standard conditions and IFB characteristics that are relevant for the simulations are given in Table 3.2.

**Table 3.2** Standard conditions and IFB characteristics for IFB model simulations.

Conditions			IFB characteristics		
$U_1 = U_3$	1.4	[m/s]	$d_{or}$	10	[mm]
$U_2$	1.0	[m/s]	$H_{orifice}^{(1)}$	35	[mm]
$U_4$	0.9	[m/s]	$H_{weir}^{(1)}$	300	[mm]
$M_{tot}$	7.0	[kg]	<sup>(1)</sup> measured from the distributor plate		
T	850	[°C]			

### 3.2.1 Orifice size and position

#### *Orifice size*

In Table 3.8, the effect of the size of the orifice on solids distribution (bed heights) and CRS is shown.

Increasing the diameter of the orifice, increases both the CRS and the gas flow through the orifice. As a result of the increased gas flow, the effective gas velocity increases in both lean beds (compartments 1 and 3) and decreases in both dense beds (compartments 2 and 4). Due to the smaller diameter of compartment 3 compared to compartment 1, the change in effective gas velocity in that bed is relatively large. This leads to a lower steady-state bed mass ( $M_{ss}$ ) and an increased voidage. The pressure drop across orifice 2-3 increases and decreases for orifice 4-1. The solids flow through orifice 4-1 thus becomes more rate limiting. As a result, the bed mass accumulates in compartment 4 and subsequently (through backflow) also in compartment 1, and reduces in compartment 2. These results are illustrated for the range of orifice diameters (10 to 30 mm) that were investigated, as shown in Table 3.3.

**Table 3.3** The effect of orifice size on the bed heights and CRS in the IFB reactor.

$d_{or}$ [mm]	$H_1$ [m]	$H_2$ [m]	$H_3$ [m]	$H_4$ [m]	CRS [g/s]
10	0.227	0.294	0.265	0.304	11.0
20	0.234	0.285	0.270	0.306	34.4
30	0.240	0.276	0.270	0.306	62.8

#### *Orifice position*

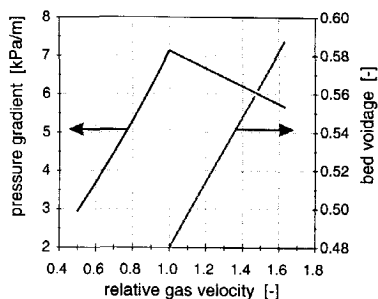
The position of the orifice with respect to the height at which it is inserted in the separating wall between compartments 2-3 and 4-1 was also investigated. In the simulations the height of the inserted orifice was equal for both orifices. The height measured from the distributor plate was varied from: 35, 50, 100 and 150 mm. The results of the model calculations are presented in Table 3.4.

**Table 3.4** The effect of orifice position on the bed heights and CRS in the IFB reactor.

$H_{or}$ [mm]	$H_1$ [m]	$H_2$ [m]	$H_3$ [m]	$H_4$ [m]	CRS [g/s]
35	0.227	0.294	0.265	0.304	11.0
50	0.227	0.295	0.264	0.303	11.1
100	0.227	0.299	0.258	0.303	11.4
150	0.228	0.300	0.251	0.301	11.7

As the height of the orifice position is increased, the solids flow increases. This is the result of the increased pressure drop across the orifice, which implies that the pressure gradient in the dense bed is smaller than the pressure gradient in the lean bed. This seems to be in conflict with the difference in bulk density of both beds. Therefore, the calculated pressure gradient and bed voidage are shown as a function of the relative gas velocity in Figure 3.8.

The pressure gradient in the bed increases with increasing gas velocity until the conditions of minimum fluidization are reached. Further increasing the gas velocity will cause the pressure gradient to decrease due to the increased bed voidage. The effective gas velocities were also calculated by the IFB model. It is found that at an orifice height of 35 mm, the effective relative gas velocities in compartments 4 and 1 are 0.82 and 1.43 respectively. In Figure 3.8 it can be seen that the pressure gradient is indeed larger in the lean bed. This is not true for orifice 2-3 as the effective gas velocities are 0.92 and 1.59 respectively. However, elevating the orifice position increases the CRS, as the flow



**Figure 3.8** Calculated pressure gradient and bed voidage as a function of the relative gas velocity.

through orifice 4-1 is rate determining. Elevating orifice 2-3 in fact reduces the pressure drop across this orifice. The bed height in compartment 2 increases and in compartment 3 the height decreases in order to establish the same driving force for solids flow through both orifices. The simulations thus show that elevating the orifice position may either increase or decrease the CRS, depending on the pressure gradients on both sides of the orifice that is rate determining.

In the simulations that were carried out, the contribution of particle stress ( $\sigma_N$ ) as a driving force is small and its decreasing influence with increasing orifice position is therefore not observed.

In practice, the best location for the orifice has thus to be determined with care. The effective gas velocities in the compartments should be determined from the gas phase balance around the orifice (see Figure 2.12). When this is known, the pressure gradient in dense and

lean bed can be determined which gives insight at what axial position the maximum driving force for solids flow can be attained.

It should be noted that elevating the orifice position is limited. At a certain height, the possibility that a part of the solids that enter the lean bed through the orifice, directly leave the bed over the weir becomes realistic. The true effect depends obviously on the specific design of the IFB reactor and the mode of operation. However, it can in general affect the performance of the IFB reactor negatively through a short-circuiting stream of solids.

It should also be noted that (due to the orifice gas flow), elevating the orifice actually divides each bed into two regions with respect to the fluidization conditions (as shown in Figure 2.12). The amount of gas that is passing the solids in the bed is either increased or decreased due to the orifice gas transfer. The model does not account for this and calculates bed voidage and bed height, on the basis of the effective gas velocity above the orifice position. In the standard case ( $H_{orifice}=35$  mm,  $H_{bed}=300$  mm, Table 3.2) this assumption is reasonable as approximately 90% of the bed material is located above the position of the orifice.

**3.2.2 Total IFB bed mass**

The total IFB bed mass will certainly affect the hydrodynamic behaviour of the IFB system. It is important to verify the influence of this operational parameter because it can be used to manipulate the process taking place in the IFB reactor. In the case of regenerative desulfurization for example it could be desirable to increase the amount of sulfur to be captured. In this specific situation, an increase in the total IFB bed mass could be used to reach this goal.

In order to determine the influence of the IFB bed mass on the hydrodynamics of the IFB pilot plant reactor, the total bed mass was varied between 6.0 and 8.5 kg. The results of the simulations are shown in Table 3.5.

**Table 3.5** The effect of the total IFB bed mass on the bed heights and CRS in the IFB reactor.

$M_{bed}$ [mm]	$H_1$ [m]	$H_2$ [m]	$H_3$ [m]	$H_4$ [m]	CRS [g/s]
6.0	0.222	0.217	0.240	0.226	3.0
6.5	0.227	0.248	0.238	0.276	8.9
7.0	0.227	0.294	0.265	0.304	11.0
7.5	0.255	0.301	0.292	0.311	9.3
8.0	0.283	0.305	0.313	0.321	7.5
8.5	0.307	0.314	0.332	0.337	6.5

Since the CRS is determined (*viz.*, limited) by the solids flow through orifice 4-1, increasing the total IFB bed mass will initially lead to accumulation of particles in compartment 4 (as observed in Table 3.5). This results in an increased pressure drop across the orifice and consequently in an increased CRS. Solids also accumulate in compartment 2 and to a lesser extent in compartment 3, in order to establish an equivalent driving force for solids flow.

Compartment 4 is filled up to the height of the weir (*i.e.*, 0.3 m) at a total IFB bed mass of 7.0 kg (see Table 3.5). Adding more solids to the IFB reactor will result in back flow of particles from compartment 4 to the lean bed compartment 3. The extra amount of solids will partly end up in compartment 1 causing the pressure drop across orifice 4-1 to decrease. The CRS will thus decrease. Due to the resistance for solids flow in orifice 2-3, the next compartment that will be filled up to the height of the weir is compartment 2. This is followed by compartments 3 and 1.

When the total bed mass is reduced, this will result in a situation in which the solids flow over the weir becomes rate limiting. It was found that for a bed mass smaller than 6.0 kg, this is the case for this specific IFB reactor and particle system. As a result, the solids will accumulate in the lean beds. This can lead to a lean bed height that exceeds the height of the dense beds. The pressure drop across the orifice can still be positive due to the pressure gradients in the beds. However, further decreasing the total bed mass will result in a situation in which no solids flow occurs due to the decreased driving forces ( $M < M_{ss}$ ). The IFB model is thus capable of predicting this phenomena. In practice, if one wants to prevent a situation of weir flow limitation, the IFB reactor can be filled up to the height of the weir at the specific gas velocities for all compartments. In that case, the solids flow through one of the orifices will be rate determining.

### 3.2.3 Gas velocities

Manipulation of the CRS by means of the gas velocities to the IFB compartments is an important consideration. The gas velocity is in practice the most straightforward and easy to use operational parameter. In order to study the possibilities of controlling the CRS by means of the gas velocity to compartment 4, the influence of the gas velocities on the CRS in the other compartments should be verified.

#### *Gas velocity to compartment 1 and 3*

Compartments 1 and 3 serve as chemical reactors in the IFB reactor. The gas velocities will therefore be fixed by the requirements concerning the chemical processes taking place. However, it is important to verify the effect of the gas velocity to these compartments on the CRS. The effect of the relative gas velocity to compartment 1 as calculated by the overall IFB model is represented in Table 3.6.

**Table 3.6** The effect of the gas velocity to compartment 1 on the bed heights and CRS in the IFB reactor.

$U_1$ [m/s]	$H_1$ [m]	$H_2$ [m]	$H_3$ [m]	$H_4$ [m]	CRS [g/s]
1.2	0.264	0.213	0.238	0.277	1.9
1.3	0.245	0.248	0.240	0.300	8.5
1.4	0.227	0.294	0.265	0.304	11.1
1.5	0.232	0.301	0.269	0.305	11.3
1.6	0.240	0.302	0.271	0.305	11.3

## Chapter 3

As a result of the reduction in steady-state bed mass ( $M_{ss}$ , Equation 3.3), the height of compartment 1 generally decreases with increasing gas velocity in compartment 1. As a consequence, the pressure drop across orifice 4-1 increases and as the solids flow through orifice 4-1 is rate determining, the CRS increases as well. The fact that the solids flow through orifice 4-1 is rate determining at these conditions is indicated by the fact that the bed height in compartment 4 ( $H_4$ ) is higher than the bed height for the other compartments (see Table 3.6), *viz.*, solids are accumulating in compartment 4.

The bed mass accumulates in the dense beds and when compartment 4 becomes filled up to the weir height, the solids start to accumulate in compartment 3. When compartment 2 also reaches the height of the weir, particles start to flow back to compartment 1. At relative gas velocities above 1.4, the height of compartment 1 increases with gas velocity. This does not result in a reduced pressure drop across orifice 4-1 due to the increased voidage and smaller pressure gradient in the bed. The CRS will only slightly increase at relative gas velocities above 1.4 (as shown in Table 3.6). The effect of the gas velocity in compartment 3 is similar to that of compartment 1.

### *Gas velocity to compartment 2*

In order to control the CRS by means of the gas velocity in compartment 4, the conditions for solids flow through orifice 2-3 should be such that the driving forces for solids flow are larger than for solids flow through orifice 4-1. When the effective gas velocity in compartment 2 is below the gas velocity in compartment 4, the solids flow through orifice 2-3 becomes rate limiting. Solids will accumulate in compartment 2 (instead of compartment 4). The effects on the CRS and solids distribution of the gas velocities to compartments 2 and 4 are similar.

To accomplish a CRS determining orifice flow through orifice 4-1, the gas velocity to compartment 2 should be set at a somewhat higher value than the gas velocity in compartment 4. This enables the CRS to be controlled by only one operational parameter, *viz.*, the gas velocity to compartment 4.

**Table 3.7** The effect of the gas velocity to compartment 4 on the bed heights and CRS in the IFB reactor.

$U_4$ [m/s]	$H_1$ [m]	$H_2$ [m]	$H_3$ [m]	$H_4$ [m]	CRS [g/s]
0.7	0.226	0.273	0.293	0.308	5.2
0.8	0.227	0.283	0.281	0.306	8.4
0.9	0.227	0.294	0.265	0.304	11.1
1.0	0.231	0.300	0.244	0.301	13.1

### *Gas velocity to compartment 4*

The relative gas velocity to compartment 4 was varied from 0.7 to 1.0. The simulation results that are shown in Table 3.7 reveal that the CRS increases by increasing the gas velocity to compartment 4. This is caused by the increased pressure drop across orifice 4-1. As the flow through orifice 4-1 becomes less rate determining, the accumulation of solids



g/s, respectively. The calculated values that are shown in Table 3.5 are 9.3 and 6.5 g/s for bed masses of 7.5 and 8.5 kg, respectively. The decrease of the CRS with increasing bed mass is thus correctly predicted by the overall IFB model. The CRS that is predicted by the IFB model for a bed mass of 8.5 kg is too high indicating that the model can predict the trend accurately while the exact values have to be considered with restriction.

Further, the modelling results can be qualitatively compared to the results that were measured in a cold four-bed experimental facility and described by Korbee *et al.* (1991). The geometry of the experimental facility resembles the IFB reactor. The compartments were  $0.1 \times 0.1 \text{ m}^2$  in size and the height of the weir was 0.3 m. The experiments were performed with glass beads ( $d_p = 511 \text{ }\mu\text{m}$  and  $\rho_p = 2880 \text{ }\mu\text{m}$ ). In the experiments an optimum pressure drop across the orifice was observed when the solids hold-up in the four-bed facility was varied. This is qualitatively in accordance with the modelling results that are shown in Table 3.5 in which a maximum solids flow is also observed.

### *Gas velocity to compartment 4*

In the experiments, the gas velocity to compartment 4 was set at 0.8, 0.9 and 1.0 m/s. For a total IFB bed mass of 7.5 kg this resulted in a CRS of 6.8, 8.3, and 9.7 g/s, respectively (see Table 3.8).

In Table 3.7, the calculated effect of the gas velocity to compartment 4 for a total IFB bed mass of 7.0 kg is shown. The trend that the CRS increases with increasing gas velocity is also observed in the experimental results. However, when the CRS is calculated by the IFB model for a bed mass of 7.5 kg, the predicted value for the CRS ( $U_4$  at 0.9 m/s, see Table 3.5) is approximately 10% too high (9.3 compared to 8.3 g/s).

### *Gas velocities to compartments 1 and 3*

During the IFB experiments, the gas velocities to compartments 1 and 3 were set at 1.4 and 1.5 m/s (see Table 3.8). No significant change in CRS was observed (8.3 and 8.2 g/s, for experiment 2 and 4, respectively).

Table 3.6 represents the calculated influence of the gas velocity to compartment 1 on the CRS. It can be seen that the IFB model also predicts a very small influence for a change in gas velocity to compartment 1 from 1.4 to 1.5 m/s. The model predictions and experimental results are therefore in accordance with each other.

In conclusion, the overall IFB model that was developed in this chapter is capable of explaining qualitatively the hydrodynamic phenomena that were experimentally observed in the IFB pilot plant reactor. The CRS, determined during the experiments, is calculated on the basis of measured pressure drops across the orifice. The added value of the overall IFB model (compared to an orifice flow model) is that it is capable of predicting the solids distribution and subsequently the CRS on the basis of the total IFB bed mass and gas velocities to the compartments.

It should be mentioned that the IFB model was not fitted to the experiments carried out in the IFB pilot plant reactor. All empirical constants and model parameters were determined in separate cold flow experiments.



### 3.3 Dynamic modelling of the IFB reactor

#### *The use of a dynamic process model*

The model that was developed in this chapter is able to predict the dynamic behaviour of the hydrodynamics of the IFB reactor. In general, a dynamic model can give insight in the dynamics of a process that affect the controllability (see Beasley, 1989 and Korving, 1995).

The general objectives of process control are (Stephanopoulos, 1984):

- ▶ deviations from setpoint caused by external disturbances should be corrected for;
- ▶ the process should run at optimum conditions;
- ▶ the operation of the process should be as safe and stable as possible.

The optimum and safe conditions should be defined first after which a control strategy can be developed. This is strongly dependent on the process characteristics. In case of the IFB reactor for regenerative desulfurization, a specific degree of sulfur retention needs to be established. An important safety aspect is the presence of hydrogen and air in one reactor vessel.

External disturbances are for example unforeseen variations in the inlet gas concentrations to the desulfurization and regeneration compartments. In chapter 6, these aspects will be treated and mathematically modelled. In the present chapter the dynamics of the IFB reactor are restricted to the hydrodynamics of the system. A mathematical model can play an important role in developing a control strategy. To control the process, manipulated variables or operational parameters have to be chosen and their influence on the process needs to be determined. This can be carried out by a mathematical process model. Providing that the model is a correct description of the process, many time-consuming and costly experiments can be omitted. The mathematical model can then predict the dynamic response of disturbances and the subsequent control action by the operational parameter.

Another, more advanced, possibility of the use of a dynamic process model is Model Predictive Control (MPC). MPC can be particularly useful for processes with cross-correlations between their multiple inputs and outputs. In the MPC approach, the dynamic process model (or a linearized version) is used to set the manipulated parameter at the desired value based on the calculated response by the dynamic process model. This yields advantages regarding the optimization and control of a process (see for example Desphande *et al.*, 1995; Gawthrop and Ponton, 1996).

#### *Dynamic simulations*

To obtain insight in the dynamics of the IFB reactor system, the responses of the hydrodynamics were calculated by means of mathematical modelling. The model that was programmed in Speedup (1993) offers the opportunity of a "*run-time environment*" in which the input variables can be changed during a dynamic simulation. This gives a direct insight in the dynamics of the IFB system.

The step-changes in characteristic operational parameters that were selected are realistic with respect to the practical feasibility during operation of the IFB reactor. The values for the operational parameters were, if not varied, equal to the values mentioned in Table 3.2.

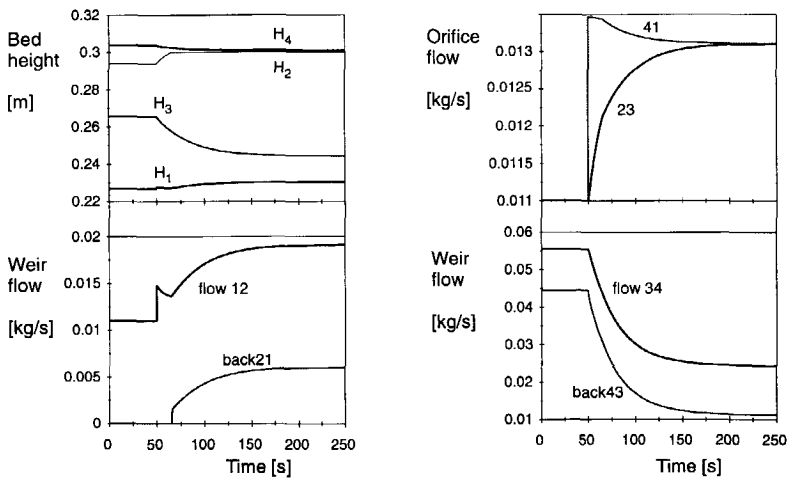
► Step-change in the gas velocity to compartment 4

In Figure 3.9, the effect of a step-change in the gas velocity to compartment 4 ( $U_4$ ) from 0.9 to 1.0 m/s is shown. The other operational parameters were kept constant during this simulation. In chapter 3.2.3, it was already shown that such an increase in  $U_4$  from 0.9 to 1.0 m/s will result in an increase in CRS from approximately 11 to 13 g/s. This is caused by the fact that the solids flow through orifice 4-1 is rate limiting with respect to the CRS. It can further be observed in Figure 3.9 that the bed heights of compartments 1 and 2 increase whereas the solids holdup in compartments 3 and 4 decreases. This is caused by the fact that orifice 4-1 becomes less rate limiting as the gas velocity becomes equivalent to the gas velocity in compartment 2.

The orifice flow and weir flow become constant when the solids are redistributed according to the new steady-state. It can be seen that the solids flow through orifice 4-1 is responding fast caused by the momentary increase of the pressure drop across the orifice. Initially, the orifice flow is even increased to a somewhat higher value than its new steady-state.

The solids flow over the weir and the back flow of solids respond according to the changes in the solids holdup in the respective compartment. This is caused by the fact that the flows are a function of the solids holdup in the compartments.

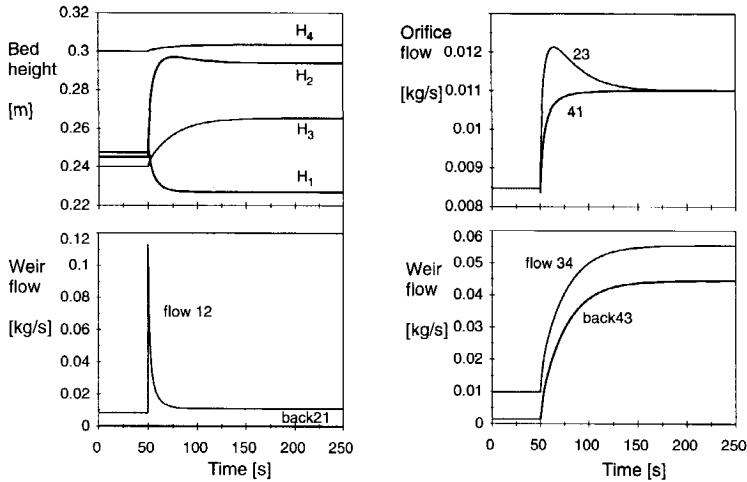
After approximately 150 s, the new steady-state is reached. The average CRS during this run is about 12 g/s at a total IFB bed mass of 7 kg. This implies that the average cycle-time of the solids is approximately 580 s (if no dead zones are considered in the dense transport compartments 2 and 4). The steady-state is reached faster than this average solids cycle-time. This is caused by the fact that the time to reach the new steady-state is proportional to the amount of solids that needs to be redistributed instead of the total IFB bed mass. The average solids residence time in compartment 4 is 150 s (calculated on the basis of an average bed mass in compartment 4 of 1.8 kg), which is equivalent to the time needed to reach the new steady-state.



**Figure 3.9** The effects of a step-change at  $t = 50$  s on the gas velocity to compartment 4 from 0.9 to 1.0 m/s. Other operational parameters are kept constant. The response is plotted for the bed heights and solids flows through the orifices and over the weirs.

► Step-change in the gas velocity to compartment 1

In chapter 3.2.3, some effects of a changing gas velocity to compartment 1 were already discussed. It was shown that for a gas velocity to compartment 1 above 1.4 m/s its influence on the CRS is negligible. However, a step-change of 1.3 to 1.4 m/s, as shown in Figure 3.10, will have a significant effect on the IFB hydrodynamics.



**Figure 3.10** The effects of a step-change at  $t = 50$  s on the gas velocity to compartment 1 from 1.3 to 1.4 m/s. Other operational parameters are kept constant.

It is observed that the solids hold-up in compartment 1 decreases fast due to the increased gas velocity. This will directly affect the bed height in the smaller compartment 2 and subsequently the driving force (pressure drop) for solids flow through orifice 2-3. This solids flow passes a maximum and then decreases to the new steady-state value.

The bed height in compartment 2 and the solids flow through orifice 2-3 show an overshoot response on the step-change in gas velocity in compartment 1. This is caused by the momentary increase in weir flow from compartment 1 to compartment 2. The orifice 2-3 cannot carry away the solids immediately causing a temporary high solids content in compartment 2 while compartment 3 contains too little solids with respect to the new steady-state. The time to reach the new steady-state, *viz.* about 150 s, is similar to the time needed in case of the step-change in the gas velocity to compartment 4 indicating that the amount of solids that needs to be redistributed is equivalent (at equal CRS).

► A stepwise addition of solids to the IFB reactor

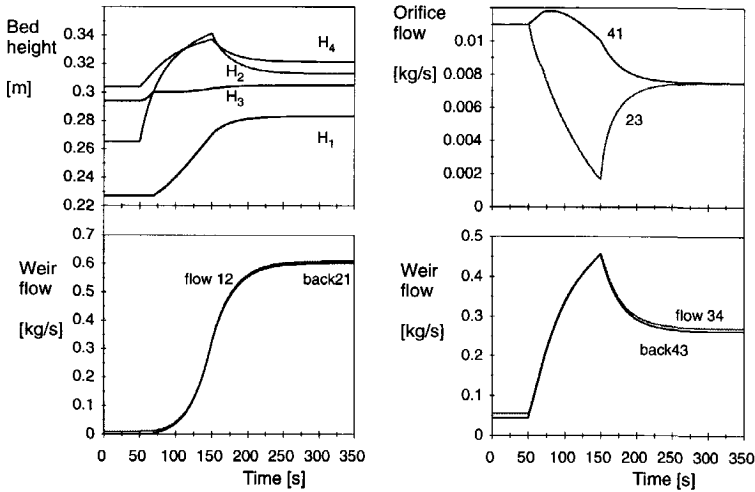
In chapter 3.2.2, effects of the total IFB bed mass on the hydrodynamics of the IFB reactor were already discussed.

In Figure 3.11, the effect of an IFB bed mass increase from 7 to 8 kg is shown. The solids are added to compartment 4 at a flowrate of 10 g/s from  $t = 50$  to  $t = 150$  seconds. At 7 kg, *i.e.*, the optimum bed mass with respect to the CRS (see Table 3.5), the bed height in compartment 4 approximately equals the height of the weir. Adding more solids to the IFB

reactor causes compartment 2 to be filled to the height of the weir. A small part of the 1 kg that is added will end up in compartment 1, causing the pressure drop across orifice 4-1 to decrease and, subsequently, the CRS decreases.

The weir flow and back flow between the compartments that are connected by a weir are significantly influenced by the increase in total IFB bed mass. At 7.0 kg, for example, no back flow occurs from compartments 2 to 1 whereas at 8.0 kg the back flow is considerable (approximately 0.6 kg/s).

The time needed to reach the new steady-state is again proportional to the amount of solids that needs to be redistributed and the average CRS in the IFB reactor. The solids are added in 100 seconds and the new steady-state is reached after another 150 seconds.



**Figure 3.11** The effects of an increase in total IFB bed mass from 7 to 8 kg. Other operational parameters are kept constant. Extra bed mass is added at a flowrate of 10 g/s from t=50 to t=150s in compartment 4.

### 3.4 Discussion and conclusions

The dynamic IFB model as described in this chapter gives information on the steady-state hydrodynamics as well as the dynamic behaviour of the IFB reactor system. This gives insight in how to operate the IFB reactor and in the effect of operational parameters that are used for process control purposes.

The mathematical model that was used consists of sub-models mentioned in chapter 3.1. The weir flow and back flow of solids over the weir between two compartments is described with an empirical model. This model was developed specifically for the IFB pilot plant reactor and the particles that were used in this study. The results are therefore difficult to be used for scale-up predictions or applied to other sized IFB reactors. It is believed however that general trends and features of the IFB reactor hydrodynamics are properly predicted by the IFB model.

The steady-state modelling results show that the influence of variations (from 1.2 to 1.6 m/s) in the gas velocities to compartments 1 and 3 on the CRS is relatively small ( $\pm 5\%$ ) as long as the solids flow through orifice 4-1 is rate limiting. Therefore, compartments 1 and 3 should be operated above 1.4 m/s and compartment 2 should be operated at a gas velocity that is 10% higher than the gas velocity in compartment 4. These conditions enable the CRS to be controlled by means of the gas velocity to compartment 4. This gas velocity therefore is a critical parameter to control the CRS in the IFB reactor.

The steady-state CRS in the IFB reactor obviously depends on the total IFB bed mass as well. It was shown that an optimum IFB bed mass exists with respect to a maximum CRS. When the bed mass in the IFB reactor is variable during operation, the CRS needs to be controlled to the value that is necessary for the regenerative process that is carried out. This can be achieved by means of adjusting the gas velocity to compartment 4. The size of the orifice should be designed such that the CRS required for the regenerative process can be achieved by variation of the gas velocity to compartment 4 with a solids hold-up in the IFB reactor that is subject to changes. From an operational point of view it will be necessary to keep the IFB bed mass within a specific range that enables the required CRS to be realized.

When a step-change is made on the operational parameters such as the gas velocity or the total IFB bed mass, care should be taken that it will not cause a high temporary solids flow that causes an overshooting response for some of the variables. See the Figures 3.9, 3.10 and 3.11. This can be accomplished by changing the operational parameters in smaller steps. The dynamic model that was developed in this chapter can be particularly useful in determining the response of the process parameters on step-changes in order to verify the controllability of the IFB reactor.

The response of solids distribution and CRS of the IFB reactor on a step-change results for all investigated operational parameters (gas velocities and IFB bed mass) in a new steady-state. The new steady-state is reached after a time that is equivalent to the time needed to redistribute the solids between the IFB compartments. This time is much smaller than the average IFB cycle-time ( $= M_{IFB}/CRS$ ) and is approximated by the average residence time in the transport compartment that is rate controlling (compartment 4).

In chapter 6, the dynamics and the influence of process dynamics on the chemical performance of the IFB reactor will be discussed. A mathematical model is used to calculate the effect of sudden changes in operational conditions on sulfur retention in the IFB reactor in case of regenerative desulfurization.

## Chapter 3

### Notation

$A_{bed}$	: bed area, surface area of the bed	[m <sup>2</sup> ]
$A_o$	: cross sectional area of the orifice	[m <sup>2</sup> ]
$C_D$	: discharge coefficient	[-]
$C_1, C_2$	: empirical constant defined by Equation 3.4	[-]
CRS	: Circulation Rate of Solids	[kg/s, g/s]
$D_e$	: effective bubble size	[m]
$d_{or}$	: orifice diameter	[m]
$d_p$	: particle diameter	[m]
$f$	: friction factor	[-]
$F(\Delta u_z)$	: solid-gas frictional force per unit bed volume or solid-gas frictional pressure drop per unit bed height	[N/m <sup>3</sup> ] [Pa/m]
$g$	: gravitational constant	[m/s <sup>2</sup> ]
$H_{bed}$	: expanded bed height	[m]
$H_{orifice}$	: height of the orifice from distributor plate	[m]
$K$	: stress ratio	[-]
$K_1, K_2$	: empirical constant defined by Equation 3.3	[-]
$L_{weir}$	: length of the weir	[m]
$M^*$	: characteristic bed mass (= $M_{bed}/A_{bed}$ )	[kg/m <sup>2</sup> <sub>bed</sub> ]
$M_{ss}$	: steady-state bed mass defined by Equation 3.3	[kg]
$M_{ss,dense}$	: steady-state bed mass of a dense bed	[kg]
$P_w$	: perimeter of dense bed	[m]
$\Delta P$	: pressure drop across the orifice	[Pa]
$T$	: temperature	[°C]
TDH	: Transport Disengaging Height	[m]
$u$	: absolute or interstitial gas velocity	[m/s]
$U$	: superficial gas velocity	[m/s]
$z$	: vertical coordinate	[m]

### Greek

$\epsilon$	: bed voidage	[m <sup>3</sup> <sub>gas</sub> /m <sup>3</sup> <sub>bed</sub> ]
$\epsilon_d$	: voidage of dense bed	[m <sup>3</sup> <sub>gas</sub> /m <sup>3</sup> <sub>bed</sub> ]
$\mu$	: dynamic viscosity of fluid	[Pa.s]
$\sigma_N$	: horizontally directed particle pressure	[Pa]
$\rho_d$	: bulk density of dense bed	[kg/m <sup>3</sup> <sub>bed</sub> ]
$\phi_m$	: solids mass flow	[kg/s]
$\phi_s$	: particle shape factor	[-]

### Subscripts

bf	: back flow
d	: dense bed
eff	: effective
exp	: experimental
g	: gas
l	: lean
or	: orifice
p	: particle
w	: wall

**References**

- Beasley, D.E., "Dynamic response of fluidized beds", Chem. Eng. Communications., 79, 115-130 (1989).
- Caram, H.S., Efes, Z., Levy, E.K., "Gas and particle motion induced by a bubble eruption at the surface of a fluidized bed", AIChE Symp. Series, 80 (234), 106-113 (1984).
- Desphande, P.B., Caldwell, J.A., Yerrapragada, S.S., Bhalodia, M.A., "Should you use constrained Model Predictive Control?", Chem. Eng. Progress, March, 65-72 (1995).
- Gawthrop, P.J., Ponton, J.W., "Improved control using dynamic process models", Trans. I.Chem.E., 74(A), January, 63-69 (1996).
- Geldart, D., "Particle entrainment and carryover", Chapter 6, in "Gas Fluidization Technology, Geldart, D. (Ed.), John Wiley & Sons, 123-153 (1986).
- Korbee, R., Schouten, J.C., Bleek van den, "Modelling Interconnected Fluidized Bed systems", AIChE Symp. Series, 281, 70-77 (1991).
- Korbee, R., Snip, O.C., Schouten, J.C., Bleek van den, C.M., "Rate of solids and gas via an orifice between partially and completely fluidized beds", Chem. Eng. Sci., 49(24B), 5819-5832 (1994).
- Korving, A., "Dynamic modelling", Chapter 8, in: "Atmospheric fluidized bed coal combustion: research development and application", 22, Coal Science and Technology, Valk, M. (Ed.), Elsevier, Amsterdam, 353-385 (1995).
- Kunii, D., Levenspiel, O., "Entrainment and elutriation from fluidized beds", Chapter 7, in: "Fluidization Engineering", 2nd Ed., Butterworth-Heineman, 165-192 (1991).
- Ling van, D.A., "Modelling the hydrodynamic behaviour of the Interconnected Fluidised Bed system", MSc report, Delft University of Technology (1996).
- Speedup, "User manual: release 5.4", Volume I and II, Aspen Technology, Inc., Cambridge Massachusetts, USA (1993).
- Stephanopoulos, G., "Chemical process control: an introduction to theory and practice", Prentice-Hall, Inc. (1984).
- Verlaat, M., "Dynamic modelling of the Interconnected Fluidized Bed reactor system", MSc report, Delft University of Technology (1995). (in Dutch)

---

## Appendix 3.A:

### Outline of the mathematical model for IFB hydrodynamics.

The model for IFB hydrodynamics was implemented in the dynamic flowsheeting program Speedup. In this appendix, the general features of Speedup modelling are presented as well as the models and model equations that were used for the mathematical modelling of the IFB hydrodynamics described in chapter 3.

#### *The structure of a Speedup problem.*

Speedup is a dynamic flowsheeting simulation program suited for chemical engineering applications. A series of unit operations is interconnected by means of process streams. Speedup can be used to model any type of process provided that this process can be described in terms of algebraic and differential equations. A process is defined in Speedup as a "problem" consisting of a number of sections.

Options: In this section, the calculation routine, the converge criterium and the maximum number of iterations are defined. If no settings are defined, Speedup will apply default settings. The time step and the number of intervals for integration can also be set. It can further be defined whether a run-time-environment is to be used or not. This run-time-environment allows the input parameters to be changed during a dynamic simulation.

Declare: The variable types are defined in the declare section. Each type of variable is defined with an initial value, a lower bound, an upper bound and a unit of measurement. Within the models, each variable is linked to a variable type. Further, the main stream (of the process) and global parameters should be defined in this section.

Model: This section provides the description of the local variables, the in- and outcoming streams, the connections of variables between units and the algebraic and/or differential equations. One model can be applied in several units.

Unit: In this section, it is indicated what model is applied for each specific unit. In the operation and flowsheet section, reference is made to the units.

Flowsheet: In the flowsheet section, the structure of the Speedup problem is given. See Figure 3.7 for the flowsheet that represents the Speedup problem concerning the IFB hydrodynamics. The in- and outcoming streams and the connections between the units are defined in the flowsheet section.

Operation: In this section, the fixed values for the variables in each unit are defined. Further, the initial values of the variables calculated as a function of time can be given.

#### *The models and units for the IFB hydrodynamics Speedup problem.*

The Speedup problem that defines the IFB hydrodynamics consists of a number of models that are used in several units as indicated in Table A.3.1.



**Table A.3.1** Models and units for the IFB hydrodynamics problem.

Model	Unit	Calculation of
Bedvoid	eps1, eps2, eps3, eps4	Voidage of the bed
Fluidbed	bed1, bed2, bed3, bed4	Momentary mass of the bed
Hopper	hopper	Addition/removal of solids to/from each bed
Orificeflow	orflow41, orflow23	Gasflow and solids flow through the orifice and effective gas velocities in each bed
Weirflow	wrflow12, wrflow34	Solids flow over the weir

The units shown in the flowsheet given in Figure 3.7 represent the Speedup problem for the IFB hydrodynamics. The units are connected as indicated in the flowsheet. The models that are used in the units are outlined below.

#### Bedvoid

The Bedvoid model defines the voidage for both fluidized and defluidized conditions. The voidage at fluidized bed conditions is estimated on the basis of bubble characteristics of the bed. The average bubble diameter and bubble rise velocities are estimated on the basis of the correlations provided by Kunii and Levenspiel (1991) (Chapter 6). The calculated bubble diameters are limited to the diameter of the bed and the rise velocity of the bubble or slug will in that case be calculated by means of a slug rise velocity correlation from Kunii and Levenspiel (1991).

#### Fluidbed

The Fluidbed model calculates the momentary bed mass for each of the compartments as defined in the units. Equation 3.2 is the differential equation that determines the solids hold-up in a compartment as a function of the inlet and outlet solids flows. The solids flow over the weir and through the orifice is calculated by the models Weirflow and Orificeflow respectively.

#### Hopper

This model enables the addition and removal of solids to each of the compartments at a user-defined flow rate. The Hopper model thus defines an inlet or outlet solids flow in addition to the orifice flow and weir flow of solids.

#### Orificeflow

The Orificeflow model defines the solids and gas flows through the orifice. The main equations describing the solids flow and gas flow are given in chapter 5.2.2 as Equations 5.2 and 5.3 respectively. The model parameters that are applied in the Orificeflow model are given in Table 5.2. The vertical particle pressure that is required for the determination of the solids flow is calculated according to Equation 2.8. The force that is exerted on the solids

### Appendix A.3

---

by the gas in vertical direction  $F(\Delta u_z)$  is calculated by the Ergun equation. An important consideration is the fact that the solids and gas flows through the orifice need to be determined simultaneously. The pressure drop across the orifice and the particle pressure are both dependent on the effective gas velocities in dense and lean bed. In Speedup, the set of equations that determines the orifice flow is solved simultaneously at each time-step during a dynamic simulation.

#### Weirflow

The weir flow phenomena in the IFB reactor are schematically shown in Figure 3.1. The Weirflow model is based on the equations for weir flow and back flow as given in chapter 3.1.2. The weir flow is a function of the steady-state bed mass (Equation 3.3) that is a function of the effective gas velocity in the lean bed and the momentary bed mass. The solids flow over the weir is calculated from Equation 3.7. The back flow, defined as the solids flow from a dense bed to a lean bed, is calculated from Equation 3.8.

The models defined above are used in the units indicated in Table A.3.1. The units are connected as indicated in Figure 3.7. The Speedup problem for the IFB hydrodynamics is used in the simulations carried out in chapter 3. In chapter 6, the model is extended with a mathematical description of the regenerative desulfurization gas-solids reactions.

# Chapter 4

## IFB pilot plant facility for regenerative desulfurization

design, construction, and operation

---

### 4.1 Design of the IFB pilot plant facility

#### 4.1.1 IFB reactor and flowsheet

The design and construction of the IFB pilot plant facility arised from the earlier work on IFB systems as described in chapter 1.2. Korbee (1995) describes the development of an Interconnected Fluidized Bed system for the purpose of regenerative desulfurization during Fluidized Bed Combustion of coal (FBC). The processes of combustion and sulfur capture are integrated with sorbent regeneration into one reactor system. The synthetic sorbent that was developed for this purpose consists of CaO on a  $\gamma$ -alumina carrier.

Furthermore, removal of H<sub>2</sub>S from coal gas originating from a gasification process was investigated at DUT which lead to the development of a steam regenerative synthetic sorbent consisting of MnO and FeO on a  $\gamma$ -alumina carrier. This work is described in detail by Wakker (1992) and Atakül *et al.* (1996).

The work in this project is focused on the IFB reactor development of a continuous high temperature, gas/solids regenerative process for the removal of SO<sub>2</sub> (FBC) or H<sub>2</sub>S (coal gasification). The purpose of the hot IFB facility was to experimentally prove the reactor concept at reaction conditions. It therefore needs to be suitable for the investigation of the high temperature desulfurization and regeneration in a continuous process.

In this chapter, an outline is given of the IFB facility design. It is not a description of a detailed design study but rather a summary of the most important design considerations and design parameters. The main results with respect to the design parameters are presented.

The relevant parameters in the IFB reactor design are:

- ▶ diameters of the beds,
- ▶ bed heights,
- ▶ gas distributor type and specific sizes,
- ▶ diameter and position of the orifice, and
- ▶ height of the freeboard.

The **IFB reactor** should be designed in such a way that the experimental results are representative for the regenerative desulfurization processes. Furthermore, it should be possible to study the influence of several reaction and hydrodynamic parameters on reactor performance.

## Chapter 4

In order to experimentally prove the concept of the IFB reactor it should consist of four compartments (see Figure 1.3). This minimum number of compartments is necessary to connect two fluidized bed reactors (sulfur capture and regeneration compartments) by means of two transport compartments. For FBC of coal processes (SO<sub>2</sub> removal), a temperature of approximately 850 °C is usually applied. High temperature coal gas desulfurization (H<sub>2</sub>S removal) temperatures vary from 450 to 650 °C. Therefore, the IFB reactor was designed such that a temperature of 400 to 900 °C can be applied.

Attention will initially be focused on the regenerative desulfurization during FBC of coal that will be studied by means of 'simulated' off-gases at atmospheric pressure. The synthetic sorbent material that will be used for regenerative sulfur capture is not a subject of investigation in this study and was produced during earlier work (Korbee, 1995). See Table 4.1 for the properties of the SGC-500 sorbent.

**Table 4.1** Particle properties of the SGC-500 sorbent (CaO on  $\gamma$ -Al<sub>2</sub>O<sub>3</sub>).

Ca-content = 8.91	[wt %]	$\epsilon_{\text{fixed}}$ = 0.463	[-]
pore volume = 0.40	[ml/g]	$\alpha_r$ = 24	[°]
$S_{\text{BET}}$ = 136.3	[m <sup>2</sup> /g]	K = 0.62	[-]
porosity = 0.56	[ml/ml]	f <sup>(1)</sup> = 0.4	[-]
$d_p$ = 2.65	[mm]	$U_{\text{mf}}$ = 0.75	[m/s]
$\rho_p$ = 1400	[kg/m <sup>3</sup> ]	(at 20 °C)	

<sup>(1)</sup> The friction factor ( $f$ ) is a particle-wall interaction parameter. Its value was determined at ambient conditions for alumina-PMMA (Poly-Methyl-MethAcrylate or perspex), (see chapter 2.6.2). Picciotti (1995) lists friction coefficients for various materials. A value of 0.4 appears to be typical for a large number of materials and is therefore also used in further calculations concerning particle wall interaction in the IFB reactor.

Korbee (1995) showed that the regeneration of the sorbent is fast compared to the sulfur capture process. The regenerator compartment can therefore be significantly smaller than the desulfurization compartment (adsorber). A size ratio of 140 was found to be appropriate in a specific preliminary design of a 100 MWe power plant (Korbee *et al.*, 1993).

In the design of the IFB pilot plant reactor, the size of the regenerator was set by a minimum bed size to particle diameter ratio. This ratio should be higher than 20 to avoid wall effects on the hydrodynamics of the fluidized bed that would result in different fluidization regimes in sulfur capture and regeneration compartments. The diameter of the regenerator is therefore set at 0.06 m ( $d_p = 2.65$  mm).

Due to the practical availability of gases (such as the maximum sizes of liquid storage tanks for nitrogen and compressors for air that can be installed at DUT) and construction limitations (such as the size of the DUT-CRE experimental building), the size ratio of 140 cannot be attained. This is not a real concern because the goal of this work was to prove the IFB reactor concept and not to design and operate a 100 MWe plant. Because of these practical considerations, the size of the IFB reactor and its compartments were fixed as indicated in Table 4.2. The square geometry of the reactor is induced by practical and constructional reasons.

One of the most important aspects that should be complied with in order to experimentally prove the IFB reactor concept, is a measurable sulfur capture and regeneration for the hydrodynamic and chemical parameters that can be varied during the experiments. Therefore, the gas-phase components of interest should be present in the IFB reactor at measurable concentrations. The latter is verified by means of an operational analysis (mentioned in chapter 4.3) and the specifications of the gas analysis equipment (chapter 4.2.2). From these results, the height of the beds (and thus, the height of the weirs) and the sizes of the orifices were determined.

**Table 4.2** Sizes in IFB reactor pilot plant facility.

Compartment size (m <sup>2</sup> )	D <sub>h</sub> <sup>(1)</sup> (m)	Distributor		Weir length (m)	d <sub>orifice</sub> (mm)	A <sub>lean</sub> /A <sub>dense</sub> (-)	H <sub>0</sub> <sup>(2)</sup> (mm)
		N <sub>hole</sub> (-)	N <sub>hole</sub> ' (·10 <sup>4</sup> /m <sup>2</sup> )				
1. 0.14x0.14	0.14	525	2.7	1→2=	10	4→1=2.33	35
2. 0.06x0.14	0.084	167	2.0	0.14	15		105
3. 0.06x0.06	0.06	96	2.7		20	2→3=0.43	175
4. 0.14x0.06	0.084	167	2.0	3→4=	25		
				0.06	30		

<sup>(1)</sup> D<sub>h</sub> = 4 x (surface of the compartment)/(perimeter of compartment)

<sup>(2)</sup> H<sub>0</sub> = position of the orifice measured from distributor plate  
H<sub>weir</sub> = 0.3 m

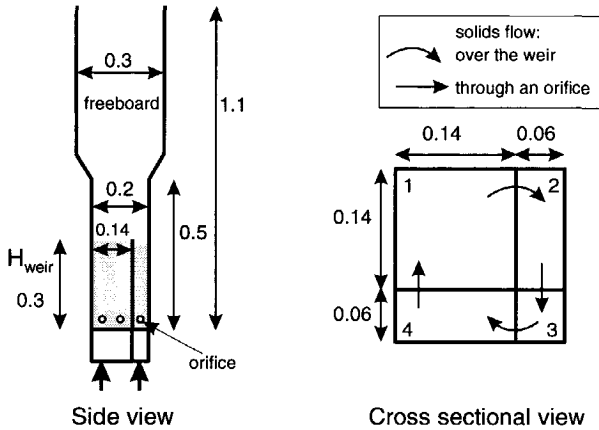
When the sizes of the IFB reactor are fixed, the gas distributor plate can be designed. The main purpose of the gas distributor is the uniform distribution of the gas into the bed. According to Sathiyamoorthy and Rao (1981) and Pell (1990) a comfortable pressure drop across the distributor is 40 to 50% of the pressure drop across the bed. A perforated plate was chosen in this design because no sintered plate (often used in laboratory units) was available that can withstand the conditions in the IFB reactor. Another reason is that a drilled plate is based on the designs of commercial scale gas distributors and therefore more representative for larger scale equipment (Pell, 1990).

An important design consideration is the gas velocity in the holes of the distributor. This velocity should not be higher than 80 m/s to prevent severe attrition of the particles in the vicinity of the jet penetrating the fluidized bed. Further, the diameter of a hole should be smaller than five times the particle diameter to prevent the smallest particles to trickle into the windbox. Geldart and Bayens (1985) give more details on these considerations as well as a design procedure. Following these guidelines and design procedure resulted in the specific design of the distributor for each of the four beds of the IFB reactor (see Table 4.2).

In order to prevent the smaller particles to be blown out of the fluidized bed in large amounts, a freeboard is used. A freeboard is often characterized by its TDH (Transport Disengagement Height). This represents the height above which the solids hold-up does not change any further. It was decided to fix the freeboard height at the transport disengaging

## Chapter 4

height. An estimation of TDH (*Zenz and Weil correlation*) can be obtained according to Geldart (1986). It is found that the TDH is approximately 0.5 m for a freeboard diameter of 0.3 m. The IFB reactor dimensions are then fixed as indicated in Figure 4.1.

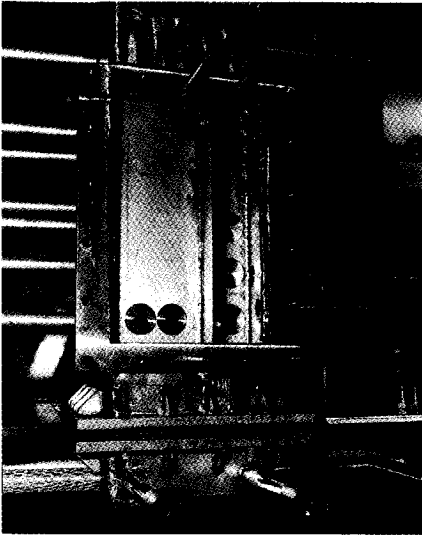


**Figure 4.1** Schematic views of the IFB reactor. In the cross-sectional view, the arrows indicate the direction of solids circulation. Compartment 1 and 3 are the sulfur capture and regeneration fluidized bed reactors respectively. Compartments 2 and 4 are transport beds operated at smaller gas velocities than the fluidized bed reactors. (sizes are indicated in meters)

The reactor material that was chosen needs to withstand high temperatures (up to 1000 °C), sulfurous gases as well as, oxidizing and reducing conditions. In practice such severe conditions will in most cases be resisted by a refractory lining. However in this small scale reactor this is not feasible. Therefore, a high temperature alloy (Haynes Alloy HR-120) was chosen that is capable of enduring the conditions mentioned. An overview of developments in high temperature alloys is given by Sorell (1994). In the HR-120 material, small additions of aluminum, silicon and rare earth elements modify protective oxides and therefore markedly improve the effectiveness of the material as a high temperature barrier for corrosion. According to Sorell (1994) a nickel-chromium (Ni-Cr) alloy such as the HR-120 is suitable for the conditions above mentioned.

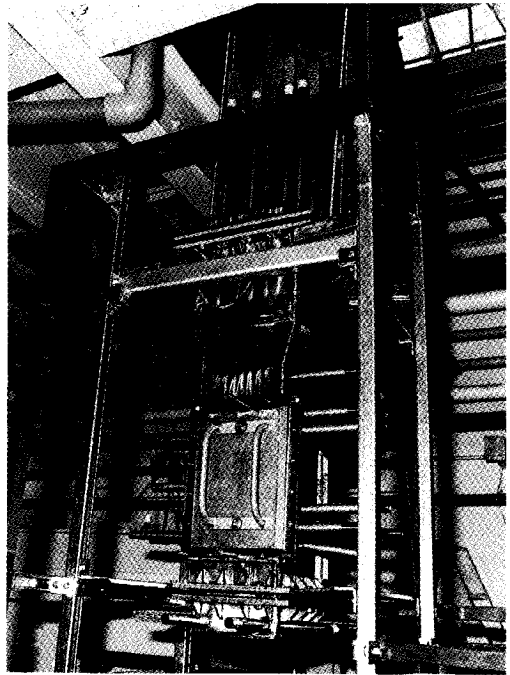
An impression of the IFB reactor and the pilot plant facility is given in the Figures 4.2, 4.3 and 4.4.

In Figure 4.2, a front view of the IFB reactor is shown. Two compartments can be observed: the regenerator at the right-hand side (smallest compartment) and the transport compartment 4 at the left-hand side. Solids flow from the regenerator over the weir (the height from the distributor plate is 300 mm) to compartment 4. From this compartment, the solids flow to the sulfur capture compartment through the orifices (or one of the orifices). The separating wall between compartment 4 and 1 in principle offers the possibility of applying one or two orifices for solids circulation as the orifices can be closed independently. The solids return to the regenerator from compartment 2 through the orifice at the right-hand side.



**Figure 4.2** Front view of the IFB reactor under construction.

A front view of the closed IFB reactor is given in Figure 4.3. Two grips are observed at the closing plate that is installed and secured (by means of high-temperature studbolts) to the square flanges that can be observed in Figure 4.2. At the top of the reactor, the sampling tubes are located for measuring bed heights (see chapter 4.2.1).



**Figure 4.3** Front view of the closed IFB reactor under construction.

The tubes at the left- and right-hand side of the reactor are used for measuring temperatures and pressures and for sampling of gas and solids. At the bottom of the reactor, two tubes are welded to the reactor for each compartment. These are used for gas supply and measuring of the pressures below the gas distributor plates. The gas distributor plates are not visible at this picture as they are positioned just below the lower flange at 35 mm of the centre of the orifice.

## Chapter 4

---

In Figure 4.4, a side view of the IFB reactor under construction is presented. The reactor can be observed as well as the afterburning section (where reducing gases are combusted) and the cyclone.

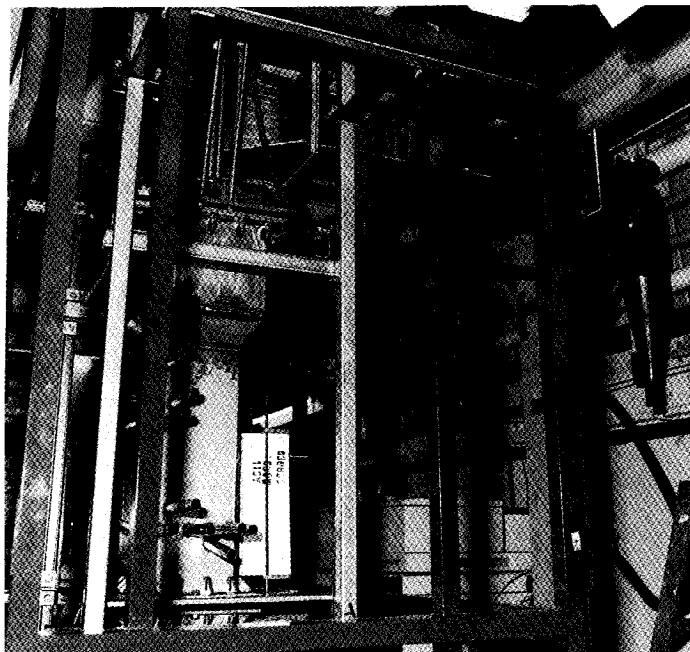


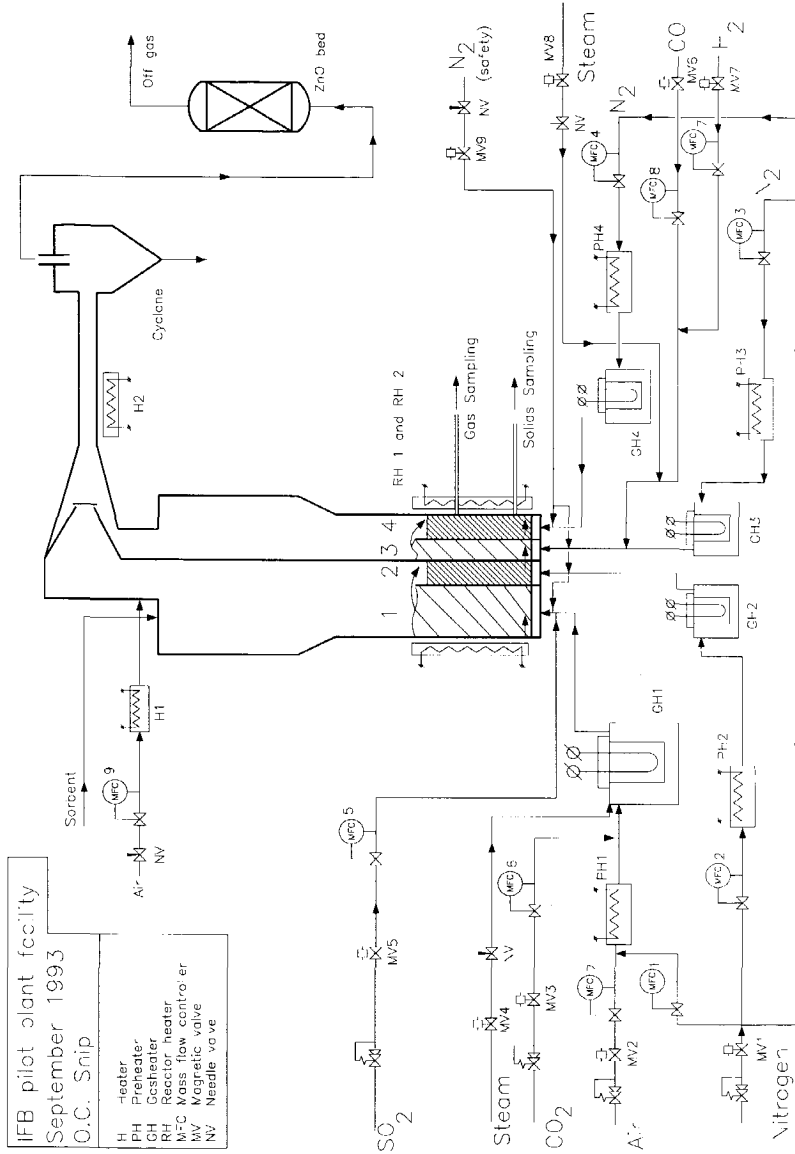
Figure 4.4 Side view of the IFB reactor under construction.

In Figure 4.5 the **flowsheet** of the pilot plant facility is given. It can be seen that the gas flow for all components is controlled by means of Magnetic Valves (MV's) and Mass Flow Controllers (MFC's). The gas dosing is fully automatic, controlled by a personal computer through a hardware interface between process and so-called *FIX* control software.

The gases are electrically heated in two steps: 20-500 °C in the preheaters (PH1 to PH4) and 500-900 °C in the gasheaters (GH1 to GH4). Furthermore, the reactor is electrically heated by means of reactor heaters (RH1 and RH2).

The two freeboards of beds 1 and 2 and of beds 3 and 4, respectively, are connected at the top of the reactor. In the afterburning section, the combustible gases are converted to their combustion products. In the cyclone, the fines are separated from the gas stream. The cyclone diameter was determined according to Coulson and Richardson (1991) at 0.17 m. The cut size diameter was set at 7  $\mu\text{m}$  ( $d_{p,50}$ ). This is the particle size of which 50% is collected. The subsequent dimensions of the cyclone geometry were taken from Perry and Green (1988). To prevent any  $\text{H}_2\text{S}$  to leave the system in the off-gas, a vessel filled with ZnO particles (type HTZ-4, Haldor Topsøe) was installed after the cyclone.





**Figure 4.5** Flowsheet of the IFB pilot plant facility. Gas supply can be opened by means of Magnetic Valves (MV) and controlled by means of Mass Flow Controllers (MFC) for all gas phase supply lines. Gases are preheated by means of PreHeaters (PH) and further heated to reaction temperatures by GasHeaters (GH). ReactorHeaters (RH) are used to directly heat the IFB reactor. The extra air for combustion of reductive gases (H<sub>2</sub>S, H<sub>2</sub> and CO) is heated by H1 and the combustion section is heated by means of heater H2. After the cyclone, the H<sub>2</sub>S that is possibly not converted is captured in the ZnO bed.

### 4.1.2 Safety

In general, the IFB reactor and pilot plant facility are guarded by continuous monitoring of pressures, temperatures, and concentrations of toxic or explosive gases. The measured values are compared to the setpoints. In case of an alarm, all magnetic valves will be closed except for the so-called safety nitrogen (MV9) which is a down-to-open type valve.

The **pressures** are measured at various positions in the reactor. The purpose is to monitor, amongst others, excess pressure that may be built up in the system. Below the gas distributor plate, the pressure is controlled for too high and too low pressure. The latter is an indication that the main gas stream to the reactor is not present. At the top of the reactor three safety relief valves were installed that will open in case of failure of the other safety measures.

All heaters are protected for overheating by means of **temperature** controllers and temperature registration by thermocouples. Further temperature safety measurements are carried out in the reactive compartments of the IFB reactor and the afterburning section.

Another issue that needs to be addressed to is the **explosion risk** in the system. To prevent explosion events, two important conditions have to be satisfied:

1. the temperature has to be higher than the auto-ignition temperature of the explosive gases ( $> 625\text{ }^{\circ}\text{C}$ ) and
2. the concentrations of these gases need to be outside the explosion limits.

The explosive or reducing gases (such as  $\text{H}_2$  or  $\text{CO}$ ) enter the reactor in the regenerator. The design of the air supply system is such that no air can be introduced in this IFB compartment. The only oxygen source could be internal leakage from compartment 1. This is not very likely to happen. Nevertheless, a minimum temperature controller was installed that is connected to the  $\text{CO}$  and  $\text{H}_2$  magnetic valves. This controller determines whether the reducing gases can be supplied or not. Further explosion risk is present in the afterburning section where the gases from the two freeboards of the IFB reactor are mixed. Here, the temperature is controlled at a minimum and excess air is supplied to ensure a surplus amount of air. When the air supply halts, a minimum pressure controller in the feeding line will close the magnetic valves for the reducing gases immediately. By means of these safety measures, the facility is considered to be sufficiently protected against explosions or any violent chemical reactions.

## 4.2 Measuring in the IFB facility

In addition to the measurements of temperature and pressure for process control, safety and operational aspects, several quantities need to be measured for the investigation of the IFB reactor behaviour as a function of the operational parameters. These measurements concern the hydrodynamics of the system and the gas-solids reactions that take place.

### 4.2.1 Hydrodynamics

The hydrodynamics of the IFB system concern those phenomena that determine the **solids distribution** and the Circulation Rate of the Solids (CRS) in the IFB reactor. These two

hydrodynamic quantities need to be determined on-line as a function of the operational parameters because the resulting sulfur retention that is achieved in the IFB reactor is depending on solids distribution as well as CRS.

***Solids distribution***

Initially, the total mass in each compartment of the IFB system is known. However, the distribution of the mass over the four compartments needs to be determined from measurements. In principle, the solids hold-up (or bed mass) of a compartment can be determined from the height of the bed and the bulk density.

Several methods and devices are available to measure the bed levels for bulk solids:

- ▶ radiation absorption
- ▶ ultrasonic ranging devices
- ▶ capacitance probes
- ▶ pressure gradient extrapolation
- ▶ laser light reflection
- ▶ visual observation

The complicating factors in the IFB reactor are the high temperature and the chemical environment in the reactor. Therefore, the measurements of the bed levels need to be carried out through a sampling tube with a limited (20 mm) inner diameter. General considerations on level-measurements are described and summarized by Knight and Pugh (1996). Experimental work was performed by Van den Hengel (1994) to test various techniques (ultrasonic, pressure gradient, visual observation and laser light reflection). Only two methods gave satisfying results with respect to the accuracy (experimental error of the measurement should be smaller than 10% of the total bed height) and practical applicability in the IFB facility:

1. Laser Light Reflection (LLR). This is a direct, temperature independent and contactless method. It is based on measurement of the time needed for a high frequency laser pulse to be reflected between the bed surface and the laser apparatus (Leica Disto). The experimental error in the bed height measurement was smaller than 0.01m at an average bed height of 0.30 m. For the measurements by means of laser light reflection, a measuring tube was installed on top of the reactor for each compartment in which a transparent piece of quartz was mounted. This allows also visual observation of the fluid bed behaviour in the IFB reactor (see Figure 4.6).
2. Pressure Gradient Extrapolation (PGE). This method is based on measuring the pressure gradient over a well-defined distance (here 0.15 m) in the bed (see Figure 4.6). It was experimentally confirmed (Van den Hengel, 1994) that a linear pressure profile in the bed can be assumed. In that case, the following relation holds:

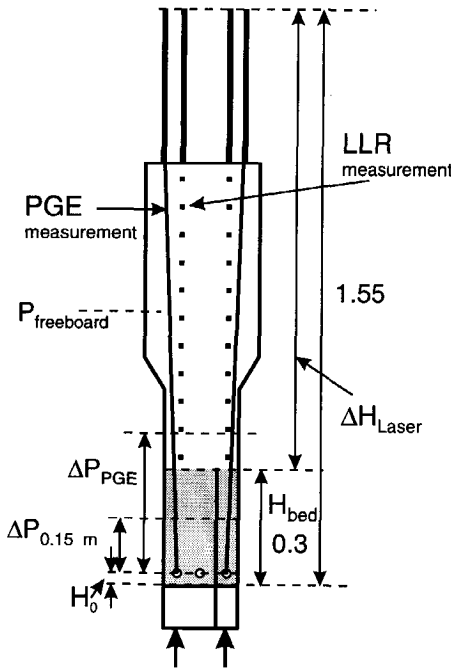
$$\frac{\Delta P_{PGE}}{(H_{bed} - H_0)} = \frac{\Delta P_{0.15m}}{0.15} \tag{4.1}$$

The terms  $\Delta P_{PGE}$  and  $\Delta P_{0.15 m}$  refer to the pressure difference between  $H_0$  (height of the center of the orifice measured from the distributor plate) and the freeboard and between

$H_0$  and a position 0.15 m higher in the bed respectively (see Figure 4.6). The value for  $H_0$  during the experimental work described in this thesis was 35 mm. The actual bed height can then be obtained from:

$$H_{bed} = H_0 + \left( \frac{\Delta P_{PGE}}{\Delta P_{0.15m}} \right) \cdot 0.15 \tag{4.2}$$

The experimental error in the measurement of  $H_{bed}$  by means of PGE was smaller than 0.02m at an average bed height of 0.30 m.



**Figure 4.6** Measuring bed heights and pressure drop across the orifice ( $\Delta P_{orifice}$ ) in the IFB reactor. The bed heights can be measured by means of Laser Light Reflection (LLR) and Pressure Gradient Extrapolation (PGE). LLR is based on the measured distance between the top of the measuring tube and the bed surface ( $\Delta H_{laser}$ ) and the known distance between the top and the distributor plate (1.55 m at 850°C). PGE is based on the measured pressure gradient in the bed ( $\Delta P_{0.15m}$ ) and the pressure in the freeboard (Equation 4.2).

Both methods will be used as complementary measuring methods, and results can thus be compared to verify the correctness of measured values. The PGE method is used on-line while the laser measurement is used for verification by means of comparing the measured bed heights of both methods.

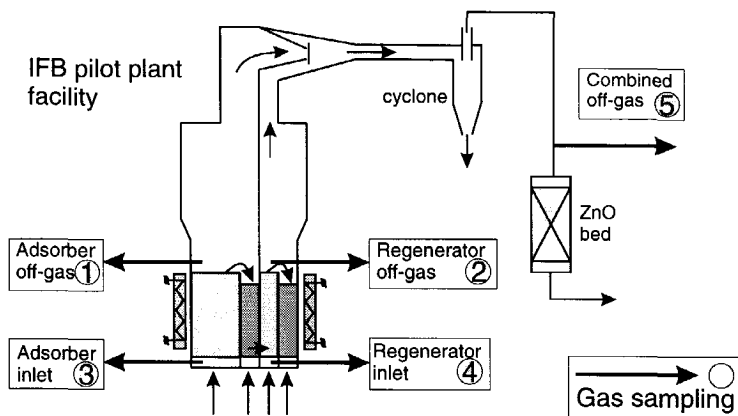
From the measured pressure gradient in the bed, it is also possible to determine the bulk density. Below the minimum fluidization velocity, the voidage is taken constant at  $\epsilon_{mf}$ . When the bed is fluidized, the pressure drop is considered to be the static height of the fluid particle mixture. The solids distribution in the IFB system can thus be determined experimentally.

### CRS

Direct measurement of the CRS in the hot IFB reactor is not a simple matter and would require additional research and extra facilities in the pilot plant. It was therefore decided to estimate the CRS on the basis of pressure drop measurements in the reactor (see Figure 4.6). The pressure drop across the orifice is a measure of the solids flow through the orifice. The possible differences in freeboard pressure are accounted for. The gas flow through the orifice is estimated on the basis of pressure gradient measurements in the dense bed (see chapter 2.6 for a detailed description).

### 4.2.2 Gas and solids analysis

A Fourier Transform Infrared (FT-IR) spectrometer, SESAM1, (System for Emission Sampling And Measurement, by Siemens AG and Nicolet Corp.) has been used for quantitative gas analysis. The inlet gas compositions and the concentration of the gases in the reactor at different positions in the IFB facility can be measured (as indicated in Figure 4.7). A PC controlled sampling program (in *FIX* control software) was developed that can switch fully automatic between 4 sampling positions.



**Figure 4.7** At the five indicated positions in the IFB facility, gas can be sampled and subsequently analyzed for its composition by means of the FT-IR spectrometer.

General features of the SESAM1 FT-IR apparatus are:

- ▶ single-pass cell (path 0.8 m; volume 1.57 ltr)
- ▶ liquid-N<sub>2</sub> cooled MCT detector
- ▶ cell temperature control ( $185 \pm 2$  °C)
- ▶ cell pressure control ( $86.5 \pm 0.1$  kPa)
- ▶ sample pump (1-10 ltr/min)
- ▶ heated gas filter and sample line ( $185 \pm 2$  °C)

The heated gas cell and the heated gas sampling system is applied in order to avoid condensation of water and water-soluble components or sulfurous gases. The components of interest in this study that can be measured by the infrared technique are: SO<sub>2</sub>, H<sub>2</sub>S, H<sub>2</sub>O, CO and COS.

The FT-IR apparatus was calibrated in the appropriate concentration ranges for these components. A detailed description of the calibration procedure is given by de Feber (1995) and Korbee *et al.* (1994a). Special attention was given to the presence of water in a gas mixture. This component shows strong absorption in the infrared spectrum and can therefore interfere the measurement of the other components of interest. Its influence can be twofold: peak overlap and component interaction.

Peak overlap occurs when water absorbs in the same range of frequencies where the component is to be measured. Component interaction can be considered as a change of the infrared 'fingerprint' of a component by the presence of another component. Both effects were accounted for in the calibration procedure. The FT-IR apparatus could then be used for simultaneous and on-line measurement of the components of interest.

In case of non-stationary behaviour of the gas-phase composition in the IFB reactor, it is important to verify the effects of gas residence time and distribution in the sample lines to the FT-IR equipment. The FT-IR apparatus measures the gas phase concentration in the cell every 2 seconds and stores an average value of these measurements every 30 seconds. The length of the tubing that is passed by the gases from sampling position in the IFB facility to the gas cell is approximately 10 m (inner diameter, 4 mm). During operation, the FT-IR sample pump was operated at a constant gas flow rate of 4 l/min. The gas residence time in the tubing is therefore less than 2 seconds which is much smaller than the non-stationary effects that were encountered during the experiments in the IFB facility (time constant in the order of minutes, see chapter 5.4). It can therefore be assumed that the effects of dead time and dispersion effects of the gas phase components in the sample lines are negligible.

Furthermore, the sorbent material can be sampled from the reactor and analyzed off-line for its contents on  $\text{CaSO}_4$  and  $\text{CaS}$  by means of wet chemical analysis.

### 4.3 Operational analysis of the IFB facility

An operational analysis of the IFB reactor was performed in order to study the influence of the reaction and the hydrodynamic parameters on reactor performance. This analysis was carried out in relation to the design of the IFB facility. The operational analysis should reveal whether the IFB reactor as presented in chapter 4.1.1, is capable of proving the IFB reactor concept. It was therefore verified whether the proposed values for the design parameters mentioned in chapter 4.1.1 result in measurable gas-phase concentrations in the sulfur capture and regeneration compartments of the IFB reactor. This should be the case for a range of operational conditions for both the hydrodynamic (gas velocities) and reaction parameters (inlet gas phase concentrations). The detailed description of the operational analysis is given by Snip *et al.* (1995), a comprehensive summary is given below.

#### 4.3.1 Modelling the IFB reactor

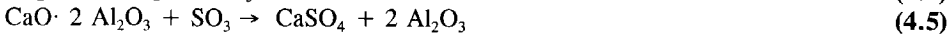
The *hydrodynamics* of the IFB reactor concern those phenomena that determine the solids circulation. In this analysis the CRS was calculated under the assumption that the solids transport from compartment 4 to compartment 1 is controlling the solids circulation (see chapter 3 of this thesis for more details on this matter). The solids flow through the connecting orifice is calculated according to:

$$\phi_m = C_D A_o \rho_d \sqrt{\frac{2(\sigma_N + \Delta P)}{\rho_p(1 - \epsilon_d)}} \quad (4.3)$$

In this relationship the pressure drop ( $\Delta P$ ) and the particle stress that is directed in horizontal direction ( $\sigma_N$ ) are considered as the driving forces for solids flow. All non-idealities are

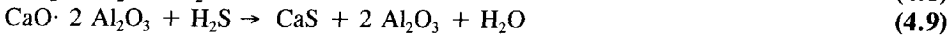
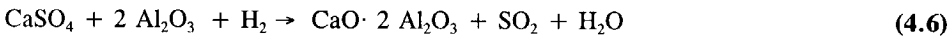
accounted for by the discharge coefficient ( $C_D$ ). A detailed description of the model is given by Korbee *et al.* (1994b) and is further discussed in chapter 2 of this thesis.

The calculated results from the hydrodynamic model need to be translated to the performance of the IFB system in terms of sulfur retention. Therefore, the *sulfur capture and regeneration* processes need to be considered. In modelling the reactors, the gas and solids phase are assumed to be ideally mixed. Residence time distribution was not taken into account. The sulfation reaction taking place in the adsorber (compartment 1), is assumed to proceed through the formation of  $\text{SO}_3$  according to:



The sulfation process is further described by an unreacted shrinking core model, the SURE2 model (Wolff *et al.*, 1991). In this model, the rate of sulfation is assumed to be first order in the  $\text{SO}_3$  concentration at the core radius and first order in the outer surface of the core. The model has previously shown that it can adequately predict the sulfation behaviour of the SGC-500 sorbent for reactors of different scale (Wolff *et al.*, 1991).

The kinetic model for the regeneration (compartment 3) is based on two gas-solid reactions and two reversible gas phase reactions (Korbee *et al.*, 1993):



The regeneration reactions are considered to be first order in the outer surface of the sorbent particles and first order in the gas concentrations. This is similar to the SURE model approach that was introduced by Schouten and Van den Bleek (1987). The appropriate kinetic parameters were obtained from fluidized bed experiments described by Korbee (1995).

The calculations commenced at the determination of the CRS through the IFB system. Then, the sulfur capture and regeneration calculations were performed resulting in the overall sulfur retention of the IFB system as a function of the hydrodynamics (*viz.*, CRS) and kinetic parameters.

### 4.3.2 Results and consequences for design and operation

#### *Hydrodynamics*

The hydrodynamic (design and operational) parameters that were varied in the model simulations are:

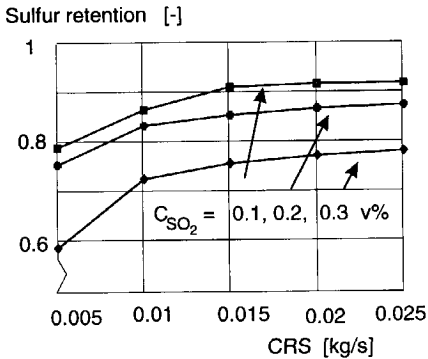
- ▶ the orifice size
- ▶ bed heights
- ▶ bed area ratio's and
- ▶ gas velocities to the compartments.

Increasing the orifice size clearly results in a higher CRS. A maximum in solids flow occurs at minimum fluidization conditions in the dense bed. The bed area ratio's (lean over dense

bed size) in the IFB reactor (2.33 and 0.43) do affect the solids flow phenomena through gas transfer phenomena. An equal amount of gas from the dense bed will decrease the bulk density of the lean bed stronger for a smaller bed area ratio. The resulting values of the CRS as a function of the design and the operational parameters were used in regenerative desulfurization calculations (mentioned below) to reveal their influence on the regenerative sulfur capture in the IFB reactor.

**Regenerative desulfurization**

The influence of the hydrodynamic parameters can be translated to the CRS dependency of sulfur retention, thereby yielding their influence on the overall sulfur retention that is achieved in the IFB reactor.



**Figure 4.8** Sulfur retention in compartment 1 of the IFB reactor as a function of the Circulation Rate of the Solids (CRS) for three inlet gas phase concentration of SO<sub>2</sub>. It was assumed that the sorbent is fully regenerated in the regenerator (compartment 3).

The input parameters (inlet gas phase concentrations) are chosen such that regeneration of the sorbent is not rate-limiting. The sorbent is thus completely regenerated. It was experimentally shown by Korbee (1995) that this is a realistic assumption. For different values of the inlet SO<sub>2</sub> concentration (corresponding to approximately 1-3 wt% sulfur in coal), the sulfur retention was calculated as a function of the CRS (see Figure 4.8). The sulfur retention increases with increasing CRS. It can be observed that for low CRS (*viz.*, higher solids residence time in the compartments) its influence is stronger. At higher CRS, the sulfur retention diminishes to a nearly constant value. This is caused by the fact that the sulfur capture rate is dependent on the degree of sulfation.

**Consequences for design and operation**

The size of the orifice is an important design parameter because the CRS is strongly depending on its size. Increasing the size of the orifice will result in a higher CRS and will subsequently lead to a higher sulfur retention. However, the increase in sulfur retention is limited at high sorbent conversions (Figure 4.8).

The major operating parameter is the aeration rate of the dense bed used for control of the solids flow rate. Adjusting the aeration rate, the CRS and therefore the sulfur retention can be controlled. The total solids hold-up in the IFB system is also important to be considered. This influences the sulfur retention in two ways. Firstly by means of the CRS and secondly through the solids distribution.

The CRS was determined as a function of the design and operational parameters. The range of CRS that could be achieved in the IFB system as a function of the operational parameters (*viz.*, gas velocities to the compartments and total IFB bedmass) was verified for regenerative desulfurization behaviour and lead to the choice of the IFB sizes (for orifice size and bed



## IFB pilot plant facility: design, construction and operation

heights) as indicated in Table 4.2. By means of determining the sulfur retention as a function of the CRS in the IFB system, it was shown (see Figure 4.8) that measurable gas-phase concentrations can be achieved in the desulfurization compartment. This was also shown for the regenerator compartment of the IFB reactor. Reference is made to Snip *et al.*, 1995) for more details on these considerations and results.

It is thus (in principle) possible to prove the IFB reactor concept by means of the IFB pilot plant facility. The experimental results that were obtained in the IFB pilot plant facility are described in chapter 5 of this thesis.

### Notation

$A_o$	: cross sectional area of the orifice	[m <sup>2</sup> ]
$A_{lean}$	: cross sectional area of lean bed	[m <sup>2</sup> ]
$A_{dense}$	: cross sectional area of dense bed	[m <sup>2</sup> ]
$C_D$	: discharge coefficient	[-]
$D_H$	: hydraulic diameter	[m]
$d_{orifice}$	: orifice diameter	[m]
$d_p$	: particle diameter	[m]
$f$	: friction factor	[-]
$H$	: height	[m]
$H_{bed}$	: expanded bed height	[m]
$H_o$	: height of the orifice measured from distributor plate	[m]
$\Delta H_{laser}$	: distance measured by means of laser light reflection	[m]
$K$	: stress ratio	[-]
$N_{hole}$	: number of holes	[-]
$N_{hole}'$	: number of holes per square meter	[m <sup>-2</sup> ]
$\Delta P$	: pressure drop across the orifice	[Pa]
$\Delta P_{0.15 m}$	: pressure drop across 0.15 m bed	[Pa]
$\Delta P_{PGE}$	: pressure difference between freeboard and orifice height	[Pa]
$S_{BET}$	: B.E.T. surface area	[m <sup>2</sup> /g]
$U$	: superficial gas velocity	[m/s]

### Greek

$\alpha_r$	: angle of repose	[°]
$\epsilon_{fixed}$	: fixed bed voidage	[m <sup>3</sup> <sub>gas</sub> /m <sup>3</sup> <sub>bed</sub> ]
$\epsilon_u$	: voidage of the upflowing bed	[m <sup>3</sup> <sub>gas</sub> /m <sup>3</sup> <sub>bed</sub> ]
$\sigma_N$	: horizontally directed particle pressure	[Pa]
$\rho_d$	: bulk density of dense bed	[kg/m <sup>3</sup> <sub>bed</sub> ]
$\rho_p$	: particle density	[kg/m <sup>3</sup> <sub>particle</sub> ]
$\phi_m$	: solids mass flow	[kg/s]

### Subscripts

bd	: bed	N	: normal
h	: hydraulic	o	: orifice
mf	: minimum fluidization	w	: wall
lean	: lean bed, operated at relatively high gas velocity		
dense	: dense bed, operated at relatively low gas velocity		

## Chapter 4

---

### References

- Atakül, H., Wakker, J.P., Gerritsen, A.W., Berg van den, P.J., "Regeneration of MnO/gamma-Al<sub>2</sub>O<sub>3</sub> used for high-temperature desulfurization of fuel gases", *Fuel*, 75 (3), 373-378 (1996).
- Coulson, J.M., Richardson, J.F., "Chemical Engineering: Design", Volume 6, Pergamon Press, Oxford, 378-379 (1991).
- Feber de, M.A.P.C., "Interconnected Fluidized Bed for regenerative desulfurization: development and testing of the IFB pilot plant facility", MSc report, Delft University of Technology (1995).
- Geldart, D., Bayens, J., "The design of distributors for gas-fluidized beds", *Powder Technol.*, 42, 67-78 (1985).
- Geldart, D., "Particle entrainment and carryover", Chapter 6, in: "Gas fluidization technology", Geldart, D. (Ed.), John Wiley & Sons Ltd., (1986).
- Hengel van den, R., "High temperature bed height measurement in the Interconnected Fluidized Bed", MSc report, Delft University of Technology (1994).
- Knight, E.A., Pugh, J.R., "Properly select level-measurement devices for bulk solids", *Chem. Eng. Progr.*, February issue, 50-55 (1996).
- Korbee, R., "Regenerative desulfurization in an Interconnected Fluidized Bed System", PhD thesis, Delft University of Technology, Delft, The Netherlands (1995).
- Korbee, R., Grievink, J., Schouten, J.C., Bleek van den, C.M., "Preliminary design of a 100 MWe power plant with regenerative desulfurization applying Interconnected Fluidized Bed technology", In: *Proceedings of the 12th International Conference on Fluidized Bed Combustion of Coal*, Vol. 2, (Eds: Rubow, L., Commonwealth, G.), San Diego, USA, 1143-1151 (1993).
- Korbee, R., Schouten, J.C., Bleek van den, C.M., "Measuring and Calibration Experience with an FT-IR system: quantitative use in complex gas mixtures", In: *proceedings of the Nordic Seminar on Gas Analysis in Combustion*, (Ed.: Hernberg, R.), Tampere, Finland, 63-76 (1994a).
- Korbee, R., Snip, O.C., Schouten, J.C., Bleek van den, C.M., "Rate of solids and gas via an orifice between partially and completely fluidized beds", *Chem. Eng. Sci.*, 49 (24B), 5819-5832 (1994b).
- Pell, M., "Gas fluidization", Chapters 3 and 10, Elsevier, 21-29 (1990).
- Perry, R.H., Green, D. (Eds.), "Perry's Chemical Engineers' Handbook", Mc-Graw-Hill, Singapore, 20-84 (1988).
- Picciotti, M., "Specify standpipes and feeder valves for packed beds", *Chem. Eng. Progr.*, January, 54-63 (1995).
- Sathiyamoorthy, D., Rao C.S., "The choice of distributor to bed pressure drop ratio in gas fluidised beds", *Powder Technol.*, 30(2), 139-143 (1981).
- Schouten, J.C., Bleek van den, C.M., "The DUT SURE model: A simple approach in the FBC sulfur retention modeling", In: *Proceedings of the 9th Conference on Fluidized Bed Combustion*, (Ed. Mustonen, J.P.), ASME, Boston, USA, Vol. 2, 749-761 (1987).
- Snip, O.C., Korbee, R., Schouten, J.C., Bleek van den, C.M., "The influence of hydrodynamics on the performance of an Interconnected Fluidized Bed system for regenerative desulfurization", *AIChE Symp. Series*, 91 (308), 82-92 (1995).
- Wakker, J.P., "Development of a high temperature steam regenerative H<sub>2</sub>S removal process based on alumina supported MnO and FeO", PhD thesis, Delft University of Technology, The Netherlands (1992).
- Wolff, E.H.P., Gerritsen, A.W., Bleek van den, C.M., "Multiple reactor testing of a synthetic sorbent for regenerative sulfur capture in fluidized bed combustion of coal", *Can. J. Chem. Eng.*, 71 (February), 83-93 (1993).

# Chapter 5

## IFB pilot plant facility for regenerative desulfurization

experimental and modelling results

---

### 5.1 Experimental work in the IFB pilot plant facility

The main aspects considering the design and the construction of the IFB pilot plant facility are described in chapter 4. The purpose of the facility was to show the suitability of the IFB reactor concept to be used in a continuous high-temperature desulfurization process. The pilot plant was designed to investigate general process performance and operability at a temperature up to 850 °C, and to assess the influence of operating conditions (fluidization velocities, sorbent inventory and inlet gas phase concentrations) on the Circulation Rate of Solids (CRS), sulfur retention and regenerator product.

The experimental work as carried out in the IFB facility concerns hydrodynamic as well as regenerative desulfurization measurements. The regenerative desulfurization was carried out as described in the previous chapter. Hydrogen was used as the regeneration gas.

Due to the complexity of the experimental facility, the experiments were carried out in the following order:

1. Introductory and hydrodynamic experiments
2. Batch experiments: sulfur capture, regeneration and successive sulfur capture and regeneration experiments including solids circulation
3. Continuous sulfur capture and regeneration experiments

#### 1. *Introductory and hydrodynamic experiments*

The introductory measurements comprehended the investigation of the proper functioning of the various utilities that were installed in the facility. Several tests were carried out to check the well functioning of all parts of the facility: gas heating system, safety measures, pressure drop measurements, bed level measurements, process control and data acquisition system and gas analysis apparatus (FT-IR).

Because of several experimental complications concerning the gas heaters, the temperature that is representative for regenerative desulfurization during Fluidized Bed Combustion (FBC) of coal (850 °C) could not be reached. Most of the experiments were therefore carried out at lower temperatures (from 650 to 750 °C).

The temperature effect and the determination of the minimum fluidization velocity of the sorbent material (that was used for all experiments mentioned in this chapter) is described in chapter 5.2. Furthermore, the determination of the CRS on the basis of pressure drop measurements is explained in this chapter as well. The determination of the steady-state CRS

## Chapter 5

was carried out and verified for the continuous regenerative desulfurization experiments (see Table 5.4 and chapter 5.5).

### 2. Batch experiments

Before continuous regenerative desulfurization experiments were started, three consecutive sulfur capture and regeneration experiments were carried out. The measured trends for both desulfurization and regeneration are given in chapter 5.4. Furthermore, the related modelling results and the consequences for modelling are described as well.

### 3. Continuous sulfur capture and regeneration experiments

Following the batch experiments, a number of continuous regenerative desulfurization experiments was carried out. Two sets of experiments can be distinguished because of a difference in temperature between the experiments (as explained in chapter 5.5). These are a five-day test and a ten-hour test of continuous operation.

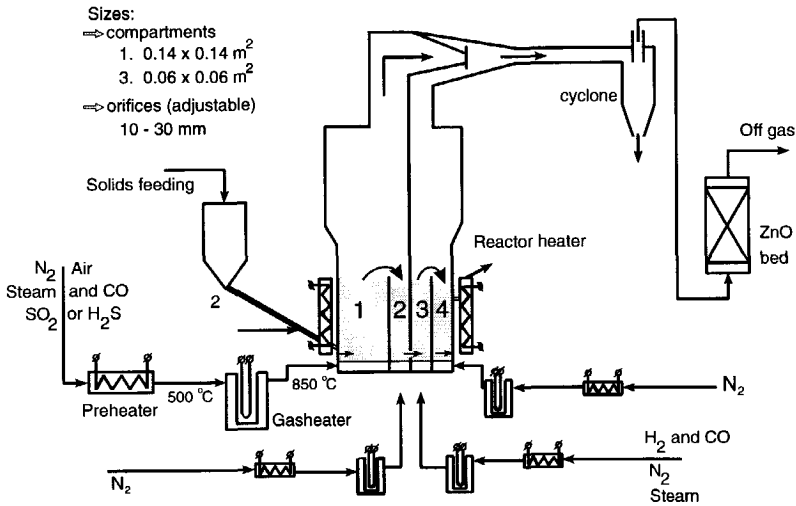


Figure 5.1 IFB pilot plant facility for high temperature regenerative desulfurization.

The experimental results obtained in the IFB pilot plant facility (see Figure 5.1) are thus presented and discussed in this chapter together with the relevant modelling considerations. It should be mentioned that during this research period no mathematical models were developed or kinetic data was measured concerning sulfur capture or regeneration. The main target of this work was to show the suitability of the IFB reactor system for a high temperature gas/solids regenerative desulfurization process. Therefore, the description of modelling work on sulfur capture and regeneration that is given in this chapter is based on earlier work carried out at DUT (Wolff, 1991; Korbee, 1995) (see chapter 5.3).

A full description of the experimental and modelling work and details concerning the measurements and the IFB facility can be found in the MSc reports of Kraijo (1996), van Ling (1996) and Smaling (1996).

## 5.2 Hydrodynamics and solids circulation in the IFB reactor at high temperature

### 5.2.1 Minimum fluidization velocity

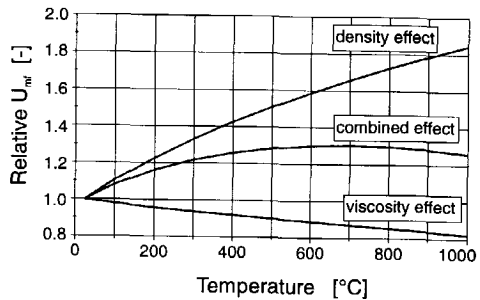
#### Temperature effect

The minimum fluidization velocity ( $U_{mf}$ ) of the sorbent is an important parameter in operating and analysing the IFB reactor. In order to describe the experiments with respect to their hydrodynamic behaviour it is important to know adequate values for  $U_{mf}$  at the elevated temperatures (650 to 850 °C) that are applied in the IFB facility.

In chapter 2, the minimum fluidization velocity was experimentally determined at ambient temperature ( $U_{mf} = 0.75$  m/s at 20 °C). Many correlations are available in literature to estimate the temperature effect on  $U_{mf}$  (Botteril, 1989; Yates, 1996). The equation that is generally used, is obtained when it is assumed that at minimum fluidization conditions the weight of the solids is balanced by the pressure drop according to the Ergun equation (Kunii and Levenspiel, 1991):

$$\frac{d_p^3 \rho_g (\rho_p - \rho_g) g}{\mu_g^2} = \frac{1.75}{\epsilon_{mf}^3 \phi_s} \left( \frac{d_p U_{mf} \rho_g}{\mu_g} \right)^2 + \frac{150 (1 - \epsilon_{mf})}{\epsilon_{mf}^3 \phi_s^2} \left( \frac{d_p U_{mf} \rho_g}{\mu_g} \right) \quad (5.1)$$

It can be seen that  $U_{mf}$  depends on gas properties ( $\rho_g$  and  $\mu_g$ ) as well as particle properties ( $d_p$ ,  $\rho_p$ ,  $\phi_s$  and  $\epsilon_{mf}$ ). In Figure 5.2 the effects of gas (air) density and viscosity are shown on the minimum fluidization velocity of the sorbent particles that are applied in the IFB reactor. The calculated value for  $U_{mf}$  is expressed as the ratio to  $U_{mf}$  at 20 °C. Variations in the minimum fluidization voidage ( $\epsilon_{mf}$ ) with temperature also affect  $U_{mf}$ . However this effect is strongly decreasing for increasing particle size (Raso *et al.*, 1992) caused by a relative decrease in particle interaction forces. Despite the predictive correlations to estimate  $U_{mf}$  at elevated temperatures it is in general better to determine the proper value of  $U_{mf}$  experimentally at reaction conditions for a given particle system.

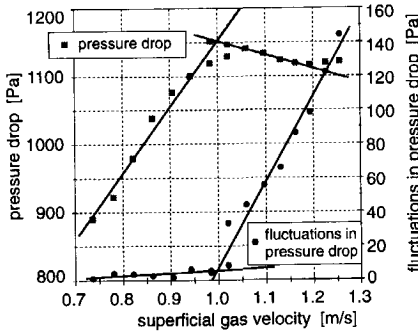


**Figure 5.2** Effect of gas density and viscosity on the minimum fluidization velocity of the sorbent particles according to Equation 5.1. The plotted value for  $U_{mf}$  is related to the value of the minimum fluidization velocity at 20 °C.

#### Experimental determination

To determine  $U_{mf}$  at high temperatures, experiments were carried out in a small scale facility (50 mm diameter quartz column). It was decided to determine the minimum fluidization velocity by means of:

1. pressure drop measurements, and by
2. measuring the pressure fluctuations.



**Figure 5.3** Measured pressure drop and pressure drop fluctuations as a function of the superficial gas velocity at 850 °C. Both type of measurements were used for the determination of  $U_{mf}$  (viz., 1 m/s).

In the second method, it is assumed that the standard deviation of the fluctuations increases linearly with the excess gas velocity ( $U-U_{mf}$ ). This method has shown to give results that are in agreement with the results from the pressure drop method (see for example: Punčochář *et al.* (1985), Hong *et al.* (1990) and Wilkinson (1995)).

In Figure 5.3, the results are shown for an experiment that was carried out at 850 °C. It can be seen that the measured values for  $U_{mf}$  are in agreement for both experimental methods. In Table 5.1, the experimental results are given for the measurements at the indicated

temperatures. The calculated values according to the Ergun equation (Equation 5.1) are in good agreement with the experimental values for  $U_{mf}$ . The particle shape factor ( $\phi_s$ ) was experimentally determined (by means of image analysis) to be 0.975.

**Table 5.1** Calculated and experimental values for the minimum fluidization velocity. The values for  $\epsilon_{mf}$  and  $U_{mf}$  were determined by Laser Light Reflection (see chapter 4.2.1) and pressure fluctuation measurements respectively.

Temperature (°C)	$\epsilon_{mf}$ exp. (-)	$U_{mf}$ exp. (m/s)	$U_{mf}$ calc. (m/s)
650	$0.418 \pm 0.002$	1.07	1.06
850	$0.410 \pm 0.002$	1.00	1.01

It is concluded that the Ergun equation can be used to estimate adequate values for  $U_{mf}$  provided that the minimum fluidization voidage is known at the specific temperature. The effect of temperature cannot be easily distracted from the two measurements listed in Table 5.1 due to the differences in  $\epsilon_{mf}$  during the experiments. A small difference in  $\epsilon_{mf}$  will strongly affect the calculated value for  $U_{mf}$ . It was calculated (by means of the Ergun equation) that the relative effect on  $U_{mf}$  of the difference in temperature (650 to 850 °C) is approximately 2%.

Further, it is shown that the pressure drop fluctuations are suitable for determination of the minimum fluidization velocity. This provides a useful opportunity for monitoring  $U_{mf}$  during operation of the IFB system. The actual value of the minimum fluidization velocity can then be used for setting the operating conditions (viz., superficial gas velocities) of the IFB system.

The effect of changing particle properties was examined in the experiments that were carried out in the pilot plant facility. The particle size and shape were analyzed during and after the experiments from samples taken from the IFB reactor. The particle shape factor (or sphericity ( $\phi_s$ )) did not change substantially. The average particle diameter changed from 2.62 to 2.58 mm during 700 hours of operation. The calculated effect on the minimum fluidization velocity is less than 2% and is therefore neglected in further analysis of the results.

In 700 hours of operation in the high-temperature IFB reactor, a limited amount of attrition is thus observed (approximately 5%, based on the reduction of the average particle diameter). Korbee (1995) showed that the mechanism for attrition for this type of sorbent material in a fluidized bed environment is abrasion (or polishing) that is obviously stronger for 'fresh' sorbent. The experimentally determined and limited rate of attrition is thus an illustration of an important advantage of the IFB reactor with respect to solids transport. Especially in comparison to high velocity pneumatic transport in which the sorbent loss is much more severe (see Wolff *et al.*, 1993a).

### 5.2.2 Circulation Rate of Solids

The Circulation Rate of the Solids (CRS) is an important parameter in analysing an IFB system. It is therefore important to determine its value during the regenerative desulfurization experiments. In chapter 3 it is explained how the CRS depends on the operational parameters: gas velocities and total solids hold-up in the IFB system.

For all experiments, the CRS was *calculated* on the basis of the solids flow model. Further, the gas flow through the orifice is *calculated*. This gas flow from one compartment to the other is important with respect to the gas analysis and mass balances for the reactive gaseous components.

A number of assumptions and model parameters are thus used to determine the solids and gas flow through an orifice in the high temperature IFB reactor. Therefore the calculated results were verified on the basis of comparable cold experimental work (Table 5.3) and a residence time distribution analysis (Figure 5.4).

The solids flow through the orifice in a steady-state situation is equivalent to the CRS in the IFB system. Details on solids and gas transport through an orifice can be found in chapter 2 of this thesis. The solids and gas flow that occurred during the experiments in the IFB pilot plant facility are calculated on the basis of the measured pressure drop across the orifice.

The solids flow is calculated according to the Ergun equation:

$$\phi_m = C_D A_{eff} \rho_d \sqrt{\frac{2(K\sigma_z + \Delta P_o)}{\rho_p(1 - \epsilon_d)}} \quad (5.2)$$

In this equation, two driving forces are taken into account: the pressure drop across the orifice ( $\Delta P_o$ ) and the horizontally directed particle pressure ( $K\sigma_z$ ) at orifice height. All other non-idealities are accounted for by the effective orifice area ( $A_{eff}$ ) and the discharge coefficient ( $C_D$ ). For the calculation and derivation of the equations that are necessary to calculate the particle stresses, reference is made to chapter 2.

## Chapter 5

The gas flow is calculated according to:

$$\Delta P_o = \frac{150}{2\pi} \left( \frac{1-\epsilon_d}{\epsilon_d} \right)^2 \frac{\mu}{(\phi_s d_p)^2} \Delta\phi \left( \frac{1}{r_o'} - \frac{1}{x} \right) + \gamma \frac{1.75}{12\pi^2} \left( \frac{1-\epsilon_d}{\epsilon_d} \right) \frac{\rho_g}{\phi_s d_p} \Delta\phi^2 \left( \frac{1}{r_o'^3} - \frac{1}{x^3} \right) \quad (5.3)$$

in which  $\gamma=1$  if  $\Delta\phi>0$  and  $\gamma=-1$  if  $\Delta\phi<0$ . The term  $\Delta\phi$  represents the difference in volumetric flow between gas and solids. The radius of the hemisphere with a surface area that equals the orifice area is represented by  $r_o'$  ( $=d_{\text{orifice}}/\sqrt{8}$ ). The term  $x$  represents the radius of the hemisphere from which the flowing gas converges towards the orifice.

In Table 5.2 the parameters that are used in Equations 5.2 and 5.3 are given. Some of these parameters ( $f$ ,  $K_o$ ,  $x$  and  $C_D$ ) were directly taken from the experimental results described in chapter 2 of this thesis.

**Table 5.2** Solids and gas flow modelling parameters used in Equations 5.2 and 5.3.

Parameter	Value	Parameter	Value
$d_p$ [mm]	2.59	$d_{\text{orifice}}$ [mm]	10
$\phi_s$ [-]	0.975	$f$ [-]	0.40
$\rho_p$ [kg/m <sup>3</sup> ]	1400	$x$ [m]	0.03
$\epsilon_d$ [-]	0.48	$K_o$ [-]	0.62
$U_{mf}$ [m/s] (650 - 850 °C)	1.0	$C_D$ [-]	0.15

For all experiments carried out in the IFB facility, the solids and gas flows were calculated based on the measured pressure drop. To verify the correctness, the calculated solids flows were compared to measurements carried out in the cold facilities described in chapter 2. In Table 5.3, two sets of experiments carried out in the twin-bed (cold) facility are compared to a calculated result in the hot IFB facility.

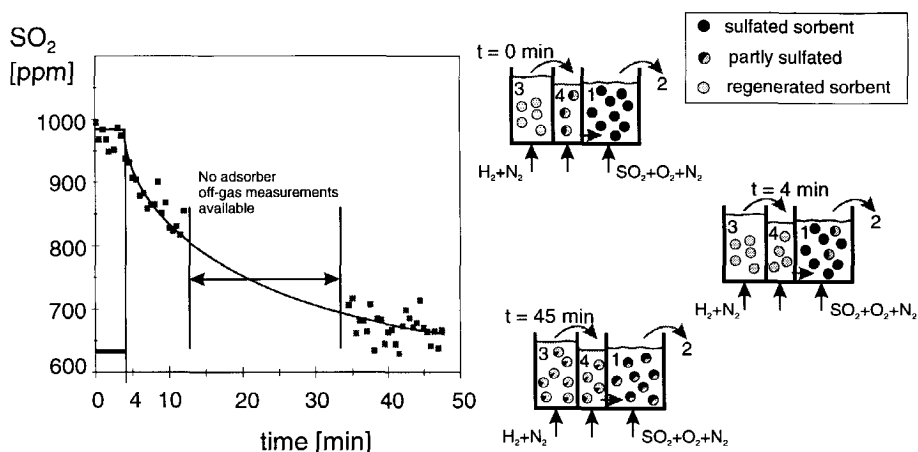
**Table 5.3** Comparison of solids flows in hot IFB and cold twin-bed facility.

	Twin-bed cold, exp.1	Twin-bed cold, exp.2	IFB fac. hot
$\Delta P_o$ [Pa]	38	40	43
$U_d/U_{mf}$ [-]	0.80	0.80	0.83
$\phi_m$ [g/s]	6.5	6.6	6.4

It is shown that the experimental solids flows measured in the cold twin-bed facility (*viz.*, 6.5 and 6.6 g/s) very well resemble the calculated solids flow in the IFB pilot plant facility. This is an indication that the model predicts accurate values for the CRS in the hot IFB facility.



Another way of estimating the solids flow in the hot IFB facility was made possible when an orifice was accidentally blocked and no solids flow occurred during a regenerative desulfurization experiment. After some time the outlet  $\text{SO}_2$  concentration of the adsorber (compartment 1) increased due to a decrease in the supply of regenerated sorbent. In the regenerator, the sorbent was regenerated to a large extent at the same moment. This situation (at  $t=0$ ) is shown in Figure 5.4. At  $t=0$ , the barrier to solids flow was removed by purging bed 4. After 4 to 5 minutes, the  $\text{SO}_2$  concentration in the adsorber off-gas starts to decrease due to the supply of regenerated sorbent. A steady-state is reached after approximately 45 minutes. The calculated residence time in bed 4 (*i.e.*,  $M_4/\phi_m$ ) is about 4 minutes which is therefore another indication that the calculated CRS is representative for the solids circulation in the IFB reactor.



**Figure 5.4** Estimation of the Circulation Rate of Solids (CRS) in the IFB reactor. At  $t=0$ , the solids flow is resuming. Regenerated sorbent is overflowing to compartment 4 and after approximately 4 minutes (equivalent to the calculated residence time in compartment 4), the solids enter the sulfur capture compartment (1). The latter is observed in the decreasing  $\text{SO}_2$  concentration above this compartment, indicating an increased sulfur retention due to the supply of regenerated sorbent to compartment 1.

The hydrodynamic parameters that were varied during the experiments in the hot IFB facility are:

1. gas velocity to compartment 4:  $U_4$  0.8, 0.9 and 1.0 m/s
2. gas velocities to compartments 1 and 3:  $U_1$  and  $U_3$  1.4 and 1.5 m/s
3. total IFB bed mass:  $M_{IFB}$  7.5 and 8.5 kg

The gas velocity in compartment 2 was set to the minimum fluidization velocity of 1.0 m/s for all experiments.

In Table 5.4, the calculated steady-state CRS is represented as a function of the hydrodynamic parameters. Each value corresponds to a continuous regenerative desulfurization experiment of 8 hours during which the hydrodynamics (gas velocities, pressures, *etc.*) and

## Chapter 5

concentrations of the relevant gases were recorded. The non-hydrodynamic results of these experiments can be found in chapter 5.5 in which the calculated values for the CRS are used for the interpretation of the results.

**Table 5.4** CRS (calculated according to Equation 5.2) as a function of the indicated hydrodynamic parameters.

Experiment		1	2	3	4	5	6
$U_4$	[m/s]	0.8	0.9	1.0	0.9	0.9	1.0
$M_{IFB}$	[kg]	7.5	7.5	7.5	7.5	8.5	8.5
$U_1 = U_3$	[m/s]	1.4	1.4	1.4	1.5	1.4	1.4
CRS	[kg/min]	0.41	0.50	0.58	0.49	0.39	0.46
	[g/s]	6.8	8.3	9.7	8.2	6.5	7.7

It can be observed that the CRS increases with increasing gas velocity in bed 4. This effect can be explained from the increasing driving force for solids flow through the flow rate determining orifice (4→1). Increasing the gas velocity in bed 1 does not affect the CRS substantially. The increasing  $U_1$  does not contribute to the driving force.

The increase in IFB bed mass (7.5→8.5) shows a decrease in CRS. This effect can be explained when the solids distribution is considered. As explained in chapter 3, an optimum (with regard to CRS) bed mass exists. When more solids are added to the IFB system this will result in solids accumulation in the lean beds and a smaller driving force for solids flow.

### 5.3 Modelling regenerative desulfurization: temperature dependency, reaction mechanisms and rate limitations

During most of the experiments in the IFB pilot plant facility, the temperature in the reactor varied between 650 and 750 °C. The reactor temperature during previous studies on regenerative desulfurization applying the synthetic sorbent (CaO/ $\gamma$ -alumina) at DUT was 850 °C (Wolff, 1991; Wolff *et al.*, 1993b; Korbee, 1995).

During this research period, no mathematical models were developed or kinetic data was measured concerning sulfur capture or regeneration. The modelling work on sulfur capture and regeneration that is presented in this chapter is based on earlier work (mentioned above) carried out at DUT. Because of the difference in temperature between the IFB experiments and the previous experiments, the temperature-dependent parameters cannot be used straightforward from the previous studies mentioned. The temperature effect on regenerative desulfurization was therefore investigated and described below together with the main features of the sulfation (SURE2) and regeneration models as developed by Wolff (1991) and Korbee (1995). The sorbent properties are represented in Table 5.5.

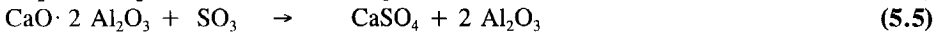
Table 5.5 Synthetic sorbent SGC-500 properties.

$\rho_p$	[kg/m <sup>3</sup> ]	1400	$V_{\text{pore}}$	[ml/g]	0.40
$d_p$	[mm]	2.60	$S_{\text{BET}}$	[m <sup>2</sup> /g]	136.3
Ca-content	[wt%]	8.91	porosity	[ml/ml]	0.56

### 5.3.1 Sulfur capture

#### SURE2 approach

The so-called SURE2 model was developed by Wolff (1991) and applied to experiments in fixed and fluidized bed reactors operated at 850 °C (Wolff *et al.*, 1993b). The model proved to be able to describe the experimental results satisfactory and is therefore used in this study. The sulfation was assumed to proceed through the formation of SO<sub>3</sub>, reaction with CaO/ $\gamma$ -alumina, and formation of calcium sulfate:



The basis for the SURE2 approach is the shrinking unreacted core model. This model assumes that the reaction first occurs at the outer skin of a particle. The reaction zone then moves into the solid particle, while a 'shell' of completely converted solid material is produced. Such a model can be applied to a porous solid in which a fast reaction takes place. In that case, diffusion into the core and chemical reaction occur in parallel. This gives rise to a thin reaction zone that advances to the center at a certain rate. The shell grows in thickness and the unreacted core of porous, still unreacted, material shrinks during reaction (Figure 5.5).

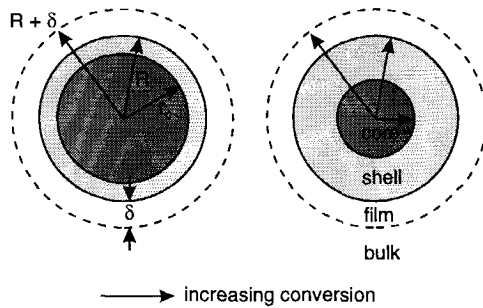


Figure 5.5 Shrinking unreacted core model. The overall rate of the process is determined by: (1) diffusion to the outer surface of the particle through the film layer, (2) diffusion through the shell to the surface of the unreacted core and (3) reaction at the shrinking core surface.

The overall rate of the process is determined by three steps:

1. Diffusion of the gaseous reactants to the outer surface of the particle. The transport parameters are the film diffusion coefficient ( $D_{\text{SO}_2, \text{film}}$ ) or the film mass transport coefficient ( $k_{\text{SO}_2, \text{film}}$ ).

2. Diffusion of the reactants through the shell to the surface of the unreacted core. This transport process is characterized by the shell diffusion coefficient ( $D_{\text{SO}_2, \text{shell}}$ ).

## Chapter 5

3. Reaction of the reactants with the solid at the core surface. The rate of conversion of CaO is considered to be first order in  $\text{SO}_3$  and proportional to the surface area of the core. The reaction rate constant is  $k_s$  ( $\text{m}^3_{\text{gas}}/\text{m}^2_{\text{core}} \cdot \text{s}$ ).

A conversion equation is then derived for one sorbent particle. The rate of shrinkage of the unreacted core is assumed to be much slower than the linear velocity of the reactants towards the unreacted core. In that case it is reasonable to assume a quasi-stationary core radius. From a mass balance for the gaseous reactants in film and shell, the  $\text{SO}_2$  concentration at the core radius ( $r_c$ ) is determined as (see Wolff, 1991; Schouten and van den Bleek, 1995):

$$C_{\text{SO}_2, r_c} = \frac{C_{\text{SO}_2, R} \delta}{1 + K_{eq} \sqrt{C_{\text{O}_2}} k_s r_c^2 (\alpha_{\text{SO}_2, \text{film}} + \alpha_{\text{SO}_2, \text{shell}})} \quad (5.6)$$

in which:

$$\alpha_{\text{SO}_2, \text{film}} = \frac{1}{D_{\text{SO}_2, \text{film}} + D_{\text{SO}_3, \text{film}} K_{eq} \sqrt{C_{\text{O}_2}}} \left( \frac{1}{R} - \frac{1}{R + \delta} \right) \quad (5.7)$$

and:

$$\alpha_{\text{SO}_2, \text{shell}} = \frac{1}{D_{\text{SO}_2, \text{shell}} + D_{\text{SO}_3, \text{shell}} K_{eq} \sqrt{C_{\text{O}_2}}} \left( \frac{1}{r_c} - \frac{1}{R} \right) \quad (5.8)$$

The term  $K_{eq}$  represents the equilibrium constant for reaction 5.4 and  $\delta$  is the film layer thickness that is estimated according to film theory (Wolff, 1991):

$$\delta = \frac{1}{\frac{k_{\text{SO}_2, \text{film}}}{D_{\text{SO}_2, \text{film}}} - \frac{1}{R}} \quad (5.9)$$

The rate of conversion of CaO (first order in core surface area and  $\text{SO}_3$  concentration) is written as:

$$\frac{dN_{\text{CaO}}}{dt} = -\Gamma k_s 4\pi r_c^2 K_{eq} \sqrt{C_{\text{O}_2}} C_{\text{SO}_2, r_c} \quad (5.10)$$

with  $N_{\text{CaO}} = \frac{4}{3} \pi r_c^3 C_{\text{CaO}}$

Equation (5.10) is written in terms of the number of moles of CaO and can be rewritten to a conversion equation in  $r_c$  or conversion of CaO (see Wolff, 1991). The stoichiometric constant  $\Gamma=1$  (mole CaO/ mole  $\text{SO}_2$ ). The conversion equation for one particle can be combined with a specific reactor model and its Residence Time Distribution (RTD) function. Then the sorbent conversion and sulfur retention of that specific reactor can be calculated. This is done for example by Korbee *et al.* (1991) who describe a general approach to FBC sulfur retention modelling. The model is based on the SURE2 approach and its use is

extended to natural sorbents (limestone and dolomites). It proved to be able to describe the experimental results for various sorbents satisfactory.

### **Reaction mechanism**

A number of studies (see Hansen *et al.*, 1991; Lin, 1994) was carried out on the temperature dependency of the reaction mechanism of desulfurization. In most of this work, the reaction between sulfur dioxide and limestone was studied. Detailed models are available that predict the sulfation behaviour of limestones under various reaction conditions (see Korbee (1995) for a literature review).

A changing reaction mechanism with varying temperature was experimentally observed by Marsh and Ulrichson (1985) and Al-Shawabkeh *et al.* (1995). This was described by a changing reaction order in SO<sub>2</sub> from zero to higher reaction order with increasing temperature.

Al-Shawabkeh *et al.* (1995), who studied limestone sulfation, measured a change in reaction order from zero at 450 °C to one at approximately 710 °C. A striking similarity was found between the sulfur capture with calcined limestone (CaO) and with the synthetic sorbent (CaO/ $\gamma$ -Al<sub>2</sub>O<sub>3</sub>). Al-Shawabkeh *et al.* (1995) reported a measured reaction order at 650 °C of 0.83 in SO<sub>2</sub>. One batch sulfation experiment carried out at 650 °C in the IFB pilot plant facility for the SGC-500 sorbent revealed also a reaction order of approximately 0.83 (a straight line was found when  $(C_{SO_2})^{0.17}$  was plotted as a function of time). This indicates that the reaction mechanism for the two types of sorbent is comparable.

A detailed quantitative elementary reaction mechanism was proposed by Dam-Johansen and Østergaard (1991b) that was able to explain the shift in reaction order. At low temperature (<700 °C), the reaction between limestone and SO<sub>2</sub> yields CaSO<sub>3</sub> that is further oxidized to CaSO<sub>4</sub>. At higher temperature the sulfation proceeds through the formation of SO<sub>3</sub> and subsequent direct oxidation of CaO to calciumsulfate. The model by Dam-Johansen and Østergaard (1991b) showed good agreement with the limited amount of experimental measurements of initial rates of sulfation available in literature.

The above mentioned findings on the reaction mechanism of sorbent sulfation (that were obtained from literature) indicate that for temperatures above approximately 700 °C, the order of reaction in SO<sub>2</sub> equals one. As the temperature was higher than 700 °C in the sulfur capture compartment of the IFB reactor during the experiments, the value of one was thus used in further modelling of sorbent sulfation.

### **Rate limitations**

For gas-solid reactions in porous particles, the rate of reaction for the particle as a whole may depend on (Levenspiel, 1993):

1. **Surface kinetics**, or reaction limited, the intrinsic rate of reaction;
2. **Pore diffusion**, which sets up an internal concentration gradient and causes the non-accessibility particle interior;
3. **Heat transfer within the particle**, temperature gradient within the particle caused by heat release or absorption during reaction;
4. **Heat transfer around the particle**, temperature gradient between the outer surface of the particle and the bulk gas;
5. **Film diffusion**, concentration gradient across the gas film.

Wolff (1991) showed that heat effects in case of sorbent sulfation are negligible and can be left out of the model.

The overall sulfation process as carried out in practice is in general controlled by physical transport processes and in particular the gas phase pore diffusion (Dam-Johansen *et al.*, 1991; Wolff *et al.*, 1993b). Modelling of the sorbent sulfation should therefore take this transport phenomenon into account (as for example in the SURE2 approach).

Dam-Johansen and Østergaard (1991a) experimentally showed significant pore diffusion limitations in limestone sulfation. They measured the intraparticle conversion profiles for sulfated limestone by means of energy-dispersive X-ray analysis. A sharp sulfur front was observed that moved inwards with increasing reaction time. For limestone, the pore diffusion limitations are however significantly larger than for the synthetic sorbent. This can be explained from the sorbent morphology. For the synthetic sorbent the pore volume is larger, the calcium distribution is more disperse and the calcium content is smaller than for limestone (Duisterwinkel, 1991).

Experimental evidence was however also provided for pore diffusion limitation in the synthetic sorbents. Wolff *et al.* (1993b) determined the intraparticle conversion profiles of the sulfated synthetic sorbent by means of EPMA-analysis (Electron-Probe X-ray MicroAnalysis). The sulfur distribution was in agreement with the more or less stepwise diffusion limited penetration of sulfur into the sorbent.

**Temperature dependency of transport processes and rate of reaction**

Both pore diffusion and reaction rate are influenced by temperature. The effect of pore diffusivity is calculated according to (Perry and Green, 1988):

$$D_{pore} = \frac{\epsilon}{\tau} \left( \frac{1}{D_{Knu}} + \frac{1}{D_{free}} \right)^{-1} \tag{5.11}$$

in which  $\epsilon$  is the internal porosity of the particle and  $\tau$  is the so-called tortuosity. For this type of particle (Table 5.5), a reasonable value for  $\tau$  is 3 (Wolff, 1991; Korbee *et al.*, 1991). The Knudsen diffusion coefficient ( $D_{Knu}$ ) is estimated by:

$$D_{Knu} = \frac{4 r_{pore}}{3} \left( \frac{2RT}{\pi M} \right)^{1/2}, \quad r_{pore} = \frac{2V_{pore}}{S_{BET}} \tag{5.12}$$

The free gas phase diffusion coefficient ( $D_{free}$ ) of component *a* that is diffusing in component *b* is calculated according to (Reid *et al.*, 1977):

$$D_{free} = \frac{1.013 \cdot 10^{-7} T^{1.75}}{P [(V_a)^{1/3} + (V_b)^{1/3}]^2} \left( \frac{1}{M_a} + \frac{1}{M_b} \right)^{0.5} \tag{5.13}$$

The terms  $V_a$  and  $V_b$  are the diffusion volume coefficients for the specific component. Its value for  $SO_2$  and  $N_2$  is 41.1 and 17.9, respectively. When it is assumed that the diffusivity is proportional to the square root of the reciprocal molar mass ( $M$ ) (Equation 5.12), it follows that the diffusion coefficient for  $SO_3$  can be estimated from:

$$D_{pore,SO_3} = 0.9 D_{pore,SO_2} \tag{5.14}$$

The influence of temperature on the rate of reaction is usually estimated on the basis of an Arrhenius expression. In many cases, the activation energy ( $E_A$ ) is fitted on experimental data of reaction rate against reciprocal temperature. The sulfation rate constant is determined from specific data obtained under different operating conditions and will in general not be representative for the intrinsic kinetics. This explains the various values that are given in literature for the activation energy of the limestone sulfation reaction (see Table 5.6).

**Table 5.6** Activation energies for the limestone sulfation reaction.

Authors	Mura <i>et al.</i> (1991)	Simons <i>et al.</i> (1987)	Marsh and Ulrichson (1985)	Hartman and Trnka (1980)
$E_A$ [kJ/mole]	117	141	80	97

Based on the results in Table 5.6, a value for  $E_A$  of 100 kJ/mole is used to estimate the temperature effect on the rate of the sulfation reaction. To estimate the effect of pore diffusion on the overall process, the effectiveness factor  $E$  is used.  $E$  is defined as the ratio of the rate at which reaction actually occurs to the rate at which reaction would occur if no concentration gradient is present and the concentration of reactant inside the particle is equal to that outside the particle. For a spherical particle and a first order irreversible reaction, the effectiveness factor is taken from the generalized Thiele modulus ( $M_T$ ) (Levenspiel, 1993):

$$E = \frac{3}{M_T} \left( \frac{1}{\tanh M_T} - \frac{1}{M_T} \right) \quad (5.15)$$

and:

$$M_T = \frac{d_p}{2} \left( \frac{S_{BET} \rho_p k}{D_{pore}} \right)^{1/2} \quad (5.16)$$

in which  $k$  is the intrinsic first order reaction rate constant. It can be evaluated in terms of the Thiele modulus and the effectiveness factor whether a shrinking unreacted core is present in the particle (that is being sulfated) as assumed in the SURE2 approach (Wolff, 1991).

In the SURE2 model, the rate of conversion ( $R_{conv}$  in mole/s) is expressed by:

$$R_{conv, SURE2} = k_s 4\pi R^2 C_{SO_3, R} \quad (5.17)$$

and in the generalized Thiele approach this is:

$$R_{conv, Thiele} = k S_{BET} \rho_p \frac{4}{3} \pi R^3 E C_{SO_3, R} \quad (5.18)$$

Both equations can be combined to (see Wolff, 1991):

$$\frac{M_T}{R} \left( \frac{1}{\tanh M_T} - \frac{1}{M_T} \right) - \frac{k_s}{D_{pore}} = 0 \quad (5.19)$$

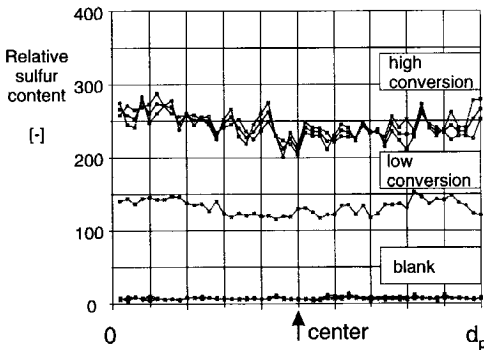
## Chapter 5

The Thiele modulus ( $M_T$ ) can then be calculated from Equation 5.19 when the sulfation reaction rate constant ( $k_s$ ) and the pore diffusion coefficient ( $D_{pore}$ ) are known. The temperature range for the experiments in the IFB pilot plant facility was 650 to 850 °C. The pore diffusion coefficient was calculated from Equation 5.11. The value for  $k_s$  at 850 °C was taken from Wolff (1991). At 650 °C,  $k_s$  can then be calculated from the Arrhenius expression. The results are shown in Table 5.7.

**Table 5.7** Temperature dependency of the rate sorbent sulfation.

T [°C]	$k_s$ [ $m^3_{gas}/m^2_{core}s$ ]	$D_{pore}$ [ $m^2_{pore}/s$ ]	$M_T$ [-]	E [-]
650	0.015	$3.95 \cdot 10^{-7}$	49	0.06
850	0.149	$4.35 \cdot 10^{-7}$	446	0.007

No resistance to pore diffusion occurs when  $M_T < 0.4$  and for  $M_T > 4$  strong pore diffusion effects determine the reaction rate (Levenspiel, 1993). As can be seen in Table 5.7, the Thiele modulus is high enough to predict significant pore diffusion effects. For a sharp concentration drop in the sorbent particle,  $M_T$  must be greater than 200 (Carberry and Goring, 1966). At high temperature (850 °C) this is the case. For the lower temperature (650 °C),  $M_T$  is considerably smaller than the required value (of 200) to establish the shell-core interface. At low temperature the shrinking unreacted core assumption is therefore according to Carberry and Goring (1966) not valid.



**Figure 5.6** Sulfur distribution across a particle diameter measured by means of EPMA analysis. The temperature during the sulfur capture experiment (from which the particles were taken) was 715 °C. The relative sulfur content is plotted for a particle that was not sulfated (blank) and for a sorbent of high and low conversion (of CaO).

diameter of sorbent particles is shown in the case of sorbent particles from a regenerative

The above calculations are carried out for a steady-state at time zero ( $r_c = R$ ). When  $r_c$  becomes smaller than  $R$ , the Thiele modulus decreases and subsequently the concentration profile will become less sharp. The shrinking core assumption will thus become more and more affected (Luss, 1968).

From these considerations it is clear that at 850 °C the SURE2 approach can be used for sorbent sulfation modelling. However, at lower temperature, the SURE2 model will not be representative for the exact phenomena that occur in a sorbent particle.

This conclusion was confirmed by the analysis of the sorbent material after sulfation at 715 °C. In Figure 5.6, the sulfur distribution across the



desulfurization experiment carried out at 715 °C. The sulfur distribution is shown in the case of high and low sorbent (CaO) conversion. The relative sulfur concentration was measured by means of EPMA analysis. Each line represents the analysis of one particle. At 715 °C it is clear that the sulfur is evenly distributed throughout the particle, indicating no diffusion limitation effects. In Figure 5.7 it is shown that at 850 °C, diffusion limitation is significant. The outer part of the particle is loaded with a higher sulfur content compared to the center of the particle.

Based on the Thiele modulus analysis and the experimentally observed sulfur distribution in the particle, the conclusion is that the shrinking core model and pseudo steady-state approximation are not fully adequate for sorbent sulfation modelling at lower temperature.

A simpler approach to sulfation modelling is the SURE model as developed by Schouten and van den Bleek (1987). This basic approach preceded the development of the SURE2 model. The main idea of the SURE model is that the rate of sulfation is assumed to be first order in the gaseous SO<sub>3</sub> concentration and first order in the total external reactive sorbent surface area. The SURE model does however not take into account pore diffusion effects that play an important role in sorbent sulfation (as is seen from Table 5.7). It was therefore decided to use the SURE2 model because it does consider pore diffusion effects, despite the fact that this model is not fully adequate for describing sorbent sulfation at low temperature. Further, the rate of SO<sub>3</sub> formation according to Equation 5.4 is assumed to be fast enough that it will not be rate limiting, viz., the SO<sub>2</sub> oxidation will be effectively catalyzed by the γ-alumina of the sorbent (Sander, 1984).

The temperature dependency of the equilibrium constant of the SO<sub>3</sub> formation is calculated according to (Barin and Knacke, 1973; Wolff, 1991):

$$RT \ln K_{eq} = -\Delta G_{r,T} = 91.9 \cdot T - 97.6 \cdot 10^3 \quad (5.20)$$

with  $300 < T < 1800$  K.

### Reactor model

In the IFB reactor, two compartments (for desulfurization and regeneration) act as chemical reactors. When the sulfation is described at particle level, one has to decide what kind of contacting model should be used to describe the reactor performance.

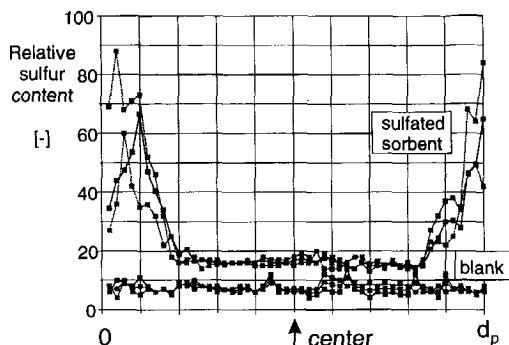


Figure 5.7 Sulfur distribution across a particle diameter measured by means of EPMA analysis. The temperature in the sulfur capture compartment was 850 °C. The relative sulfur content is plotted for a sorbent that was not sulfated (blank) and for a sorbent that was sampled from the high-temperature regenerative desulfurization experiment.

## Chapter 5

For fluidized bed reactors, a variety of basic and complex reactor models is available in literature (Grace, 1986; Kunii and Levenspiel, 1991). The models' characteristics depend on the specific fluidized bed behaviour or operating regime.

Depending on particle type and mode of operation, the bed is in a bubbling, slugging or turbulent regime. In the IFB pilot plant facility, the fluidized bed operating regime is typically slugging. This may also be characteristic for a bubbling fluidized bed combustor at commercial scale due to various heat transfer facilities in the fluidized bed (Schouten, 1988).

Due to severe mixing characteristics in this type of regime, no further mass transfer limitations (contrary to the bubbling regime) are present in the fluid bed reactor. It can therefore be assumed that both gas and solids phase are ideally mixed. This assumption was confirmed by de Feber (1994) who reviewed gas and solids dispersion in this type of gas-solid fluidized beds. Based on literature data, the mixing times were calculated for the solids phase. These appeared to be significantly smaller (more than 10 times) than the smallest particle residence time that will be encountered in the IFB reactor compartments.

In chapter 6 of this thesis, a detailed analysis is given on the modelling of regenerative desulfurization in the IFB reactor including the effects of residence time distribution. In this chapter the main equations are presented that were used to calculate the sulfur retention in the IFB reactor.

The molar balance for CaO in the fluidized bed adsorption compartment of the IFB reactor can be written as:

$$\phi_{s,out} \alpha = \phi_{s,in} \alpha_{in} + r_{\alpha} M_{bed} - \frac{d(M_{bed} \alpha)}{dt} \quad (5.21)$$

in which  $\alpha$  is the fraction of CaO that is converted to CaSO<sub>4</sub>,  $\phi_{s,out}$  and  $\phi_{s,in}$  are the outlet and inlet mass flows respectively,  $r_{\alpha}$  is the rate of conversion for one sorbent particle and  $M_{bed}$  is the solids hold-up in the bed. The term  $r_{\alpha}$  is calculated according to the SURE2 model (Equation 5.10). When the bedmass in the adsorption compartment is constant in time and the inlet and outlet mass flow are equal, Equation 5.21 can be written as:

$$\frac{d\alpha}{dt} = \frac{\phi_{sorb}}{M_{bed}} (\alpha_{in} - \alpha) + r_{\alpha} \quad (5.22)$$

The term  $\phi_{sorb}$  is the steady-state solids flow through the IFB system (equal to the CRS). The gas phase balance for SO<sub>2</sub> for a constant gas phase volume ( $V_g$ ) can be written as:

$$\frac{d C_{SO_2}}{dt} = \frac{\phi_v}{V_g} (C_{SO_2,in} - C_{SO_2}) - \frac{f_{Ca} M_{bed}}{M_{Ca} \Gamma} r_{\alpha} \quad (5.23)$$

in which  $f_{Ca}$  is the calcium weight fraction of the sorbent,  $M_{Ca}$  is the molar mass of calcium,  $\Gamma$  is the stoichiometric coefficient for the sulfation reaction (mole CaO/mole SO<sub>2</sub>) and  $V_g$  can be determined from:

$$V_g = \frac{M_{bed}}{\rho_p} \left( \frac{\epsilon}{1 - \epsilon} \right) \quad (5.24)$$

With the above given equations and considerations, the sorbent sulfation behaviour that was experimentally observed will be interpreted.

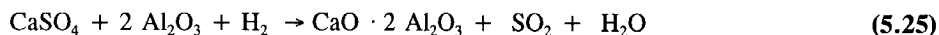
### 5.3.2 Sorbent regeneration

#### *Reactions and experimental observations*

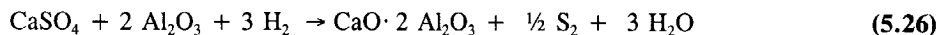
The sulfated synthetic sorbent can be regenerated at relative low temperatures compared to the high temperature (>1100 °C) that is needed for limestone regeneration. This can be explained from a thermodynamic point of view and is based on the formation of calcium aluminates (Duisterwinkel, 1991; Wolff, 1991). The aluminate form of the synthetic sorbent is represented in the reaction equations as:  $\text{CaO} \cdot \text{Al}_2\text{O}_3$ .

Wolff (1991) studied the regeneration characteristics of the sorbent using hydrogen, carbon monoxide, or a mixture of these components as reducing agent. It was experimentally shown that regeneration is effectively possible for both  $\text{H}_2$  and  $\text{CO}$ . Which type of reducing agent is preferred depends mainly on the regeneration products that are preferred for downstream processing and the availability of specific reducing gases.

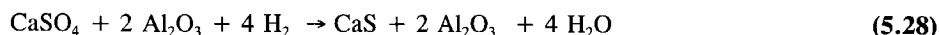
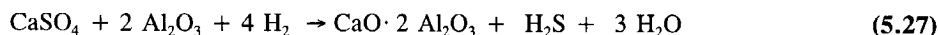
When hydrogen is used, the main regeneration reaction can be written as (Korbee, 1995):



Next to sulfur dioxide, also elemental sulfur, hydrogen sulfide and calcium sulfide may be formed during regeneration with hydrogen. The overall reactions can be represented as:

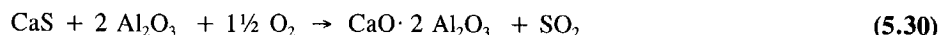
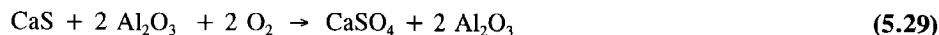


Elemental sulfur is represented as  $\frac{1}{2}\text{S}_2$  because at temperatures (650-850 °C) encountered in the IFB reactor, it will be mainly present in this ( $\text{S}_2$ ) form (Sander, 1984).



The latter reaction is unfavourable for two reasons. Firstly, the reaction does not contribute to a desired high concentration of sulfur compounds in the gas phase of the regenerator. Secondly, the sorbent material is returned to the sulfur capture compartment in which the  $\text{CaS}$  is not directly useful for desulfurization.

When  $\text{CaS}$  is brought in contact with oxygen present in the combustor (or desulfurization compartment), two oxidation pathways are possible:



According to Wolff (1991), 95% of the  $\text{CaS}$  is oxidized to  $\text{CaSO}_4$  (reaction 5.29). The  $\text{CaS}$  formation will deteriorate the performance of the desulfurization process. It was

experimentally shown by Wolff (1991) and Korbee (1995) that adding H<sub>2</sub>O and CO<sub>2</sub> to the regenerator can effectively suppress CaS formation.

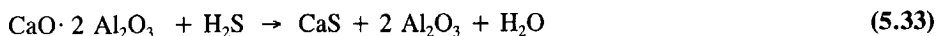
The true reaction mechanism of regeneration for natural as well as synthetic sorbents, is according to Korbee (1995), still not completely understood. It is difficult to obtain the true kinetic parameters from batch regeneration experiments. The reason is that the reactions are fast and complex. A large number of reactants and products are present in both the solids and gas phase. Further, it is believed that especially pore diffusion plays a rate limiting role in the overall regeneration process (Snyder *et al.*, 1975).

Some general features on the regeneration of synthetic sorbents can be obtained from the experimental observations that are available in literature (Snyder *et al.*, 1975; Wolff, 1991; Korbee, 1995). The reductive decomposition of CaSO<sub>4</sub> is in general much faster than the sulfation of CaO. The ratio between the experimentally determined sulfation and regeneration times can be up to 30.

It is further believed that CaSO<sub>4</sub> is first reduced to CaO during which the SO<sub>2</sub> is released. Subsequently, the sulfur dioxide can react together with the reducing agent, *e.g.* H<sub>2</sub>, and CaO to CaS. When the sorbent is regenerated with hydrogen, the following gas phase equilibrium reactions are likely to occur:



Korbee (1995) found experimentally that the above reactions are strongly catalyzed by the alumina based sorbent (SGC-500). It was further observed that the sorbent can be sulfided by H<sub>2</sub>S. The sulfidation is represented by the following overall reaction:



It is thus believed that H<sub>2</sub>S plays an important role in the formation of CaS. The general sequence of the reactions for the gas phase components then would be:

- ▶ formation of SO<sub>2</sub>: reaction (5.25)
- ▶ reduction of SO<sub>2</sub> to elemental sulfur (½ S<sub>2</sub>): reaction (5.31)
- ▶ formation of hydrogen sulfide (H<sub>2</sub>S) to elemental sulfur: reaction (5.32)
- ▶ reaction of H<sub>2</sub>S and CaO to CaS: reaction (5.33)

A number of batch regeneration experiments with the SGC-500 sorbent was reported by Korbee (1995). The experiments were carried out at 850 °C and hydrogen was used as reducing agent. The amount of SO<sub>2</sub> released varied inversely proportional with the hydrogen concentration in the feed gas. With increasing H<sub>2</sub> concentration, more H<sub>2</sub>S and also more CaS and/or S<sub>2</sub> was formed. This supports the suggested role of H<sub>2</sub>S in the formation of CaS. A moderate hydrogen (or reducing agent) concentration and a relatively short sorbent residence time in the regenerator can therefore also be used to suppress CaS formation.

### ***Regeneration modelling***

Korbee (1995) developed a model for the synthetic sorbent regeneration based on the above mentioned reaction scheme. The model resembles the SURE2 model (for sorbent sulfation).

It takes into account three rate limiting phenomena: film diffusion, pore diffusion, and gas-solid/gas-gas reactions.

Reactions 5.31 and 5.32 are treated as reversible gas phase reactions, not necessarily at equilibrium. The solid-gas reactions are assumed to be first order in solid and gas phase reactants. The rate constants were estimated from a batch regeneration experiment carried out at 850 °C.

The model calculations showed strong pore diffusion effects that influence the concentration gradient in the sorbent particle and subsequently the reactions taking place. The model was further capable of predicting the experimentally observed and above mentioned regeneration behaviour during batch experiments carried out at 850 °C. To apply the regeneration model to other experiments requires the estimation of the reaction rate constants at the specific temperatures used in the experiments. Due to the limited amount of experimental data that was available for the lower temperature (650 °C), the parameter estimation was not possible. The regeneration model by Korbee (1995) could therefore not be used for predicting the regeneration behaviour at lower temperature that was observed in the IFB reactor.

A model such as developed by Korbee (1995) can certainly be of use to estimate the effect of rate limitations (especially due to pore diffusion) as a function of process conditions. The insight thus obtained in sorbent regeneration behaviour can be particularly useful in verifying the correctness of an engineering model that is based on a simpler description of the regeneration. An example of such a model is described by Korbee *et al.* (1993). It is used in a preliminary design study of a regenerative desulfurization process in an IFB system. The reaction scheme is equal to that described in this chapter.

#### Temperature influence and rate limitations during regeneration

The temperature in the regenerator during most of the IFB pilot plant experiments of 650 °C was attained. This is significantly lower than the temperature (850°C) during the experiments described by Korbee (1995). It is therefore necessary to analyze temperature effects on the regeneration process in order to be able to compare the results.

In the temperature range of 650 to 850 °C, it is not expected that the reaction mechanism will change. The temperature will however certainly influence the rate of reactions and the mass transfer. The effect of temperature on the rate of reaction can be estimated according to an Arrhenius relation. An estimation of the activation energy for the regeneration of a synthetic sorbent (CaO on  $\alpha$ -alumina) by means of hydrogen was determined by Snyder *et al.* (1975). A value of 62.4 kJ/mole was reported.

This results in a decrease in reaction rate of approximately a factor 4.3 when temperature decreases from 850 to 650 °C.

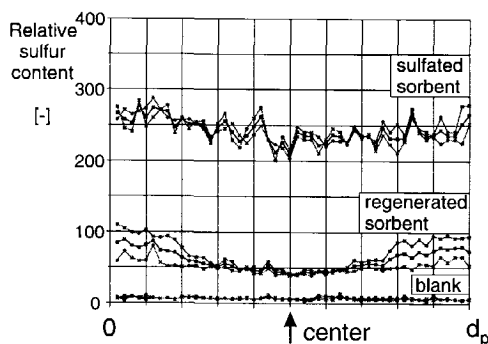


Figure 5.8 Sulfur distribution across a particle diameter measured by means of EPMA analysis. The relative sulfur content is plotted for a sorbent that was not used for experiments (blank), for a sorbent that was sulfated at 715 °C, and for a sorbent that was regenerated at 650 °C.

The temperature influence on pore diffusion is calculated according to Equation 5.11. It is found that the decrease in diffusivity for hydrogen in nitrogen is 10% when the temperature decreases as mentioned. It is further found that the diffusivity of hydrogen is five times higher than that for sulfur dioxide. This indicates the importance of treating the reactants and products of reaction separately with respect to pore diffusion.

From these considerations it is clear that temperature influence is much stronger on the rate of reaction than on the pore diffusion process. Analogous to the sulfation, at low temperatures, pore diffusion limitation is less pronounced than it is at high temperature. Line scan EPMA analysis was carried out for sorbent particles taken from the regenerator operated at 650 °C in a steady-state regenerative desulfurization experiment. The results are shown in Figure 5.8. It can be seen that the sulfur is more or less equally distributed across the particle diameter. This indicates a reaction limited process and not a pore diffusion limited phenomenon.

Temperature can also play an important role in the gas phase equilibrium reactions 5.31 and 5.32. The temperature effect on the equilibrium of these reactions was calculated on the basis of thermodynamic data from Barin and Knacke (1973) and Equation 5.20. The equilibrium constants for the elemental sulfur ( $\frac{1}{2}S_2$ ) formation (reaction 5.31) and hydrogen sulfide ( $H_2S$ ) formation (reaction 5.32) and the ratio of the equilibrium constants for the indicated temperatures are shown in Table 5.8.

**Table 5.8** Temperature influence on equilibrium reactions for the formation of elemental sulfur and hydrogen sulfide.

T (°C)	850	650	$K_{Eq,650} / K_{Eq,850}$
$K_{eq}$ reaction (5.31) $\frac{1}{2} S_2$ formation	$2.2 \cdot 10^4$	$5.9 \cdot 10^4$	27
$K_{eq}$ reaction (5.32) $H_2S$ formation	43	399	9

From these results it is clear that thermodynamics are strongly in favour of elemental sulfur and hydrogen sulfide at lower temperature: a decrease in temperature will result in higher concentrations of elemental sulfur and  $H_2S$ . The amount of sulfur dioxide will therefore be less at lower temperature. It must however be said that according to Korbee (1995) these equilibria will most probably not be reached. Experimental and modelling results (at 850 °C) showed that the composition of the components in the gas phase was far from that at equilibrium. Apparently, the rates of these equilibrium reactions are such that the equilibrium will not be reached within the gas residence time in the regenerator.

## 5.4 Batch experiments

Following the introductory tests of the IFB pilot plant facility, experiments were performed in batch-mode to verify proper functioning of each of the sub-processes. Desulfurization and regeneration were carried out serial instead of parallel.

### 5.4.1 Sulfur capture: experiments and modelling

#### Batch experiments

During the first batch experiments in the IFB facility, the orifices were closed and no solids flow occurred between the compartments. The experiments were carried out by sulfating the sorbent in one of the IFB compartments. The  $\text{SO}_2$  was introduced in the gas stream and when the measured concentration above the fluidized bed levelled off, oxygen (air) was added to the gas stream too. Concentrations of the reactive gas phase components were fixed during the experiments at approximately:  $C_{\text{SO}_2, \text{in}} = 2000 \text{ ppm}$  and  $C_{\text{O}_2, \text{in}} = 4 \text{ v\%}$ .

The required oxygen concentration is established by combining air and nitrogen gas streams. The gas phase concentrations for  $\text{SO}_2$  and  $\text{O}_2$  represent typical values for a commercial fluidized bed combustor (Wolff, 1991). The simulated FBC gas phase in the IFB reactor did not contain other combustion products such as  $\text{H}_2\text{O}$  or  $\text{CO}_2$ .

The  $\text{SO}_2$  concentration measured above the bed is shown in Figure 5.9. The experiment started with fresh sorbent. Solids samples were afterwards analyzed for their sulfate content. The sulfate analysis of samples taken from the IFB reactor was executed by means of wet chemical analysis (titration). Relative errors were limited in all experimentally determined sulfate contents to 5%. The error is caused by the method of analysis and by sampling from an inhomogeneous mixture of

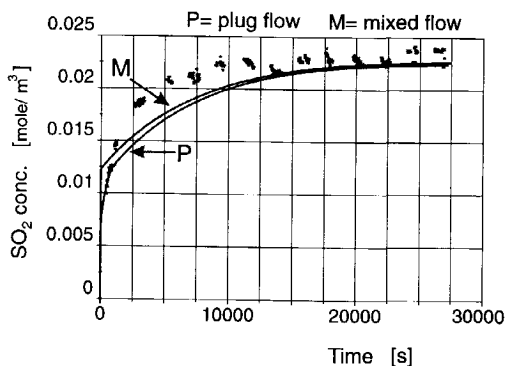
sorbent particles from the reactor. For this experiment,  $\text{CaO}$  appeared to be sulfated to  $\text{CaSO}_4$  for 73%.

From the measured  $\text{SO}_2$  concentration it can be seen that the retention (= relative amount of  $\text{SO}_2$  captured) is gradually decreasing until the measured  $\text{SO}_2$  concentration above the bed equals the inlet concentration.

An attempt was made to describe the batch sulfation behaviour by means of a mathematical model.

As mentioned in the previous section, the SURE2 approach was applied.

Some of the model parameters were experimentally determined ( $M_1$ ,  $H_1$ ,  $\epsilon_1$  and  $T_1$ ) and some were calculated. The pore and film diffusion coefficients ( $D_{\text{pore}}$  and



**Figure 5.9** Batch sulfation experiment in the IFB reactor (compartment 1) at 715 °C. The  $\text{SO}_2$  off-gas concentration is plotted as a function of time. The sorbent material is not circulating between the compartments. The two curves represent the calculated  $\text{SO}_2$  concentration by means of a mathematical model in which the gas phase is considered to be in plug flow and mixed flow. The parameters that were used in the model are given in Table 5.9.

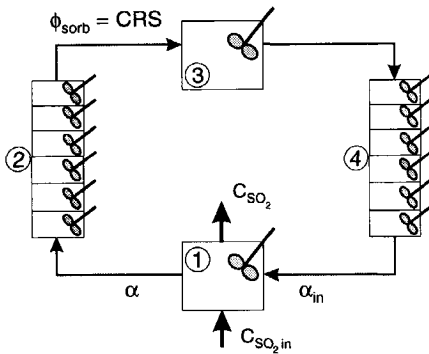
**Chapter 5**

$D_{free}$ ) were estimated by Equations 5.11 and 5.13 respectively. The reaction rate constant ( $k_r$ ) was determined from a measured value at 850 °C by Wolff (1991) and an estimated activation energy of 100 kJ/ mole (see Chapter 5.3.1). All parameters used in the sulfation modelling are listed in Table 5.9.

**Table 5.9** Model parameters for modelling sorbent sulfation behaviour of synthetic sorbent (SGC-500) at 715 °C.

Experimental parameters			Calculated parameters		
$M_1$	2.95	[kg]	$K_{Eq}$	2.3	[-]
$\epsilon_1$	0.62	[-]	$D_{pore, SO_2}$	$4.1 \cdot 10^{-7}$	$[m^2_{pore}/s]$
$T_1$	715	[°C]	$D_{free, SO_2}$	$1.1 \cdot 10^{-4}$	$[m^2/s]$
$U_1$	1.4	[m/s]	$k_s$	0.034	$[m^3_{gas}/m^2_{core}s]$
$C_{SO_2, in}$	0.024	$[mol/m^3]$			
$C_{O_2, in}$	0.494	$[mol/m^3]$			

The sulfur capture process was modelled applying the parameters listed in Table 5.9 and the balances for CaO and SO<sub>2</sub> (Equations 5.22 and 5.23). The result is shown in Figure 5.9. The model shows reasonable agreement with the experimental results. It was also tested whether a plug flow assumption for the gas phase would give better results in comparison to the experiments. The model was adapted for this situation by using a tanks-in-series model (Levenspiel, 1993). It appeared that the calculated results did not change substantially with increasing number of tanks for larger numbers than six. This value was therefore used for plug flow modelling of the gas phase. The plug flow model (see Figure 5.9) does not appear to be a significant improvement in describing the experimental data compared to mixed flow



**Figure 5.10** Solids circulation through the IFB reactor. The solids flow model is indicated for each compartment. Compartment 1 is used for desulfurization of the gas phase, resulting in an average conversion ( $\alpha$ ) of the synthetic sorbent material.

conditions for the gas phase. The true flow pattern and corresponding model for the gas-phase can therefore not be determined from this experiment.

**Batch experiments including solids flow**

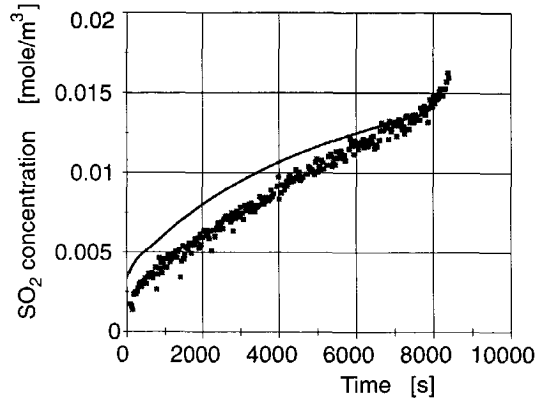
Batch sulfation of the sorbent (without regeneration) with solids circulation through the IFB reactor was also experimentally investigated.

The Circulation Rate of the Solids (CRS) and the accompanying gas flow through the orifice were determined as explained in chapter 5.2.2 and is based on the experimentally determined pressure drop across the orifice.

The sorbent particles recirculate between the compartments as shown in Figure 5.10. Compartments 2 and 4 are both



represented by six tanks-in-series. This plug flow character for the solids phase flow in these compartments is caused by a gas velocity that is set at approximately (or somewhat below) the minimum fluidization velocity. The number of six tanks was chosen for pragmatic reasons. No significantly deviating results were calculated when higher values for the number of tanks were applied.



**Figure 5.11** Batch sulfation experiment in the IFB reactor at 715 °C including solids circulation. The model assumes plug flow behaviour for the gas phase. The parameters that were used in modelling are listed in Table 5.9 and 5.10.

The experimental data is shown in Figure 5.11 together with the modelling results. During this experiment after 10.000 seconds (a little less than 3 hours) no steady-state was reached. The temperature of the IFB reactor decreased significantly (due to heater break down) at this time resulting in an accelerated decrease in sulfur retention. The most important model parameters that are different from the above mentioned batch sulfation model (see Table 5.9) are represented in Table 5.10.

**Table 5.10** Experimentally determined model parameters for a sulfation experiment at 715 °C in the IFB reactor including solids circulation.

$\phi_{\text{sorb}} = \text{CRS}$	<b>7.1</b>	[g/s]	$M_2$	<b>1.8</b>	[kg]
$\epsilon_1$	<b>0.64</b>	[-]	$M_3$	<b>0.6</b>	[kg]
$M_1$	<b>2.7</b>	[kg]	$M_4$	<b>1.9</b>	[kg]

The gas phase was modelled as plug flow (Figure 5.10). The deviation between model predictions and experimental results is clear (Figure 5.11).

A sensitivity analysis of the model parameters ( $M_1$ ,  $\epsilon_1$ ,  $\phi_{\text{sorb}}$ ,  $C_{\text{SO}_2, \text{in}}$  and  $k_s$ ) revealed that only a difference in reaction rate constant  $k_s$  could explain the differences between model and experimental results. The reaction rate constant is determined from a rough estimation of the activation energy ( $E_A$ ) (see chapter 5.3.1) and can therefore deviate significantly from the actual value. Without additional experimental work it is however not possible to determine a more reliable value.

Another complicating factor is already mentioned and concerns the validity of the SURE2 approach. It was experimentally shown (Figure 5.6) and theoretically made plausible that the SO<sub>2</sub> is not strictly penetrating the sorbent particle progressively as assumed in the SURE2 approach. In practice this means that more CaO is available for sulfur capture than assumed by the SURE2 model. This is especially the case at the start of the experiment. This would result in a higher sulfur retention and thus partly explain the deviation between model and experimental results.

Further, physical adsorption of SO<sub>2</sub> on the sorbent can explain part of the deviation between model and experimental results. This phenomenon is not considered in the sulfur capture model. The SO<sub>2</sub> can be adsorbed in compartment 1 and released in one of the other compartments. In that case it will appear to be captured by the sorbent. From the sulfur balance (that was made for all experiments) it was shown that physical adsorption can be up to 5% of the amount of SO<sub>2</sub> that was introduced in the desulfurization compartment. The adsorption process as a function of SO<sub>2</sub> concentration, temperature, sorbent conversion and CRS is however not known in detail.

The overall conclusion is that the model as presented has too many limitations to predict sorbent sulfation adequately at lower temperature ( $\approx 700^\circ\text{C}$ ). At higher temperature ( $850^\circ\text{C}$ ), the model proved to be able to predict the sorbent sulfation behaviour satisfactory (Wolff *et al.*, 1993b).

If further work on sorbent sulfation at lower temperature is to be carried out, the sulfur capture model should be improved on several aspects for more adequate predictions of sorbent sulfation at this temperature. First, the SURE2 assumptions are not completely valid (at lower temperature) and should be substituted for a model taking into account diffusional effects without assuming a pseudo steady-state and a step-wise penetration of SO<sub>2</sub> in the sorbent particle. Another important aspect is the temperature dependency of both diffusional effects and reaction rates that should be investigated and verified by more experiments at different temperatures. Further, the physical adsorption effects should be given more attention.

### 5.4.2 Sorbent regeneration: experiments and consequences for modelling

After the batch sulfation experiments described previously, the same sorbent was regenerated by means of hydrogen.

#### *Experimental considerations*

Batch regeneration experiments were carried out at approximately  $650^\circ\text{C}$ . This relative low temperature affects the regeneration process as discussed in chapter 5.3.2. The most important aspect is that the sorbent is still regenerable at a temperature that is  $200^\circ\text{C}$  lower than the temperature for which it was developed. During the experiments, the hydrogen feed concentration to the regenerator was fixed at 10 v% (unless another value is mentioned).

The gas concentration measurements at the positions indicated in Figure 4.4 (chapter 4) started when the hydrogen was added to the regeneration IFB compartment. Three gas phase components can be detected by means of the FTIR analyzer: SO<sub>2</sub>, H<sub>2</sub>S and H<sub>2</sub>O.

The elemental sulfur that is formed during regeneration is not directly detectable in the regenerator off-gas. There are however two ways to determine the amount of  $\frac{1}{2}\text{S}_2$  that is released:

1. Measuring the off-gas composition from the IFB pilot plant facility. All sulfur components will be oxidized in the combustion section to  $\text{SO}_2$ .
2. Calculation from the measured  $\text{H}_2\text{O}$  concentration in the regenerator and the reaction scheme (see chapter 5.3.2).

Further, samples of the sorbent particles were taken after each experiment to determine their sulfate and sulfide ( $\text{CaSO}_4$  and  $\text{CaS}$ ) content by means of wet chemical analysis. It appeared that during all IFB experiments no significant amount of  $\text{CaS}$  was formed. The results of the  $\text{CaS}$  determination were confirmed when it was attempted to oxidize the  $\text{CaS}$  on the sorbent. No sulfur products were released indicating that no  $\text{CaS}$  was formed in the regenerator. When  $\text{CaS}$  is not formed, the reaction scheme that can be used to determine the amount of elemental sulfur in the regenerator simplifies to reactions 5.25, 5.26 and 5.27. In these regeneration reactions sulfur dioxide, elemental sulfur and hydrogen sulfide are formed. The formation of 1 mole of  $\text{SO}_2$  is accompanied by 1 mole of water. During the formation of  $\frac{1}{2}\text{S}_2$  and  $\text{H}_2\text{S}$ , 3 moles of  $\text{H}_2\text{O}$  are formed. This results in the following 'relationship' (sulfur molar balance) to determine the elemental sulfur concentration:

$$\frac{1}{2} \text{S}_2 = \frac{1}{3} (\text{H}_2\text{O} - \text{SO}_2 - 3 \text{H}_2\text{S}) \quad (5.34)$$

In this balance, the components are the molar gas phase concentrations measured in the regenerator. The elemental sulfur concentration can thus be determined from the measured  $\text{H}_2\text{O}$ ,  $\text{SO}_2$  and  $\text{H}_2\text{S}$  concentrations in the regenerator. This method is preferred over determination from the measured  $\text{SO}_2$  concentration in the IFB off-gas measurement. Due to dilution in the combustion section, the accuracy of this method will be limited. Further, the regenerator off-gas composition was determined continuously during the experiments while the IFB off-gas measurements were carried out at intervals of 15 to 20 minutes.

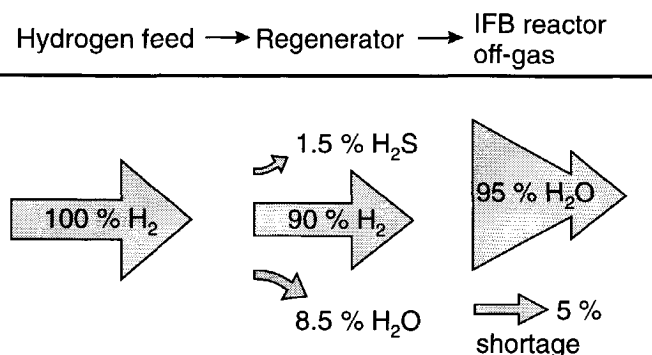
#### *Molar balances*

The molar balances are an important tool to verify the correctness of the measured gas phase concentrations. For all experiments carried out in the IFB facility, the balances were set up for sulfur and hydrogen. To provide insight in the molar balances for sulfur and hydrogen, these are presented in Table 5.12 for the continuous regenerative desulfurization experiments that were carried out in the IFB pilot plant facility and described in chapter 5.5.

Sulfur can only be introduced in the system in compartment 1, *i.e.*, the desulfurization compartment. It can then be measured in the off-gases of compartment 1 (as  $\text{SO}_2$ ) and 3 (as  $\text{SO}_2$ ,  $\frac{1}{2}\text{S}_2$  and  $\text{H}_2\text{S}$ ) or as sulfate or sulfide on the sorbent particles.

A complicating factor is the elemental sulfur determination in the regenerator. The concentration of this component is actually determined from a molar balance. The sulfur balance was therefore based on the IFB off-gas measurement after combustion. The total amount of sulfur in the various terms of the balance were calculated for all experiments. The balance fitted within 10% for most of the experiments carried out (see Table 5.12). This gives an indication of the accuracy of the  $\text{SO}_2$  concentration measurements. It is believed that most of the inaccuracies find their origin in the sorbent sulfur content determination (see chapter 5.4.1) and the IFB off-gas measurement.

The hydrogen balance is important with respect to the analysis of the regenerator performance. The regenerator feed gas was identified as the only hydrogen source for the IFB reactor. The water content of the other gases (nitrogen and air) was measured and appeared to be negligible compared to the hydrogen feed in the regenerator. The total amount of  $H_2$  added to the system can then be calculated for the experiments.



**Figure 5.12** Representative hydrogen balance for regeneration experiments in the IFB reactor. Approximately 10% of the hydrogen added to the regenerator is used for regeneration. In most of the experiments, a  $H_2$  shortage was observed in the IFB reactor off-gas as shown in Table 5.12.

During most of the experiments, the hydrogen balance can be presented as shown in Figure 5.12 (see Table 5.12). The  $H_2O$  and  $H_2S$  concentrations are measured. Hydrogen itself cannot be detected by means of the FTIR analyzer. It can be observed that approximately 10% of the hydrogen is used for the regeneration reactions (formation of  $H_2S$  and  $H_2O$ ). In the IFB off-gas measurements an average shortage of 5%  $H_2$  was found throughout the experiments. The only possible explanation for this shortage is the accuracy of the FTIR analyzer for the components  $H_2S$  and  $H_2O$ . The deviations of the hydrogen balance are in agreement with the range of systematic errors in the calibration measurements of the FTIR apparatus (see de Feber (1995) and Korbee *et al.* (1994) for a detailed description of the calibration features).

### Batch experiments

A typical example of a batch regeneration experiment is shown in Figure 5.13. The elemental sulfur concentration is determined according to Equation 5.13. The concentration curves follow a typical pattern of sequential reactions. It can be seen that at the start of the experiment large amounts of  $SO_2$  are released and after approximately 100 minutes the concentration is levelled off to very small values. The  $H_2S$  is formed after the formation of elemental sulfur.

From the regeneration curves shown in Figure 5.13, the total amount of sulfur that is released from the sorbent is determined (by means of calculating the total amount of moles that was released for each component during the regeneration experiment). In Table 5.11 the resulting product distribution is shown for the IFB batch regeneration experiment and compared to the product distribution determined by Korbee (1995). The temperatures for the regeneration experiments are 650 and 850 °C, respectively.

## IFB pilot plant facility: experimental and modelling results

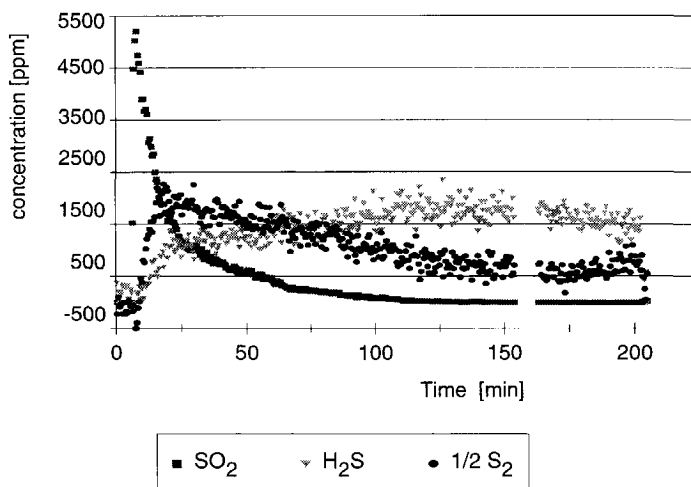
**Table 5.11** Batch regeneration product distribution measured in the IFB reactor at 650 °C and by Korbee (1995) at 850 °C for the same synthetic sorbent.

	SO <sub>2</sub> [%]	½ S <sub>2</sub> [%]	H <sub>2</sub> S [%]
IFB regeneration experiment	14	36	50
Regeneration experiment by Korbee (1995)	39	27	34

It must be mentioned that after 200 minutes the regeneration in the IFB reactor was not complete. However, due to the decreased amount of SO<sub>2</sub>, it is clear that at low temperature in the IFB reactor less SO<sub>2</sub> will be released. This was already expected on the basis of the gas phase equilibrium reactions analysis (Table 5.8). At low temperature both equilibrium reactions are more in favour of the elemental sulfur and H<sub>2</sub>S formation. This is in accordance with the experimental results at 850 and 650 °C (Table 5.11).

On the basis of the measured gas phase concentrations at  $t=100$  minutes, it was calculated that equilibrium was not reached for the equilibrium reactions (5.31) and (5.32). The calculated value for the equilibrium constants (Table 5.8) was not found. For the elemental sulfur and H<sub>2</sub>S formation reaction, values of 2.3 and 8.7 were respectively found. At the regeneration temperature of 650 °C much higher values should be found (Table 5.8) if equilibrium was reached.

The regeneration described in chapter 5.3.2 is in correspondence (with respect to the sequential reaction scheme) to the regeneration behaviour that was experimentally observed in the IFB pilot plant facility. This is illustrated in Figure 5.13.



**Figure 5.13** Batch regeneration experiment carried out in the IFB pilot plant facility at 650 °C. No solids circulation occurred and 10 v% H<sub>2</sub> was applied in the feed gas.

### *Consequences for modelling*

From the reaction scheme proposed by Korbee (1995) and described in chapter 5.3.2 the experimental regeneration behaviour observed in the IFB facility can be explained. This is a strong indication that at lower temperature (650 °C in the IFB facility compared to 850 °C in the experiments by Korbee, 1995), the reaction mechanism for reductive sorbent regeneration is equivalent to that at higher temperature. Further modelling efforts can therefore be based on the above mentioned reaction scheme. A complicating feature is however the determination of the role of diffusion limitation. From the line scan EPMA analysis of regenerated sorbent particles, a more or less evenly distributed sulfur content across the particle was observed. This is an indication of reaction limitation more than diffusion limitation.

The number of experiments and the range of experimental conditions (temperature and hydrogen concentration in the feed gas) are too limited to determine these parameters from the IFB regeneration experiments. Although the sulfur distribution in the regenerated particle (Figure 5.8) does not reveal strong pore diffusion effects, the diffusion of the regeneration products in the particle will play an important role in the product distribution of the reactor. The outer part of the sulfated sorbent is first regenerated and the regeneration product SO<sub>2</sub> is released and can diffuse out of the particle in a relative short time. When the regeneration proceeds, the sulfur will be released deeper in the particle. This will result in higher residence times of the regeneration products in the pore of the particle and a higher conversion of SO<sub>2</sub> to elemental sulfur and H<sub>2</sub>S. Subsequently, the product distribution of the regenerator will change in time as observed in the regeneration curves shown in Figure 5.13. This effect should certainly be taken into account for proper regeneration modelling.

For experiments including solids circulation the physical adsorption effects should also be investigated for the regeneration process (see chapter 5.4.1 for physical adsorption effects during sorbent sulfation).

The solids residence time in the regenerator ranged from 1 to 4 minutes and the gas residence time is approximately 0.2 seconds ( $H_3/U_3 = 0.3/1.5$ ) during the IFB experiments described in this chapter. It should therefore also be investigated whether the process at particle scale can be treated as stationary (as in the model developed by Korbee, 1995). When the penetration time (according to penetration theory) is calculated for a spherical particle of 2.6 mm for a gas with a diffusion coefficient of  $4.1 \cdot 10^{-7}$  m<sup>2</sup>/s (Table 5.9), a value of 1.3 seconds is found. This rough estimation indicates that diffusion effects can be of influence on the regeneration process through the relative large residence time of the gas phase regeneration products in the particle interior.

For further regeneration modelling, the most important drawback is the lack of appropriate kinetic parameters that could not be determined (as explained above) from the IFB experiments. The main purpose of the experiments described in this chapter was to prove the IFB reactor concept for regenerative desulfurization.

## 5.5 Continuous regenerative desulfurization experiments

During the continuous regenerative desulfurization experiments, the hydrodynamic parameters were varied as indicated in chapter 5.2.2. In Table 5.12 an overview is given of the experiments that were carried out in the IFB pilot plant facility

## IFB pilot plant facility: experimental and modelling results

**Table 5.12** Continuous regenerative desulfurization experiments. Variations in the operational parameters and the molar balances for sulfur and hydrogen are given.

Nr	$U_4$ [m/s] (1)	$U_1$ [m/s] (1)	$M_{IFB}$ [kg]	$SO_{2,in}$ [mole] (2)	$SO_{2,1}$ [mole] (3)	$SO_{2,off}$ [mole] (4)	$\Delta(CaSO_4)$ [mole] (5)	error [%] (6)	$H_{2,in}$ [mole] (7)	$H_2O_{off}$ [%] (8)
1	0.8	1.4	7.5	18.55	17.02	16.34	0.88	-7.2	192.3	93.2
2	0.9	1.4	7.5	24.44	4.92	21.12	4.61	5.3	256.4	96.0
3	1.0	1.4	7.5	25.58	16.46	21.92	4.13	1.8	262.7	90.3
4	0.9	1.5	7.5	32.27	15.25	32.67	-0.71	-0.96	330.3	93.5
5	0.9	1.4	8.5	23.67	21.79	20.81	1.97	-3.8	245.0	102.9
6	1.0	1.4	8.5	30.10	15.26	26.57	0.08	-11.5	319.4	100.4
7 (9)	0.9	1.4	7.5	20.75	16.82	19.20	2.22	3.2	327.5	87.5
8 (9)	0.9	1.4	7.5	25.74	21.23	25.01	0.94	0.82	135.4	108.1
9	0.9	1.5	7.5	15.49	0.98	21.77	-4.06	14.3	141.2	94.0

- (1) The gas velocities to compartment 1 ( $U_1$ ) and 3 ( $U_3$ ) were the same for all experiments. The gas velocity to compartment 2 ( $U_2$ ) was set at 1.0 m/s for all experiments.
- (2) Cumulative number of moles  $SO_2$  that were added to compartment 1 during the experiment.
- (3) Total amount of  $SO_2$  that was determined in the off-gas of compartment 1.
- (4) Total amount of  $SO_2$  that was measured in the IFB reactor off-gas (see Figure 4.4, position 5).
- (5) Difference between the number of moles  $CaSO_4$  on the sorbent material at the end and at the start of the experiment. ( $\Delta(CaSO_4) = [(CaSO_4_{end}) - (CaSO_4_{start})]$ )
- (6) Percentage defined as:  $(SO_{2,off} + \Delta CaSO_4 - SO_{2,in}) / SO_{2,in}$
- (7) Cumulative number of moles  $H_2$  that were added to compartment 3 during the experiment.
- (8) Percentage of the hydrogen added to compartment 3 that was measured in the IFB off-gas.
- (9) In all experiments, the  $H_2$  concentration in the feed gas to compartment 3 was 10 v%, except for experiment 7 and 8 in which 15 and 5 v% were respectively applied.

### 5.5.1 Five-day test with step changes in operating parameters

The IFB facility was continuously operated for five days during which the experiments 1 to 8 (as given in Table 5.12) were carried out. The temperatures of the regeneration and sulfur capture compartment were 650 and 715 °C respectively. The operational parameters that were varied are: the superficial gas velocities to the compartments, the total bed mass in the IFB reactor, and the hydrogen concentration in the regenerator.

A total of eight different experimental settings for hydrodynamic and reaction parameters was investigated during this test (as indicated in Table 5.12). The operating parameters were changed step-wise after which a steady-state could be reached.

## Chapter 5

In this chapter, the main results and considerations are presented. For one experiment, an overview of measured data is given.

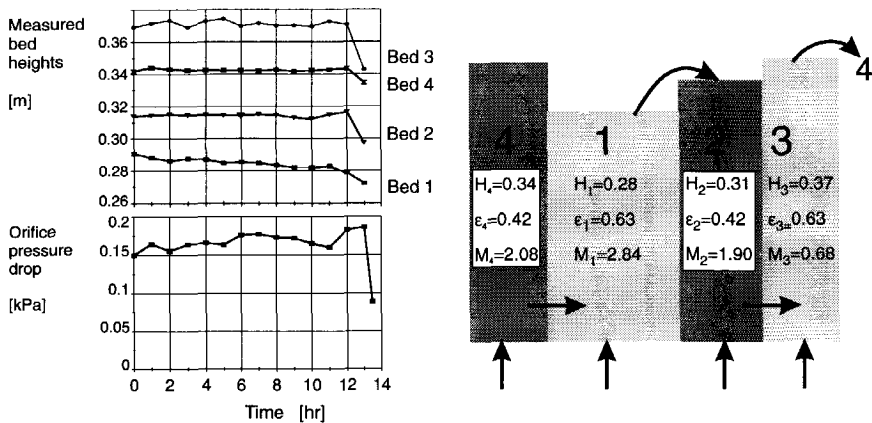
### *Analysis of a continuous regenerative desulfurization experiment*

This specific experiment corresponds to experiment 4 in Table 5.12. The inlet concentrations of the reactive gas phase components and the hydrodynamic parameters were set as indicated in Table 5.13.

**Table 5.13** Hydrodynamic and reaction parameters during a continuous regenerative desulfurization experiment at indicated settings (experiment 4; Table 5.12).

Hydrodynamic parameters			Gas phase concentrations		
$U_4$	0.9	[m/s]	$C_{SO_2, in}$	0.25	[v%]
$U_1 = U_3$	1.5	[m/s]	$C_{O_2, in}$	4	[v%]
$U_2$	1.0	[m/s]	$C_{H_2, in}$	10	[v%]
$M_{IFB}$	7.5	[kg]			

The temperature during the experiment in the desulfurization and regeneration compartments was constant at 715 and 650 °C, respectively. The most important hydrodynamic measurements during the IFB experiment are the bed heights in the IFB compartments and the pressure drop across the orifice between compartments 4 and 1. The hourly-averaged experimental data are shown in Figure 5.14.



**Figure 5.14** Hourly averaged measured bed heights and pressure drop across the orifice between compartment 4 and 1 during a high temperature desulfurization experiment in the IFB facility. See Table 5.13 for the experimental settings.

From these data it can be concluded that the IFB reactor was operated in a hydrodynamic steady-state. The measured bed heights and pressure drop across the orifice are more or less constant. The stationary CRS (calculated in chapter 5.2.2, Table 5.4) was 8.2 g/s.

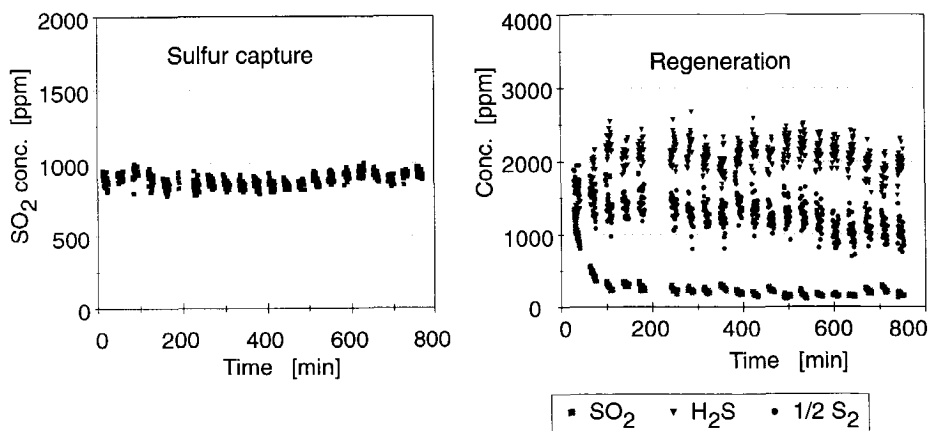


The solids distribution based on the measured bed levels illustrates that the orifice flow between compartments 4 and 1 is rate determining. The solids accumulate in bed 4 and subsequently flow back to bed 3 causing the highest bed level in these compartments. This is an important observation because the IFB reactor is operated as such.

The voidage in the chemical reactive compartments was estimated on the basis of pressure drop measurements over a fixed height in the bed. For both compartments (equal gas velocities), the voidage during this experiment was estimated as 0.63. The bed mass or solids distribution can then be determined on the basis of voidage and bed heights. From a total of 7.5 kg, the compartments 1, 2, 3, and 4 contained 2.84, 1.90, 0.68 and 2.08 kg sorbent material respectively.

In Figure 5.15, the measured off-gases of compartments 1 and 3 are represented. A steady-state sulfur retention of approximately 54% is achieved during this experiment.

The sulfur balance (see Table 5.12) showed that during this experiment, the amount of SO<sub>2</sub> that is captured in compartment 1 is also regenerated from the sorbent. The IFB reactor is thus in steady-state concerning the regenerative desulfurization. The balance fitted within 1% difference between the inlet and outlet amounts of sulfur that were determined for this specific experiment.



**Figure 5.15** Measured concentrations in the regenerator and sulfur capture compartment at 650 and 715 °C respectively during regenerative desulfurization. See Table 5.13 for the experimental settings.

The hydrogen balance indicated that 13.3 % of the H<sub>2</sub> added to the regenerator was used for regeneration. This is the difference between the hydrogen that was added to compartment 3 and the amount that was found in the off-gas of this compartment in the form of H<sub>2</sub>S and H<sub>2</sub>O. In the regenerator, the H<sub>2</sub> was converted to H<sub>2</sub>S and H<sub>2</sub>O for 2.2 and 11.1 %, respectively. In the IFB off-gas 93.5 % of the H<sub>2</sub> was measured as H<sub>2</sub>O (see Table 5.12). This H<sub>2</sub> shortage of 6.5% in hydrogen in the IFB reactor off-gas was more or less typical for the IFB experiments as discussed in chapter 5.4.2.

The product distribution in the regenerator changed from a relative high concentration of SO<sub>2</sub> at the start of the experiment to a constant low value after approximately 100 minutes. The scatter in the measured H<sub>2</sub>S and ½S<sub>2</sub> concentrations is considerable. The concentration of elemental sulfur is calculated according to Equation 5.34 and based on the measured H<sub>2</sub>O, SO<sub>2</sub>, and H<sub>2</sub>S concentrations. From the average concentrations during the experiment, it was found that the sulfur was released as SO<sub>2</sub>, H<sub>2</sub>S, and ½S<sub>2</sub> for 7.2, 57.1 and 35.7 %, respectively.

### *General considerations*

The influence of the hydrodynamics on the regenerative desulfurization process will be discussed in chapter 5.5.3. During the five-day test, the IFB reactor was continuously and successfully operated.

The average regeneration product distribution at a regeneration temperature of 650 °C shows a few percent SO<sub>2</sub>, 65 % H<sub>2</sub>S, and 30 % elemental sulfur. The sequential reaction scheme as observed in the batch regeneration experiments (chapter 5.4.2) also holds during continuous regenerative desulfurization.

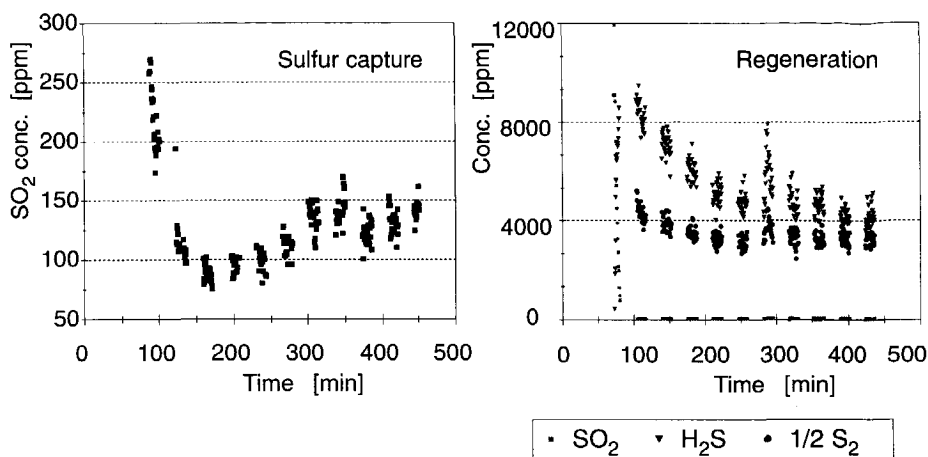
The influence of the hydrogen feed concentration on the regeneration performance and regeneration product distribution was not as expected from earlier observations (Snyder *et al.*, 1975; Wolff, 1991; Korbee, 1995). Neither the performance nor the product distribution did show a significant change when the hydrogen feed concentration was changed. This is an indication that the regeneration process is not limited in hydrogen concentration. In the regenerator an excess amount of H<sub>2</sub> is present. However, the H<sub>2</sub> concentration is expected to influence the regeneration product distribution and the rate of the regeneration reactions. No reasonable explanation on the basis of the experimental data could be found for the fact that this is not the case during regeneration in the IFB experiments.

### **5.5.2 A ten-hour high temperature experiment**

During a ten-hour test (experiment 9 in Table 5.12), the IFB reactor was operated at high temperature. The desulfurization compartment and regenerator were operated at temperatures of 850 and 795 °C, respectively. The hydrodynamic and reaction parameters are equal to the settings given in Table 5.13 except for the higher temperature.

The off-gas concentrations that were measured in the desulfurization compartment and regenerator are shown in Figure 5.16. A steady-state sulfur retention of 93% was achieved. A higher temperature apparently improves the sulfur retention of the IFB reactor significantly. At lower temperature (715 °C, see Figure 5.15), a maximum sulfur retention of 54% was established. The regeneration is also strongly affected by temperature. The higher temperature in the regenerator shifts the product distribution to elemental sulfur (43 v%) at the cost of SO<sub>2</sub> and mainly H<sub>2</sub>S. At lower temperature in the regenerator (650 °C, see Figure 5.15), the regeneration product consisted of a few percent SO<sub>2</sub>, 65 v% H<sub>2</sub>S and 30 v% elemental sulfur.

The steady-state sulfur retention of the pilot plant facility operated at high temperature was predicted by a mathematical model (see Snip *et al.* (1995) and chapter 4.3.2 of this thesis). It is interesting to compare the modelling results to the experimentally determined sulfur



**Figure 5.16** Measured concentrations in the regenerator and sulfur capture compartment at 795 and 850 °C respectively during regenerative desulfurization (experiment 9).

retention. Based on the measured pressure drop across the rate limiting orifice (4→1), the CRS was calculated to be 0.576 kg/min (see chapter 5.5.2 for details on the method of calculation). For this CRS (see Figure 4.5), the mathematical model predicts the sulfur retention to be 87%. This is close to the value that was experimentally found (93%). This indicates that the mathematical model is capable of predicting a reasonable estimation of the IFB reactor performance for high-temperature regenerative desulfurization.

Another aspect that was already mentioned in chapter 5.3.1 is the increasing effect of pore diffusion during sorbent sulfation at high temperature (850 °C) compared to lower temperature (715 °C). This is illustrated in Figure 5.7 and Table 5.7.

### 5.5.3 Sulfur retention as a function of IFB hydrodynamics

The influence of IFB hydrodynamics on reactor performance is an important aspect of this study. The IFB hydrodynamics are those phenomena that determine the solids circulation and solids distribution in the IFB reactor.

In Figure 5.17, the influence of hydrodynamics on the IFB reactor performance is schematically illustrated. The solids distribution and CRS dependency of the hydrodynamic parameters is discussed in chapter 3 of this thesis.

In this experimental study, the influence of the hydrodynamics of the IFB reactor on the sulfur retention was studied experimentally by means of variation of the important hydrodynamic parameters as indicated in chapter 5.5.1 and Table 5.12. The relevant data collected during the experiments are presented in Table 5.14 for three experiments that resulted in a steady-state concerning the sulfur retention.

## Chapter 5

**Table 5.14** Steady-state sulfur retention and hydrodynamic data measured during regenerative desulfurization experiments in the IFB facility.

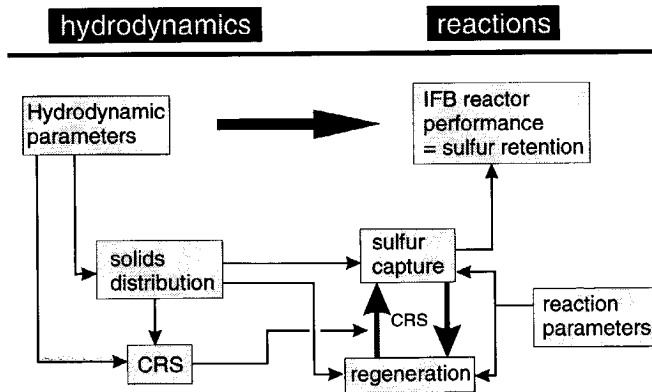
(1)	$U_1=U_3$ [m/s]	CRS [kg/min]	$M_1$ [kg]	$M_3$ [kg]	$\epsilon_1=\epsilon_3$ [m <sup>3</sup> <sub>gas</sub> /m <sup>3</sup> <sub>bed</sub> ]	$H_1$ [cm]	$H_3$ [cm]	Sulfur retention [%]
4.	1.5	0.49	2.84	0.68	0.63	28.3	36.7	54
8.	1.4	0.39	3.01	0.64	0.60	27.7	32.3	13
7.	1.4	0.41	2.93	0.67	0.61	27.7	34.4	14

(1) The numbers of the experiments correspond to the numbering in Table 5.12.

The difference between experiment 8 and 7 is the hydrogen feed concentration that was 5 and 15 v%, respectively. A close look at Table 5.14 learns that the main difference in hydrodynamic settings for the experiments is a difference CRS.

Another difference that stands out is the measured bed height in the regenerator ( $H_3$ ) for experiment 4. This value seems to be overestimated by the pressure gradient extrapolation method. The bed height was also measured by means of laser light reflection (see chapter 4.2.1 for details concerning bed height measurements). It appeared that the regenerator bed height could be overestimated by 3 to 4 cm in compartment 3. For the other compartments, the measured bed heights by means of both methods were in agreement within the range of experimental error (*i.e.*, 1 to 2 cm).

The sulfur retention of the IFB reactor is determined by the solids distribution and CRS, and the rate of sulfur capture and regeneration reactions as schematically shown in Figure 5.17. For the above mentioned experiments the solids distribution ( $M_1$  and  $M_3$ ) is not significantly different. The regeneration was shown to be not rate limiting in the regenerative desulfurization process (see chapter 5.5.1). The difference in sulfur retention or reactor performance can thus be explained by the CRS.



**Figure 5.17** A schematic representation of the influence of hydrodynamic parameters on the IFB chemical reactor performance through the solids distribution and the CRS.

The sulfur retention increases with increasing CRS. This is similar to what was expected on the basis of IFB regenerative desulfurization modelling (Snip *et al.*, 1995). The modelling results cannot be directly compared to the experimental data because the temperatures are different; in chapter 5.3 this is explained.

Although the experimental data are limited, the trend is clear that by increasing the CRS, the IFB sulfur retention will also increase.

### 5.6 Discussion and conclusions

The IFB facility was designed and constructed to show the suitability of the IFB reactor concept for a continuous high-temperature desulfurization process. The experimental results showed that the IFB reactor is capable of integrating sulfur capture and regeneration by means of solids circulation within one reactor vessel.

The IFB pilot plant facility was operated continuously in a five-day period at a sulfur capture and regeneration temperature of 715 and 650 °C, respectively. In a ten-hour test, the optimum sulfur capture temperature (Wolff, 1991; Korbee, 1995) was reached. Retention and regeneration temperatures of 850 and 795 °C were respectively effected. Further, various batch sulfur capture and regeneration experiments were carried out to investigate these sub-processes.

#### *Hydrodynamics*

The experiments concerned the determination of the temperature effect on the minimum fluidization velocity ( $U_{mf}$ ). It was experimentally shown by means of pressure drop and pressure fluctuation measurements that within the range of temperatures (650-850 °C) during the IFB experiments the temperature did not affect  $U_{mf}$  significantly. The difference in  $U_{mf}$  between high temperature and ambient conditions is strong (1.0 to 0.75 m/s) and was therefore taken into account.

The Circulation Rate of Solids (CRS) was determined on the basis of pressure drop measurements across the rate limiting orifice and a solids flow model (chapter 5.2.2). Comparison to cold IFB experimental work and a residence time distribution analysis (Figure 5.4) indicated that a reasonable estimation of the CRS could be determined during the IFB experiments.

#### *Sulfur capture*

The temperature influence on reaction mechanism, rate of reaction and pore diffusion was investigated. It was shown that reaction mechanism and pore diffusion were not significantly affected by temperature in the range that was applied in the experiments.

By means of an analysis on rate limitations it was shown that the role of pore diffusion significantly decreases due to a strong negative temperature effect on the reaction rate of sulfation. This was experimentally confirmed by means of a detailed (EPMA) particle analysis. It was shown that at 850 °C, SO<sub>2</sub> penetrates the sorbent particle according to a pore diffusion limited process (Figure 5.7). At 715 °C this is not the case, implicating more reaction limitation.

Based on a rough estimation of the activation energy (100 kJ/mole), the reaction rate at 715 °C was estimated. This value was used for batch sulfation modelling. The results were in fair

agreement with the experimental data. The discrepancy can be explained mainly from the uncertainties in the sulfation reaction rate constant and the role of pore diffusion at lower temperature.

### *Regeneration*

During the experiments, the sorbent was regenerated by means of hydrogen as a reducing agent. As for sulfation, the influence of temperature causes the rate limiting process to shift from diffusion at 850 °C to reaction rate limitation at 715 °C. This was shown by means of particle analysis (Figure 5.7 and 5.8).

An important observation was that even at a low temperature (compared to 850 °C) of 650 °C, the sorbent can be regenerated by means of hydrogen.

A sequential reaction scheme was observed in both batch and continuous regenerative desulfurization experiments:  $\text{CaSO}_4 \rightarrow \text{SO}_2 \rightarrow \frac{1}{2}\text{S}_2 \rightarrow \text{H}_2\text{S} \rightarrow \text{CaS}$ .

This sequence of reactions is in agreement with earlier work on sorbent regeneration (Korbee, 1995). No significant amount of CaS was formed during the experiments. The influence of the hydrogen feed concentration was weak and not completely understood.

The elemental sulfur concentration in the regenerator off-gas was estimated on the basis of the measured  $\text{H}_2\text{O}$ ,  $\text{H}_2\text{S}$  and  $\text{SO}_2$  concentration (Equation 5.34). These components were directly and on-line measured by means of an FTIR analyzer.

The gas phase components in the regenerator are far from thermodynamic equilibrium. Composition of the regenerator gas phase therefore depends on the kinetics of the proposed equilibrium reactions. For proper regeneration modelling, adequate values for the kinetic parameters are therefore needed. The solids and gas residence times in the regeneration compartment were compared to the penetration time of the gas phase components in the particle. This revealed that is necessary to investigate the non-stationary regeneration process at particle scale.

### *Reactor performance*

The IFB reactor performance was analyzed in terms of the influence of the hydrodynamics on the IFB sulfur retention. The hydrodynamics do influence the sulfur retention through the CRS and the solids distribution in the IFB reactor (Figure 5.17).

The experiments in which a steady-state sulfur retention was reached are represented in Table 5.14. It was shown that by increasing the CRS, the sulfur retention also increases. This is in agreement with the model predictions. During the high temperature regenerative desulfurization experiment, a maximum steady-state sulfur retention of 93% was reached. The temperature for sulfur capture and regeneration were 850 and 795 °C, respectively.

### *General considerations*

Although a limited set of experiments was carried out in the IFB pilot plant facility, some important findings must be emphasized:

- ▶ the IFB reactor proved to work at reaction conditions with respect to continuous solids circulation, sulfur capture and regeneration;
- ▶ reactor performance could be controlled by means of manipulating the hydrodynamics (gas velocities and bed mass) through the CRS;
- ▶ a relative high (>90%) sulfur retention can be achieved in the IFB reactor that is thus suitable for regenerative desulfurization

## IFB pilot plant facility: experimental and modelling results

More experiments are needed to support the above mentioned conclusions. These experiments should also provide the appropriate kinetic data concerning the chemical reactions and physical adsorption effects. This information is needed for further modelling of the sulfur capture and regeneration process.

The hydrodynamic parameters such as: the size of the orifice, the gas velocities and the IFB bed mass, should be varied systematically in order to verify the correctness of the solids flow model that was used to predict the CRS in the IFB reactor.

This study and further experimental work carried out in the IFB pilot facility can provide information on how to design and operate the process of regenerative desulfurization in the IFB reactor.

### Notation

$A_{\text{eff}}$	: effective orifice area (Equation 2.1; Chapter 2)	[m <sup>2</sup> ]
$A_o$	: cross sectional area of the orifice	[m <sup>2</sup> ]
$C$	: gas phase concentration	[mole/ m <sup>3</sup> ]
$C_{\text{CaO}}$	: CaO content of sorbent	[mole CaO/ m <sup>3</sup> sorbent]
$C_D$	: discharge coefficient	[-]
CRS	: Circulation Rate of Solids	[g/s]
$d_{\text{orifice}}$	: orifice diameter	[m]
$d_p$	: particle diameter	[m]
$D_{\text{pore}}$	: pore diffusion coefficient	[m <sup>2</sup> pore/s]
$D$	: diffusion coefficient for component x	[m <sup>2</sup> /s]
$E$	: Effectiveness factor	[-]
$E_A$	: activation energy	[J/mole]
$f$	: friction factor	[-]
$f_{\text{Ca}}$	: calcium content (fraction) of the sorbent	[kg Ca/kg sorbent]
$\Delta G$	: Gibbs function of reaction	[J/ mole]
$K$	: stress ratio	[-]
$k$	: intrinsic reaction rate constant	[m <sup>3</sup> gas/m <sup>2</sup> surface.s]
$K_{\text{Eq}}$	: equilibrium constant	[-]
$k_s$	: sulfation reaction rate constant	[m <sup>3</sup> gas/m <sup>2</sup> core.s]
$k_{\text{SO}_2}$	: mass transport coefficient	[m <sup>2</sup> /s]
$M_{\text{bed}}$	: solids hold-up in IFB compartment	[kg]
$M_{\text{Ca}}$	: molar mass of Ca	[kg Ca/ mole Ca]
$M_T$	: Thiele modulus	[-]
$N_{\text{CaO}}$	: amount of CaO in the core of one sorbent particle	[mole CaO]
$\Delta P$	: pressure drop across the orifice	[Pa]
$r_c$	: core radius	[m]
$r_\alpha$	: rate of conversion of one sorbent particle	[(mole CaSO <sub>4</sub> /mole Ca)/s]
$R$	: radius of sorbent particle	[m]
$R_{\text{conv}}$	: rate of conversion	[mole/s]
$S_{\text{BET}}$	: B.E.T. surface area	[m <sup>2</sup> /g]
$T$	: temperature	[°C]
$U$	: superficial gas velocity	[m/s]
$V_g$	: gas volume of the fluidized bed compartment	[m <sup>3</sup> gas]
$V_{\text{pore}}$	: sorbent pore volume	[ml/g]

## Chapter 5

### Greek

$\alpha$	: sorbent (or CaO) conversion	[mole CaSO <sub>4</sub> /mole Ca]
$\alpha_r$	: angle of repose	[°]
$\Gamma$	: stoichiometric coefficient	[mole CaO/ mole SO <sub>2</sub> ]
$\delta$	: film layer thickness	[m]
$\epsilon_{\text{fixed}}$	: fixed bed voidage	[m <sup>3</sup> <sub>gas</sub> /m <sup>3</sup> <sub>bed</sub> ]
$\epsilon_u$	: voidage of the upflowing bed	[m <sup>3</sup> <sub>gas</sub> /m <sup>3</sup> <sub>bed</sub> ]
$\mu$	: viscosity	[Pa s]
$\sigma_N$	: horizontally directed particle pressure	[Pa]
$\rho_d$	: bulk density of dense bed	[kg/m <sup>3</sup> <sub>bed</sub> ]
$\rho_p$	: particle density	[kg/m <sup>3</sup> <sub>particle</sub> ]
$\tau$	: tortuosity factor	[m <sup>2</sup> <sub>gas</sub> / m <sup>2</sup> <sub>particle</sub> ]
$\phi_m$	: solids mass flow	[kg/s]
$\phi_s$	: particle shape factor	[-]
$\phi_v$	: volumetric flow	[m <sup>3</sup> /s]

### Subscripts

bd	: bed
dense	: dense bed, operated at relatively low gas velocity
eff	: effective
Knu	: Knudsen
lean	: lean bed, operated at relatively high gas velocity
mf	: minimum fluidization
N	: normal
o	: orifice

### References

- Al-Shawabkeh, A., Lin, S-Y, Matsuda, H., Hasatani, M., "Formation of CaSO<sub>3</sub> during high-temperature desulfurization with Ca-based sorbents", J. of Chem. Eng. of Jap., 28(6), 689-696 (1995).
- Barin, I., Knacke, O., "Thermochemical properties of inorganic substances", Springer-Verlag, Berlin (1973).
- Bischoff, K.B., "Accuracy of the pseudo steady state approximation for moving boundary diffusion problems", Chem. Eng. Sci., 18, 711-713 (1963).
- Botteril, J.S.M., "Fluidized bed behaviour at high temperature and pressures", In: Transport in fluidized particle systems (Eds: Doraiswamy, L.K., Mujumdar, A.S.), Elsevier, Amsterdam, 33-70 (1989).
- Carberry, J.J., Goring, R.L., "Time-dependent pore-mouth poisoning of catalysts", J. of Catalysis, 5, 529-535 (1966).
- Coulson, J.M., Richardson, J.F., "Chemical Engineering: Design", Volume 6, Pergamon Press, Oxford, 254-255 (1991).
- Dam-Johansen, K., Østergaard, K., "High temperature reaction between sulfur dioxide and limestone-II. An improved experimental basis for a mathematical model", Chem. Eng. Sci., 46(3), 839-845 (1991a).
- Dam-Johansen, K., Hansen, P.F.B., Østergaard, K., "High temperature reaction between sulfur dioxide and limestone- III. A grain-micrograin model and its verification", Chem. Eng. Sci., 46(3), 847-853 (1991).



## IFB pilot plant facility: experimental and modelling results

- Dam-Johansen, K., Østergaard, K., "High temperature reaction between sulfur dioxide and limestone-IV. A discussion of chemical reaction mechanisms and kinetics", *Chem. Eng. Sci.*, 46(3), 855-859 (1991b).
- Duisterwinkel, A.E., "Clean coal combustion with in-situ impregnated sol-gel sorbent", PhD thesis, Delft University of Technology, Delft, The Netherlands (1991).
- Feber de, M.A.P.C., "Gas and solids dispersion in fluidized beds: prediction of contacting models in the IFB pilot plant facility with aid of literature dispersion data", Internal report, Delft University of Technology (1994).
- Feber de, M.A.P.C., "Interconnected Fluidized Bed for regenerative desulfurization: development and testing of the IFB pilot plant facility", MSc report, Delft University of Technology (1995).
- Grace, J.R., "Fluid Beds as Chemical Reactors", Chapter 12, in "Gas Fluidization Technology, Geldart, D. (Ed.), John Wiley & Sons, 285-339 (1986).
- Hansen, P.F.B., Dam-Johansen, K., Bank, L.H., Østergaard, K., "Sulfur retention on limestone under fluidized bed combustion conditions- An experimental study", in: proceedings of the 11th Int. Conf. on Fluidized Bed Combustion, (Ed: Anthony, E.J.), Montreal, Canada, vol 1, 73-82 (1991).
- Hartman, M., Trnka, O., "Influence of temperature on the reactivity of limestone particles with sulfur dioxide", *Chem. Eng. Sci.*, 35, 1189-1194 (1980).
- Hong, S.C., Jo, B.R., Doh, D.S., Choi, C.S., "Determination of minimum fluidization velocity by statistical analysis of pressure fluctuations in a gas-solid fluidized bed", *Powder Techn.*, 60, 215-221 (1990).
- Hsia, C., St.Pierre, G.R., Raghunathan, K., Fan, L.S., "Diffusion through  $\text{CaSO}_4$  formed during the reaction of  $\text{CaO}$  with  $\text{SO}_2$  and  $\text{O}_2$ ", *AIChE J.* 39(4), 698-700 (1993).
- Korbee, R., "Regenerative desulfurization in an Interconnected Fluidized Bed System", PhD thesis, Delft University of Technology, Delft, The Netherlands (1995).
- Korbee, R., Grievink, J., Schouten, J.C., Van den Bleek, C.M., "Preliminary design of a 100 MWE power plant with regenerative desulfurization, applying Interconnected Fluidized Bed Combustion", in: proceedings of 12th Int. Conf. on Fluidized Bed Combustion, (Eds: Rubow, L., Commonwealth, G.), San Diego, USA, vol. 2, 1143-1151 (1993).
- Korbee, R., Schouten, J.C., Bleek van den, C.M., "Measuring and Calibration Experience with an FT-IR system: quantitative use in complex gas mixtures", In: proceedings of the Nordic Seminar on Gas Analysis in Combustion, (Ed.: Hernberg, R.), Tampere, Finland, 63-76 (1994).
- Korbee, R., Wolff, E.H.P., Bleek van den, C.M., "A general approach to FBC sulfur retention modelling", in: proceedings of the 11th Int. Conf. on Fluidized Bed Combustion, (Ed: Anthony, E.J.), Montreal, Canada, vol 2, 907-916 (1991).
- Kraijo, G., "Regenerative desulfurization in an Interconnected Fluidised Bed reactor: experimental study and modelling of the sulfur retention", MSc report, Delft University of Technology (1996).
- Kunii, D., Levenspiel, O., "Fluidization Engineering", Chapters 3 and 12, 2nd Ed., Butterworth-Heinemann, 61-94 (1991).
- Levenspiel, O., "The Chemical Reactor Omnibook", 4th version, OSU Book Stores, Inc., Corvallis, Oregon, USA, Chapter 22 (1993).
- Lin, W., "Interactions between  $\text{SO}_2$  and  $\text{NO}_x$  emissions in fluidized bed combustion of coal", PhD thesis, Delft University of Technology, Delft, The Netherlands (1994).
- Ling van, D.A., "Modelling the hydrodynamic behaviour of the Interconnected Fluidised Bed system", MSc report, Delft University of Technology (1996).
- Luss, D., "On the pseudo steady state approximation for gas solid reactions", *The Can. J. of Chem. Eng.*, 46, June, 154-156 (1968).
- Marsh, D.W., Ulrichson, D.L., "Rate and diffusional study of the reaction of calcium oxide with sulfur dioxide", *Chem. Eng. Sci.*, 40 (3), 423-433 (1985).

## Chapter 5

---

- Mura, G., Lallai, A., Olla, P., "On the kinetics of dry desulfurization with calcium oxide", *The Chem. Eng. J.*, 46, 119-128 (1991).
- Perry, R.H., Green, D. (Eds.), "Perry's Chemical Engineers' Handbook", Mc-Graw-Hill, Singapore, 20-84 (1988).
- Punčochář, M., Drahoš, J., Čermák, J., Selucký, "Evaluation of minimum fluidizing velocity in gas fluidized beds from pressure fluctuations", *Chem. Eng. Comm.*, 35, 81-87 (1985).
- Rapagna, S., Foscolo, P.U., Gibilaro, L.G., "The influence of temperature on the quality of gas fluidization", *Int. J. of Multiphase Flow* 10(2), 305-313 (1994).
- Raso, G., D'Amore, M., Formisani, B., Lignola, P.G., "The influence of temperature on the properties of the particulate phase at incipient fluidization", *Powder Technol.*, 72, 71-76 (1992).
- Reid, R.C., Prausnitz, J.C., Sherwood, T.K., "The properties of gases and liquids", 3rd ed., McGraw-Hill, New York, USA, 553-555 (1977).
- Sander, U.H.F., "Sulphur, sulphur dioxide and sulfuric acid", The British Sulphur Corporation Ltd., (1984).
- Schouten, J.C., "Sulfur retention and particle motion during fluidized bed combustion of coal", PhD thesis, Delft University of Technology, Delft, The Netherlands (1988).
- Schouten, J.C., Bleek van den, C.M., "The DUT SURE model: A simple approach in the FBC sulfur retention modelling", In: *Proceedings of the 9th Conference on Fluidized Bed Combustion*, (Ed. Mustonen, J.P.), ASME, Boston, USA, Vol. 2, 749-761 (1987).
- Schouten, J.C., Bleek van den, C.M., "Sulfur retention and NOx reduction: the SURE model", in: "Atmospheric fluidized bed coal combustion - research, development and application", 22, *Coal Science and Technology*, (Ed: Valk, M.), Elsevier, Amsterdam, The Netherlands, 227-257 (1995).
- Simons, G.A., Garman, A.R., Boni, A.A., "The kinetic rate of SO<sub>2</sub> sorption by CaO", *AIChE J.*, 33(1), 211-247 (1987).
- Smaling, C.M., "Experimental study on the continuous regenerative desulfurization in an Interconnected Fluidized Bed reactor: regeneration of the synthetic sorbent SGC 500", MSc report, Delft University of Technology (1996).
- Snip, O.C., Korbee, R., Schouten, J.C., Bleek van den, C.M., "The influence of hydrodynamics on the performance of an Interconnected Fluidized Bed system for regenerative desulfurization", *AIChE Symp. Series*, 91 (308), 82-92 (1995).
- Snyder, R.B., Wilson, W.I., Vogel, G.J., Jonke, A.A., "Sulfation and regeneration of synthetic additives", In: *Proceedings of the 4th International Conference on Fluidized Bed Combustion*, McLean, Virginia, USA, 439-455 (1975).
- Wilkinson, D., "Determination of minimum fluidization velocity by pressure fluctuation measurement", *Can. J. of Chem. Eng.*, 73, 562-565 (1995).
- Wolff, E.H.P., "Regenerative sulfur capture in fluidized bed combustion of coal: A fixed bed sorption study", PhD thesis, Delft University of Technology, Delft, The Netherlands (1991).
- Wolff, E.H.P., Gerritsen, A.W., Verheijen, P.J.T., "Attrition of an alumina-based synthetic sorbent for regenerative sulphur capture from flue gas in a fluidised bed", *Powder Technol.*, 76, 47-55 (1993a).
- Wolff, E.H.P., Gerritsen, A.W., Bleek van den, C.M., "Multiple reactor testing of a synthetic sorbent for regenerative sulfur capture in fluidized bed combustion of coal", *Can. J. Chem. Eng.*, 71 (February), 83-93 (1993b).
- Yates, J.G., "Effects of temperature and pressure on gas-solid fluidization", *Chem. Eng. Sci.*, 51, 167-205 (1996).

# Chapter 6

## Gas-solids reactions in the IFB system

influence of dynamics and particle residence time distribution on IFB reactor performance

---

### 6.1 Dynamic modelling of regenerative desulfurization in the IFB reactor

The influence of the Residence Time Distribution (RTD) of the particles on the average conversion in the IFB reactor compartments is not considered in the equations presented in chapter 6.1. The modelling and consequences of particle RTD on regenerative desulfurization in an IFB reactor are outlined in chapter 6.3.

#### *An overall dynamic model for IFB hydrodynamics*

In chapter 3, a dynamic model was developed for the prediction of the non-steady state hydrodynamic behaviour of the IFB reactor system. This model is the basis of an extension to the dynamic model for regenerative desulfurization in the IFB reactor as presented in this chapter. The calculations that were carried out and are presented in this chapter have been adapted to the IFB reactor of the pilot plant facility (described in chapters 4 and 5).

The hydrodynamic model as outlined in chapter 3.1 is based on mass balances for the solids phase in each of the IFB compartments:

$$\frac{dM_i}{dt} = \phi_{s,in,i} - \phi_{s,out,i} \quad (6.1)$$

in which  $M_i$  is the bed mass of compartment  $i$ . The terms  $\phi_{s,in,i}$  and  $\phi_{s,out,i}$  represent the inlet and outlet solids flows of the compartment.

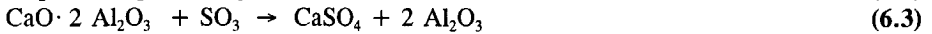
Depending on the operating conditions, a compartment is either a dense (low gas velocity) or a lean bed (high gas velocity). The inlet and outlet terms can be either solids flow through an orifice or solids flow over a weir depending on the specific conditions in the compartment (see Figure 3.1). The weir flow model, as developed in chapter 3.1, estimates the solids flow as a function of the actual bed mass in a lean bed compartment and the gas velocity that is applied. The solids flow through the orifice depends on the hydrodynamic conditions in the compartments at both sides of the orifice.

The mass balances for each compartment and the models for weir flow and orifice flow enable the prediction of the IFB hydrodynamics as a function of design (*i.e.*, IFB sizes and particle properties) and operational parameters (*i.e.*, gas velocities and total IFB bed mass). The overall IFB model was implemented in the dynamic flowsheeting simulator Speedup (1993). The structure of the Speedup model for IFB hydrodynamics is outlined in chapter 3

(appendix 3.A). The modelling results were compared to experimental results and it was shown that the overall IFB model is well capable of predicting qualitatively the hydrodynamic phenomena that were observed in the IFB pilot plant reactor.

**Regenerative desulfurization**

Sulfur capture modelling by means of a synthetic sorbent was extensively studied at DUT. This is described by Wolff *et al.* (1993) and Korbee (1995). The so-called SURE2 approach was developed. This approach is based on a shrinking unreacted core at the sorbent particle level. A stepwise penetration of the SO<sub>2</sub> into the sorbent particle is assumed. The reaction is assumed to proceed through the formation of SO<sub>3</sub>, reaction with CaO/ $\gamma$ -alumina, and formation of calcium sulfate:



The SURE2 model proved to be able to describe the experimentally observed sulfur capture behaviour adequately. In chapter 5.3 of this thesis, the SURE2 model is briefly outlined and emphasis is given on the temperature dependency of the model parameters.

For the fluidized bed desulfurization compartment in the IFB reactor, the solids and gas phases can be assumed as ideally mixed (see chapter 5.3). The conversion of CaO of a sorbent particle is defined as  $\alpha$  (mole CaSO<sub>4</sub>/mole Ca). The solids phase (CaO) balance for the sulfur capture compartment is represented as:

$$\text{out} = \text{in} - \text{conversion} - \text{accumulation} \tag{6.4}$$

which is written in terms of conversion ( $\alpha$ ) as:

$$\phi_{s,out} \alpha = \phi_{s,in} \alpha_{in} + r_\alpha M - \frac{d(M\alpha)}{dt} \tag{6.5}$$

where  $\phi_{s,out}$  and  $\phi_{s,in}$  are the outlet and inlet mass flows,  $r_\alpha$  is the rate of conversion for one sorbent particle [(mole CaO/mole Ca)/s], and  $M$  is the total solids hold-up in the desulfurization compartment. The reaction rate term  $r_\alpha$  follows from Equation 5.10 (chapter 5.3) as a result of the SURE2 model. The shrinking core radius ( $r_c$ ) of the sorbent particle (of radius  $R$ ) is related to the conversion  $\alpha$  according to:

$$\alpha = 1 - \left(\frac{r_c}{R}\right)^3 \tag{6.6}$$

Equation 6.5 can be rewritten to:

$$\frac{d\alpha}{dt} = \frac{\phi_{s,in}}{M} \alpha_{in} - \frac{\phi_{s,out}}{M} \alpha + r_\alpha - \frac{\alpha}{M} \frac{dM}{dt} \tag{6.7}$$

The gas phase balance for SO<sub>2</sub> (assuming mixed flow conditions) can be written as:

$$\frac{dV_g C_{SO_2}}{dt} = \phi_v (C_{SO_2,in} - C_{SO_2}) - \frac{f_{Ca} M}{M_{Ca} \Gamma} r_\alpha + \frac{1}{10} \frac{f_{Ca}}{M_{Ca}} \phi_{s,in} \alpha_3 \tag{6.8}$$

in which  $V_g$  is the gas phase volume of the fluidized bed adsorber,  $\phi_v$  is the volumetric flow rate through the bed,  $C_{SO_2}$  is the gas phase  $SO_2$  concentration in the adsorber. Further,  $f_{Ca}$  represents the mass fraction Ca of the sorbent,  $M_{Ca}$  is the molar mass of Ca and  $\Gamma$  is the stoichiometric coefficient (number moles  $SO_3$  that react with CaO, according to Equation 6.3 its value is 1). The last term in Equation 6.8 originates from the fact that in the regenerator not all  $CaSO_4$  is regenerated to CaO. A fraction  $\alpha_3$  is converted to CaS (see Equations 6.12 to 6.15).

It was experimentally observed by Wolff (1991) that CaS (on a  $\gamma$ -alumina carrier) is oxidized according to the following reactions:



Wolff (1991) determined that 10% of the CaS is converted to CaO (reaction 6.9) and 90% to  $CaSO_4$  (reaction 6.10). This will also affect the  $\alpha_{in}$  term in Equation 6.7:

$$\alpha_{in} = \alpha_1 + \frac{9}{10}\alpha_3 \quad (6.11)$$

in which  $\alpha_1$  is the mole fraction of  $CaSO_4$  in the regenerator. CaS ( $\alpha_3$ ) is converted for 90% to  $CaSO_4$  in the adsorber.

In chapter 6.3, the effects of particle residence time distribution on the average conversion will be calculated. In first instance, the average sulfur retention and the average sorbent conversion are used in the calculations. In the above equations no particle residence time distribution was therefore taken into account. It is shown (see chapter 6.3) that this assumption is reasonable for a shrinking core particle conversion model when the conversion ( $\alpha$ ) is limited.

### ***Sorbent regeneration***

Sorbent regeneration was studied by Korbee (1995) who developed a mathematical model to predict the sorbent regeneration behaviour. The general reaction scheme and the temperature influence of the model parameters for regeneration modelling are represented in chapter 5.3.2 of this thesis. Based on experimental observations, Korbee (1995) proposed an engineering model for sorbent regeneration. It is assumed that the calcium is present at the outer surface of the sorbent particle as  $CaSO_4$ , CaO, or CaS, with respective mole fractions of  $\alpha_1$ ,  $\alpha_2$  and  $\alpha_3$ . The model further assumes first order reaction in gas phase concentration and outer surface area.

The main reactions according to which the regeneration is assumed to take place are:



## Chapter 6

Kinetic parameters and thermodynamic properties are given for a temperature of 850°C and were taken from Korbee (1995).

For the regenerator, ideally mixed flow conditions are assumed (see chapter 5.3.2). Each of the three sorbent components (CaSO<sub>4</sub>, CaO and, CaS) is characterized as:

$$\begin{aligned}\alpha_1 &= \text{number of moles CaSO}_4 \text{ per mole Ca} & [\text{mole CaSO}_4/\text{mole Ca}] \\ \alpha_2 &= \text{number of moles CaO per mole Ca} & [\text{mole CaO/mole Ca}] \\ \alpha_3 &= \text{number of moles CaS per mole Ca} & [\text{mole CaS/mole Ca}]\end{aligned}$$

The solids phase molar balances for these components can be written in the general form (see Equations 6.4 and 6.5). For  $\alpha_1$  (CaSO<sub>4</sub>) this results in:

$$\phi_{s,out} \alpha_1 = \phi_{s,in} \alpha - \frac{k_1 \alpha_1 C_{H_2}}{q} M - \frac{d(M \alpha_1)}{dt} \quad (6.16)$$

in which  $\phi_{s,out}$  and  $\phi_{s,in}$  are the outlet and inlet mass flows for the regenerator,  $\alpha$  is the conversion of the sorbent in the adsorber that is transported to the regenerator,  $q$  is the CaO surface concentration (in mole Ca/m<sup>2</sup> sorbent),  $M$  is the amount of sorbent (bed mass) in the regenerator,  $k_1$  is the rate constant of reaction 6.12, and  $C_{H_2}$  is the gas phase hydrogen concentration. The molar balance (Equation 6.16) can be rewritten into the following differential equation describing  $\alpha_1$ :

$$\frac{d\alpha_1}{dt} = \frac{\phi_{s,in}}{M} \alpha - \frac{\phi_{s,out}}{M} \alpha_1 - \frac{k_1 \alpha_1 C_{H_2}}{q} - \frac{\alpha_1}{M} \frac{dM}{dt} \quad (6.17)$$

For the fraction of CaO, rewriting of the molar balance results in:

$$\frac{d\alpha_2}{dt} = \frac{\phi_{s,in}}{M} (1-\alpha) - \frac{\phi_{s,out}}{M} \alpha_2 + \frac{k_1 \alpha_1 C_{H_2}}{q} - \frac{k_4 C_{H_2S} \alpha_2}{q} - \frac{\alpha_2}{M} \frac{dM}{dt} \quad (6.18)$$

When  $\alpha_1$  and  $\alpha_2$  are known, the fraction of CaS can be calculated according to:

$$\alpha_3 = 1 - \alpha_1 - \alpha_2 \quad (6.19)$$

The balances for the gas phase components in the regenerator are set up assuming mixed flow conditions. The gas phase equilibrium reactions are taken into account assuming that equilibrium is reached within the regenerator. At 850 °C, the equilibrium constants for reactions 6.13 and 6.14 are 23.5·10<sup>3</sup> and 43.9 respectively indicating that the equilibrium compositions are strongly in favour of the right hand side products. The chemical reactions 6.12, 6.13 and 6.14 can then be written as:



The reaction rate of this overall reaction is equal to that of reaction 6.12 and can therefore be calculated by the reaction rate constant  $k_1$ .

For hydrogen ( $H_2$ ), the molar balance results in the following equation:

$$\frac{d(V_g C_{H_2})}{dt} = \phi_v (C_{H_2, in} - C_{H_2}) - 4k_1 \alpha_1 C_{H_2} M \frac{f_{Ca}}{M_{Ca}} \quad (6.21)$$

in which  $V_g$  is the gas phase volume of the regenerator,  $\phi_v$  is the volumetric flow rate through the bed and  $C_{H_2}$  is the hydrogen concentration in the bed.

For  $H_2S$  and  $H_2O$ , the following equations can be derived on the basis of the molar balances for these components:

$$\frac{d(V_g C_{H_2S})}{dt} = \phi_v (C_{H_2S, in} - C_{H_2S}) + (k_1 \alpha_1 C_{H_2} - k_4 \alpha_2 C_{H_2S}) M \frac{f_{Ca}}{M_{Ca}} \quad (6.22)$$

$$\frac{d(V_g C_{H_2O})}{dt} = \phi_v (C_{H_2O, in} - C_{H_2O}) + (3k_1 \alpha_1 C_{H_2} + k_4 \alpha_2 C_{H_2S}) M \frac{f_{Ca}}{M_{Ca}} \quad (6.23)$$

in which  $C_{H_2S}$  and  $C_{H_2O}$  are the gas phase concentrations in the regenerator of hydrogen sulfide and water respectively.

### *Solids circulation*

The sorbent is circulating between adsorber and regenerator. In the transport compartments of the four-bed IFB reactor no chemical reactions take place. In Figure 3.1 it is shown that for a transport compartment, three types of solids flow can be recognized:

- ▶  $\phi_{s, weir}$  : solids flow over the weir,
- ▶  $\phi_{s, back}$  : back flow over the weir, and
- ▶  $\phi_{s, orifice}$  : solids flow through the orifice to the adjacent fluidized bed reactor compartment.

The sorbent is transported from the adsorber over the weir to compartment 2. This bed is operated as a fluidized bed and can therefore be described as ideally mixed (particle residence time is much larger than the time needed for complete mixing). The effect of solids mixing on the average composition of the solids flow leaving the bed is taken into account by solving the molar balances for each solids phase component. The general form of the molar balance (Equation 6.4) is applied while omitting the conversion term. For the component  $CaSO_4$ , this results in:

$$\phi_{s, back} \alpha + \phi_{s, orifice} \alpha_1 = \phi_{s, weir} \alpha - \frac{d(M\alpha_1)}{dt} \quad (6.24)$$

It is assumed that the sorbent particles that flow back from compartment 2 to the adsorber still have an average conversion equal to that in the adsorber ( $\alpha$ ). The term  $\alpha_1$  represents the actual average  $CaSO_4$  content in compartment 2. Equation 6.24 can be rewritten to:

$$\frac{d\alpha_1}{dt} = \frac{(\phi_{s, weir} - \phi_{s, back})}{M} \alpha - \frac{\phi_{s, orifice}}{M} \alpha_1 - \frac{\alpha_1}{M} \frac{dM}{dt} \quad (6.25)$$

## Chapter 6

A similar equation for the average CaO content of the sorbent ( $\alpha_2$ ) can be derived from the molar balance:

$$\frac{d\alpha_2}{dt} = \frac{(\phi_{s,weir} - \phi_{s,back})}{M} \alpha_{2,ads} - \frac{\phi_{s,orifice}}{M} \alpha_2 - \frac{\alpha_2}{M} \frac{dM}{dt} \quad (6.26)$$

in which the term  $\alpha_{2,ads}$  is the average CaO content of the sorbent in the adsorber and  $\alpha_2$  is the average sorbent CaO content in compartment 2. The average CaS content of the sorbent ( $\alpha_3$ ) is calculated by means of Equation 6.19.

The regenerated sorbent is transported from the regenerator over the weir to compartment 4 that is operated below the minimum fluidization velocity. The solids move in plug flow through this compartment as experimentally shown by Stellema *et al.* (1996). The solids flow in this transport compartment was therefore modelled as such; no dead zones nor non-moving solids were taken into account.

The average composition of the outgoing sorbent (through the orifice to the adsorber) with respect to  $\text{CaSO}_4$  ( $\alpha_1$ ) and CaO ( $\alpha_2$ ) content is then given by:

$$\alpha_{1,out}(t) = \alpha_{1,in}(t - \tau) \quad (6.27)$$

$$\alpha_{2,out}(t) = \alpha_{2,in}(t - \tau) \quad (6.28)$$

in which the average residence time of the solids  $\tau$  is given by:

$$\tau = \frac{M}{\phi_{s,out}} \quad (6.29)$$

The term  $\phi_{s,out}$  is the solids flow from compartment 4 through the orifice to the adsorber and  $M$  is the bed mass of the transport compartment.

The above outlined equations for regenerative desulfurization were implemented in the dynamic model for IFB hydrodynamics in the flowsheeting program Speedup. The simulations and results are presented in chapter 6.2.

### 6.2 Dynamic simulations

The dynamic simulations were specifically suited to the IFB pilot plant reactor (with respect to the IFB sizes) as presented in chapter 4 of this thesis. The regenerative desulfurization experimental results that were obtained and modelling considerations are presented in chapter 5. Experiments were carried out by means of adding  $\text{SO}_2$  and  $\text{O}_2$  in relevant concentrations (respectively 0.1 to 0.2 and 4 v%) to the sulfur capture compartment. The gas phase concentrations and gas velocities to the IFB compartments that were experimentally applied served as the standard conditions in the dynamic simulations.

The high-temperature experiment described in chapter 5.5.2 was carried out at adsorption and regeneration temperatures of 850 and 795 °C, respectively. The results showed that the



sorbent was approximately fully regenerated to CaO and the amount of CaS formed during regeneration was negligible. As a consequence, the reaction rate constant  $k_4$  (Equation 6.15) was set at a value of zero during the simulations.

The values of the hydrodynamic model parameters are similar to the ones used in the calculations described in chapter 3. The standard conditions and model parameters concerning the regenerative desulfurization are given in Table 6.1 (see also chapter 5.3.1).

**Table 6.1** Standard conditions in the IFB reactor and model parameters concerning the regenerative desulfurization process.

Compartment	<b>1</b>	<b>2</b>	<b>3</b>	<b>4</b>	
Gas velocity	1.4 [m/s]	1.0 [m/s]	1.4 [m/s]	0.9 [m/s]	
Conditions and properties	<b>T</b> 850 [°C]	<b>P</b> 1.05 [bar]	<b>C</b> <sub>SO<sub>2</sub>, inlet</sub> 0.2 [v%]	<b>M</b> <sub>IFB</sub> 7.5 [kg]	<b>U</b> <sub>mf</sub> 1.0 [m/s]
Model parameters	<b>k</b> <sub>s</sub> 0.149 [m/s]	<b>K</b> <sub>Eq</sub> 0.614 [-]	<b>D</b> <sub>SO<sub>2</sub>, film</sub> 1.34·10 <sup>-4</sup> [m <sup>2</sup> /s]	<b>D</b> <sub>SO<sub>2</sub>, shell</sub> 7.53·10 <sup>-7</sup> [m <sup>3</sup> <sub>gas</sub> /m <sup>2</sup> <sub>shell</sub> /s]	<b>k</b> <sub>SO<sub>2</sub>, film</sub> 1.0 [m/s]

In order to study the dynamic behaviour of the IFB reactor system, step-changes were made on the IFB parameters that can be varied during operation. The dynamic response of the IFB system and in particular, the response on sulfur capture was studied. The latter should reveal what control action is needed to maintain a certain sulfur retention at variable conditions in the IFB reactor.

### 6.2.1 Step-changes on the operating parameters

Step-changes were made on the following operating parameters:

- ▶ gas velocity to compartment 4 :  $U_4$  0.8 → **0.9** [m/s]
- ▶ total IFB bed mass :  $M_{bed}$  **7.5** → 7.75 [kg]
- ▶ inlet gas phase SO<sub>2</sub> concentration :  $C_{SO_2}$  **0.2** → 0.1 [v%]

In Table 6.2, the steady-state situations before and after the simulated step-changes are summarized.

The standard conditions with respect to the operating parameters are indicated in **bold**. Other important parameters are the gas velocities to compartments 2 (1 m/s), 1 and 3 (1.4 m/s). The low conversions of the sorbent in compartment 1 (the adsorber) and the high sulfur retention correspond to the experimental results obtained in the IFB pilot plant facility (see chapter 5.3.1). For the low conversions of the sorbent it is shown in chapter 6.3 that the neglect of the particle residence time distribution is acceptable, since its influence at the low sorbent conversion is very small.

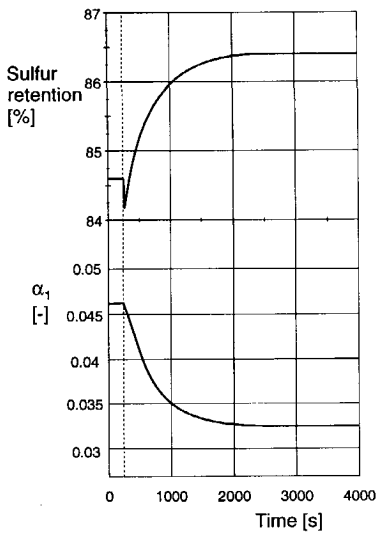
## Chapter 6

**Table 6.2** Simulation results for regenerative desulfurization in the IFB pilot plant reactor. Influence of the operational parameters  $U_4$ ,  $M_{IFB}$  and  $C_{SO_2}$  on hydrodynamics and chemistry in the IFB reactor system.

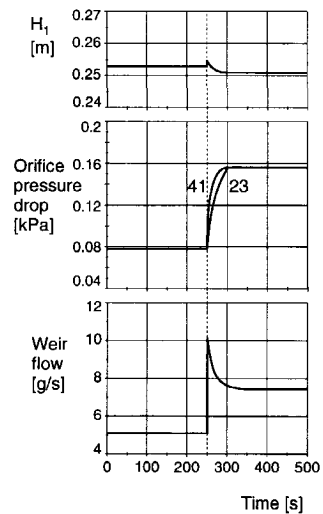
	$U_4$ 0.8 → 0.9 [m/s]	$M_{IFB}$ 7.5 → 7.75 [kg]	$C_{SO_2}$ 0.2 → 0.1 [v%]
<b>hydrodynamics</b>			
$M_1$ [kg]	3.25 3.20	3.20 3.40	3.20 3.20
CRS [g/s]	5.1 7.5	7.5 5.7	7.5 7.5
$\tau_1$ [s]	641 428	428 591	428 428
<b>chemistry</b>			
$\alpha_1$ [-]	0.05 0.03	0.03 0.05	0.03 0.02
Retention [%]	84.6 86.4	86.4 85.8	86.4 89.0

### Gas velocity to compartment 4

In Table 6.2, it can be seen that increasing the gas velocity to compartment 4 from 0.8 to 0.9 m/s results in an increase of the CRS. This leads to a decreasing average sorbent conversion (no regeneration limitations) and an increased sulfur retention.



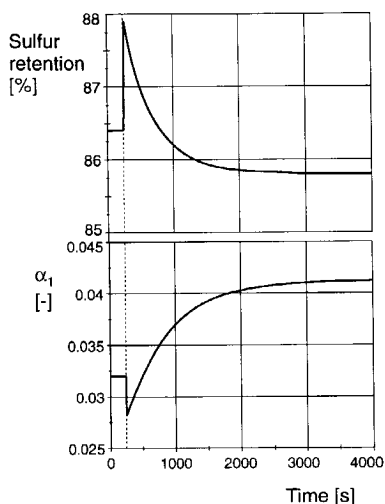
**Figure 6.1** Sulfur retention and sorbent conversion in the adsorption compartment of the IFB reactor. A step-change is made on the gas velocity to compartment 4 at  $t=250$  s from 0.8 to 0.9 m/s as indicated in Table 6.1.



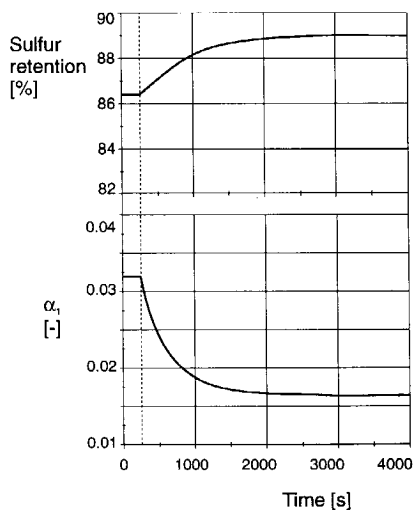
**Figure 6.2** A step-change is made on the gas velocity to compartment 4 at  $t=250$  s as indicated in Table 6.1. The dynamic response of the following hydrodynamic parameters is plotted: the solids hold-up in compartment 1, the weir flow from compartment 1 to 2 and the pressure drop as a driving force for orifice flow through the two connecting orifices (4→1 and 2→3).

In Figure 6.1, the dynamic response to the step-change in gas velocity at  $t=250$  s is shown. It is observed that the sulfur retention shows an inverse response. It first decreases and then increases to its new steady-state value. This type of response is caused by the hydrodynamics of the IFB system (see Figure 6.2). When the gas velocity to compartment 4 is suddenly increased, the driving force for solids and gas flow increases accordingly. The increased gas flow will cause a small but abrupt increase in gas velocity in compartment 1, resulting in an increase in weir flow to compartment 2. Consequently, the bed mass in compartment 1 will temporarily be smaller. The sulfur retention will thus be lower as long as the hydrodynamics of the IFB system have not reached the new steady-state.

After approximately 50 seconds, the hydrodynamics have reached the new steady-state and then the sulfur retention starts to increase and reaches its new steady-state value. The time required to reach this steady-state is 2500 seconds which is approximately equal to five times the average solids residence time in compartment 1. This is in agreement with the RTD distribution of an ideally mixed vessel in which more than 99% of the solids that were present at the time of the step-change has been replaced after five times the average solids residence time.



**Figure 6.3** Sulfur retention and sorbent conversion in the adsorption compartment of the IFB reactor. Between  $t=250$  and  $t=275$  s, 0.25 kg of sorbent material is added to compartment 4 of the IFB system.



**Figure 6.4** Sulfur retention and sorbent conversion in the adsorption compartment of the IFB reactor. At  $t=250$  s, a step-change is made on the inlet  $\text{SO}_2$  gas phase concentration as indicated in Table 6.1.

### Total IFB bed mass

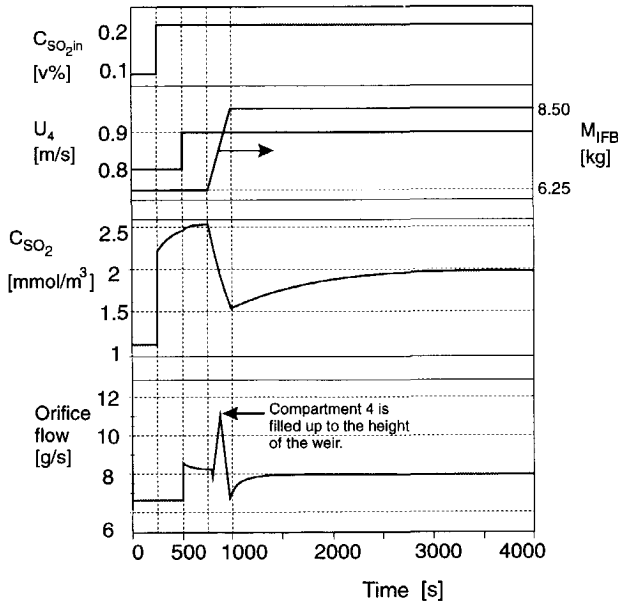
After an increase in IFB bed mass as indicated in Table 6.2, it could be expected that the sulfur retention increases caused by the extra sorbent material available for sulfur retention. This is however in this situation not true. Due to the increased bed mass the overall driving force for solids circulation decreases as explained in chapter 3.2.2. The decreased CRS will cause an effectively smaller sulfur retention.

Again an inverse response is observed (see Figure 6.3) for the average conversion and the sulfur retention. This is also caused by the IFB hydrodynamics. The solids that are added to compartment 4 are distributed over the IFB compartments. When this process is finished after approximately 100 seconds, the sorbent conversion and sulfur retention start to proceed to their steady-state values.

**Inlet gas phase SO<sub>2</sub> concentration**

The effect of a step-change of the inlet gas phase SO<sub>2</sub> concentration from 0.2 to 0.1 v% on the average sorbent conversion and sulfur retention is shown in Figure 6.4. The hydrodynamics of the IFB system are obviously not affected by this operational parameter. The average sorbent conversion decreases and consequently the sulfur retention increases as the inlet SO<sub>2</sub> concentration is lowered. No inverse response or other complicating features are observed. A new steady-state is reached for sulfur retention and sorbent conversion after approximately five times the average solids residence time in compartment 1 ( $\tau_1$ ).

**6.2.2 Controlling the sulfur retention in an IFB reactor**



**Figure 6.5** At  $t=250$  s the inlet gas phase SO<sub>2</sub> concentration is increased from 0.1 to 0.2 v%. By means of adjusting the IFB hydrodynamics, the increased outlet gas phase concentration of the adsorber is controlled to a lower level. At  $t=500$  s, the gas velocity to compartment 4 ( $U_4$ ) is increased from 0.8 to 0.9 m/s. The total IFB bed mass is increased between 750 and 925 s from 6.25 to 8.5 kg. The outlet and inlet SO<sub>2</sub> concentrations, the orifice flow through orifice 4-1, the total IFB bed mass and the gas velocity to bed 4 are plotted as a function of time. The solids flow through orifice 4-1 is increasing when the IFB bed mass is increased until compartment 4 is filled up to the height of the weir. Extra solids added to the IFB reactor cause a decrease in the driving force for solids flow because of the increasing bed mass of compartment 1.

The sulfur capture performance of the IFB reactor depends on the hydrodynamics of the IFB system. The effects on sulfur retention of the indicated step-changes on the gas velocity to compartment 4 and on the total IFB bed mass are shown in Table 6.2. The change of the operational parameters affects the solids hold-up in the adsorber ( $M_s$ ) and the Circulation Rate of the Solids (CRS), thus explaining the shifts in sulfur retention. The operational parameters mentioned above ( $U_4$  and  $M_{IFB}$ ) can therefore be used to control the sulfur retention of the IFB system.

When the supply of sulfur dioxide to the adsorber (representing an increase in sulfur content of the coal that is used in fluidized bed combustion) increases, a certain  $\text{SO}_2$  off-gas concentration needs to be maintained, generally due to environmental regulations. By means of the dynamic IFB model described in this chapter it is possible to determine what control actions are required to keep the  $\text{SO}_2$  off-gas concentration at an obligatory level.

An illustration of this is given in Figure 6.5. At  $t=250$  s, the inlet gas phase  $\text{SO}_2$  concentration is increased from 0.1 to 0.2 v%. In practice this would correspond to a sudden change of coal feed that contains twice the amount of sulfur compared to the previously used coal. It is observed that the  $\text{SO}_2$  off-gas concentration rapidly increases from 1.1 to 2.5  $\text{mmol/m}^3$ . When the maximum permissible off-gas concentration would be 2  $\text{mmol/m}^3$ , a control action is required to reduce the off-gas concentration.

At  $t=500$  s (see Figure 6.5), the gas velocity to compartment 4 ( $U_4$ ) is therefore changed step-wise from 0.8 to 0.9 m/s. This results in a decrease of the  $\text{SO}_2$  off-gas concentration due to an increased CRS and a decreased average solids residence time in the adsorber ( $\tau_1$ ) (see Table 6.2). A further decrease of the  $\text{SO}_2$  off-gas concentration is achieved when the total IFB bed mass ( $M_{IFB}$ ) is increased from 6.25 to 8.50 kg starting at  $t=750$  s until  $t=975$  s (see Figure 6.5) at a solids flow rate of 0.01 kg/s to compartment 1. In practice, the IFB bed mass can be increased by using a solids feeding device connected to a hopper. At  $t=3000$  s, the new steady-state is reached at an  $\text{SO}_2$  off-gas concentration that is below the required value of 2.0  $\text{mmol/m}^3$ .

It is thus shown that by means of adjusting the hydrodynamic operational parameters:

- ▶  $U_4$ , the gas velocity to compartment 4, and
- ▶  $M_{IFB}$ , the total IFB bed mass,

the sulfur capture performance of the IFB facility can be adequately controlled.

### 6.3 Particle residence time distribution

#### 6.3.1 The influence of particle RTD on the average conversion in a fluidized bed reactor

In a fluidized bed reactor (or reactive compartment of an IFB system), the particles need to be considered as segregated objects. This means that each particle will have its specific conversion. The distribution of conversions of the particles is determined by the Residence Time Distribution (RTD) of the particles in the reactor. The use of the RTD concept as developed by Danckwerts (1953) has found wide application in chemical reaction engineering. It is mainly used for modelling non-ideal flow in continuous flow systems.

The RTD is determined by the fluid dynamics of the reactor (the degree of mixing). Experimental investigations of particle RTD in a multi-compartment or Interconnected Fluidized Bed system were carried out by Pajongwit and Jovanovic (1994) and Stellema *et al.* (1996). It was confirmed by these authors that the solids in a fluidized bed in general can be considered as ideally mixed. The degree of mixing depends however on the average residence time of the particles compared to the mixing time in the fluidized bed. The dense beds in an IFB system showed plug flow behaviour including dead or stagnant zones consisting of particles that do not participate in solids circulation (Stellema *et al.*, 1996). This behaviour is caused by the fact that the dense beds are operated *at or below* the conditions of minimum fluidization. The degree of mixing under these conditions is very small. The size of the dead regions in the dense beds appeared to be a function of the aeration rate. It decreases with increasing aeration rate. At the conditions of minimum fluidization, the size of the dead regions is reduced to a negligible size (Stellema *et al.*, 1994).

The penetration of particles in a fluidized bed reactor from a solids feeding line can seriously affect the flow pattern in the bed and subsequently the RTD of the solids. This is especially the case for high velocity pneumatic transport systems. Brinkert (1993) and Brinkert and Davidson (1993) investigated the penetration of jets formed by the entering particles into fluidized beds. It was found that for high velocity jets the penetration can cause serious short circuiting that will affect the performance of the reactor. The penetration effect should therefore be considered in the design of a fluidized bed reactor.

An extension of the RTD concept was presented by Villiermaux (1996) who developed the Trajectory Length Distribution (TLD) concept. This represents the distribution of distances covered by fluid elements (or particles) in the system. It provides a characterization of the flow field allowing discrimination between different flow patterns. A macromixing index is defined by comparing the mean trajectory length to a characteristic dimension of the vessel. This approach can provide useful information on flow patterns in a specific chemical reactor. The RTD concept will in practice however be sufficient to characterize the fluid dynamics of fluidized bed reactors in order to determine the average conversion.

See Figure 6.6 for a schematical representation of residence time distribution in a fluidized bed reactor. For steady-state operation of a fluidized bed reactor, the particle conversion can be calculated on the basis of the particle RTD according to:

$$\alpha_{RTD} = \int_0^{\infty} E(t) \alpha(t) dt \tag{6.30}$$

The term  $\alpha(t)$  represents the batch conversion equation depending on the kinetics of the reactions taking place.  $E(t)$  represents the residence time distribution function for a given fluidized bed reactor. For a Continuously Stirred Tank Reactor (CSTR), the  $E(t)$  function is given by:

$$E(t) = \frac{1}{\tau} \exp\left(-\frac{t}{\tau}\right) \tag{6.31}$$

The parameter  $\tau$  represents the average residence time of the particles in the bed and corresponds to the first moment of the RTD function (Equation 6.31). It is calculated according to:

$$\tau = \frac{M_{bed}}{\phi_m} \quad (6.32)$$

with  $M_{bed}$  and  $\phi_m$  representing the bed mass and the mass flow rate of the particles respectively.

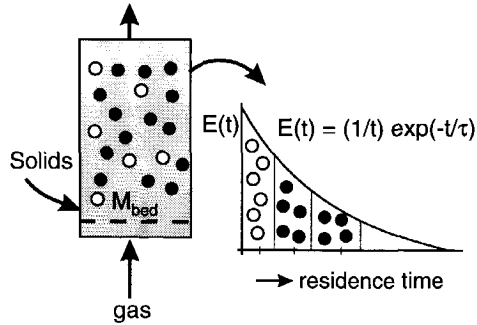
If the fluidized bed is considered as a CSTR (gas and solids phases are ideally mixed), the average conversion of the solids phase and the gas phase conversion can thus be calculated from Equations 6.30 to 6.32.

The conversion distribution caused by the particle RTD in the reactor results in an overall reactivity (towards the gas phase) of the bed material. The overall reactivity finally determines the average conversion in the gas phase and with this the performance of the reactor. The order of reaction of the gas-solids reactions taking place in the reactor determines the influence of conversion distribution. For first order reactions there is no influence and the reactivity of the particles can be characterized by the *average* conversion in the reactor (*i.e.*, the conversion at the average residence time). For non-first order reactions, the conversion distribution needs to be considered and will influence the performance of the reactor. The extent of the influence is determined by the kinetics (*viz.*, deviation from first order) and the average conversion of the particles (for very small conversions, the influence is negligible).

Heesink *et al.* (1994) evaluated the effect of particle RTD on the average conversion rate (or reactivity) of particles undergoing a non-catalytic gas-solid reaction in a continuously and stationary operated fluidized bed reactor. A so-called  $\beta$ -factor was defined representing the ratio of the actual reactivity in the reactor and the reactivity of a batch of particles that react under similar circumstances and that all have a conversion that is equal to the average conversion in the reactor.

A factor that directly relates the conversions calculated with ( $\alpha_{RTD}$ ) and without ( $\alpha_{NRTD}$ ) taking into account residence time distribution is believed to give more insight in the effect of RTD on the average conversion and was therefore introduced in this study. This factor ( $\beta''$ ) is thus defined as:

$$\beta'' = \frac{\alpha_{RTD}}{\alpha_{NRTD}} \quad (6.33)$$



**Figure 6.6** Schematic representation of the residence time distribution in an ideally mixed fluidized bed reactor. Each of the particles has its specific residence time in the reactor. The distribution of residence times is given by the distribution function  $E(t)$ .

## Chapter 6

The term  $\alpha_{RTD}$  can in general be calculated according to Equation 6.30. The conversion equation  $\alpha(t)$  for  $n$ -th order reaction is obtained from:

$$\frac{d\alpha}{dt} = k_r (1 - \alpha)^n \quad (6.34)$$

in which  $k_r$  is the reaction rate constant.

However, for reaction order smaller than one ( $n < 1$ ), the maximum conversion (one in this study) is reached at time  $T_{max}$  (for which:  $0 < T_{max} < \infty$ ). For reaction orders larger than one, the maximum conversion cannot be reached before infinite time. As a consequence,  $\alpha_{RTD}$  can be calculated by means of Equation 6.30 for  $n > 1$ . For  $n < 1$ ,  $\alpha_{RTD}$  is calculated according to:

$$\alpha_{RTD} = \int_0^{T_{max}} \alpha(t) E(t) dt + \int_{T_{max}}^{\infty} \alpha_{max} E(t) dt \quad (6.35)$$

in which  $E(t)$  is the residence time distribution function as defined for an ideally mixed vessel by Equation 6.31. For zero- and  $1/2$ -order reactions,  $T_{max}$  equals  $(1/k_r)$  and  $(2/k_r)$  respectively. From the molar balance for an ideally mixed reactor, the following equation can be derived by neglecting the influence of RTD for the conversion (and  $\alpha_{in} = 0$ ):

$$k_r (1 - \alpha_{NRTD})^n = \frac{\alpha_{NRTD}}{\tau} \quad (6.36)$$

In Table 6.3, the equations are presented that were obtained from the application of Equations 6.30, 6.35 and 6.36 for the indicated order of reaction to calculate  $\alpha_{RTD}$  and  $\alpha_{NRTD}$ .

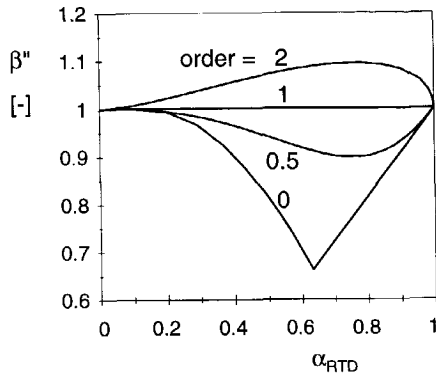
**Table 6.3** Summary of the equations to calculate  $\alpha_{RTD}$  and  $\alpha_{NRTD}$  for reaction order 0,  $1/2$ , 1 and 2. The residence time distribution function  $E(t)$  is defined by Equation 6.30.

Reaction order	$\alpha_{RTD}$	$\alpha_{NRTD}$
0	$\int_0^{1/k_r} E(t) k_r t dt + \int_{1/k_r}^{\infty} E(t) dt$	$k_r \tau$ for $k_r \tau < 1$ and 1 for $k_r \tau > 1$
$1/2$	$\int_0^{2/k_r} E(t) \left( k_r t - \frac{1}{4} k_r^2 t^2 \right) dt + \int_{2/k_r}^{\infty} E(t) dt$	$-1/2 \left( k_r^2 \tau^2 - \sqrt{k_r^4 \tau^4 + 4 k_r^2 \tau^2} \right)$ for $k_r \tau < 2$ and 1 for $k_r \tau > 2$
1	$\int_0^{\infty} E(t) (1 - \exp(-k_r t)) dt$	$\frac{k_r \tau}{k_r \tau + 1}$
2	$\int_0^{\infty} E(t) \left( \frac{k_r t}{k_r t + 1} \right) dt$	$\frac{2k_r \tau + 1 - \sqrt{4k_r \tau + 1}}{2k_r \tau}$



In Figure 6.7, the results of the calculations based on the equations given in Table 6.3 for  $\alpha_{RTD}$  and  $\alpha_{NRTD}$  are shown by plotting  $\beta^n$  as a function of the true conversion in the reactor ( $\alpha_{RTD}$ ). For *first* order reactions, no influence of RTD is observed. For *second* order reaction, a positive influence is found. This means that the true conversion in the reactor is higher than the conversion that is calculated when the RTD influence is neglected. The opposite effect is found for *zero* and  $\frac{1}{2}$  order reactions. These results are in agreement with the general conclusions given by Westerterp *et al.* (1984).

The influence of particle-RTD in case of shrinking core limitation, product-layer diffusion, and grain reaction limitation was elaborated by Heesink *et al.* (1994). Depending on the diffusion phenomena and kinetics of the gas-solid reactions taking place, the average reactivity of the particles in a fluidized bed reactor is affected. It was shown that in case of shrinking core reaction limitation, the apparent order of reaction corresponds to  $n$ th order of reaction,  $n$  being  $2/3$ . The negative RTD effect with respect to conversion for this type of reaction can be roughly evaluated from Figure 6.7. For product layer diffusion it was found that the RTD influence was positive. A higher conversion is thus found in reality compared to the calculated conversion where no RTD effects are taken into account. This positive influence was found for conversions up to 0.7.



**Figure 6.7** The  $\beta^n$ -factor plotted as a function of the average conversion in a chemical reactor for the indicated orders of reaction.

In case of stationary operated fluidized bed reactors, a  $\beta$ -factor approach (as proposed by Heesink *et al.* (1994)) can be applied to determine the effect of particle-RTD on the average conversion in a fluidized bed reactor. For non steady-state operation of a fluidized bed reactor, the situation becomes more complicated as explained and outlined in chapter 6.3.2.

### 6.3.2 Dynamic RTD in the IFB reactor

For non steady-state operation of a fluidized bed reactor the influence of RTD on fluidized bed reactor performance is more complicated mainly because the characteristic RTD function changes in time. When a step-change is made on one of the operational parameters in the IFB reactor system, the actual RTD function also changes. The result is that particles which are present in the reactor before the step-change, will experience a new RTD function while their conversion is also a function of their *history* in the reactor.

Another effect occurs when a step-change is made in the inlet gas phase concentration. The particles that are present in the reactor experience a new gas phase concentration while their conversion is also a function of the former gas phase concentration and thus also depends on the *history* of the process.

To account for the *history* effects of both particle RTD and gas phase dynamics of the process (variable average gas phase concentration in the reactor), a modelling approach needs to be considered that includes these effects.

**Population balance modelling**

The common way of modelling dynamically operated chemical reactors is the application of a population balance. This balance accounts for the transient behaviour of a distribution of a conversion (or for example crystal size or age). In this way the conversion distribution can be calculated as a function of time.

Himmelblau and Bischoff (1986) derive on the basis of a microscopic population balance, a macroscopic population balance model by means of integration over the geometric volume  $V$  which is constant in time. Application of this macroscopic model for the conversion of sorbent particles ( $\alpha$ ) in a fluidized bed reactor results in:

$$\frac{\partial \Psi}{\partial t} + \frac{\partial}{\partial \alpha} \left( \frac{\partial \alpha}{\partial t} \Psi \right) = \frac{1}{V} (\phi_{v,in} \Psi_{in} - \phi_{v,out} \Psi_{out}) \tag{6.37}$$

The term  $\psi$  represents the distribution (or density) of conversion as a function of time [ $\psi = \psi(\alpha, t)$ ]. The above equation can be modified to:

$$\frac{\partial \Psi}{\partial t} + \Psi \frac{\partial}{\partial t} \left( \frac{\partial \alpha}{\partial t} \right) + \frac{\partial \alpha}{\partial t} \frac{\partial \Psi}{\partial \alpha} = \frac{1}{V} (\phi_{v,in} \Psi_{in} - \phi_{v,out} \Psi_{out}) \tag{6.38}$$

This partial differential equation describes the distribution function  $\psi$  as a function of time and conversion. In general such a type of equation is solved by discretizing the term  $(\partial \psi / \partial \alpha)$  into a finite number of conversion classes. The remaining differential equation in time can then be solved for each class. In this way, the distribution function  $\psi$  is calculated as a function of time. Some recent examples of the application of population balances for chemical reactors are presented by Rubisov and Papangelakis (1996) and Zacca *et al.* (1996).

Modelling by means of population balances becomes increasingly complicated for non-ideal residence time distribution functions. So-called multi-compartment models are usually applied in that case (Kiparissides, 1996). The compartments are ideally mixed and linked by means of interconnecting material flows. For each compartment, the whole set of population balance equations needs to be solved.

**Dynamic Residence Time Distribution function**

The application of Residence Time Distribution (RTD) theory to calculate the chemical conversion in a reactor consisting of segregated objects is well-known. Nauman (1969) extended the classical analysis to unsteady stirred tank reactors. This is of interest in modelling the conversion of the sorbent in the IFB reactor when operated under dynamic conditions.

The derivation of a general dynamic RTD function according to Nauman (1969) starts at time  $t-t'$  at which the inlet concentration of an ideally mixed reactor changes from  $C=0$  to  $C=C_0$ . The inlet concentration for times larger than  $t-t'$  equals  $C_0$ . The molar balance in that case

can be written as:

$$\phi_{v,i} C_0 - \phi_{v,out} C = \frac{d(VC)}{dt} \quad (6.39)$$

in which (mass balance when density is constant):

$$\frac{dV}{dt} = \phi_{v,i} - \phi_{v,out} \quad (6.40)$$

Equation (6.39) can then be rewritten as:

$$V \frac{dC}{dt} = \phi_{v,i} (C_0 - C) \quad (6.41)$$

In this equation the inlet flow ( $\phi_{v,i}$ ) and reactor volume ( $V$ ) are a function of time. Integration therefore yields:

$$1 - \frac{C}{C_0} = \exp \left( \int_{t-t'}^t \frac{-\phi_{v,i}}{V} dt \right) = F(t, t') \quad (6.42)$$

It can be seen that  $(1-C/C_0)$  is the fraction of material in the exit stream at time  $t$  which has remained in the reactor for a duration greater than  $t'$ . It represents the dynamic response function of a step-change at the inlet of the reactor. This is often referred to as the  $F$ -function which is typical for a specific RTD of a reactor. The dynamic RTD (or  $E$ -function) can be obtained from the  $F$ -function:

$$E(t, t') = \frac{-dF(t, t')}{dt'} \quad (6.43)$$

The result is:

$$E(t, t') = \frac{\phi_{v,i}(t-t')}{V(t-t')} \exp \left( \int_{t-t'}^t \frac{-\phi_{v,i}}{V} dt \right) \quad (6.44)$$

$E(t, t')$  represents the RTD frequency function. The above given analysis is similar to the classical analysis of steady-state systems. In unsteady operation, any RTD can be achieved for material exiting at time  $t$ . If the tank reactor is segregated however, the system will remain segregated regardless of the unsteady operation. To find an expression for the conversion at time  $t$  for the unsteady tank reactor, the dynamic RTD function can be used to characterize the reactor.

When a portion of fluid enters the reactor at time  $t-t'$  this will remain intact and can be treated as a small batch reactor. The conversion of this batch reactor depends on the inlet concentration at time  $t-t'$  ( $= C_i(t-t')$ ) and the residence time  $t'$  in the reactor. For a first order reaction this gives:

$$B(C_i(t-t'), t') = C_i(t-t') \exp(-kt') \quad (6.45)$$

in which  $B$  is the batch conversion that is a function of  $t-t'$  (time at which the fluid is entering the reactor) and  $t'$  (the residence time in the reactor).

The average exit concentration at time  $t$  is found by integrating over all possible  $t'$ :

$$C(t) = \int_0^{\infty} B(C_i(t-t'), t') E(t, t') dt' \quad (6.46)$$

For the case  $C_i$  is constant, this is the standard result for segregated reactors with RTD frequency function  $E(t, t')$ . It represents a generalization of the classical result.

### 6.3.3 The dynamic E(t) model

Recent applications of a dynamic RTD approach are presented by Zenger (1995) and Fernández-Sempere *et al.* (1995). These applications however do only concern the physical RTD of tracers in order to characterize a non steady-state flow system.

To apply the dynamic RTD approach to fluidized bed reactors it is thus necessary to extend the concept of Nauman (1969) who used a dynamic RTD approach to calculate the conversion of a dynamically operated stirred tank reactor. This is possible because these concepts do also apply for fluidized bed reactors in which the particles undergo a certain type of reaction. The particles can be considered as segregated objects.

In this study, the dynamic E(t) model was developed that is based on the dynamic RTD approach. This model takes into account the non-stationary as well as the steady-state effects of RTD in the fluidized bed chemical reactive compartments of the IFB reactor (*viz.*, the adsorber and regenerator for sulfur capture and sorbent regeneration, respectively). A detailed outline of the model that was implemented in the dynamic flowsheeting program Speedup (1993) is given in appendix 6.A.

The following equation (similar to Equation 6.46) is used to calculate the average sorbent conversion taking into account the effects of non-stationary residence time distribution:

$$\alpha_{RTD} = \int_0^{\infty} E(t, t') \alpha(t') dt' \quad (6.47)$$

The dynamic residence time distribution function  $E(t, t')$  is given by:

$$E(t, t') = \frac{\phi_{s,in}(t-t')}{M_{bed}(t-t')} \exp\left(-\int_{t-t'}^t \frac{\phi_{s,in}}{M_{bed}} dt\right) \quad (6.48)$$

in which  $\phi_{s,in}$  and  $M_{bed}$  are the inlet solids flow and the bed mass of the adsorber respectively. The batch conversion equation  $\alpha(t')$  was derived from the sorbent sulfation model according to the SURE2 kinetics. The batch conversion equations for the regenerator were derived on the basis of the regeneration model presented in chapter 6.1. The equations that were used in modelling the sulfur capture and sorbent regeneration are outlined in appendix 6.A.

The gas phase is modelled as ideally mixed. The concentration of the gaseous reactants surrounding the particle may vary due to the chemical reaction (in the vicinity of a sorbent

particle) or mixing characteristics of the fluidized bed. In the present study such variation is neglected. The gas phase concentration is assumed to be homogeneous throughout the bed and equal to the surface concentration of the sorbent particles. This assumption is allowed if the following conditions are satisfied:

$$\tau_{conv} \gg \tau_{mix}, \quad \tau \gg \tau_{mix} \quad (6.49)$$

in which  $\tau_{conv}$  is the time needed for complete conversion of a sorbent particle and  $\tau_{mix}$  is the time needed for complete mixing of the particles. The average residence time of the particles is represented as  $\tau$ . The above mentioned conditions are well satisfied for the reactions taking place in the IFB reactor (see chapter 5.3.1).

A complicating feature of reaction-regenerator systems in which the particles react according to a shrinking core model is identified by Levenspiel (1993). Due to the residence time distributions in the reactor and regenerator in combination with a shrinking core reaction, the particles will have a varying number of concentric rings of converted and non-converted material. In the case of regenerative desulfurization, this means rings of sulfated and non-sulfated sorbent material. In the present study these effects are not considered. This is allowed since the simulations were carried out for situations of complete regeneration. For this reason, no inlet conversion distributions have to be taken into account.

The dynamic E(t) model was used for the calculation of the sulfur retention and sorbent conversion in the IFB reactor that is operated at non steady-state conditions. A detailed description of the dynamic E(t) model is given by Rijk (1997) and is further outlined in appendix 6.A.

### 6.3.4 Results of dynamic E(t) model simulations

In the simulations, the sorbent is treated as fully regenerated in agreement with the high temperature experiment described in chapter 5.5.2. Besides the calculation of  $\alpha_{RTD}$  (according to Equation 6.47),  $\alpha_{NRTD}$  was calculated as well (as outlined in chapter 6.1). The effects of particle RTD on the average conversion are represented by the  $\beta''$  factor (according to Equation 6.33).

Two sets of hydrodynamic conditions were concerned which can be characterized by the difference in the average residence times in the IFB compartments (see Table 6.1). In the first situation, the gas velocity to compartment 4 ( $U_4$ ) is 0.9 m/s, the solids discharge coefficient ( $C_D$ ) is 0.2, and the inlet SO<sub>2</sub> concentration is 0.1 v%. This results in a relatively high CRS and small average residence times in the IFB compartments (Small Residence Times, *SRT*) (see Table 6.4). For the second situation, in which  $U_4$  is set at 0.8 m/s and  $C_D$  is 0.01, a Large average Residence Time (*LRT*) is obtained in the IFB compartments (see Table 6.4). The small value of the solids discharge coefficient was used in the simulations. In practice this would correspond to a lower value of  $U_4$  resulting in the same CRS. The inlet gas phase SO<sub>2</sub> concentration is also 0.1 v%.

**Table 6.4** Hydrodynamic conditions in the IFB reactor for two situations. The resulting average residence times characterize different situations: Small Residence Times (*SRT*) and Large Residence Times (*LRT*).

Compartment		1	2	3	4	CRS
		Adsorber		Regenerator		[g/s]
<b>SRT</b>	U [m/s]	1.4	1.0	1.4	0.9	7.5
	$\tau$ [s]	428	245	84	247	
<b>LRT</b>	U [m/s]	1.4	1.0	1.4	0.8	0.3
	$\tau$ [s]	10500	6070	2170	6130	

**Steady-state simulations**

For both situations given in Table 6.4, the effects of particle RTD were investigated. For the steady-state simulations (see Table 6.5) the reaction rate constant  $k_s$  was varied in order to verify the influence of the sulfation kinetics on the RTD effects on the average sorbent conversion. The standard value for  $k_s$  (see Table 6.1) is lowered by a factor 10 (corresponding to a temperature decrease of 200 °C, see Table 5.7) and increased with a similar factor (corresponding to a temperature increase of 300 °C).

**Table 6.5** Steady-state sorbent conversions ( $\alpha_{RTD}$  and  $\alpha_{NRTD}$ ) for the indicated situations in the IFB reactor in Table 6.4 at different values for the sulfation rate constant ( $k_s$ ).

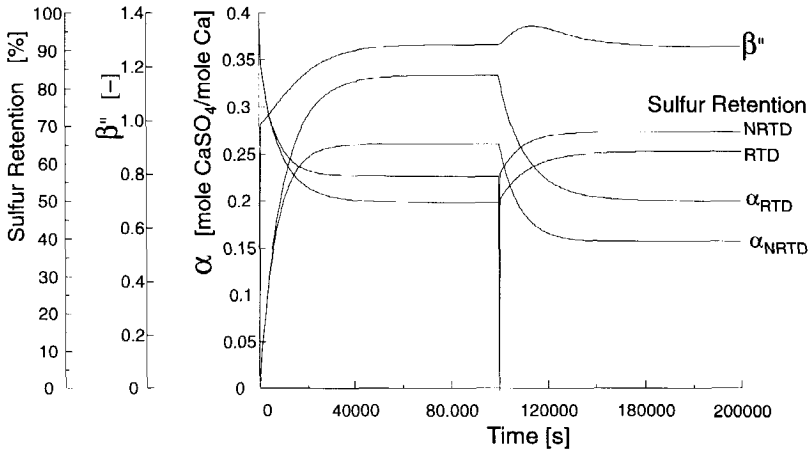
		Situation 1: SRT		Situation 2: LRT	
$k_s = 0.149$ [m/s]	$\alpha_{NRTD}$	0.0165	$\beta'' = 1.045$	0.261	$\beta'' = 1.281$
	$\alpha_{RTD}$	0.0173		0.334	
$k_s = 0.0149$ [m/s]	$\alpha_{NRTD}$	0.00994	$\beta'' = 0.996$	0.190	$\beta'' = 1.058$
	$\alpha_{RTD}$	0.00990		0.201	
$k_s = 1.49$ [m/s]	$\alpha_{NRTD}$	0.0177	$\beta'' = 1.310$	0.270	$\beta'' = 1.338$
	$\alpha_{RTD}$	0.0232		0.361	

The results in Table 6.5 show that the conversions are, as expected, higher for the *LRT* situation than for the *SRT* situation. The influence of particle RTD on sorbent conversion is more significant ( $\beta''_{LRT} > \beta''_{SRT}$ ) for the *LRT* situation than for the *SRT* situation. This is in agreement with the results in Figure 6.7. For higher conversions (up to a maximum value that is depending on the specific order of reaction), the values for  $\beta''$  are larger indicating a more significant effect of particle RTD on sorbent conversion.

In Table 6.5, it can further be seen that the values for  $\beta''$  change with changing reaction rate constant ( $k_s$ ). For an increase of the rate constant,  $\beta''$  decreases. The overall rate of sulfation becomes less diffusion-limited and more core-reaction-limited when  $k_s$  increases. For a decreasing  $k_s$ , the diffusion limitation increases and  $\beta''$  increases. These results are in agreement with those of Heesink *et al.* (1994) who found a negative effect for core-reaction limitation and positive effects for product-layer diffusion limitation. Negative and positive effects are here defined as:  $\beta'' < 1$  and  $\beta'' > 1$ , respectively.

### Dynamic simulations

In Figure 6.8, the dynamic response is given of a step-change in the  $\text{SO}_2$  inlet concentration from 0.1 to 0.05 v% at  $t=1 \cdot 10^5$  s. These results were obtained in the *LRT* situation (see Table 6.5). For the *SRT* situation, the results are similar but less significant. The values for  $\alpha_{NRTD}$  and  $\alpha_{RTD}$  are more different for the *LRT* situation than for the *SRT* situation. This is due to the smaller average conversion for which the effects of particle RTD are less significant (see Figure 6.7).



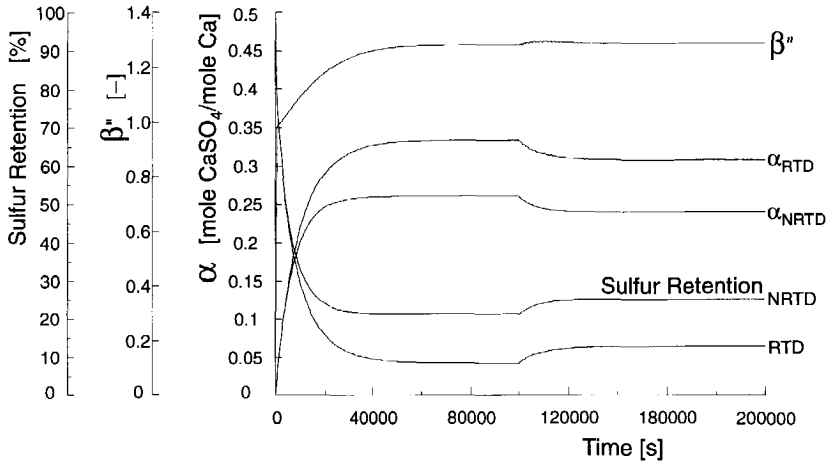
**Figure 6.8** Dynamic simulation for the *LRT* situation (Table 6.5) for a step-change in the  $\text{SO}_2$  inlet concentration from 0.1 to 0.05 v% at  $t=1 \cdot 10^5$  s. The values for  $\alpha_{RTD}$  and  $\alpha_{NRTD}$  as well as the ratio of these two conversions and the sulfur retention for both calculations are plotted as a function of time.

It is observed that the average sorbent conversion decreases for the lower  $\text{SO}_2$  inlet concentration. Subsequently, the sulfur retention increases as expected. This is the case for the results calculated by including RTD as well as for the results obtained by neglecting the effects of RTD. The momentary decrease in sulfur retention is caused by the momentary change of the inlet  $\text{SO}_2$  concentration while the  $\text{SO}_2$  concentration in the bed changes in a time that is proportional to the gas residence time in the bed ( $H_f/U_f=0.3/1.4=0.21$  s).

It can further be recognized that the  $\beta''$ -factor goes through a maximum and then reaches a new steady-state value. This is caused by the fact that directly after the step-change the sorbent particles that are present in the adsorber compartment have a different conversion and thus a different  $\beta''$ -factor compared to the steady-state value. After approximately five times the average residence time of the particles, the steady-state is reached. This is explained by the fact that after this period of time, more than 99% of the particles that were present at the time of the step-change has been replaced from the fluidized bed adsorber.

In Figure 6.9, the dynamic response is shown of a step-change in the gas velocity to compartment 4 from 0.8 to 0.85 m/s at  $t=1 \cdot 10^5$  s. The CRS increases from 0.30 to 0.34 g/s; the average sorbent conversion ( $\alpha_{RTD}$  and  $\alpha_{NRTD}$ ) decreases. Consequently, the sulfur retention increases. The  $\beta''$ -factor characterizing the effects of particle RTD increases from 1.281 to

1.282 for a decrease in  $\alpha_{RTD}$  from 0.3337 to 0.3075. The value of the  $\beta''$ -factor is for both conditions larger than one indicating an apparent order of reaction, larger than one. The small increase of the  $\beta''$ -factor for a decrease in sorbent conversion thus indicates that the sorbent conversion (before and after the step-change) is above the conversion with maximum particle RTD influence (see Figure 6.7).



**Figure 6.9** Dynamic simulation starting at the LRT situation (Table 6.5) for a step-change in the gas velocity to compartment 4 from 0.8 to 0.85 m/s at  $t=1 \cdot 10^5$  s. The CRS increases from 0.30 to 0.34 g/s. The values for  $\alpha_{RTD}$  and  $\alpha_{NRTD}$  as well as the ratio of these two conversions ( $\beta''$ ) and the sulfur retention for both calculations are plotted as a function of time.

## 6.4 Discussion and conclusions

### *Dynamic behaviour of the IFB reactor for regenerative desulfurization*

In chapter 6.2 it is shown that step-changes on the hydrodynamic operating parameters (*viz.*, gas velocity to the CRS determining transport compartment, and total IFB bed mass) can cause inverse responses with respect to the sulfur retention of the IFB system. This information can be used in deciding what control action is required to maintain a prescribed level of desulfurization.

The dynamic response of the IFB hydrodynamics on step-changes of the operational parameters is much faster than the response of the IFB sulfur capture chemistry. This is caused by the fact that the time to reach a new steady-state with respect to the IFB hydrodynamics is proportional to the amount of solids that need to be redistributed over the IFB compartments. It was found that the time needed to reach a new steady-state for the sulfur retention of the process takes approximately five times the average residence time of compartment 1. This is explained from the fact that according to the RTD distribution of an ideally mixed vessel, more than 99% of the solids that were present at the time of the step-change has been replaced after five times the average solids residence time. When it is



assumed that approximately 10% of the IFB bed mass needs to be redistributed to reach a new steady-state and compartment 1 contains 50% of the IFB bed mass, the response of the hydrodynamics is a factor 25 faster than the response of the chemistry in the IFB reactor.

On the basis of the simulation results given in chapter 6.2.2, it can be concluded that by means of adjusting the hydrodynamic operational parameters:

- ▶  $U_4$ , the gas velocity to compartment 4 and
- ▶  $M_{IFB}$ , the total IFB bed mass,

the sulfur capture performance of the IFB facility can be controlled at a required level. The sulfur retention is influenced by the average solids residence time and the bed mass in the desulfurization compartment. These characteristic properties ( $\tau_1$  and  $M_1$ ) can be adjusted by the hydrodynamic operational parameters mentioned.

### *The influence of particle-RTD in dynamically operated fluidized bed reactors*

An alternative approach was presented in addition to population balance modelling for taking into account the effect of particle RTD in a dynamically operated fluidized bed reactor in which a gas-solids reaction occurs: the so-called dynamic RTD approach. This approach, as developed by Nauman (1969), was extended in the present study for the use of modelling non-stationary operated fluidized bed reactors.

A full dynamic approach is presented by the dynamic E(t) model. It enables the modelling of a non-stationary operated fluidized bed reactor taking into account the effects of particle RTD. Furthermore, the *history* effects are taken into account. These effects concern the variable conditions for the particles during their stay in the reactor. The conditions may vary due to changes in the operational parameters (*i.e.*, gas velocities to the IFB compartments, inlet gas phase concentrations).

The modelling results indicate that the dynamic RTD approach can be applied for modelling gas-solids reactions in a dynamically operated IFB reactor. It was found that for the regenerative desulfurization process carried out in the IFB reactor, the effects of particle RTD on the average conversion of the sorbent can be up to 30%. The so-called  $\beta$ "-factor is proposed to characterize the particle RTD effects. This factor represents the ratio of the conversion taking into account the RTD and the conversion when the particle RTD effects are neglected. The values for the  $\beta$ "-factor deviating from *one* indicate that particle RTD should be taken into account for regenerative desulfurization in the IFB reactor. The  $\beta$ "-factor proved to be a useful characterization of the particle RTD effect in fluidized bed reactors and can therefore be used as such.

In practice, reactor vessels are non-ideal with respect to their mixing characteristics. The degree of mixing in a reactor depends in general on the ratio of the power that is added to the reactor to the power that is transferred to kinetic energy. Obviously, this depends on the specific type of reactor vessel, mixing devices, and the fluid properties of the reactor content. Due to non-ideal mixing characteristics, only two possibilities are available for the modelling of reactors that are used for the production of polymers (Kiparissides, 1996). These are: (1) the combination of population balances and multi-compartment models and (2) Computational Fluid Dynamics (CFD) in combination with population balance modelling.

## Chapter 6

The dynamic  $E(t)$  model could be an attractive alternative for the above mentioned possibilities. It offers an advantage due to the flexibility of the model with respect to the RTD distribution function that can be easily adjusted to the specific reactor vessel RTD characteristics. This is in contrast with population balance modelling in which multi-compartment modelling is required. Another advantage of the  $E(t)$  model is the fact that a variable volume of the reactor content is taken into account. This is not possible in the macroscopic population balance model as derived by Himmelblau and Bischoff (1986) (see chapter 6.3.2).

### Notation

B	: batch conversion	[-]
C	: gas phase concentration	[mole/ m <sup>3</sup> ]
C <sub>D</sub>	: solids discharge coefficient	[-]
CRS	: Circulation Rate of Solids	[g/s]
D <sub>SO<sub>2</sub>,film</sub>	: diffusion coefficient of SO <sub>2</sub> in the film	[m <sup>2</sup> /s]
D <sub>SO<sub>2</sub>,shell</sub>	: diffusion coefficient of SO <sub>2</sub> in the shell	[m <sup>2</sup> <sub>shell</sub> /s]
E(t)	: Residence Time Distribution function	[s <sup>-1</sup> ]
f <sub>Ca</sub>	: calcium content (fraction) of the sorbent	[kg Ca/kg sorbent]
ΔG	: Gibbs function of reaction	[J/ mole]
k	: intrinsic reaction rate constant	[m <sup>3</sup> <sub>gas</sub> /m <sup>2</sup> <sub>surface</sub> s]
K <sub>Eq</sub>	: equilibrium constant	[-]
k <sub>s</sub>	: sulfation reaction rate constant	[m <sup>3</sup> <sub>gas</sub> /m <sup>2</sup> <sub>core</sub> s]
k <sub>SO<sub>2</sub>,film</sub>	: SO <sub>2</sub> film mass transport coefficient	[m/s]
M <sub>Ca</sub>	: molar mass of Ca	[kg Ca/ mole Ca]
M <sub>i</sub>	: solids hold-up in IFB compartment i	[kg]
q	: CaO surface concentration	[mole Ca/ m <sup>2</sup> sorbent]
r <sub>α</sub>	: rate of conversion of one sorbent particle	[(mole CaSO <sub>4</sub> /mole Ca)/s]
r <sub>c</sub>	: core radius	[m]
R	: radius of sorbent particle	[m]
T	: temperature	[°C]
T <sub>max</sub>	: time needed to reach maximum conversion	[s]
t	: time	[s]
t'	: residence time	[s]
U	: superficial gas velocity	[m/s]
V	: reactor volume	[m <sup>3</sup> ]
V <sub>g</sub>	: gas volume of the fluidized bed compartment	[m <sup>3</sup> <sub>gas</sub> ]
x	: constant fraction under the E(t) curve in the E(t)-tank model	[-]
<b>Greek</b>		
α	: conversion of CaO in adsorber	[mole CaSO <sub>4</sub> /mole Ca]
α <sub>1</sub>	: mole fraction CaSO <sub>4</sub> in regenerator	[mole CaSO <sub>4</sub> /mole Ca]
α <sub>2</sub>	: mole fraction CaO in regenerator	[mole CaO/mole Ca]

$\alpha_3$	: mole fraction CaS in regenerator	[mole CaS/ mole Ca]
$\alpha_{RTD}$	: average conversion calculated by taking into account RTD	[-]
$\alpha_{NRTD}$	: average conversion calculated without taking into account RTD	[-]
$\beta$	: factor, quantifying the influence of particle-RTD on reactivity	[-]
$\beta''$	: factor defined by Equation 6.33	[-]
$\Gamma$	: stoichiometric coefficient	[mole CaO/ mole SO <sub>3</sub> ]
$\rho_d$	: bulk density of dense bed	[kg/m <sup>3</sup> <sub>bed</sub> ]
$\rho_p$	: particle density	[kg/m <sup>3</sup> <sub>particle</sub> ]
$\tau$	: average residence time	[s]
$\tau_{conv}$	: time needed for complete conversion of a sorbent particle	[-]
$\tau_{mix}$	: time needed for complete mixing of the particles	[-]
$\phi_{s, in}, \phi_{s, out}$	: solids mass flow	[kg/s]
$\phi_v$	: volumetric flow	[m <sup>3</sup> /s]
$\psi$	: distribution function in a population balance model	[-]

**Subscripts**

bd	: bed
dense	: dense bed, operated at relatively low gas velocity
eff	: effective
lean	: lean bed, operated at relatively high gas velocity
mf	: minimum fluidization

**References**

Brinkert, J., "Particle jets in fluidised beds", PhD Dissertation, University of Cambridge, Cambridge (1993).

Brinkert, J., Davidson, J.F., "Particle jets in fluidised beds", *Trans. of the Inst. of Chem. Eng.*, 71(A), 334-336 (1993).

Danckwerts, P.V., "Continuous flow systems; distribution of residence times", *Chem. Eng. Sci.*, 2, 1-11 (1953).

Fernández-Sempere, J., Font-Montesinos, R., Espejo-Alcaraz, O., "Residence time distribution for unsteady-state systems", *Chem. Eng. Sci.*, 50(2), 223-230 (1995).

Heesink, A.B.M., Klaus, J., Swaaij van, W.P.M., "The influence of particle residence time distribution on the reactivity in fluidized bed reactors", *Chem. Eng. Sci.* 49(14), 2243-2261 (1994).

Himmelblau, D.M., Bischoff, K.B., "Process analysis and simulation: deterministic systems", Chapters 4 and 6 ("Population-balance models" and "Applications of Population-balance models"), John Wiley & Sons Inc. (1968).

Kiparissides, C., "Polymerization process modelling: a review of recent developments and future directions", Plenary Lecture at the 14th International Symposium on Chemical Reaction Engineering, May 8, Brugge, Belgium (1996).

Korbee, R., "Regenerative desulfurization in an Interconnected Fluidized Bed System", PhD thesis, Delft University of Technology, Delft, The Netherlands (1995).

Levenspiel, O., "The Chemical Reactor Omnibook", 4th version, OSU Book Stores, Inc., Corvallis, Oregon, USA, Chapter 53, 53.5-53.6 (1993).

Ling van, D.A., "Modelling the hydrodynamic behaviour of the Interconnected Fluidised Bed system", MSc report, Delft University of Technology (1996).

## Chapter 6

---

- Nauman, E.B., "Residence time distribution theory for unsteady stirred tank reactors", *Chem. Eng. Sci.*, 24, 1461-1470 (1969).
- Oosterbaan van, G., "Dynamic modelling of gas-solid reactions in the IFB reactor system using Speedup: implementation of the conversion distribution", MSc report, Delft University of Technology (1996)
- Pajongwit, P., Jovanovic, G., "Residence time distribution of solids in a multi-compartment fluidized bed system", In: Preprints on Fluidization and Fluid-Particle Systems, special supplement to the 1994 Annual Meeting of the AIChE, November 13-18, San Francisco, USA (1994).
- Rijk, J.M., "Modelling of dynamic residence time distribution in the Interconnected Fluidised Bed reactor system", MSc report, Delft University of Technology (1997).
- Rubisov, D.H., Papangelakis, V.G., "Mathematical modelling of the transient behaviour of CSTRs with reactive particulates: Part 1- The Population Balance Framework; Part 2- Application to Pyrite Pressure Oxidation", *Can. J. Chem. Eng.*, 74(June), 353-371 (1996).
- Speedup, "User manual: release 5.4", Volume I and II, Aspen Technology, Inc., Cambridge Massachusetts, USA (1993).
- Stellema, C.S., Kolar, Z.I., Goeij de, J.J.M., Schouten, J.C., Bleek van den, C.M., "Solids residence time distribution in Interconnected Fluidized Beds", in: Fluidization and Fluid Particle Systems, Preprints of the 1996 AIChE Annual Meeting, (Eds.: Chen, Y.M. and Arastoopour, H.), November 10-15, Chicago, USA, 79-84 (1996).
- Villiermaux, J., "Trajectory length distribution (TLD), a novel concept to characterize mixing in flow systems", *Chem. Eng. Sci.*, 51(10), 1939-1946 (1996).
- Westerterp, K.R., Van Swaaij, W.P.M., Beenackers, A.A.C.M., "Chemical reactor design and operation", Wiley, Chichester, Chapter 5, 229-232 (1984).
- Wolff, E.H.P., "Regenerative sulfur capture in fluidized bed combustion of coal: A fixed bed sorption study", PhD thesis, Delft University of Technology, Delft, The Netherlands (1991).
- Wolff, E.H.P., Gerritsen, A.W., Bleek van den, C.M., "Multiple reactor testing of a synthetic sorbent for regenerative sulfur capture in fluidized bed combustion of coal", *Can. J. Chem. Eng.*, 71 (February), 83-93 (1993).
- Zacca, J.J., Debling, J.A., Ray, W.H., "Reactor residence time distribution effects on the multistage polymerization of olefins—I. Basic principles and illustrative examples, propylene", *Chem. Eng. Sci.*, 51(21), 4859-4886 (1996).
- Zenger, K., "Time-variable models for mixing processes under unsteady flow and volume", in: Dynamics and control of chemical reactors, distillation columns and batch processes; Preprints from the IFAC Symposium, (Ed.: Brawlings, J.B.), Helsingør, Denmark, 7-9 June 57-62 (1995).

## Appendix 6.A:

### Outline of the dynamic E(t) model for IFB regenerative desulfurization.

In this appendix, the mathematical models for IFB regenerative desulfurization that are used in chapter 6 are outlined. This includes the dynamic residence time distribution effects on the average conversions in the IFB reactor compartments. Further, the implementation in the dynamic simulation program Speedup is described.

#### *Dynamic modelling of regenerative desulfurization.*

Application of Equations 6.47 and 6.48 enables the calculation of the average conversion of the sorbent particles in a fluidized bed reactor taking into account the effects of Residence Time Distribution (RTD) of the particles. This is explained in chapter 6.3.2. The calculation requires the batch conversion ( $\alpha(t')$ ) equation for the sorbent undergoing a gas-solids reaction.

#### Sorbent sulfation

The sorbent sulfation is assumed to proceed according to the SURE2 model (chapter 5.3). The equation for the rate of conversion of one sorbent particle ( $r_c$ ) follows from Equation 5.10 and can be written in terms of the shrinking core radius ( $r_c$ ) as:

$$\frac{dr_c}{dt} = \frac{C_1 C_{SO_2}}{C_2 + C_4 r_c + (C_3 - C_4 C_5) r_c} \quad (\text{A.6.1})$$

in which:

$$C_1 = \frac{\Gamma}{C_{CaO}} \quad (\text{A.6.2})$$

$$C_2 = \frac{1}{k_s K_{Eq} \sqrt{C_{O_2}}} \quad (\text{A.6.3})$$

$$C_3 = \frac{1}{D_{SO_2, film} + D_{SO_3, film} K_{Eq} \sqrt{C_{O_2}}} \left( \frac{1}{R} - \frac{1}{R + \delta} \right) \quad (\text{A.6.4})$$

$$C_4 = \frac{1}{D_{SO_2, shell} + D_{SO_3, shell} K_{Eq} \sqrt{C_{O_2}}} \quad (\text{A.6.5})$$

$$C_5 = \frac{1}{R} \quad (\text{A.6.6})$$

Details on the SURE2 model and its model parameters can be found in chapter 5.3 of this thesis. The batch conversion equation ( $\alpha(t')$ ) is obtained from integration of Equation A.6.1. It should be noted that the gas phase  $SO_2$  concentration is in a non-stationary situation also a function of time and should thus be considered as such. The conversion  $\alpha$  is related to the

## Appendix 6.A

shrinking core radius ( $r_c$ ) according to:

$$r_c = R(1-\alpha)^{\frac{1}{3}} \quad (\text{A.6.7})$$

The sorbent particle enters the desulfurization compartment at a conversion  $\alpha_m$  at  $t=t'$ . After a certain time  $t$ , a conversion  $\alpha$  is reached. This conversion is a function of time according to the batch conversion equation that is obtained from integration of Equation A.6.1:

$$\begin{aligned} & C_2 R(1-\alpha)^{\frac{1}{3}} + \frac{1}{2} C_4 R^2(1-\alpha)^{\frac{2}{3}} + \frac{1}{3} (C_3 - C_4 C_5) R^3(1-\alpha) \\ = & -C_1 \int_{t-t'}^t C_{SO_2} dt + C_2 R(1-\alpha_m)^{\frac{1}{3}} + \frac{1}{2} C_4 R^2(1-\alpha_m)^{\frac{2}{3}} + \frac{1}{3} (C_3 - C_4 C_5) R^3(1-\alpha_m) \end{aligned} \quad (\text{A.6.8})$$

This equation implicitly defines the conversion  $\alpha$  as a function of  $t$ . The average conversion is thus calculated taking into account the particle RTD according to Equations 6.47 and 6.48. The value for the average sorbent conversion that is obtained, is applied in Equation 6.8 to determine the gas phase  $SO_2$  concentration.

### Sorbent regeneration

The sorbent regeneration can be modelled identically to the sorbent sulfation with respect to the influence of particle-RTD. The regeneration is assumed to take place according to reactions 6.12, 6.13, 6.14 and 6.15. For the simulation results presented in chapter 6.3.4, it was assumed that the sorbent is fully regenerated in the regeneration compartment of the IFB reactor. The chemical reactions were thus modelled as explained in chapter 6.1.

### *Implementation in Speedup.*

The structure of the Speedup problem is identical to that described in Appendix 3.A. Four models and units are added to the Speedup problem describing the IFB hydrodynamics. In Table 6.A.1 these models are indicated. The models *Ads* and *Reg* are based on the sulfur capture and regeneration models outlined above. The RTD for compartments 2 and 4 are modelled as ideally mixed (*CSTR*) and plugflow (*Hopperbed*) respectively.

**Table 6.A.1** Models and units for the calculation of the average sorbent conversion in each of the IFB compartments.

Model	Unit	Calculation of
Ads, bed1	adsorber	Average sorbent conversion ( $\alpha$ ), gas phase $SO_2$ concentration and sulfur retention
CSTR, bed2	CSTR	Average sorbent conversion
Reg, bed3	regenerator	Average sorbent conversions ( $\alpha_1$ , $\alpha_2$ and $\alpha_3$ ) and the gas phase concentrations $C_{H_2}$ , $C_{H_2S}$ and $C_{H_2O}$
Hopperbed, bed4	hopperbed	Average sorbent conversions ( $\alpha_1$ , $\alpha_2$ and $\alpha_3$ )

# Chapter 7

## Combined NO<sub>x</sub> and SO<sub>2</sub> abatement

### IFB possibilities for the NOXSO process

---

#### 7.1 Introduction

The work presented in this chapter is an illustration of a possible application of IFB reactor technology. The process that is studied in detail is the so-called NOXSO process. This is a process for the regenerative removal of NO<sub>x</sub> and SO<sub>2</sub> from a flue gas stream. In the process, a regenerable sorbent is transported between fluidized beds. The NOXSO process is owned and was developed by the NOXSO Corporation (described in U.S. Patent No. 4.798.711). The NOXSO process is placed in perspective of other technologies for combined NO<sub>x</sub> and SO<sub>2</sub> abatement. Reference is made to an exergy analysis in which a number of processes is analyzed in terms of energy efficiency expressed in this thermodynamic quantity (see chapter 7.4.1).

The IFB reactor design for the NOXSO process is described by Snip *et al.* (1996) and outlined in chapter 7.3. One of the main concerns of the NOXSO process is the solids circulation and the loss of sorbent during this transport. To obtain insight in the possible advantages of the use of an IFB reactor system for the NOXSO process, the design study as presented in this chapter was initiated. The NOXSO process that is carried out in an IFB reactor system is referred to as the IFB-NOXSO process.

The NOXSO process and the IFB-NOXSO process are compared on the basis of exergy losses and costs. The final design is believed to have interesting advantages compared to the original NOXSO reactor configuration.

#### 7.2 Combined NO<sub>x</sub> and SO<sub>2</sub> removal processes

The combined abatement of SO<sub>2</sub> and NO<sub>x</sub> is a key issue in electric power production. During the coal combustion process a flue gas stream containing these components is produced. Many processes are available and under development that cope with this problem.

The Electrical Power Research Institute (EPRI, USA) has performed an engineering evaluation of combined NO<sub>x</sub> and SO<sub>2</sub> control technologies (Cichanowicz *et al.*, 1991). This evaluation was based on more than 70 candidate processes and showed only a few removal technologies that are attractive alternatives to conventional flue gas desulfurization (FGD) and selective catalytic reduction (SCR).

According to Cichanowicz *et al.* (1991), processes that combine SO<sub>2</sub> and NO<sub>x</sub> removal into one step or separate steps with synergistic interactions are preferable to conventional technologies in cost, reliability and environmental effects. The category of solid adsorption/

regeneration appears to be the most prolific development. One of the leading contenders is a process developed by the NOXSO Corporation. NOXSO combines the removal of SO<sub>2</sub> and NO<sub>x</sub> in one step in a solid adsorption/regeneration process. The NOXSO process therefore is a promising technology for combined NO<sub>x</sub> and SO<sub>2</sub> removal (Bell *et al.*, 1995).

Another serious candidate process, selected by Cichanowicz *et al.* (1991), that can compete the conventional removal techniques and the NOXSO process, is the WSA/SNOX reduction/oxidation process.

The SCR/FGD and WSA/SNOX processes are briefly mentioned in order to compare these processes to the NOXSO process. The new processes (WSA/SNOX and NOXSO) and the conventional processes (SCR/FGD) are competitors in the field of combined NO<sub>x</sub> and SO<sub>2</sub> abatement.

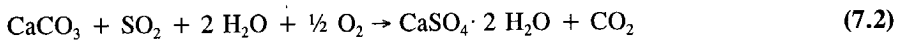
### SCR/FGD

Selective Catalytic Reduction (SCR) and Flue Gas Desulfurization (FGD) are at this moment the most common techniques to remove NO<sub>x</sub> and SO<sub>2</sub> from flue gas streams. Various specific configurations are available for SCR/FGD (Gutberlet and Schallert, 1993) especially with respect to SCR and FGD reactor technology.

In general the SCR reactor is located after the economizer that preheats the boiler feed water. The SCR temperature is approximately 350 °C. The nitrogen oxides are reduced by ammonia on a specific SCR catalyst. This can be represented by the following overall reaction:



After removal of NO<sub>x</sub>, the flue gas is generally passed through an air preheater and the particulates are removed. The SO<sub>2</sub> removal is carried out in a spray tower. A limestone slurry is introduced in the gas stream providing proper contact between SO<sub>2</sub> and limestone. At a temperature of 50 °C, gypsum is formed according to the following overall reaction between limestone and sulfur dioxide:



### WSA/SNOX

In this process, developed by Haldor Topsøe A/S (Lyngby, Denmark), NO<sub>x</sub> is catalytically reduced by ammonia to nitrogen and water. The flue gas is cooled to approximately 200 °C after which the fly-ash is removed. The gas is then heated to 390 °C at which the SCR takes place according to the overall reaction 7.1.

After removal of the NO<sub>x</sub>, the SO<sub>2</sub> is oxidized to sulfur trioxide (SO<sub>3</sub>) at a temperature of 420 °C. Any ammonia that is still present from the SCR reaction is oxidized in the SO<sub>3</sub> oxidation reactor to nitrogen and water. The off-gas from the sulfur-trioxide reactor is used to heat the flue-gas from 200 to 390 °C before the SCR reactor. The latter is an example of the fact that heat integration is an important feature of this process.

The SO<sub>2</sub> is catalytically converted to SO<sub>3</sub> according to the following overall reaction:





The gas is then cooled during which the bulk of the sulfur trioxide reacts with water to sulfuric acid according to:



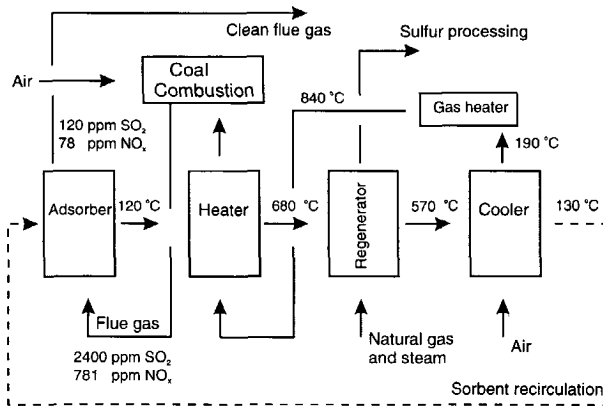
The sulfuric acid is condensed in the WSA tower. This is an air cooled falling film condenser. In this tower the flue gas passes through tubes made of borosilicate glass that are cooled by ambient air and in which the sulfuric acid condenses.

### 7.3 The NOXSO process in an IFB reactor

#### 7.3.1 NOXSO process layout

The NOXSO process is a dry flue gas treatment technology that uses a regenerable sorbent to simultaneously remove 90% of the SO<sub>2</sub> and 70-90% of the NO<sub>x</sub> from flue gas generated from the combustion of coal. The process has been successfully tested at different scales. A Life-Cycle Test Unit (0.06 MW) was operated to determine long-term effects of the process on sorbent reactivity and attrition properties. The test results were published by Ma *et al.* (1991) and Yeh *et al.* (1992). The Proof-of-Concept (POC) Test (5 MW) was the last test prior to full-scale demonstration. The test collected all design information for the full-scale NOXSO plant. The results were published by Ma and Haslbeck (1993).

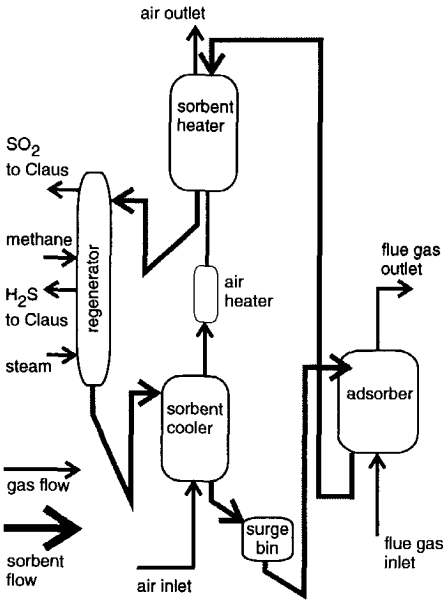
In Figure 7.1, a schematic view of the NOXSO process is given. Flue gas from the coal-fired power plant flows through the fluid-bed adsorber. Water is sprayed directly into the fluid bed as required to lower the temperature to the adsorption temperature of 120 °C by evaporative cooling.



**Figure 7.1** Schematic view of the NOXSO process. The SO<sub>2</sub> and NO<sub>x</sub> are removed from a flue gas originating from a coal-fired power plant. A solid adsorbent is recirculating between adsorber and regenerator. The sulfur is released in the regenerator and can be further processed. The NO<sub>x</sub> is released in the sorbent heater and is returned to the boiler for destruction.

Spent sorbent from the adsorber flows into a dense-phase conveying system which lifts the sorbent to the top of the sorbent heater vessel. The sorbent flows through the multi-stage fluid-bed sorbent heater (counterflow to the heating gas) in which the sorbent is heated to the regeneration temperature of 680 °C.

In the sorbent heating process, the NO<sub>x</sub> is driven from the sorbent and carried to the power plant boiler in the NO<sub>x</sub> recycle stream. The excess heat input in the heater is recovered for 60% by using the NO<sub>x</sub> recycle stream to heat part of the power plant's feedwater. The



**Figure 7.2** Solids flow path in the NOXSO reactor set-up. Solids are transported between the different reactor vessels by means of pneumatic transport lines.

cooled, NO<sub>x</sub>-rich recycle stream replaces a portion of the boilers combustion air; it hereby reduces the formation of NO<sub>x</sub> in the boiler resulting in a net destruction of NO<sub>x</sub>.

The heated sorbent enters the moving bed regenerator where it is contacted with natural gas. Through a series of chemical reactions, the sulfur on the sorbent reacts with the methane to form SO<sub>2</sub> and H<sub>2</sub>S. Additional regeneration occurs in the steam treater where the sorbent is contacted with steam and the remaining sulfur on the sorbent is converted to H<sub>2</sub>S. The regenerator and steam treater off-gas streams are combined and directed to a sulfur recovery plant where H<sub>2</sub>S and SO<sub>2</sub> are converted to a sulfur by-product.

High temperature sorbent from the steam treater passes the multi-stage fluid-bed sorbent cooler. The sorbent flows counter to the ambient air which cools the sorbent. Regenerated sorbent exits the cooler at 130 °C. It is directed to the adsorber completing the sorbent cycle. The preheated air from the sorbent cooler is heated up to 840 °C and used in the sorbent heater.

In the NOXSO process sorbent needs to be recirculated between the fluidized bed reactors. The "solids flow path" is presented in Figure 7.2. It can be seen that the solids move through a series of pneumatic transport lines and non-mechanical valves. An alternative for this reactors and solids transport system is the IFB reactor system.

**7.3.2 Modelling the IFB-NOXSO process**

**IFB technology**

The most important advantages of the IFB reactor technology are: (1) the sorbent is transported in a fluidized mode at moderate particle velocities minimizing attrition and loss of sorbent, and (2) the IFB reactor can be very compact due to the absence of solids transportation systems. The IFB reactor consists of multiple sets of dense and lean bed

compartments. The transport of solids is induced and controlled by means of differently aerated compartments. In turn, the solids flow *over* a weir and *through* an orifice which connect the respective compartments. The solids upflow compartments act as chemical reactors and the downflow compartments serve as strippers between two reactors.

The main difference between the NOXSO process in the conventional set-up and the alternate IFB set-up is that in the IFB system all reactors, coolers and heaters are constructed in one vessel. Therefore no conveying lines or any solids transport system are needed. For the NOXSO process multiple sets of these connected beds are necessary to run the process.

It was found that the solids flow rate through a system of multiple sets of dense and lean beds can be well controlled by operating one of the transport beds below or at the condition of minimum fluidization (see chapter 3 of this thesis).

Only one set of dense and lean beds will dictate the Circulation Rate of Solids (CRS) through the IFB system. The CRS is equal to the solids flow in the rate limiting orifice. The solids flow ( $\phi_m$ ) can be calculated according to the model described by Korbee *et al.* (1995). In this model, the solids are assumed to be driven by:

- ▶ a net horizontally directed normal stress caused by the presence of the particles at both sides of the orifice ( $\Delta\sigma_N$ ), and
- ▶ the gas pressure drop across the orifice ( $\Delta P_o$ ).

This is represented by the following equation (see also chapter 2.3 of this thesis):

$$\phi_m = C_D A_{orifice} \sqrt{\rho_p (1-\epsilon) 2 (\Delta\sigma_N + \Delta P_o)} \quad (7.5)$$

A simplification was made to the model in this design study. The normal stress ( $\sigma_N$ ) is assumed to have no influence on solids flow in the range of conditions applied in the IFB system. Its contribution is negligible compared to the gas pressure drop. The discharge coefficient ( $C_D$ ) was set to a constant value of 0.5, according to Davies and Fenton (1995) and Zhang and Rudolph (1991), accounting for friction losses in the region of solids flow between dense and lean beds.

#### ***NOXSO chemistry: adsorption and regeneration***

The NOXSO sorbent is a  $\gamma$ -alumina bead impregnated with sodium carbonate. The sodium content is 5.2 wt% and the average particle size is 1.2 mm. The active ingredients on the NOXSO sorbent are sodium and alumina. These components contribute to the sorbent's capacity to *adsorb* SO<sub>2</sub> and NO<sub>x</sub> from the flue gas. Several adsorption tests verified the following phenomena:

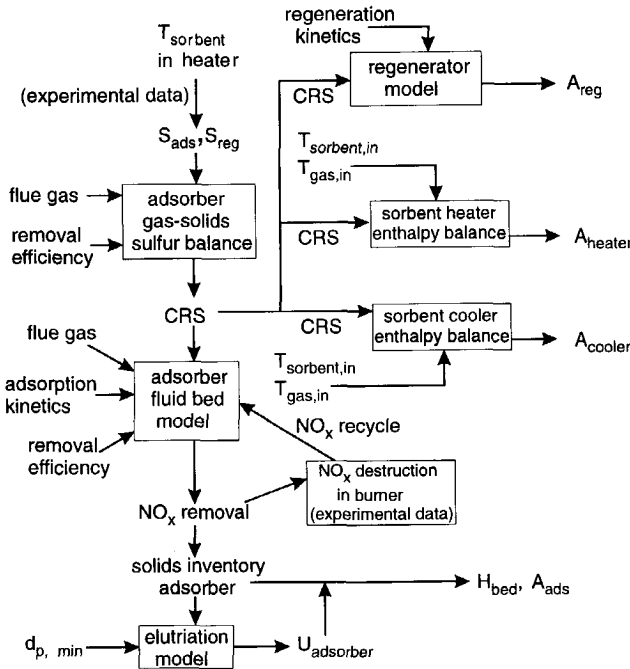
1. presence of oxygen and steam enhances the NO<sub>x</sub> and SO<sub>2</sub> sorption on the sorbent,
2. NO<sub>x</sub> is removed only if SO<sub>2</sub> is also present in the flue gas,
3. sorbed NO<sub>x</sub> will desorb if more SO<sub>2</sub> is fed to the reactor, and
4. the NO<sub>x</sub> and SO<sub>2</sub> sorption is limited by the NO<sub>x</sub> sorption.

A detailed reaction scheme is given by Ma *et al.* (1995). The adsorption model used for design purposes in the present study is taken from Ma and Haslbeck (1993). The kinetics are based on the above mentioned experimental observations. In order to incorporate the adsorption mechanism into a fluid bed adsorber model, a time-averaged sorbent conversion

and mean gas concentration are used. The adsorber is modelled by assuming plug flow for the gas phase and mixed-flow of the solids phase. The values for the kinetic parameters used in this design are estimated by Ma and Haslbeck (1993) from experimental data obtained in a flue gas treatment plant capable of cleaning the flue gas stream of a 5 MW power plant. A gas-solid sulfur balance gives insight to the relation between the molar flue gas stream ( $\phi_{mol, flue\ gas}$ ), the mole fraction  $SO_2$  in flue gas ( $y_{SO_2}$ ), the Circulation Rate of the Solids (CRS) and the sulfur load after adsorption and regeneration ( $S_{ads}$  and  $S_{reg}$ ):

$$\phi_{mol, flue\ gas} M_s (y_{SO_2, in} - y_{SO_2, out}) = \frac{CRS}{100} (S_{ads} - S_{reg}) \quad (7.6)$$

The  $NO_x$  that is removed in the adsorber is completely evolved in the sorbent heater. The sulfur needs to be regenerated by contacting the heated sorbent with methane and steam respectively. The rate of sulfur regeneration for the spent sorbent can be predicted according to a  $1/2$ -order rate equation in the sulfur content of the sorbent. The agreement between experimental data and model predictions is reasonable and therefore the model can be used to size the regenerator (Ma and Haslbeck, 1993).



**Figure 7.3** Calculation scheme that was used to design the IFB reactor system for the  $NO_xSO$  process. The temperature in the sorbent heater determines the sulfur content of the sorbent in adsorber and regenerator ( $S_{ads}$  and  $S_{reg}$ ). By means of the sulfur balance, fluid bed adsorber model, minimum particle size that needs to stay in the bed ( $d_{p, min}$ ) and the superficial gas velocity ( $U_{adsorber}$ ), the size of the adsorber is determined. The cross-sectional bed area ( $A_{bed}$ ) of the regenerator, heater and cooler is determined by the regenerator model and enthalpy balances.

### *Process requirements and method of calculation*

The flue gas stream that needs to be treated is fixed by the fact that it is originating from a specific power plant (150 MWe): 172.3 Nm<sup>3</sup>/s containing 2400 ppm SO<sub>2</sub> and 781 ppm NO<sub>x</sub>. The requirements of the process were set to: 95% SO<sub>2</sub> and 90% NO<sub>x</sub> removal. The size of the power plant (150 MWe) and the removal efficiencies of SO<sub>2</sub> and NO<sub>x</sub> were chosen such that the present IFB design provides relevant information that can be compared to design data that was available from the original NOXSO setup.

The calculation scheme that was applied in this design is shown in Figure 7.3. It is based on the following considerations. Test results made clear that the temperature in the sorbent heater determines the sulfur content of the sorbent for the whole process. The sulfur content increases linearly with decreasing temperature. Further, the difference in sulfur content between spent sorbent ( $S_{ads}$ ) and regenerated sorbent ( $S_{reg}$ ) appears to be constant (Ma and Haslbeck, 1993). A low regeneration temperature is preferred in terms of energy conservation and sorbent life but for the sake of process safety the temperature in the sorbent heater is controlled well above the auto-ignition temperature of natural gas (602 °C). Any natural gas that slips into the sorbent heater due to the process upset will burn spontaneously. The fixed sulfur content of the sorbent ( $S_{ads}$  and  $S_{reg}$ ), the amount of flue gas and the removal efficiency of SO<sub>2</sub> determine the appropriate Circulation Rate of Solids (CRS). The CRS is calculated from Equation 7.6.

According to the fluid bed adsorber model (described in the previous section), the solids inventory in the adsorber can be calculated. To calculate the fraction of the NO<sub>x</sub> that is removed, the efficiency of the NO<sub>x</sub> destruction in the burner has to be taken into account as well. This is due to the recycle stream that returns the NO<sub>x</sub> rich stream (from the sorbent heater) to the burner where part of the NO<sub>x</sub> is destroyed. When the NO<sub>x</sub> removal is satisfactory, the resulting bed inventory and CRS are known.

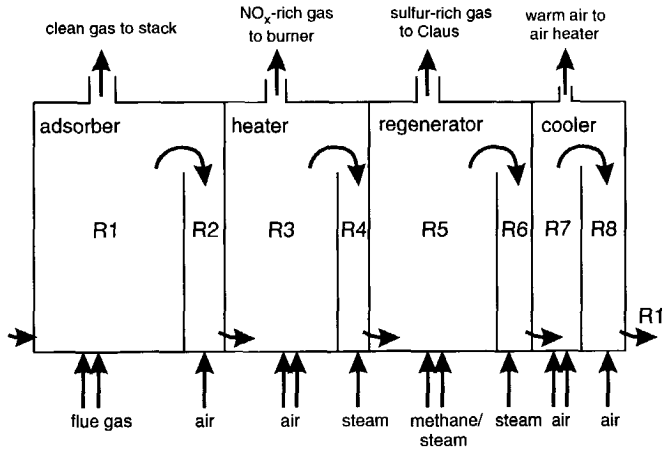
The inventory of the regenerator is calculated based on the known CRS and the regeneration model that is described in the previous section (Ma and Haslbeck, 1993).

### 7.3.3 Design of the IFB reactor system

#### *Adsorber and regenerator*

When the CRS and the inventories of adsorber and regenerator are known, the IFB reactor system can be further designed (Figure 7.3). The overall *schematic* picture of the IFB reactor is shown in Figure 7.4. The IFB reactor system consists of four sets of beds as indicated in Table 7.1. All compartments have a specific function and are therefore necessary for proper operation of the NOXSO process in the IFB reactor.

The first step in designing the IFB reactor system is the design of the individual compartments. The CRS and the solids inventories of the adsorber and regenerator are already known. The size (bed height, area) and gas velocity for all compartments are still to be fixed.



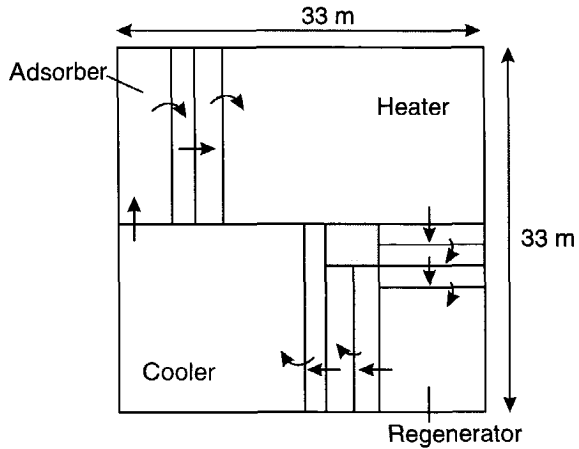
**Figure 7.4** View of the simplified IFB reactor configuration. The IFB-NOXSO reactor consists of four sets of dense and lean (or overflowing) beds.

The adsorber (R1) is used for flue gas cleaning and the connected transport bed (R2) is used for controlling the CRS. The gas velocity in the adsorber is set to a value that is equivalent to the terminal velocity ( $U_t$ ) of the smallest particle that has to stay in the bed (in this design:  $d_{p, min} = 840 \mu\text{m}$  and the corresponding  $U_t = 2.8 \text{ m/s}$ ). The gas velocity is set on this value and the corresponding size, bed height and other related properties can be evaluated. In the transport bed (like in all the beds in this IFB system), the superficial gas velocity is actually a slip velocity (gas and solids are moving in counter-current mode). The expanded bed height of the adsorber is 2.5 m. This height is also taken for the height of the weirs in the other sets of lean and dense beds.

**Table 7.1** Simplified configuration of the IFB-NOXSO reactor system: function and destination of off-gas.

Set of dense/ lean bed	Lean bed: a) function b) fluidization gas	Dense bed: a) function b) fluidization gas	a) Off-gas to: b) Consisting of:
1 a) b)	adsorber raw flue gas	transport bed air	stack clean flue gas
2 a) b)	heater air	transport bed stripping steam	NO <sub>x</sub> to burner NO <sub>x</sub> rich gas stream
3 a) b)	regenerator methane	stripping + regeneration steam	sulfur plant sulfur rich gas
4 a) b)	cooler air	transport bed air	sorbent heater preheated air

The regenerator (R5) is designed according to equivalent considerations as given in the adsorber design. The difference however is that it was chosen to accommodate the regeneration process in a transport compartment. In this way, a counter-current mode of operation is possible enabling an equivalent regeneration efficiency as obtained in the original NOXSO reactor configuration. As shown in Figure 7.5, additional transport compartments are used to prevent any air to be contacted with methane in the regenerator and to strip residual sulfur that is still present on the sorbent.

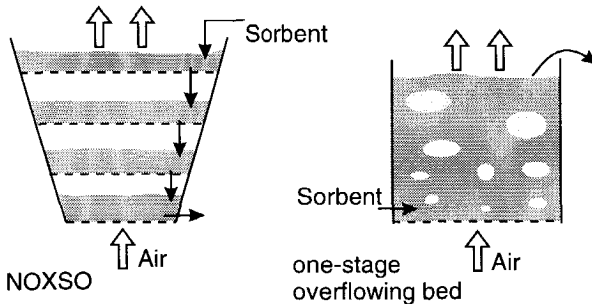


**Figure 7.5** Cross-sectional view of the IFB-NOXSO design. The sorbent is transported between the dense bed and lean bed (overflowing) compartments.

**Cooler and heater**

In the original NOXSO reactor configuration, the sorbent undergoes a cycle of heating and cooling (see Figure 7.1). Heat transfer is therefore an important consideration for reactor design.

In Figure 7.6, the original NOXSO and a one-stage heat exchange configuration are shown. It is known that counter-current heat exchange is preferable compared to co-current operation. The NOXSO heat exchange facility operates counter-currently in multiple stages. This results in a much better heat transfer efficiency than for the one-stage heat exchanger in which the heat transfer is carried out in a well-mixed fluidized bed. This would result in a much higher natural gas consumption for this configuration compared to the original NOXSO heat exchange facility.



**Figure 7.6** Heat exchange in the sorbent cooler between sorbent and gas in the original NOXSO process and in a one-stage overflowing bed facility.

In literature, various reactor configurations can be found that were developed to improve physical operations such as heat transfer between gas and solids (see for example Kunii and Levenspiel (1991) and Papa and Zenz (1995) ).

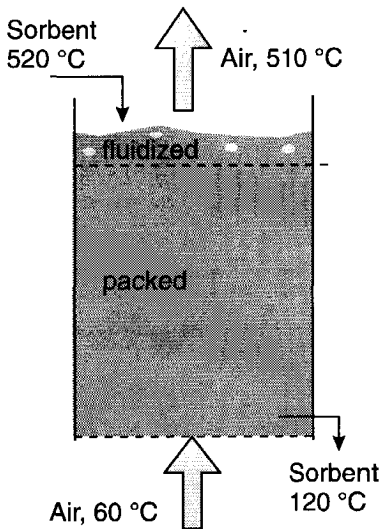
In the dense beds of the IFB reactor, the solids and gas are moving in counter-current mode approaching plug flow. This offers the opportunity for heat transfer between gas and solids in a counter-current mode for heater as well as sorbent cooler.

Two parameters are important for a heater and cooler design in a counter-current downflow moving bed. These are:

- ▶ the superficial gas velocity, and
- ▶ the cross-sectional bed area.

When a large bed area is chosen, a low superficial gas velocity can be applied. For a high superficial gas velocity, a small bed can be used. The superficial gas velocity is limited to the minimum fluidization velocity for two reasons:

1. The solids need to flow in moving bed mode countercurrent to the air flow that is heating or cooling the sorbent in order to improve the heat transfer efficiency.
2. The solids have to be transported from dense to lean bed. This can only be achieved when there is an effective driving force. Hence, the gas velocity in the dense bed needs to be below the minimum fluidization velocity.



**Figure 7.7** Moving bed counter-current heat exchange in a dense transport bed of the IFB-NOXSO reactor. The gas is heated from 60 °C to 510 °C. This causes an increase of the superficial gas velocity and is the reason that the upper part of the bed is just fluidized.

Due to the exchange of heat between gas and solid phases, the temperature and, consequently, the gas density changes with height. It was chosen to accommodate the heater and cooler together with adsorber and regenerator in one IFB-NOXSO facility. It was therefore decided not to apply any special features such as tapering or staging.

Due to the changing temperature, the gas velocity in the heater and cooler will change with height. In order to minimize the size of the IFB-NOXSO reactor, the heater and cooler were designed such that the maximum gas velocity that was attained equals the minimum fluidization velocity.

***Design of the sorbent cooler***

The design of the sorbent cooler is briefly outlined in order to give some insight in the straightforward design procedure that was followed.

The sorbent flow through the NOXSO



process is shown in Figure 7.1. When the sorbent is regenerated at a high temperature of approximately 600 °C, it is cooled by air before it is directed to the adsorber. A schematic representation of the cooler is shown in Figure 7.7.

The inlet temperatures of solids and gas are fixed and indicated in Figure 7.7. The required outlet temperature of the sorbent is determined by the adsorption process of NO<sub>x</sub> and SO<sub>2</sub> that is carried out 120 °C.

The recovery of heat would be maximum when the sorbent is cooled to the inlet temperature of air or when air is heated to the inlet temperature of the sorbent. In the cooler, the latter situation is preferred.

To achieve a reasonable heat transfer rate however, a certain temperature difference between gas and solids needs to be set throughout the bed. In this design, a temperature difference between the inlet solids temperature and the outlet gas temperature of 10 °C was used.

The gas outlet temperature is then fixed at 510 °C. The cooler is designed in such a way that the outlet superficial gas velocity equals the minimum fluidization velocity. In this way, the minimum size of the bed is attained and the moving bed mode of the cooler is ensured. The cooler size and inlet superficial gas velocity are then determined by the heat balances for gas and solid phases in the moving bed. The resulting inlet superficial gas velocity ( $U_0$ ) and bed area are indicated in Table 7.2.

The design of the heater was carried out analogous to the cooler design. The heater and cooler were then fitted into one IFB-NOXSO reactor. The results of the calculations for heater and cooler are given in Table 7.2 and the cross-sectional sizes of the IFB-NOXSO design are shown in Figure 7.5. A number of extra transport compartments is needed with respect to the simplified IFB-NOXSO facility shown in Figure 7.4. These extra compartments serve as separation zones to prevent mixing of the gas from the regenerator (methane) with air (oxygen) that is used in cooler and heater. These compartments and their sizes are indicated in Figure 7.5.

**Table 7.2** Cooler and heater specifications of the IFB-NOXSO design.

	<b>Solids flow direction</b>	<b>Bed area [m<sup>2</sup>]</b>	<b><math>U_0/U_{mf}</math> [-]</b>
<b>Cooler</b>	upflow	12	2
	downflow	300	0.43
<b>Heater</b>	upflow	20.4	2
	downflow	440	1.01

It should however be mentioned that the IFB-NOXSO design is based on the assumption that it is functioning well with respect to the heat transfer in the cooler and heater compartments. According to Woods (1996), operation of the IFB reactor downflow compartments is in principle possible and would result in an effective heat transfer.

### 7.3.4 Results and discussion

From the CRS and the pressure drops across the orifice, the size of the orifices can be calculated. The CRS is known and its value in case of this specific IFB-NOXSO design is 43.5 kg/s. This is the circulation rate through all compartments. Under the assumption that the normal stress is zero, the driving force for solids flow comes down to the difference in density between the connected beds. The area of the orifice that is necessary for adsorber and regenerator, was calculated from Equation 7.5. Solids fluxes are obtained between 150 and 350 kg/m<sup>2</sup>s.

In practice the design of the orifices between the compartments will be such that one of these provides a restriction in solids flow. This is an advantage because in that case the solids flow, and therefore the CRS, can be controlled by adjusting the gas velocity to one transport bed. The most appropriate bed in this set-up is R2 (see Figure 7.4), the transport bed after the adsorber, because it has no other function than transporting solids.

The gas flow through the orifice was calculated by application of the model of Korbee *et al.* (1995) on the specific conditions in the IFB system. This gas flow is negligible with respect to its influence on the lean bed. However, the influence is significant on the gas velocity in the dense bed. The results were obtained taking this effect into account on all dense bed gas velocities.

This IFB-NOXSO design shows that an IFB reactor system can accommodate the NOXSO process. The IFB reactor system has certain advantages compared to the NOXSO reactor set-up for solids transport. The main advantages are:

1. less attrition due to a lack of transport lines,
2. the IFB system is compact, and
3. less compressed gas is needed for solids transport (all vessels are at ground level).

The first advantage is difficult to quantify without more appropriate attrition data. More investigation is necessary to obtain the relevant attrition data of the NOXSO sorbent under relevant process conditions. It is important to determine in which part of the NOXSO set-up for solids circulation most of the attrition occurs. According to Leonard *et al.* (1994), solids make-up consists of approximately 35% of the operational and maintenance costs. Limiting attrition therefore will substantially contribute to improved process economics.

The IFB system seems to be an attractive alternative set-up for solids transport in the NOXSO process. A more detailed evaluation is needed to quantify these advantages. This type of analysis is described in chapter 7.4.

## 7.4 Analysis and comparison of the NOXSO and IFB-NOXSO processes

### 7.4.1 Exergy analysis

An exergy analysis was performed to compare a number of combined NO<sub>x</sub> and SO<sub>2</sub> removal processes. The term exergy refers to a concept of thermodynamics that accounts for the quality of energy and its degradation in real processes. The idea is that an exergy analysis

can give insight into the nature of irreversibilities associated with specific processes. In this chapter, only the results of an exergy analysis will be given without going into detail on theoretical backgrounds. For a detailed description of theory and the implementation of exergy analysis in a flowsheeting simulator, reference is made to the work of Hinderink *et al.* (1996).

The definition of exergy can be formulated as: *exergy is the amount of work that can be obtained from a process stream by bringing it into equilibrium with its natural environment.* According to this definition, exergy (*Ex*) can be represented as:

$$Ex = (H - H_0) - T_0(S - S_0) \quad (7.7)$$

in which  $H_0$ ,  $T_0$  and  $S_0$  refer respectively to the standard enthalpy, temperature and entropy at reference environment conditions. The nature of exergy can be (1) chemical, (2) physical or (3) based on the mixing of pure components.

The chemical exergy refers to the difference in chemical potential between the pure components and the reference environment. The physical exergy is the maximum obtainable amount of shaft work when a process stream is brought in equilibrium with its environment by reversible processes. The reference environment that was used in this analysis and in most exergy studies in literature was defined by Szargut *et al.* (1988). It defines reference temperature and pressure ( $T_0 = 298$  K;  $p_0 = 1.10^5$  Pa) and chemical composition.

The total exergy flow rates in a process can be determined by multiplying the sum of exergies by the total molar flow rate. This does not require new physical property models. The physical exergy and the exergy change of mixing are based on enthalpy, entropy and phase behaviour calculations. Chemical exergies can be obtained by determining a standard chemical exergy based on a well-defined reference environment (Szargut *et al.*, 1988).

A detailed description of the exergy analysis of a number of combined NO<sub>x</sub> and SO<sub>2</sub> removal processes is given by de Loë (1996). The data was obtained from simulation of a 500 MWE power station by Aspen plus. The final results are presented in Table 7.3.

**Table 7.3** Results of exergy analysis for the indicated NO<sub>x</sub> and SO<sub>2</sub> removal processes.

Process	SO <sub>2</sub> removal	NO <sub>x</sub> removal	Product	Exergy loss (MW)
SCR/FGD	Scrubbing with limestone slurry	Catalytic reduction	Gypsum	102
SNOX	Oxidation and condensation to sulfuric acid	Catalytic reduction	Sulfuric acid	104
NOXSO	Adsorption <sup>(1)</sup>	Adsorption <sup>(1)</sup>	Sulfur	160
IFB-NOXSO	Adsorption <sup>(1)</sup>	Adsorption <sup>(1)</sup>	Sulfur	161

<sup>(1)</sup> adsorption on Na<sub>2</sub>O/γ-Al<sub>2</sub>O<sub>3</sub>

## Chapter 7

From these results it could be concluded that the NOXSO process and especially the IFB-NOXSO process are not efficient with respect to exergy and should therefore not be chosen for combined NO<sub>x</sub> and SO<sub>2</sub> removal. However, the final choice to be made will be eventually determined by process economics. This is described in chapter 7.4.2.

### 7.4.2 Economic evaluation

The economics of the SNOX and SCR/FGD processes were analyzed by Borio and Kingston (1993). The prices for the main chemicals that are used in the SNOX process were set at 150 and 50 \$/ton for ammonia and sulfuric acid respectively. The economic numbers for the SNOX and SCR/FGD processes were calculated by Borio and Kingston (1993) and are presented in Table 7.4.

The NOXSO process was economically analyzed by Leonard *et al.* (1994). The most important economic parameters that were used in this NOXSO process analysis are:

- ▶ electricity                    0.018 \$/ kWh
- ▶ NOXSO sorbent            3.3 \$/ kg
- ▶ natural gas                0.002 \$/ MJ
- ▶ net sulfur value            40 \$/ ton

The economic analysis that is carried out here for the IFB-NOXSO process are based on the economic data of Leonard *et al.* (1994). As a rough approximation, it was assumed that the capital costs regarding the total plant costs, working capital and startup expenses are identical for the NOXSO and the IFB-NOXSO process. The economic parameters that were taken into account are listed above. It was further assumed that the costs for sorbent make-up in the IFB-NOXSO design were 50% of the make-up costs in the original NOXSO process. Obviously, the numbers that are given in Table 7.4 have to be considered with reservation because they are based on rough estimations of various prices and costs. These can vary considerable for a different scale of operation or specific design. The numbers do however represent important features of the processes and are therefore presented as such.

**Table 7.4** Results of economic analysis for the indicated NO<sub>x</sub> and SO<sub>2</sub> removal processes.

Process	Capital charges [10 <sup>-3</sup> \$ /kWh]	Operating and maintenance costs [10 <sup>-3</sup> \$ /kWh]	Total costs [10 <sup>-3</sup> \$ /kWh]
SCR/FGD	3.4	3.8	7.3
SNOX	6.3	1.0	7.3
NOXSO	1.0	3.3	4.3
IFB-NOXSO	2.0	2.2	4.2

It is found that the SNOX process was most advantageous with respect to direct operating and maintenance costs compared to the NOXSO and the conventional SCR/FGD processes. Comparison of the total costs, including capital costs, results in a different picture. This is mainly due to the high costs of the SNOX equipment. The capital costs for the SNOX process are significantly higher than for the other processes. One of the major cost factors in the SNOX process is the WSA tower, in which the sulfuric acid is condensed in tubes made of borosilicate glass (see chapter 7.2).

The IFB-NOXSO design is more cost effective with respect to the other processes. This has to be considered with some technical restrictions that are mentioned in chapter 7.3.3.

Borio and Kingston (1993) as well as Leonard *et al.* (1994) performed a sensitivity analysis to determine the effect on the net operating and maintenance costs of:

- ▶ the net sale price of sulfur and sulfuric acid,
- ▶ the unit cost of natural gas, sorbent and ammonia, and
- ▶ the price and lifetime of the SCR and SO<sub>2</sub> oxidation catalysts.

Their conclusion was that the costs for SO<sub>2</sub> and NO<sub>x</sub> removal varies considerable with variation in the above mentioned cost factors. Both processes (*viz.*, SNOX and NOXSO) however still appeared to be economically attractive with respect to conventional SCR/FGD processes.

The results of the analysis, shown in Table 7.4, indicate that the IFB-NOXSO process might be an economically attractive reactor configuration to accommodate and further improve the NOXSO process.

### 7.4.3 Discussion and comparison of exergy and economic analysis

Despite the usefulness of exergy analysis, eventually a process needs to be analyzed on the basis of its total costs. A process that is attractive with respect to small exergy losses is not necessarily economically attractive. This is well illustrated by the SNOX process. In Table 7.3, it is shown that this process is preferable with respect to exergy losses. In Table 7.4 however, it appears that the process economics are not as favourable as the exergy analysis suggested.

The comparison of exergy and economic analysis shows that an exergy analysis can be useful in terms of economically improving a process. This is the case when an exergy loss in a process can be attributed to a certain part of the process operation and when this part can be technically improved.

## 7.5 Discussion and conclusions

In this chapter, a comprehensive overview is given of the preliminary design of an IFB reactor system for regenerative SO<sub>2</sub> and NO<sub>x</sub> removal from flue gas.

## Chapter 7

---

An important advantage of the IFB reactor set-up is the limited sorbent attrition due to a lack of transport lines. This advantage is however difficult to quantify yet without more appropriate attrition data. More investigation is necessary to obtain the relevant attrition data of the NOXSO sorbent under relevant process conditions. It is important to determine in which part of the NOXSO reactor set-up most of the attrition occurs.

Exergy analysis and economic evaluation were carried out in order to quantify and compare the energy requirements and economic performance of the original NOXSO and IFB-NOXSO processes. An exergy analysis is only useful when the exergy loss is economically important and when the cause of this exergy loss can be technically improved. It was illustrated that when a process is attractive with respect to small exergy losses, it is not necessarily economically attractive. It is therefore concluded that despite the usefulness of an exergy analysis, eventually a process needs to be analyzed on the basis of its costs.

The economic analysis was made on the basis of rough estimations of prices and costs. The true costs of the processes might therefore deviate considerably. The economic numbers do however represent important features of the processes and are therefore evaluated. It was shown that the IFB reactor can be an attractive alternative for solids circulation in the NOXSO process.

### Notation

A	surface area	[m <sup>2</sup> ]
C <sub>D</sub>	solids discharge coefficient	[-]
CRS	Circulation Rate of Solids	[kg/s]
Ex	exergy (defined by Equation 7.7)	[J/mole]
H	height	[m]
H	enthalpy	[J/mole]
M	molar mass	[kg/kmol]
P	pressure	[N/m <sup>2</sup> ]
S	sulfur content of sorbent	[wt%]
S	entropy	[J/(mole K)]
T	temperature	[°C]
U	superficial gas velocity	[m/s]
y	mole fraction	[-]

### Greek

ε	bed voidage	[-]
σ	stress	[N/m <sup>2</sup> ]
ρ	density	[kg/m <sup>3</sup> ]
φ	flow rate	[kmol/s, kg/s]

**Subscripts**

0	reference conditions
ads	adsorber
m	mass
min	minimal
mol	molar
p	particle
reg	regenerator
s	sorbent
t	terminal

**References**

- Bell, A. T., Manzer, L. E., Chen, N. Y., Weekman, V. W., Hegedus, L. L., Pereira, C. J., "Protecting the environment through catalysis", *Chem. Eng. Progr.*, 91 (February), 26-34 (1995).
- Borio, D. C., Kingston, W. H., "Efficient and cost effective NO<sub>x</sub> and SO<sub>2</sub> removal from flue gases with SNOX process", in: *Proceedings of the 5th Conference on Processing and Utilization of High-Sulfur Coals*, Elsevier, Amsterdam (1993).
- Cichanowicz, J. E., Dene, C. E., DePriest, W., Gaikwad, R., Jarvis, J., "Engineering Evaluation of Combined NO<sub>x</sub>/SO<sub>2</sub> Controls for Utility Application", EPRI, USA (1991).
- Davies, C., Fenton, K., "Particle size effects in the discharge of fluidized solids through orifices and vertical slots", in: *Proceedings of the International Symposium of the Engineering Foundation, Fluidization VIII*, Tours, France, 1059-1066 (1995).
- Gutberlet, H., Schallert, B., "Selective Catalytic Reduction of NO<sub>x</sub> from coal fired power plants", *Catal. Today*, 16(2), 207-236 (1993).
- Hinderink, A. P., Kerkhof, F. P. J. M., Lie, A. B. K., Swaan Arons de, J., Kooi van der, H. J., "Exergy analysis with a flowsheeting simulator—I. Theory; Calculating exergies of material streams", *Chem. Eng. Sci.*, 51 (20), 4693-4700 (1996).
- Korbee, R., "Regenerative desulfurization in an Interconnected Fluidized Bed system", PhD thesis, Delft University of Technology, Delft, The Netherlands (1995).
- Korbee, R., Snip, O. C., Schouten, J. C., Bleek van den, C. M., "Rate of solids and gas transfer via an orifice between partially and completely fluidized beds", *Chem. Eng. Sci.*, 49 (24B), 5819-5832 (1995).
- Kunii, D., Levenspiel, O., "Design for physical operations", Chapter 16, in: "Fluidization Engineering", 2nd Ed., Butterworth-Heinemann, 397-427 (1991).
- Leonard, C. A., Haslbeck, J. L., Friedrich, J. J., Woods, M. C., "NOXSO process economics", Presented at the conference on Comparative Economics of Emerging Clean Coal Technologies III, (1994).
- Loë de, C. J. B., "Exergy analysis of combined NO<sub>x</sub> and SO<sub>2</sub> removal from flue gas: foundation, application and evaluation", MSc thesis, Delft University of Technology (1996).
- Ma, W. T., Haslbeck, J. L., Neal, L. G., Yeh, J. T., "Life Cycle Test of the NOXSO SO<sub>2</sub> and NO<sub>x</sub> Flue Gas Treatment Process: Process Modelling", *Sep. Techn.*, 1, 195-204 (1991).
- Ma, W. T., Haslbeck, J. L., "NOXSO SO<sub>2</sub>/NO<sub>x</sub> Flue Gas Treatment Process: Proof-of-Concept Test", *Env. Progr.*, 12(3), 163-168 (1993).
- Ma, W. T., Chang, A. M., Haslbeck, J. L., Neal, L. G., "NOXSO SO<sub>2</sub>/NO<sub>x</sub> Flue Gas Treatment Process Adsorption Chemistry and Kinetics", *AIChE Symp. Ser.*, 91 (309), 18-31 (1995).
- Papa, G., Zenz, F. A., "Optimize performance of fluidized-bed reactors", *Chem. Eng. Progress*, April, 32-36 (1995).

## Chapter 7

---

- Snip, O.C., Woods, M., Korbee, R., Schouten, J.C., Bleek van den, C.M., "Regenerative removal of  $\text{SO}_2$  and  $\text{NO}_x$  for a 150 MWe power plant in an Interconnected Fluidized Bed facility", *Chem. Eng. Sci.*, 51A (10), 2021-2029 (1996).
- Snip, O.C., Korbee, R., Schouten, J.C., Bleek van den, C.M., "The influence of hydrodynamics on the performance of an Interconnected Fluidized Bed system for regenerative desulfurization", *AIChE Symp. Ser.*, 91 (308), 82-92 (1995).
- Szargut, J., Morris, D.R., Steward, F.R., "Exergy analysis of thermal chemical and metallurgical processes", Hemisphere Publishing, New York (1988).
- Woods, M., "Personal Communication", NOXSO Corporation, Bethel Park, PA, USA (1996).
- Yeh, J.T., Ma, W.T., Penline, H.W., Haslbeck, J.L., Joubert, J.I., Gromicko, F.N., "Integrated testing of the NOXSO Process: Simultaneous Removal of  $\text{SO}_2$  and  $\text{NO}_x$  from Flue Gas", *Chem. Eng. Comm.*, 114, 65-88 (1992).
- Zhang, J.Y., Rudolph, V., "Effect of Shear Friction on Solid Flow through an Orifice", *Ind. Eng. Chem. Res.*, 30 (8), 1977-1981 (1991).



# Chapter 8

## Outlook and applications of IFB technology

---

### 8.1 General design and operational considerations

In general, the IFB reactor consists of fluidized bed reactor compartments and transport compartments that are successively connected by means of orifices and weirs. See Figure 2.1. Kinetics of the gas-solids reactions or solid catalyzed gas-phase reactions and mass transfer between gas and solids determine the design of the fluidized bed reactor compartments. Designing fluidized bed reactors is extensively discussed in textbooks such as Geldart (1986) and Kunii and Levenspiel (1991) and will therefore not be treated.

In chapters 5 and 6 of this thesis it was shown that IFB (chemical) reactor performance depends to a large extent on the hydrodynamics of the IFB system. The term hydrodynamics refers to those phenomena that determine the solids distribution and the Circulation Rate of the Solids (CRS) in the IFB reactor. The hydrodynamic parameters can be subdivided in design and operational parameters:

#### Design parameters:

1. **particle properties:** density, size (and size distribution), sphericity and frictional properties;
2. **IFB geometry:** orifice size, weir height and width, bed diameter and sizes of the respective compartments.

#### Operational parameters:

3. **gas velocities** to the compartments and
4. **total IFB bed mass.**

#### *Design*

The IFB reactor system should be designed such that it is possible to control the CRS through the IFB reactor by means of the hydrodynamic operational parameters (such as the gas velocity). By means of mathematical modelling and experimental confirmation, see chapters 3 and 5 respectively, it was shown that this can be achieved by limiting the solids flow through one of the connecting orifices.

The particle properties of the solids that are used in the IFB reactor will be mainly determined by the desired fluidization characteristics in the fluidized bed compartments. These considerations are not specific for the IFB reactor and are also treated in the above mentioned textbooks.

## Chapter 8

---

The influence of the IFB sizes is most importantly related to the connecting orifice. The size of the orifice clearly influences the CRS in the IFB system. The solids flow rate through the orifice as a function of the pressure drop (or driving force) increases proportional to the orifice cross-sectional area. Depending on the required CRS for a specific application, the size of the orifice can be determined by means of solids flow relationships that were developed and described in chapter 2.

The shape of the orifice can be of importance when gas transport that accompanies the solids flow needs to be minimized. This is however only of importance in case of a small scale IFB facility or in processes in which the CRS is small. In those cases, the orifice size will be relatively small compared to the particle size. See chapter 2.2 (non-mechanical valves) for a more detailed analysis of this subject.

The position of the orifice and in particular the height relative to the distributor plate can be of influence with respect to the CRS in the IFB reactor. Depending on the pressure gradients at both sides of the orifice, this height should be minimized or maximized with respect to the optimum driving force for solids flow. In general, the position of the orifice should be chosen such that no short-circuiting will be created. This, however, depends also strongly on the mixing characteristics and average residence time in the reactor.

The design and scale-up of IFB reactors can be compared to 'normal' fluidized bed reactors. All aspects that need to be considered for fluidized bed reactor design do also apply for IFB reactors. Additional attention needs to be given to the solids flow between the compartments. Solids flow over the weir (from a high velocity upflowing bed to a low velocity downflowing bed) and the residence time distribution in large IFB compartments are the main aspects of the IFB reactor that will be sensitive to its size and are therefore of importance in scaling of IFB reactor systems.

An important effect concerning freeboard pressures was identified by Ishida and Shirai (1976) who studied the equilibrium bed heights between a fixed and a fluidized bed. Their experimental set-up was similar to the IFB system discussed in this thesis. The main difference was that the bed columns were contracted at the gas exit. It was therefore possible to analyze the pressure balances and the effect of contracting the bed columns at the gas exit. In the IFB modelling and experimental work presented in this thesis, the freeboard pressures in the beds that are connected by means of an orifice were equal ( $\Delta P_{\text{freeboard}}=0$ ). Whether this difference in freeboard pressure does influence the CRS through the IFB reactor depends on the magnitude of the difference in pressure drop between the freeboards and the pressure drop across the orifice.

Depending on downstream equipment, the influence of freeboard pressure difference can be estimated during stationary and non-stationary operation of the IFB reactor. This effect could influence the IFB reactor design with respect to bed heights and connecting orifice sizes if one wants to minimize the freeboard influence on IFB hydrodynamics.

### *Operational*

As shown above, freeboard pressure differences due to downstream equipment specifications can seriously affect the IFB hydrodynamics. If one wants to minimize the influence of freeboard pressure differences in an IFB system, operation of the process should be such that the freeboards are controlled at equal pressure. In that case, the IFB hydrodynamics determine the CRS through the IFB system. This mode of operation is further analyzed since it was shown that the IFB reactor hydrodynamics can be well controlled by means of manipulation of the IFB hydrodynamic operational parameters.

The dynamic IFB simulations described in chapter 3 and the experiments described in chapter 5 showed that the 4-bed IFB reactor can be operated such that the solids flow through one of the orifices is rate limiting. In that case, the CRS in the IFB reactor can be controlled by means of the gas velocity to one of the transport compartments. To achieve this condition, the gas velocity to the rate limiting dense bed should be somewhat below the minimum fluidization velocity. The gas velocity to the other transport compartment should be somewhat higher than the gas velocity to the rate determining transport bed. The latter is necessary to ensure a higher driving force across the connecting orifice. For more details on this analysis, reference is made to chapter 3.2.3.

It was further shown that an optimum IFB bedmass exists with respect to a maximum CRS. Changing the solids hold-up of the IFB system will thus influence the CRS. This effect should be taken into account and can be used to control the CRS during operation of the IFB reactor.

The solids distribution and CRS in the IFB reactor can be controlled by means of the operational hydrodynamic parameters. The combination of reaction parameters (inlet gas-phase concentrations) and hydrodynamics will finally determine the IFB chemical reactor performance.

## **8.2 Applications of IFB technology: processes with solids circulation**

### **8.2.1 Reaction-regeneration processes**

In general, as mentioned in chapter 1, possible applications of IFB technology can be found in processes in which a solid material needs to be transported between fluidized bed type reactors. In case of a four-bed IFB reactor, the two upflow beds can act as chemical reactors and the two downflow beds can be used for transport of solids and separation of the chemical environments of the two fluidized bed reactors.

Potential applications can generally be found in processes in which:

- ▶ a sorbent needs to be regenerated,
- ▶ the catalyst deactivates fast, and
- ▶ intermediates are the desired product.

Typical examples of sorbent regenerative processes can be found elsewhere in this thesis. The developments of regenerative desulfurization during fluidized bed combustion of coal (SO<sub>2</sub> removal) are described in chapter 1.3. Experimental results with respect to this process were obtained in a small scale IFB pilot plant facility. This facility was designed and constructed at Delft University of Technology (DUT) for the investigation of regenerative desulfurization, by means of a synthetic sorbent, during Fluidized Bed Combustion (FBC) of coal (see chapter 5 of this thesis).

It was experimentally shown (by means of simulated FBC gas) that the IFB reactor is suitable for regenerative desulfurization during atmospheric FBC of coal. This process is economically attractive in comparison to other types of fluidized bed combustion for plant sizes smaller than 25-50 MWe (Anthony, 1996). The size of the combustor in an IFB reactor can be optimized because the sorbent conversion can to a certain extent be considered as a degree of freedom. Korbee *et al.* (1993) showed that this can significantly reduce the capital charges.

The IFB concept combines a compact reactor system and a minimum solids waste stream. Further, the sulfur is regenerated and processed to a desired product (for example elemental sulfur or sulfuric acid). The NO<sub>x</sub> can be thermally reduced to nitrogen by means of ammonia injection in the freeboard of the combustor (Duo, 1990). This eliminates the need of expensive selective catalytic reduction of the large flue gas stream.

These advantages and considerations show that a combination of the IFB reactor and regenerative desulfurization by means of a synthetic sorbent can be particularly attractive for a *small scale* application of fluidized bed combustion of coal.

Another example of a regenerative process is the NOXSO process described in chapter 7. The IFB technology can also be applied in regenerative H<sub>2</sub>S removal from coal gas originating from a coal gasifier. Wakker *et al.* (1993), developed a dry sorbent (based on MnO and/or FeO supported by alumina) that can be used for this purpose. Transport of sorbent between capture and regeneration compartments can be achieved by means of IFB reactor technology (see Bakker *et al.*, 1996).

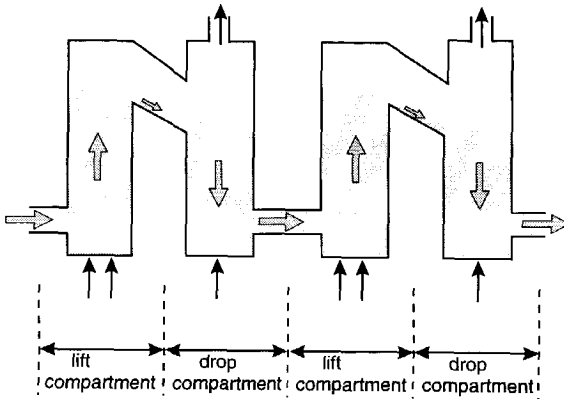
Other interesting processes in which IFB reactor technology can be considered as an alternative for conventional reactors are listed and discussed below.

### ***Fluidized Catalytic Cracking and related oil processes***

A well known example in this field of chemical engineering is Fluidized Catalytic Cracking (FCC) of crude oil to gasoline. King (1992) and Avidan (1997) provide an overview of developments of the process and its reactor technology. From fluidized bed reactors, riser reactor technology was developed. This type of reactor has some important advantages over fluidized beds. The residence time of the catalyst is shorter and the spread in residence time is less. This will positively affect the reactor performance.

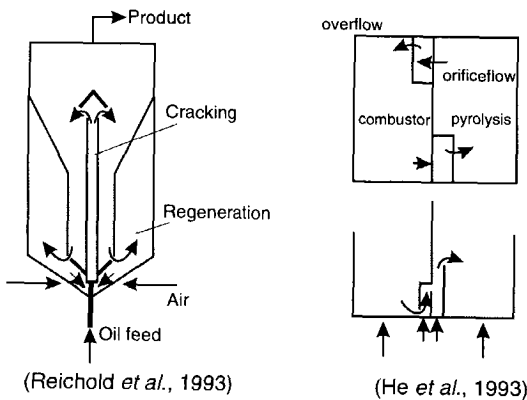
Despite the advantages, it was also appreciated that riser technology has some disadvantages. For example, the attrition of the catalyst and the erosion of the reactor vessels are important concerns of the FCC process. Therefore other type of reactors are still under investigation. Zhu and Wei (1995) report on developments of downer reactors in which the oil vapour is contacted with the cracking catalyst that flows counter-current to the upflowing oil gas-phase.

In this reactor, the contact time between oil and catalyst can be even further reduced compared to a riser reactor, minimizing coke formation.



**Figure 8.1** Low profile fluid catalytic cracking apparatus (by Thacker *et al.*, 1990). Solids circulation is established for the purpose of fluid catalytic cracking by means of connecting 'drop' and 'lift' compartments. Multiple compartments are used for cracking and regeneration.

Identical advantages are claimed by Thacker *et al.* (1990) who developed a so-called low profile fluid catalytic cracking apparatus. This reactor consists of a succession of low profile catalyst chambers that are alternately connected in sequence by openings below the catalyst level and thereabove (see Figure 8.1). This apparatus strongly resembles the IFB reactor. The catalyst residence time in the reactor is narrow due to the number ( $> 10$ ) of well mixed compartments in series. According to Thacker *et al.* (1990) this results in a compact reactor and improved reactor performance compared to a riser reactor in combination with a fluidized bed regenerator.



**Figure 8.2** Schematic representations of Internally Circulating Fluidized Beds. Reactor configurations for upgrading of heavy oils (Reichold *et al.*, 1993) and oil shale retort (He *et al.*, 1993).

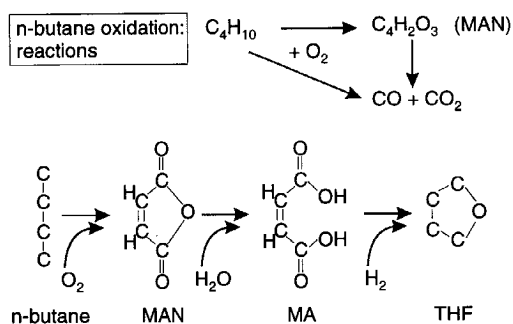
Other developments in this area are referred to as Internally Circulating Fluidized Beds (Milne *et al.*, 1992; Reichold *et al.*, 1996). See Figure 8.2 for a schematic representation of this type of reactor. According to the authors and experimentally shown by Reichold *et al.* (1996) this reactor is suitable for upgrading of heavy oils. The main advantage of these circulating fluidized bed systems lies in their compact design. It is further reported that this reactor configuration is also suitable for the cracking or upgrading of oils from biological sources and of pyrolysis oils.

The above mentioned oil cracking or upgrading processes have in common that they can also be carried out in an IFB reactor system. Depending on the specific application, a detailed analysis should reveal whether it is economically attractive to apply the IFB reactor.

Another dense-phase circulating fluidized bed system was investigated by He *et al.* (1993) for the use of a continuous oil shale retort. See Figure 8.2, for a schematic representation of this reactor system. In this application, one compartment is used for the combustion of the excess carbon off the shale. The other compartment, fluidized by recycled product gas, acts as the pyrolysis reactor where the oil is distilled off. For this process, the IFB reactor seems to be a suitable candidate because of the strong similarity with the circulating fluidized bed reactor presented by He *et al.* (1993).

### Selective oxidation of *n*-butane to maleic anhydride

The production of maleic anhydride (MAN) as an intermediate in the manufacturing of tetrahydrofuran (THF) was an important subject of investigation for many years (Lerou and Mills, 1993). It appeared to be most advantageous to use *n*-butane as a feedstock. The butane is catalytically oxidized to MAN. The reaction scheme from *n*-butane to THF is shown in Figure 8.3.

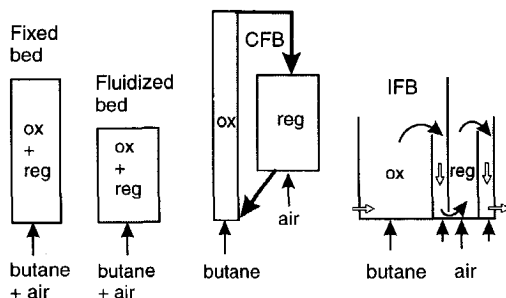


**Figure 8.3** Reaction network from *n*-butane to maleic anhydride (MAN), maleic acid (MA) and tetrahydrofuran (THF).

The oxidation step in this process represents an important class of industrial oxidation processes that have a number of common features:

- ▶ the reactions are highly exothermal,
- ▶ an explosive mixture can be formed by the reactants and air, and
- ▶ the chemistry needs to be halted at the right step.

Industrial oxidation processes are reviewed from the standpoint of reactor technology by Mills *et al.* (1995). Three main types of reactors are described that can be used for selective oxidation of butane. In Figure 8.4, these reactors are shown together with the IFB reactor. The fixed bed or multi-tubular and fluidized bed reactor are the conventional reactors being used for butane oxidation. Butane and air are brought in contact in the presence of a Vanadium-Phosphorous-Oxide (VPO) catalyst. As shown in Figure 8.3, the danger is present that butane is directly oxidized to the undesired CO and CO<sub>2</sub> and MAN can be further oxidized. This is especially the case when free gas phase oxygen is in contact with butane.



**Figure 8.4** Possible reactor configurations for selective butane oxidation. (ox= oxidation of butane and reg= regeneration of the oxidation catalyst)

The most important innovation of the recirculating solids reactor or Circulating Fluidized Bed (CFB) by Du Pont (Mills *et al.*, 1995) is the fact that the catalyst is regenerated in a fluidized bed regenerator. The reactant is selectively oxidized in a separate transport bed or riser reactor. The reduced catalyst from the riser is separated from the product gas, stripped from any carbonaceous species and returned to the regenerator. The recirculating catalyst remains in a transient cyclic state. Much higher (70-80%) selectivities, compared to conventional fixed and fluidized bed reactors (40-50%), can be obtained by means of the new reactor technology.

The IFB reactor is added to the reactor technologies to be compared on the basis of important features that determine the attractiveness of a certain reactor type. This is represented in Table 8.1.

**Table 8.1** Comparison of reactor technologies suitable for butane oxidation.

A + and -, respectively stand for a positive and negative property of the reactor type compared to the others.

System parameter	Fixed bed	Fluidized Bed	CFB	IFB
heat removal	-	+	+	+
maximum feed conc. %	1.8-2.1	4	> 10	> 15
pressure drop	--	+	+/-	+
catalyst attrition	+	-	--	-
selectivity	-	-	+	+

It is clear that the CFB (riser/regenerator) and IFB reactor offer important advantages with respect to selectivity due to the separate catalyst reoxidation in a regenerator. Possible advantages of the IFB reactor compared to the CFB reactor configuration are:

1. The compressor costs can be less for the IFB reactor. In the riser of the CFB reactor, the catalyst needs to be accelerated to high solids transport velocities and height. This will give rise to pressure drops that can be relatively higher than for a fluidized bed compartment in the IFB reactor.
2. The butane feed concentration can be increased to higher values in the IFB reactor than in the CFB riser. The limited solids entrainment rate is often referred to as the saturation carrying capacity of the gas phase. The limitations are encountered in this process due to the fact that a large amount of catalyst is needed to oxidize butane. As a general guideline it is stated that only 2 gram of butane can be converted by 1000 g of catalyst (Bej and Rao, 1992). For the riser reactor, this results in a maximum butane feed concentration that will be somewhat less than for the IFB reactor. This idea is confirmed by Golbig and Werther (1996) who found by means of process simulations that the catalyst circulation rate is limiting for the butane conversion in the riser.
3. The catalyst attrition will be more severe in a riser than in a fluidized bed reactor. To overcome this, Du Pont (Lerou and Mills, 1993) developed a method of preparation for an attrition resistant VPO catalyst. The catalyst is more or less encapsulated in a micro-porous silica shell. Although this innovation can solve the attrition problem, it remains a major concern in riser reactor technology. In a fluidized bed (IFB) reactor this problem will be less.

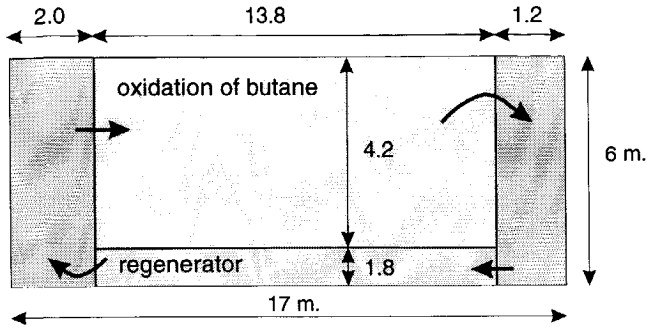
To investigate the possibilities of IFB reactor technology with respect to butane oxidation, a preliminary design was made for the production of THF (Maaskant and Verlaan, 1994). This design is equivalent in size (45.000 ton/year) compared to the commercial THF plant mentioned by Lerou and Mills (1993).

The IFB reactor was designed according to the oxidation kinetics of Sharma *et al.* (1991) and the three-phase fluidized bed reactor model of Kunii and Levenspiel (1991) consisting of bubble, cloud and emulsion phase. The oxidation kinetics were fitted to the experimental results by Contractor (1991).

Reactor calculations were performed and the dimensions of the IFB reactor and the Circulation Rate of Solids were determined. By means of the simplified solids flow model (see chapter 7.3.2), the transport compartments and size of the IFB reactor were fixed. A detailed description of the IFB reactor design and the plant for THF production is given by Maaskant and Verlaan (1994). The main sizes are shown in the cross-sectional view of the IFB reactor in Figure 8.5.

The IFB reactor design for selective butane oxidation showed that technically, the IFB reactor can be used for this oxidation process. In order to make the right reactor selection, more investigation is needed that economically quantifies the possible advantages of the IFB reactor. Du Pont developed a riser/regenerator reactor system for selective oxidation. A 45.000 ton/year THF plant, applying the CFB reactor for butane oxidation, was constructed in Asturias, Spain (ECN, 1996). The IFB reactor seems nevertheless an interesting option for butane oxidation technology and for this type of reactions in general.





**Figure 8.5** Cross-sectional view of the IFB reactor that was designed for the selective butane oxidation to maleic anhydride as an intermediate for the production of tetrahydrofuran. The reactor was sized for a plant size of 45,000 ton THF/year.

#### More reaction-regeneration processes

Potential applications for a CFB reactor are listed by Berruti *et al.* (1995) and Zhu and Bi (1995). The processes mentioned can also be considered as possible applications for the IFB reactor. This is illustrated by the above mentioned analysis of selective butane oxidation to maleic anhydride.

Many processes have been patented that claim substantial advantages of the use of circulating fluidized bed type reactors over more conventional fixed and fluidized beds. They have however not been commercialized because of a number of factors associated with new process development (Berruti *et al.*, 1995): scale-up uncertainty, process equipment complexity, need for attrition resistant catalyst, and large scale requirements to justify process economics.

It is interesting however to identify the possible advantages of IFB reactor technology for a number of processes. The use of an IFB reactor becomes particularly attractive when a high solids/gas ratio is required to perform a specific reaction.

Potential applications for IFB reactor technology include partial oxidation of alkanes and alkenes, epoxidation, ammoxidation and oxidative dehydrogenation (Berruti *et al.*, 1995; Zhu and Bi, 1995). Examples of these processes are:

#### Reaction

- ▶ phthalic anhydride from *o*-xylene
- ▶ acrolein from propylene
- ▶ acrylonitrile from propylene
- ▶ benzonitrile from toluene and acrylonitrile from propylene
- ▶ ethylene oxide from ethylene
- ▶ ethyl benzene to styrene
- ▶ ethylene from ethane
- ▶ hydrogen chloride to chlorine

#### Reference

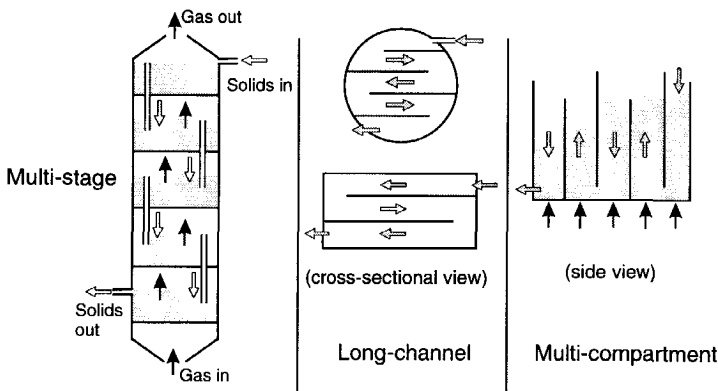
- Gelbein (1981)
- Patience and Mills (1994)
- Beuther *et al.* (1978)
- Gianetto *et al.* (1990)
- Park and Gau (1986)
- Debras *et al.* (1992)
- Coudurier *et al.* (1993)
- Mortensen *et al.* (1996)

For the above mentioned processes, it could be attractive to apply the IFB reactor. A detailed analysis should reveal whether the technical advantages can make the processes economically more attractive.

### 8.2.2 Processes for physical operation

Physical operation of a fluidized bed generally concerns the treatment of a solid material by means of a gas stream. Examples of such processes are drying, heating, cooling, coating and adsorption. Another typical example, investigated by Martin-Gullon *et al.* (1995), is the activation of carbon.

In all these processes *counter-current operation* is preferred with respect to the effectiveness of the process that needs to be carried out. In this mode of operation the optimum driving force for the desired physical transport phenomenon is achieved. In a counter-current contacting mode, the solids generally flow downwards against the upflowing gas. The apparatus will in most cases be equipped with multiple stages (see Figure 8.6).



**Figure 8.6** Three types of fluidized beds for physical operation. The contacting pattern is counter-current (*multi-stage*) or cross-flow (*long-channel* and *multi-compartment*).

For a one-stage facility, the solids will approximate mixed flow. The spread in Residence Time Distribution (RTD) and subsequent product distribution will be significant. In a multi-stage fluidized bed, consisting of a number of mixed stages in series, the spread in RTD will be limited resulting in a more uniform product.

In practice however, physical operations (especially drying) are often carried out in so-called cross-flow fluidized beds. The reason is that this type of fluidized is more easily operated than the multi-stage fluidized bed (Kunii and Levenspiel, 1991).

The cross-flow devices can be subdivided in two classes: long-channel and multi-compartment beds (see Figure 8.6). The advantages compared to one-stage physical operation are the increased efficiency of the process and the more uniform product distribution.

The so-called long-channel beds are described by Krishnaiah *et al.* (1982). In this type of facility, the solids enter at one side of the bed and are moving in forced plug-flow, due to vertical plates that are mounted at the gas distributor plate, to the other side of the bed.

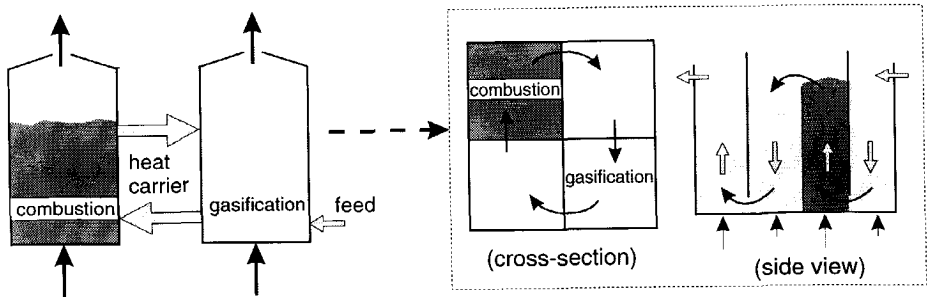
Another example and direct application of an IFB reactor is the multi-compartment cross-flow device. See for example Beran and Lutchka (1975) and Ormós *et al.* (1975). In this type of apparatus, the solids are forced to circulate through a concatenation of compartments. The driving force is, similar to the IFB reactor, the difference in aeration. In the same manner, the IFB system can therefore also be used as a cross-flow fluidized bed for physical operation.

### 8.2.3 Combined gasification and novel combustion processes

Fluidized bed combustion is a suitable combustion technique for many fuels such as coal or other alternative fuels because of its fuel flexibility. This originates from the fact that in the combustor, the fuel is present to a low level and is burnt in the mass of a thermally inert bed material (typically sand). Anthony (1995) provides an overview of alternative solid fuels that are suitable for fluidized bed combustion. Examples are paper waste, petroleum coke, solid and industrial wastes and agricultural/food processing wastes.

The inert material that is present in a fluidized bed combustion chamber can also be used as a heat-carrier and transported to a reactor in which a heat consuming process such as gasification takes place.

Kunii (1980) proposed and investigated the integration of the two fluidized beds (combustor and gasification reactor) into a single reactor vessel. This vessel was separated by means of two partition plates through which the thermal energy could be transferred from the combustor to the gasifier. This idea is identical to the IFB reactor concept. See Figure 8.7 for a schematic representation of the combustion-gasification concept and the integration of the two processes in one reactor vessel. In many cases, the transportation of the heat carrier between gasifier and combustor is accompanied by the non- or difficult gasifiable products. These products are converted in the combustion compartment. By means of combustion, the thermal energy is produced that is used in the gasification process.



**Figure 8.7** Schematical representation of a combustion-gasification process and its integration in a single reactor vessel. An inert material (typically sand) is circulated between combustion and gasification section.

The concept of combustion-gasification can be applied to a number of solid fuels such as biomass, oil products, several types of waste from various sources or coal (Masson, 1989; Lin *et al.*, 1995). Masson (1989) further describes the development of an integrated combustor-gasifier reactor. The reactor concept is identical to the IFB reactor system. Especially biomass seems to be an attractive fuel in a combined combustion-gasification or pyrolysis process with respect to the environmental impact and availability. Various options are available with respect to the reactor configuration (Wagenaar *et al.*, 1994) and combined processes (Anthony, 1995; Masson, 1989; Stassen, 1994).

A process for regenerative desulfurization during gasification of sulfur rich fuel oil is presented by McMillan and Zoldak (1977). The sulfur that is released as  $H_2S$  during gasification (at 850 °C) is captured by limestone. The sulfated limestone is transported to a high temperature (1050 °C) combustion chamber in which the limestone is regenerated and a sulfur rich gas stream is produced. This is a typical example of the application of IFB reactor technology for regenerative desulfurization. The process that was developed and described by McMillan and Zoldak (1977) could be seriously improved if a synthetic sorbent (as described in chapter 5 of this thesis) was used. The loss of sorbent due to attrition is reduced and regeneration can be carried out at a temperature that is equivalent to the gasification temperature of approximately 850 °C.

Another circulating fluidized bed system is proposed by Yuen *et al.* (1993) that is suitable for the combustion of high moisture wastes. Special attention is given to the combustion of paper de-inking waste. In this IFB like reactor configuration, a downflow compartment is used to dry the solids. After drying, the solids are transported to a fluidized combustion compartment. A heat carrying material (sand) is transported from combustion to drying compartment to provide the heat that is necessary for the drying process.

### 8.3 Frequently asked questions: with answers

A number of important features of the IFB reactor system is identified in the top-10 of Frequently Asked Questions (FAQ's). The FAQ's were raised by people who were confronted with the IFB reactor system during presentations at conferences or other occasions. The list of FAQ's is given below. It is believed that this will give a direct insight in relevant aspects of the IFB reactor. The answers refer to the appropriate parts of this thesis for more details on the subject involved.

#### 1. How is the CRS controlled and what is the influence on the process?

The CRS in the IFB reactor can be controlled by means of manipulation of the gas velocity to one of the transport compartments. The change in CRS can be achieved without actually disturbing the chemical processes taking place in the fluidized bed compartments. This is explained in chapter 2.1. A limited influence is expected of gas transfer from dense to lean bed. See also question number 3.

### 2. Why did you choose to make your reactor geometry square?

The reason is constructional simplicity. It is not a specific feature of an IFB reactor as shown by Kunii (1980) who introduced an IFB system consisting of a circular vessel divided in four sections by means of partition plates. Further, it can be stated that square fluidized beds are commonly used, especially for high temperature applications. See for example experimental data listed by Kunii and Levenspiel (1991).

### 3. Don't you have the problem of gas leakage and subsequent unwanted reactions?

Gas leakage is inherent to solids circulation systems. It is therefore stated that gas transport accompanying the solids flow in the IFB reactor is not more than in other solids circulation systems. See chapter 2.2, non-mechanical valves. In the small scale IFB pilot plant facility (chapter 5), it was experimentally shown that no problems were encountered with respect to hydrogen and air present in one reactor vessel.

### 4. Instead of the trend of using CFB reactors operated at high gas velocities, the IFB reactor operates at moderate gas velocity. Why?

This question refers to the main advantage of the IFB reactor system compared to other CFB type reactors. In an IFB system, the transport velocities of the solid material will be an order of magnitude (factor 10) smaller than in a CFB riser. This will cause a significant decrease in attrition of the solid material (sorbent or catalyst) that is circulating between reactor vessels or compartments.

### 5. In a CFB it is possible to change the inventory of the reactor during operation. Is this also possible in the IFB reactor?

In an IFB reactor this is possible as well. As long as the orifice flow through one of the connecting orifices is rate determining, the inventory of the system can be changed during operation while maintaining an equivalent CRS. Weirflow can become limiting when the bedmass decreases to a lower limit. Obviously, an upper limit of solids hold-up is determined by the reactor height. Within these limits it is possible to change the inventory of the IFB system without disturbing the process with respect to the CRS. See chapter 3 for more details on this subject.

### 6. Why do you use the upflow (and not the downflow) compartments as chemical reactors?

Which type of compartment is used as a chemical reactor depends on the requirements that are determined by the process itself. Depending on its specifications, a reaction needs to be carried out in a fluidized bed (mixing or heat transfer) or dense transport bed (counter-current, in case of physical operation, see chapter 8.2.2). Accordingly, the other type of compartment will function as a transport compartment. From an operational point of view it is preferred to use a dense downflowing bed for CRS controlling purposes (chapter 3).

### 7. How good are your solids flow models at hot conditions and at larger scale?

The solids flow models were developed from experimental work in cold IFB facilities (chapter 2). The models were subsequently applied for predicting the CRS in the small scale high-temperature IFB facility. For this purpose, temperature influence was taken into account (see chapter 5.2). This proved to result in a reasonable estimation of the CRS and it can therefore be concluded that the solids flow model can be used for high temperature application.

The design and scale-up of IFB reactors can be compared to that of 'normal' fluidized bed reactors. All aspects that need to be considered for fluidized bed reactor design do also apply for IFB reactors. Solids flow over the weir from a high velocity (upflowing) bed to a low velocity (downflowing) bed and the residence time distribution in large IFB compartments are the main aspects of the IFB reactor that will be sensitive to scale effects.

### 8. What is the controllability of the CRS in an IFB reactor?

The CRS can be controlled between zero and a maximum solids 'flow. The maximum CRS that can be attained is determined by the IFB design parameters. The actual CRS can be manipulated by means of the independent operational parameters: total IFB bedmass and the gas velocity to one of the transport compartments. The aspects of controllability are treated in chapter 3.2.

### 9. Is it possible to adjust the gas and solids residence times independently?

This is certainly possible. In chapter 3.2, it is shown that the influence of the gas velocity (gas residence time) to the upflow fluidized compartments on the CRS (solids residence time) is small (<5%). This is true providing that the orifice flow through one of the connecting orifices is rate determining.

### 10. What is really new about the IFB reactor?

In an IFB reactor, a gas-solids regenerative process can be continuously operated in a compact reactor with a minimum attrition of the recirculating solid material. The IFB reactor is particularly new with respect to the reactor technology and mode of operation that is currently applied for a number of applications (fixed beds in swing operation and riser-regenerator reactor systems). Potential and new applications are identified in chapter 8.2.

References

- Anthony, E.J., "Fluidized bed combustion of alternative solid fuels; status, successes and problems of the technology", *Prog. Energy Combust. Sci.*, 21, 239-268 (1995).
- Anthony, E.J., "Size of bubbling fluidized beds", Personal Communication (1996).
- Avidan, A.A., "Fluid catalytic cracking", Chapter 13 in "Circulating Fluidized Beds" (Ed. Grace, J.R., *et al.*), Chapman & Hall, London, 466-487 (1997).
- Bakker, W.J.W., Kapteijn, F., Moulijn, J.A., Korbee, R., Liang, B., Snip, O.C., Schouten, J.C., Bleek van den, C.M., "Regenerative sulphur capture in gases from coal gasifiers", Final report for the Joule-II Clean Coal Technology Contract No. JOU2/CT93/043, Delft University of Technology, The Netherlands (1996).
- Bej, S.K., Rao, M.S., "Selective oxidation of n-butane to maleic anhydride: 4", *Ind. Eng. Chem. Res.*, 31, 2075-2079 (1992).
- Beran, Z., Lutcha, J., "Optimising particle residence time in a fluidised bed drier", *Chem. Eng.*, 303, 678-681 (1975).
- Berruti, F., Chaouki, J., Godfroy, L., Pugsley, T.S., Patience, G.S., "Hydrodynamics of Circulating Fluidized Bed Risers: A Review", *Can. J. Chem. Eng.*, 73, October, 579-602 (1995).
- Beuther, H., Innes, R.A., Swift, H.E., "Process for preparing acrylonitrile", U.S. patent 4,102,914 assigned to Gulf Research and Development Co., July 25 (1978).
- Contractor, R.M., "Vapour phase catalytic oxidation of butane to maleic anhydride", U.S. patent 5,021,588 assigned to Du Pont, June 4 (1991).
- Coudurier, G., Decottignies, D., Loukah, M., Vadrine, J.C., "Vanadium and chromium based phosphates as catalysts for oxidative dehydrogenation of ethane", presented at the 13<sup>th</sup> North American Meeting of the Catalysis Society, Pittsburgh, PA, May 2 (1993).
- Debras, G.J., Grootjans, J., Delorme, L., "Process for the catalytic dehydrogenation of alkylaromatic hydrocarbons", European Patent No. 0 482 276 A1 (1992).
- Duo, W., "Kinetic studies of the reactions involved in selective non-catalytic reduction of nitric oxide", PhD thesis, Technical University of Denmark, Lyngby, Denmark (1990).
- ECN, "DuPont brings innovative THF technology onstream", *European Chemical News*, 2-8 September, 23 (1996).
- Gelbein, A.P., "Phthalic anhydride reaction system", U.S. Patent 4,261,899, assigned to Chem. Systems Inc., April 14 (1981).
- Geldart, D. (Ed.), "Gas fluidization technology", John Wiley & Sons Ltd., (1986)
- Gianetto, A., Pagliolico, S., Rovero, G., Ruggeri, B., "Theoretical and practical aspects of Circulating Fluidized Bed Reactors (CFBRs) for complex chemical systems", *Chem. Eng. Sci.*, 45, 2219-2225 (1990).
- Golbig, K.G., Werther, J., "Selective synthesis of maleic anhydride in a riser/regenerator system", in: CFB5; preprints of the 5th International Conference on Circulating Fluidized Beds, May 28 to June 1, Beijing, Peoples Republic of China, Pr15 (1996).
- He, Y., Rudolph, V., Nicklin, D.J., Chong, Y.O., "Circulating fluidized oil shale retort", *Fuel* 72(6), 879-883 (1993).
- Ishida, M., Shirai, T., "Equilibrium bed heights when a fluidized and a fixed bed are connected through an opening - effect of contracting the bed columns at the gas exit -", *J. Chem. Eng. Jpn.*, 9(3), 249-250 (1976).
- Korbee, R., Grievink, J., Schouten, J.C., Bleek van den, C.M., "Preliminary design of a 100 MWe power plant with regenerative desulfurization applying Interconnected Fluidized Bed technology", In: Proceedings of the 12th International Conference on Fluidized Bed Combustion of coal, Vol. 2, (Eds: Rubow, L., Commonwealth, G.), San Diego, USA, 1143-1151 (1993).

## Chapter 8

---

- King, D., "Fluidized Catalytic Crackers: an engineering review", In: Fluidization VII; Proceedings of the 7th Engineering Foundation Conference on Fluidization (Eds: Potter, O.E.; Nicklin, D.J.), Brisbane, Australia, 15-26 (1992).
- Krishnaiah, K., Pydisetty, Y., Varma, Y.B.G., "Residence time distribution of solids in multistage fluidisation", *Chem. Eng. Sci.*, 37, 1371-1377 (1982).
- Kunii, D., "Chemical reaction engineering and research and development of gas solid systems", *Chem. Eng. Sci.*, 35, 1887-1911 (1980).
- Kunii, D., Levenspiel, O., "Fluidization Engineering", 2nd Ed., Butterworth-Heineman, Chapters 2, 6 and 17 (1991).
- Lerou, J.J., Mills, P.L., "Du Pont butane oxidation process", in: Precision Process Technology, perspectives for pollution prevention, (Eds.: Weijnen, M.P.C., Drinkenburg, A.A.H.), Kluwer Academic Publishers, 175-195 (1993).
- Lin, W., Dam-Johansen, K., Bleek van den, C.M., "Novel designs of fluidized bed combustors for low pollutant emissions", in: Proceedings of the 13th ASME International Conference on Fluidized Bed Combustion (Ed.: Heinschel, K.J.), Orlando, FL, USA, 2, 1343-1349 (1995).
- Maaskant, E.A.R., Verlaan, M.L., "Tetrahydrofuran production with the Interconnected Fluidized Bed reactor from butane and air", Preliminary design report 3090, Delft University of Technology, Delft (1994).
- McMillan, R.E., Zoldak, F.D., "A discussion of the chemically active fluid bed process (CAFB)", paper prepared for the Conference on Frontiers of Power Technology, Oklahoma State University, Stillwater, Oklahoma, USA by Foster Wheeler Energy Corporation (1977).
- Masson, H.A., "The AVSA fluid bed combustor-gasifier project", Report for the Commission of the European Communities (Contract No ESE-R-087-B), University of Brussels, Belgium (1989).
- Martin-Gullon, I., Marcilla, A., Asensio, M., "Stable operating velocity range for multistage fluidized bed reactors with downcomers", *Powder Technol.*, 85, 193-201 (1995).
- Mills, P.L., Harold, M.P., Lerou, J.J., "Industrial oxidation processes", in: Catalytic oxidation principles and applications, NIOK, Netherlands Institute for Catalysis Research (Eds.: Sheldon, R.A., Santen van, R.A.), World Scientific, 291-369 (1995).
- Milne, B.J., Berruti, F., Behie, L.A. "The Internally Circulating Fluidized Bed (ICFB): A novel solution to gas bypassing in spouted beds", *Can. J. Chem. Eng.*, 70, 910-915 (1992).
- Mortensen, M., Minet, R.G., Tsotsis, T.T., Benson, S., "A two-stage cyclic fluidized bed process for converting hydrogen chloride to chlorine", *Chem. Eng. Sci.*, 51(10), 2031-2039 (1996).
- Ormós, Z., Csukás, B., Pataki, K., "Mehrzellen-Wirbelschicht Verfahren", *Chem. Anl. Verf.*, January, 49-52 (1975).
- Park, D.W., Gau, G., "Simulation of ethylene epoxidation in a multitubular transport reactor", *Chem. Eng. Sci.*, 143-150 (1986).
- Patience, G.S., Mills, P.L., "Modelling of propylene oxidation in a circulating fluidized bed reactor", in: New developments in selective oxidation II, (Eds.: Corberan, V.C., VicBellon, S.), Elsevier, New York, 1-18 (1994).
- Reichold, A., Hofbauer, H., Krobath, P.H., "Internally circulating fluidized bed as a reaction-regeneration system for catalytic cracking", in: CFB5; preprints of the 5th International Conference on Circulating Fluidized Beds, May 28 to June 1, Beijing, Peoples Republic of China, Pr18 (1996).
- Sharma, R.K., Cresswell, D.L., Neuson, E.J., "Kinetics and Fixed-bed reactor modeling of butane oxidation to maleic anhydride, *AIChE J.*, 37, 39-47 (1991).
- Stassen, H.E.M., "Biogas and biomass technology; energy generation from biomass in the Netherlands", *Renewable Energy*, 5 (II), 819-823 (1994).
- Thacker, M.B., Limburg, J.M., Memmott, V.J., "Low profile fluid catalytic cracking apparatus", U.S. patent 4,925,632, May 15 (1990).



## Outlook and applications of IFB technology

---

- Yuen, H.C., Chiu, J.H., Jukkola, G.D., Douglas, M.A., Morrison, S.A., Wong, S.Y., "Internal Circulation Fluidized Bed (ICFB) combustor", U.S. Patent 5,401,130 assigned to Combustion Engineering Inc., December 23 (1993).
- Wagenaar, B.M., Prins, W., Swaaij van, W.P.M., "Pyrolysis of biomass in the rotating cone reactor: modelling and experimental justification", *Chem. Eng. Sci.*, 49(24B), 5109-5126 (1994).
- Wakker, J.P., Gerritsen, A.W., Moulijn, J.A., "High temperature H<sub>2</sub>S and COS removal with MnO and FeO on gamma-Al<sub>2</sub>O<sub>3</sub> acceptors", *Ind. Eng. Chem. Res.*, 32, 139-149 (1993).
- Zhu, J-X., Bi, H-T., "Distinctions between low density and high density circulating fluidized beds", *Can. J. Chem. Eng.*, 73, October, 644-649 (1995).
- Zhu, J.-X., Wei, F., "Recent developments of downer reactors and other types of short contact reactors", In: *Fluidization VIII; Proceedings of the 8th Engineering Foundation Conference of Fluidization*, Vol. 2, Tours, France, 907-914 (1995).

---

## Samenvatting

Dit proefschrift behandelt de ontwikkeling van de 'Interconnected Fluidized Bed' (IFB) reactor technologie voor gas-vast regeneratieve processen. De IFB-reactor combineert een grote deeltjescirculatie met een minimale attritie. Een IFB-reactor-systeem bestaat uit meerdere fluïde bed reactoren die onderling zijn gekoppeld door middel van gefluïdiseerde (of beluchte) transportcompartimenten. De drijvende kracht voor deeltjestransport in de IFB-reactor berust op het toepassen van verschillende gassnelheden in de compartimenten. De deeltjes stromen beurtelings door een opening en via een overlooprand. Eén van de doelen in deze studie was het ontwerpen en bouwen van een IFB 'pilot plant' opstelling om de werking van het reactor-concept te testen. Een ander doel was de ontwikkeling van inzicht in de hydrodynamica (deeltjescirculatie en deeltjesverdeling) om te bepalen hoe IFB-reactoren moeten worden ontworpen en bedreven.

De chemische prestatie van de IFB-reactor hangt af van de hoeveelheid deeltjes die tussen de IFB-compartimenten circuleert, de CRS. In het algemeen hangt de CRS in een IFB reactor af van ontwerpparameters: 1. IFB-geometrie, 2. deeltjeseigenschappen, en van operationele parameters: 3. gassnelheden in de compartimenten en 4. de totale IFB-bedmassa.

De deeltjesstroming door de opening die twee compartimenten verbindt is in detail bestudeerd. Een algemeen stromingsmodel voor de stroming door een opening is geformuleerd op basis van de belangrijkste drijvende en weerstandskrachten. Dit macroscopische model is afgeleid op basis van microscopische beschouwingen van de stromingsverschijnselen. Het effectief doorstroomde deel van de opening wordt bepaald volgens de *lege-ring* benadering. De *gas-vast meesleepkracht* wordt beschouwd als de belangrijkste drijvende kracht voor deeltjesstroming. Het verschil in horizontaal gerichte *deeltjesspanning* tussen het beluchte transportcompartiment en het gefluïdiseerde reactor-compartiment bepaalt of dit een drijvende dan wel een weerstandskracht is. De deeltjesspanning in het beluchte bed wordt berekend op basis van een krachtenbalans en in het gefluïdiseerde bed bepaald met behulp van een empirische correlatie. De berekening van de *wrijvingskrachten* is gebaseerd op een impulsbalans over de stroming naar de opening toe. Een macroscopische drukvalrelatie legt een verband tussen de wrijvingsverliezen en de schijnbare viscositeit van het gas-vast mengsel. Op basis van gegevens uit de literatuur is een correlatie opgesteld voor de schijnbare viscositeit van het beluchte of gefluïdiseerde bed als functie van de deeltjeseigenschappen en operationele parameters. De modelparameters die zijn gerelateerd aan deeltjeseigenschappen werden bepaald door middel van kleinschalige experimenten. Het model is gevalideerd met behulp van resultaten die zijn verkregen in twee koude experimentele opstellingen: de 'twin'-bed en de 'jet'-opstelling. Deze opstellingen zijn vereenvoudigingen van het IFB-systeem en maken de directe meting van gas- en deeltjesstroming mogelijk. Het model bleek goed in staat te zijn de resultaten in beide opstellingen te beschrijven.

Het model voor stroming door de opening is gecombineerd met modellen voor stroming over de overlooprand en deeltjesverdeling in de IFB-reactor. Met behulp van het resulterende model zijn de hydrodynamische verschijnselen die experimenteel zijn waargenomen kwalitatief correct door het model voorspelt. De invloed van de totale bedmassa en de gassnelheden in de compartimenten op de IFB-hydrodynamica (CRS en deeltjesverdeling) is opgehelderd. Het is verder aangetoond dat de gassnelheid naar één van de transportcompartimenten gebruikt kan worden om de CRS te regelen.

De totstandkoming van de hoge-temperatuur-IFB-opstelling wordt beschouwd als één van de belangrijkste wapenfeiten van dit onderzoek. De 'pilot plant' opstelling is geschikt voor regeneratieve ontwaveling bij wervelbedverbranding van steenkool. Door de extreme omstandigheden vanwege de verschillende chemische milieu's (reducerend, oxiderend en zwavelhoudend) en de hoge temperatuur (tot 1000 °C), is er speciale aandacht geschonken aan de keuze van het reactormateriaal. Verder zijn er verschillende veiligheidsmaatregelen getroffen in het ontwerp en door middel van regelapparatuur. Om de deeltjesverdeling te bepalen in de IFB-reactor zijn de bedhoogtes in de vier compartimenten gemeten. Twee experimentele methodes zijn hiervoor ontwikkeld: Laser-Licht-Reflectie en Drukgradient-Extrapolatie. Deze twee methodes kunnen aanvullend worden gebruikt. De meting van de gassamenstellingen in de IFB-reactor is uitgevoerd met een FT-IR analyse-apparaat die is gecalibreerd en geschikt gemaakt voor metingen in de IFB-opstelling.

De experimentele resultaten laten zien dat in de IFB-reactor, zwavelafvangst, regeneratie van het sorbent en deeltjescirculatie kunnen worden geïntegreerd in één reactorsysteem. Gedurende een vijf-daagse periode is de IFB 'pilot plant' opstelling zonder problemen bedreven waarbij continue regeneratieve zwavelvangst is uitgevoerd. Verder is er een 10-uur test en zijn er verschillende zwavelvangst en regeneratie experimenten ladingsgewijs uitgevoerd.

De CRS in de IFB-reactor werd bepaald volgens het stromingsmodel door de opening en op basis van drukvalmetingen over de openingen. De invloed van de temperatuur op de zwavelvangst en regeneratie is bestudeerd.

De volgende belangrijke experimentele bevindingen kunnen worden onderscheiden:

- ▶ de IFB-reactor blijkt naar behoren te functioneren op een hoge temperatuur inclusief continue deeltjescirculatie, zwavelafvangst en regeneratie van het sorbent;
- ▶ de reactorprestatie kon worden geregeld door variatie van de CRS door middel van het instellen van de IFB-hydrodynamica (gassnelheden en bedmassa);
- ▶ een hoge (>90%) zwavelretentie is bereikt waarmee nadrukkelijk de geschiktheid van de IFB reactor voor regeneratieve ontwaveling is aangetoond.

Een dynamisch model is opgesteld voor de IFB-hydrodynamica. Dit model is in staat om de dynamische respons van stapveranderingen op de operationele parameters (gassnelheden en IFB-bedmassa) te voorspellen. Het is aangetoond dat de nieuwe stationaire toestand bereikt wordt in de tijd die nodig is om de deeltjes te herverdelen over de IFB compartimenten. Deze tijd is ruim kleiner dan de gemiddelde IFB-deeltjescirculatielijktijd. Het is verder aangetoond door middel van dynamisch modelleren dat het ongeveer vijf keer de gemiddelde circulatielijktijd van de deeltjes duurt om een nieuwe stationaire toestand te bereiken met betrekking tot de gas-vast reacties. Voor het modelleren van de verblijftijdspreiding (RTD) in een niet-stationair bedreven wervelbedreactor waarin gas-vast reacties plaatsvinden, is naast modelleren op basis van populatiebalansen, een alternatieve aanpak ontwikkeld. Deze dynamische RTD aanpak is toegepast op de regeneratieve ontwaveling uitgevoerd in een IFB-reactor. Het blijkt dat het effect van verblijftijdspreiding op de gemiddelde omzetting (van sorbent) kan oplopen tot 30%.

De conclusie is dat de IFB-reactor technisch gerealiseerd kan worden en mogelijk economisch aantrekkelijk is voor processen waarin deeltjescirculatie is vereist. Dit is ook duidelijk gemaakt middels een voorontwerp van een proces voor regeneratieve NO<sub>x</sub>- en SO<sub>2</sub>-verwijdering uit rookgassen. Deze ontwerp-studie is uitgevoerd in samenwerking met het bedrijf NOXSO in de Verenigde Staten. Bovendien wordt een aantal andere mogelijke toepassingen van de IFB technologie gepresenteerd.

## List of abbreviations

CFB	Circulating Fluidized Bed
CFD	Computational Fluid Dynamics
CRS	Circulation Rate of Solids
DUT	Delft University of Technology
EPMA	Electron-Probe X-ray MicroAnalysis
FCC	Fluidized Catalytic Cracking
FBC	Fluidized Bed Combustion
FT-IR	Fourier Transform-InfraRed
GH	Gas Heater
IFB	Interconnected Fluidized Bed
LLR	Laser Light Reflection
MFC	Mass Flow Controller
MPC	Model Predictive Control
MV	Magnetic Valve
PGE	Pressure Gradient Extrapolation
PH	PreHeater
IGCC	Integrated Gasification Combined Cycle
RH	Reactor Heater
RTD	Residence Time Distribution
TDH	Transport Disengaging Height

## List of publications

- Snip, O.C., Korbee, R., Schouten, J.C., Bleek van den, C.M., "The influence of hydrodynamics on the performance of an Interconnected Fluidized Bed system for regenerative desulfurization", Proceedings of the 1995 IChemE Research Event, Vol. 1, Edinburgh, UK, January 5-6, 592-594 (1995).
- Korbee, R., Snip, O.C., Schouten, J.C., Bleek van den, C.M., "Solids and gas transfer via an orifice between partly and completely fluidized beds - design equations and considerations for operation", Proceedings of the International Symposium of the Engineering Foundation, Fluidization VIII, Tours, France, May 14-19, 665-672 (1995).
- Snip, O.C., Korbee, R., Schouten, J.C., Bleek van den, C.M., "Regenerative desulfurization in coal conversion processes applying the Interconnected Fluidized Bed system", Proceedings of the 8th International Conference on Coal Science, Coal Science and Technology 24, Oviedo, Spain, September 10-15, 1847-1850 (1995).
- Snip, O.C., Korbee, R., Schouten, J.C., Bleek van den, C.M., "The influence of hydrodynamics on the performance of an Interconnected Fluidized Bed system for regenerative desulfurization", AIChE Symp. Series, 91 (308), 82-92 (1995).
- Korbee, R., Snip, O.C., Schouten, J.C., Bleek van den, C.M., "Rate of solids and gas transfer via an orifice between partially and completely fluidized beds", Chem. Eng. Sci., 49 (24B), 5819-5832 (1995).
- Snip, O.C., Korbee, R., Schouten, J.C., Bleek van den, C.M., "Solids and gas transport from and between aerated and fluidized beds", AIChE Symp. Series, 92 (313), 76-80 (1996).
- Snip, O.C., Woods, M., Korbee, R., Schouten, J.C., Bleek van den, C.M., "Regenerative removal of SO<sub>2</sub> and NO<sub>x</sub> for a 150 MWe power plant in an Interconnected Fluidized Bed facility", Chem. Eng. Sci., 51A (10), 2021-2029 (1996).
- Snip, O.C., Schouten, J.C., Bleek van den, C.M., "Micro- and macroscopic transport phenomena - on the use of transport equations: theory and experiments", to be submitted to Chem. Eng. Education (1997).
- Snip, O.C., Schouten, J.C., Bleek van den, C.M., "Solids and gas flow through orifices in Interconnected Fluidized Beds: the influence of shear friction", to be submitted to Journal of Fluid Mechanics (1997).
- Snip, O.C., Schouten, J.C., Bleek van den, C.M., "Regenerative desulfurization in an Interconnected Fluidized Bed reactor system", to be submitted to Fuel (1997).

## Dankwoord

Eigenlijk is het gek dat een woord van dank achterin het proefschrift is opgenomen. Zonder de bijdragen van vele personen hadden de resultaten namelijk helemaal niet tot stand kunnen komen.

Speciaal is dit het geval omdat een belangrijk deel van het werk zich heeft gericht op het bouwen en aan de praat krijgen van een hoge temperatuur pilot-plant-opstelling. Vanwege de complexiteit en de omvang van de apparatuur hebben velen een bijdrage geleverd aan het tot stand komen van de resultaten. Met betrekking tot deze opstelling wil ik iedereen van de werkplaats, instrumentmakerij, tekenkamer en analyse-laboratorium erg bedanken voor het werk dat ze in het kader van dit project hebben verricht. In het bijzonder noem ik het kleurrijke trio Wim Dumay, Ben Hak en Tom de Kruijff die de opstelling in de proeffabriek in belangrijke mate hebben vormgegeven.

Tevens bedank ik de afstudeerders die erg veel werk hebben verzet aan: de hete IFB opstelling, de 'koude' IFB (twin-bed- en jet-) opstellingen en IFB-modelleer-werk. In min of meer chronologische volgorde: Roy vd Hengel, Rudi Mulder, Dick Roodenburg, Gert-Jan vd Bilt, Karin Iversen (TU Denmark, Lyngby), Mike Verlaat, Matthijs Stevens, Marga de Feber, Gerard van Oosterbaan, David van Ling, Carel de Loë, Gitta Kraijo, Marco Smaling, Marit van Lieshout en Nanda Rijk. Zonder jullie inspanningen had ik niet dit proefschrift kunnen schrijven. Ook een klein leger aan research-praktikanten, 3e jaars-praktikanten en FVO'ers heeft een belangrijke bijdrage geleverd aan de resultaten. Een aantal Fabrieks-Voor-Ontwerpen van processen waarin de IFB reactor centraal stond is gemaakt in samenwerking met bedrijven waarvoor ik de NOXSO Corporation (Mark Woods) en DuPont (Jan Lerou) wil bedanken. Erg nuttig waren de grondige evaluatie's van de ontwerpen door Cees Luteijn en Johan Grievink. Laatstgenoemde heeft tevens een drietal afstudeerders op het gebied van dynamisch modelleren mede begeleid. Professor Molodtsov van de Université de Technologie in Compiègne wil ik bedanken voor de nuttige samenwerking en de uitwisseling en het begeleiden van één van de studenten. Verder ben ik professor Bird van de University of Wisconsin dankbaar voor de nuttige discussie's over fysische transportverschijnselen en het gebruik van balansen in het bijzonder.

Het leven in en om de Proeffabriek heb ik gedurende mijn AIO-tijd als bijzonder aangenaam ervaren. Hiervoor zijn in belangrijke mate de volgende personen verantwoordelijk: Albert Gerritsen, Ad Heymans, Anton Hexspoor, Jaap van Raamt en Ton de Vreese. Zij hebben ieder op hun geheel eigen wijze mij met raad en daad bijgestaan. Verder dank ik alle collega \*IO's die hebben bijgedragen tot een prettige werksfeer. In het bijzonder wil ik hier noemen mijn kamergenoten Weigang Lin, Cees Stellema en Geuch Zijlma en mijn collega filmer, acteur en luchtschip-liefhebber Otto Oudshoorn.

Erg graag wil ik Cock van den Bleek bedanken die mij de mogelijkheid heeft geboden dit onderzoek te gaan doen en mij samen met Jaap Schouten en Rob Korbee in deze periode heeft begeleid. Bedankt voor jullie enthousiasme, inzichten, kritieken, medeleven, vertrouwen en de vrijheid die ik heb gekregen om onderzoek te doen. Dit heeft er voor gezorgd dat ik de afgelopen 4 jaar veel meer heb kunnen doen en leren dan ik aan het begin had kunnen vermoeden.

Redenen te veel zijn er om Esther te bedanken. Het schrijven van dit proefschrift is voor jou soms ook afzien geweest. Jouw relativeringen en steun had ik niet kunnen missen.

## Curriculum vitae

Onno C. Snip werd op 7 augustus 1968 geboren te Groningen.

- 1980 - 1986 : Voorbereidend Wetenschappelijk Onderwijs werd gevolgd aan scholengemeenschap "de Waezenburg" te Leek (G).
- 1986 - 1992 : Scheikundige Technologie aan de Technische Universiteit Delft. Op 25 augustus 1992 werd het ingenieursdiploma behaald.  
Het afstudeeronderzoek naar radiale dispersie in trickle-bed reactoren werd uitgevoerd bij het Koninklijke/Shell Laboratorium te Amsterdam in samenwerking met de sectie chemische reactorkunde van prof.ir. C.M. van den Bleek.
- 1992 - 1997 : Na een korte carrière als reisleader in het verre oosten vervolgens op 1 november 1992 gestart met het promotieonderzoek als Assistent In Opleiding (AIO). Het onderzoek naar IFB-reactoren dat grotendeels is beschreven in dit proefschrift is uitgevoerd binnen de sectie chemische reactorkunde van de vakgroep chemische procestechnologie aan de Technische Universiteit Delft.